



**HAL**  
open science

# Dendritic functionalization of core-shell magnetic nanoparticles for biotechnology

Liubov Artiomenko Mitcova

► **To cite this version:**

Liubov Artiomenko Mitcova. Dendritic functionalization of core-shell magnetic nanoparticles for biotechnology. Organic chemistry. Université de Bordeaux, 2014. English. NNT : 2014BORD0025 . tel-01312378

**HAL Id: tel-01312378**

**<https://theses.hal.science/tel-01312378>**

Submitted on 6 May 2016

**HAL** is a multi-disciplinary open access archive for the deposit and dissemination of scientific research documents, whether they are published or not. The documents may come from teaching and research institutions in France or abroad, or from public or private research centers.

L'archive ouverte pluridisciplinaire **HAL**, est destinée au dépôt et à la diffusion de documents scientifiques de niveau recherche, publiés ou non, émanant des établissements d'enseignement et de recherche français ou étrangers, des laboratoires publics ou privés.

# THÈSE

Présentée à

**L'UNIVERSITÉ DE BORDEAUX**

École doctorale des sciences chimiques

par

**LIUBOV ARTIOMENCO MITCOVA**

Pour obtenir le grade de

**DOCTEUR**

SPÉCIALITÉ : Chimie Organique

---

Dendritic functionalization of core-shell  
magnetic nanoparticles for biotechnology

---

*Soutenue le 17 Avril 2014*

*Devant la commission d'examen formée de :*

Mme. Sofia Dembski	Chercheur, Fraunhofer-Institut für Silikatforschung (Würzburg, Allemagne)	Examineur
M. Jean-Olivier Durand	Directeur de recherche, CNRS (Université Montpellier 2)	Rapporteur
M. Eric Fouquet	Professeur (Université de Bordeaux)	Examineur
Mme. Karine Heuzé	Chargée de recherche, CNRS (Université de Bordeaux)	Directrice de thèse
M. Stéphane Parola	Professeur, (ENS Lyon)	Rapporteur
M. Luc Vellutini	Maître de Conférences (Université de Bordeaux)	Directeur de thèse



# **Résumé**



Actuellement, les nanoparticules magnétiques (MNPs) font l'objet d'intenses recherches dans beaucoup de domaines, comme celui des fluides magnétiques,<sup>1</sup> de la biotechnologie/biomédecine,<sup>2</sup> de la catalyse<sup>3</sup> et de l'environnement.<sup>4</sup> Toutes ces disciplines présentent une demande de plus en plus forte en MNPs spécifiques, en terme de géométries et de propriétés physiques/chimiques. Ainsi, le développement de nouvelles stratégies de synthèse de MNPs a permis un meilleur contrôle de leur taille, de leur structure et de leurs propriétés magnétiques. De plus, les développements de techniques de protection et de stabilisation de ces matériaux (par un enrobage organique ou inorganique, ou par encapsulation dans des matrices organiques ou inorganiques) ont permis d'améliorer les dispersions des MNPs dans les milieux aqueux et/ou organiques. Ces couches de protection présentent également des groupes fonctionnels de surface, qui vont pouvoir servir de plate-forme pour la fonctionnalisation des MNPs.

En particulier, dans le domaine de la biotechnologie (tels que la protéomique, la bio-catalyse et les biomatériaux), la purification et la manipulation contrôlées des biomolécules (protéines, enzymes, anticorps, peptides, lipides, acides nucléiques, etc) est un enjeu majeur. Jusqu'à présent, les protocoles classiques utilisés dans ce domaine (comme la chromatographie, l'électrophorèse, l'ultrafiltration, etc.) font appel à un matériel spécifique, sont difficiles à mettre en œuvre et nécessitent beaucoup de temps. Ainsi, le développement de MNPs fonctionnelles destinées à l'immobilisation spécifique de biomolécules est un axe de recherche permettant de répondre à cet enjeu.<sup>5</sup> Les MNPs de tailles inférieures à 10-20 nm sont des matériaux de choix en raison de leurs propriétés de superparamagnétisme (SP). Elles peuvent être facilement concentrées sous l'influence d'un champ magnétique externe (généralement un simple aimant) et récupérer un état colloïdal stable en l'absence de ce champ (Figure 1).



**Figure 1.** Concentration de MNPs sous l'influence d'un champ magnétique (les particules se collent aux parois du flacon), et retrouvent leur état colloïdal en l'absence de ce champ.

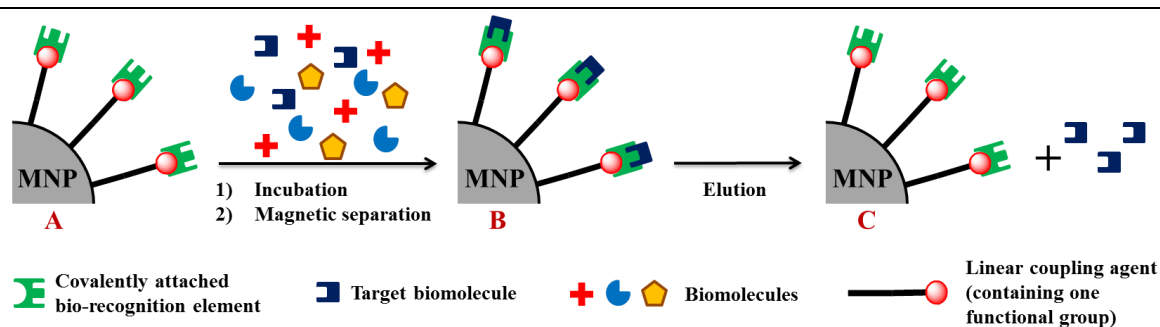


**Figure 2.** Principe de la séparation magnétique d'une biomolécule cible: (A) MNPs fonctionnelles porteuses d'un élément de biorecognition lié de manière covalente à la surface de la particule. Addition de ces MNPs dans un mélange biologique complexe contenant la biomolécule cible; (B) Les MNPs fonctionnelles reconnaissent la biomolécule cible. (C) La biomolécule cible est relarguée par clivage.

Contrairement, aux méthodes conventionnelles de séparations, la technique de décantation magnétique est simple, rapide et efficace. Ainsi, les MNPs fonctionnelles porteuses d'un biorécepteur (comme un marqueur d'affinité, des groupes d'échange d'ions, ou un oligonucléotide) lié de manière covalente à la surface, sont ajoutées à un mélange biologique complexe contenant la biomolécule cible (Figure 2). Après incubation, les MNPs reconnaissent la biomolécule cible. Puis les MNPs sont isolées par décantation magnétique et les contaminants sont éliminés. Enfin, les MNPs porteuses des biomolécules cibles sont isolées et ces dernières peuvent être récupérées par un clivage approprié. Ainsi, l'utilisation de MNPs comme plate-forme pour l'immobilisation, la séparation et de la purification de biomolécules est une méthode rapide, économique et facile à mettre en œuvre.

Le but de ce travail est de concevoir des MNPs fonctionnalisées stables, dispersibles dans l'eau et qui assureront une immobilisation covalente, sélective et efficace des biomolécules. Bien qu'un large choix de MNPs soit disponible dans le commerce, la modification chimique de surface des MNPs reste une étape indispensable à l'élaboration de matériaux spécifiques. Un contrôle précis de la fonctionnalisation de surface des MNPs est cruciale, car vont en découler leurs propriétés physico-chimiques, leur stabilité colloïdale, et la préservation de l'activité biologique de la biomolécule immobilisée.

L'efficacité de l'immobilisation et la quantité de biomolécules immobilisées de manière covalente est déterminée par le nombre de groupes fonctionnels disponibles à la surface des MNPs. Généralement, la fonctionnalisation des MNPs ne permet l'introduction que d'un nombre limité de groupements fonctionnels accessibles à la surface, ce qui ne conduit *in fine* qu'à une faible quantité de biomolécules immobilisées. Dans ce travail, nous proposons d'augmenter le nombre de groupes fonctionnels accessibles à la surface des MNPs en modifiant celle-ci par des agents de couplages dendritiques. L'efficacité de ces surfaces pour immobiliser des biomolécules ou des modèles de biomolécules est comparée avec celle obtenue pour des surfaces fonctionnalisées par un agent de couplage analogue linéaire (Figure 3) à travers l'étude de l'effet dendritique.

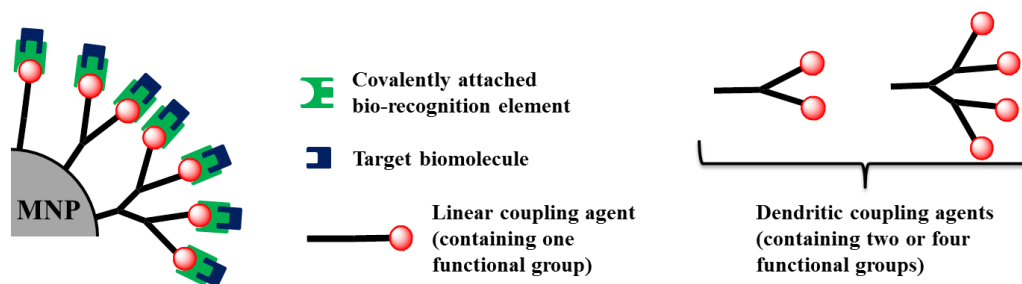


**Figure 3.** Fonctionnalisation de surface avec: un agent de couplage linéaire (contenant un groupe fonctionnel); un agent de couplage dendritique à deux branches (contenant deux groupes fonctionnels) et un agent de couplage dendritique à quatre branches (contenant quatre groupes fonctionnels).

Dans ce travail nous avons étudié deux types de nanoparticules SP cœur-écorce ( $\gamma\text{-Fe}_2\text{O}_3$ ) de 300 nm qui se composent d'une maghémite (noyau ferrofluide,  $\gamma\text{-Fe}_2\text{O}_3$ ) et d'une écorce soit: (I) de polymère (Figure 4 a) soit (II) de silice (Figure 4 b). Les deux types de nanoparticules SP cœur-écorce sont développées et commercialisées par Ademtech SA.<sup>6</sup>

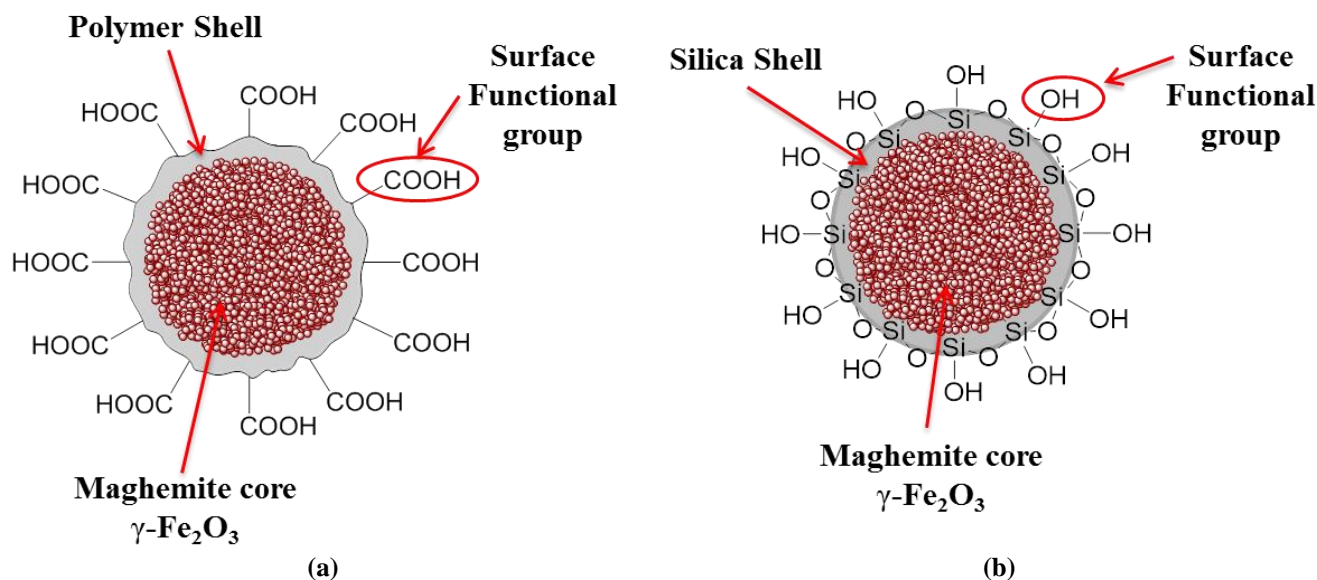


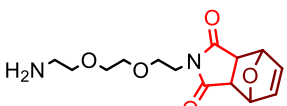
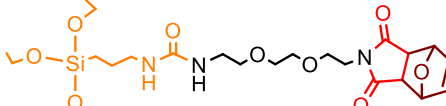
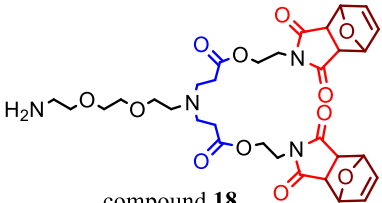
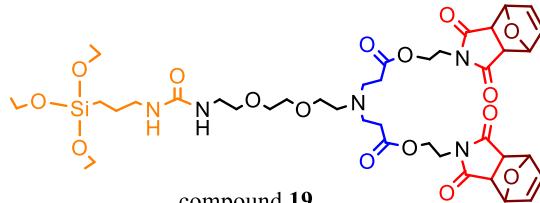
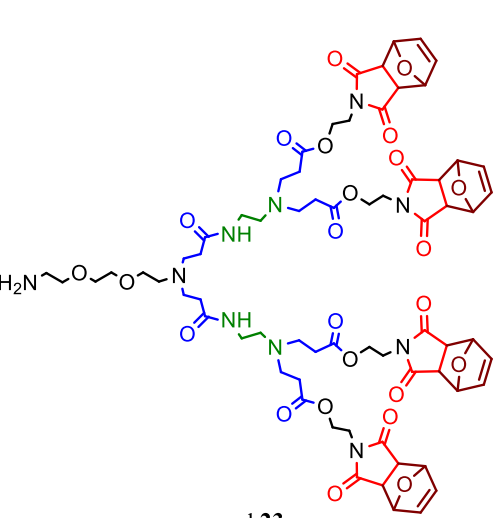
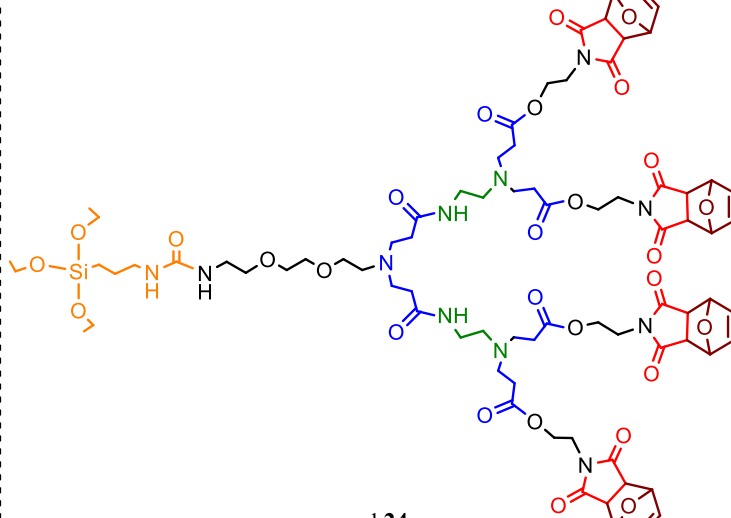
**Figure 4.** (a) MNP cœur-écorce ( $\gamma\text{-Fe}_2\text{O}_3$ /Polymer); et (b) MNP cœur-écorce ( $\gamma\text{-Fe}_2\text{O}_3$ /SiO<sub>2</sub>).

Le cœur ferrofluide est composé de particules de  $\gamma\text{-Fe}_2\text{O}_3$  de tailles nanométriques (diamètre inférieur à 10 nm, constituant des monodomains magnétiques) qui sont stabilisées dans un fluide (tensioactifs). Ces petites particules sont magnétiquement indépendantes préservant ainsi le comportement de SP de l'ensemble de la particule de 300 nm. Aussi, ces MNPs, possède une teneur magnétique élevée (70%) et manifestent donc une réponse rapide et forte à un champ magnétique externe (aimantation à saturation: env. 40 cm<sup>3</sup>/g à 300 K), ainsi leur séparation magnétique d'un milieu réactionnel est supérieure à 99% en 1 min., ce qui en fait est une méthode simple, rapide et économique.



Ce manuscrit est organisé en quatre chapitres. Dans le premier chapitre, le lecteur trouvera une étude bibliographique, ainsi qu'une brève introduction sur les MNPs, leur synthèse, leur protection/stabilisation et les techniques utilisées pour leur fonctionnalisation. Egalement, les méthodes d'immobilisation de biomolécules (chimique, physique et par médiation biologique) sont décrites. Le design et la synthèse d'agents de couplage linéaires et dendritiques sont détaillés dans le deuxième chapitre. Deux types de surfaces de MNPs cœur-écorce (avec une écorce du polymère ou de la silice) sont utilisées ce qui implique la synthèse de deux familles d'agents de couplage (aminés et silanes) (Tableau 1). Afin d'étudier l'effet «dendritique» sur la fonctionnalisation de surface, trois types d'agents de couplage ont été conçus: des agents de couplage linéaires (contenant un groupe fonctionnel: composés **10** et **11**), les agents de couplage dendritiques à deux branches (contenant deux groupes fonctionnels: composés **18** et **19**) et des agents de couplage dendritiques à quatre branches (contenant quatre groupes fonctionnels: composés **23** et **24**).

**Table 1.** Agents de couplage pour la modification chimique de MNPs cœur-écorce ( $\gamma$ -Fe<sub>2</sub>O<sub>3</sub>/polymère ou silice).

The "family" of coupling agents designed for chemical modification of MNPs with polymer shell	The "family" of silylated coupling agents designed for chemical modification of MNPs with silica shell
<p style="text-align: center;"><b>linear coupling agents:</b></p>  <p style="text-align: center;">compound <b>10</b></p>	 <p style="text-align: center;">compound <b>11</b></p>
<p style="text-align: center;"><b>two-branched coupling agents (dendrons G1):</b></p>  <p style="text-align: center;">compound <b>18</b></p>	 <p style="text-align: center;">compound <b>19</b></p>
<p style="text-align: center;"><b>four-branched coupling agents (dendrons G2):</b></p>  <p style="text-align: center;">compound <b>23</b></p>	 <p style="text-align: center;">compound <b>24</b></p>

Chaque famille d'agents de couplage possède d'une part, un site d'ancrage (amine ou silane), capable de former une liaison covalente avec les groupements disponibles à la surface des MNPs (carboxyle ou silanol) et d'autre part, un groupe fonctionnel spécifique (maléimide). Le groupement maléimide étant sensible aux nucléophiles, il a été protégé par un furane. La régénération du maléimide est facilement obtenue par une réaction de rétro-Diels-Alder. En outre, puisque la majorité des tests de bio-immobilisation sont effectués en milieu aqueux, il était indispensable de concevoir des agents de couplage hydrophiles. Ainsi, des chaînes de PEG et/ou des chaînes PAMAM (polyamidoamine) ont été introduites dans la structure des agents de couplage que nous proposons. De plus, les structures PEG sont considérées comme l'un des groupes chimiques qui limitent au maximum l'adsorption non spécifique des protéines.<sup>7</sup>

Le troisième chapitre est consacré au greffage des agents de couplage fonctionnalisés par des groupes maléimides sur des MNPs cœur-écorce ( $\gamma\text{-Fe}_2\text{O}_3/\text{Polymer-COOH}$ ) et à leur caractérisation. La fonctionnalisation de surface de ces MNPs ( $\gamma\text{-Fe}_2\text{O}_3/\text{Pol@10}$ ,  $\gamma\text{-Fe}_2\text{O}_3/\text{Pol@18}$  et  $\gamma\text{-Fe}_2\text{O}_3/\text{Pol@23}$ ) a été obtenue par le greffage des agents de couplage aminés (linéaire **10**, dendritique à deux branches **18** et dendritique à quatre branches **23**) sur les fonctions acide carboxylique accessibles à la surface des MNPs (par un couplage de type EDC/NHS). Cette étape a été suivie et caractérisée par spectroscopie FT-IR en suivant la bande d'absorption à  $1703\text{ cm}^{-1}$  correspondant au mode  $\nu\text{C=O}$  en opposition de phase (d'imides cycliques). Nous avons ainsi mis en évidence que le rendement de greffage dépend fortement de la quantité d'agents de couplage utilisée dans l'étape de greffage (Figure 5).

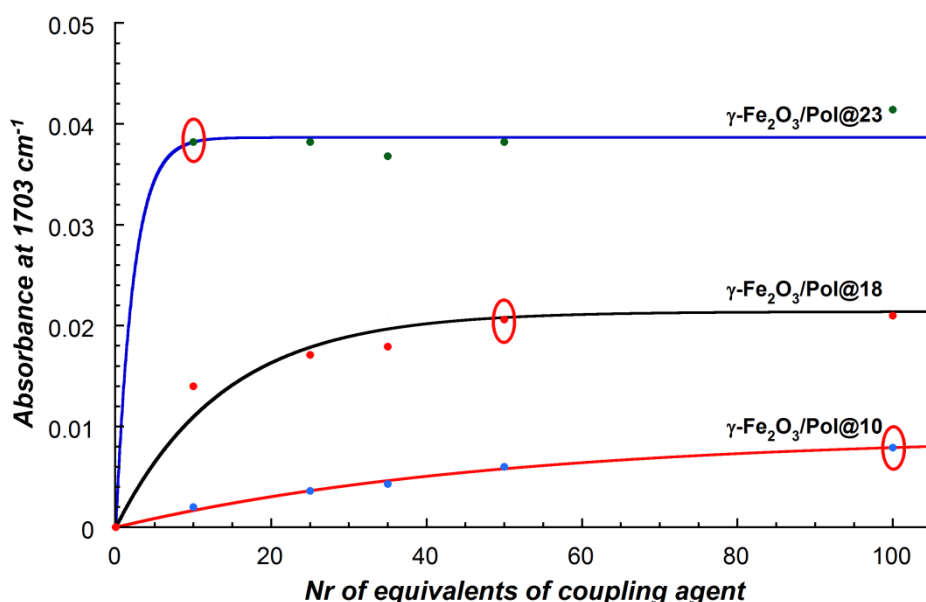


**Figure 5.** Etude IR de la fonctionnalisation de surface par l'agent de couplage linéaire **10** (courbe rouge); l'agent de couplage dendritique à deux branches **18** (courbe noire); et l'agent de couplage dendritique à quatre branches **23** (courbe bleue).

Ainsi, le maximum de fonctionnalisation de surface avec l'agent de couplage linéaire **10** a été obtenu par addition de 100 équivalents de ce composé ; avec l'agent de couplage deux branches **18**, 50 équivalents de ce composé ont été nécessaires, tandis qu'avec l'agent de couplage à quatre branches **23**, nous avons obtenu le maximum de fonctionnalisation de surface en ajoutant seulement 10 équivalents de ce composé. En outre, la quantité de groupes fonctionnels sur la surface des MNPs augmente avec la génération du dendron. Egalement, cette quantité est directement proportionnelle au nombre de groupes fonctionnels présents dans la structure de l'agent de couplage, mettant en évidence un effet dendritique positif sur la fonctionnalisation de surface. La fonctionnalisation de surface a également été confirmée par des mesures ATG couplées à la masse et des mesures de potentiel zêta. Les MNPs ( $\gamma$ -Fe<sub>2</sub>O<sub>3</sub>/Pol@**10/18/23**) modifiées par ces agents de couplage fonctionnels (maléimide) ont conservé leur intégrité ainsi que leur stabilité colloïdale. En effet, une bonne dispersion dans des solutions aqueuses et des solvants polaires a été maintenue. La capacité des MNPs ( $\gamma$ -Fe<sub>2</sub>O<sub>3</sub>/Pol@**10/18/23**) modifiées par des groupes maléimide pour immobiliser des biomolécules ou des modèles de biomolécules a été étudiée par une série de tests d'immobilisation. Tous ont permis d'immobiliser des biomolécules contenant un groupe thiol, de plus un effet dendritique positif a été mis en évidence sur la fonctionnalisation de surface. En outre, la réactivité des MNPs ( $\gamma$ -Fe<sub>2</sub>O<sub>3</sub>/Pol@**10/18/23**) modifiées par des groupes maléimide envers les groupements amine (de biomolécules), dans des conditions de réaction types utilisées pour l'immobilisation des thiols (c'est à dire dans des conditions de pH 6.5 - 7.5), a été explorée. Il a été confirmé que les fonctions amine de biomolécules peuvent être immobilisées, cependant, en quantité négligeable par rapport aux quantités des biomolécules porteuses de groupements thiol. Cette expérience nous a permis de montrer la bio-spécificité de l'immobilisation de biomolécules par ces MNPs ( $\gamma$ -Fe<sub>2</sub>O<sub>3</sub>/Pol@**10/18/23**) modifiées par des groupes maléimide.

Le quatrième chapitre est consacré à la fonctionnalisation et la caractérisation de MNPs cœur-écorce ( $\gamma$ -Fe<sub>2</sub>O<sub>3</sub>/SiO<sub>2</sub>) par des groupes maléimide. La modification chimique de surface de ces MNPs a été obtenue par réaction d'hydrolyse-condensation de groupes silanol de l'écorce de silice avec les groupements silane des agents de couplage (agent de couplage linéaire **11**, agent de couplage dendritique à deux branches **19** et agent de couplage dendritique à quatre branches **24**). La modification de surface est suivie par spectroscopie IR. Cette étude a permis de caractériser le greffage par les agents de couplage (**11**, **19** et **24**) et à montrer que la quantité de groupes fonctionnels présents sur la surface des MNPs ( $\gamma$ -Fe<sub>2</sub>O<sub>3</sub>/SiO<sub>2</sub>@**11/19/24**) augmente avec la génération du dendron. La plus grande quantité de groupes fonctionnels à la surface de ces MNPs a été obtenue par le greffage de l'agent de couplage dendritique à quatre branches **24**, mettant en évidence l'efficacité des structures dendritiques pour la modification de surface et démontrant encore une fois un effet dendritique positif sur la fonctionnalisation de celle-ci. La modification chimique de surface a également été confirmée

par des mesures ATG couplées avec la masse et des mesures de potentiel zêta. La microscopie MET a montré que ces MNPs ( $\gamma\text{-Fe}_2\text{O}_3/\text{SiO}_2@11/19/24$ ) ont conservé leur morphologie et leur intégrité, tandis qu'une légère augmentation de l'épaisseur de l'écorce suggère la formation d'une couche mince homogène d'agents de couplage sur leur surface. Egalement, on note que ces particules fonctionnalisées conservent une bonne stabilité colloïdale en milieux aqueux. Enfin, la capacité de ces MNPs ( $\gamma\text{-Fe}_2\text{O}_3/\text{SiO}_2@11/19/24$ ) à immobiliser des biomolécules a été étudiée au moyen de deux tests d'immobilisation: (I) l'immobilisation de biotine modifiée par un groupement thiol (HS-PEG-Biot) (Figure 6 a) et (II) l'immobilisation d'un oligonucléotide modifié par un groupement thiol (HS-dT) (Figure 7).

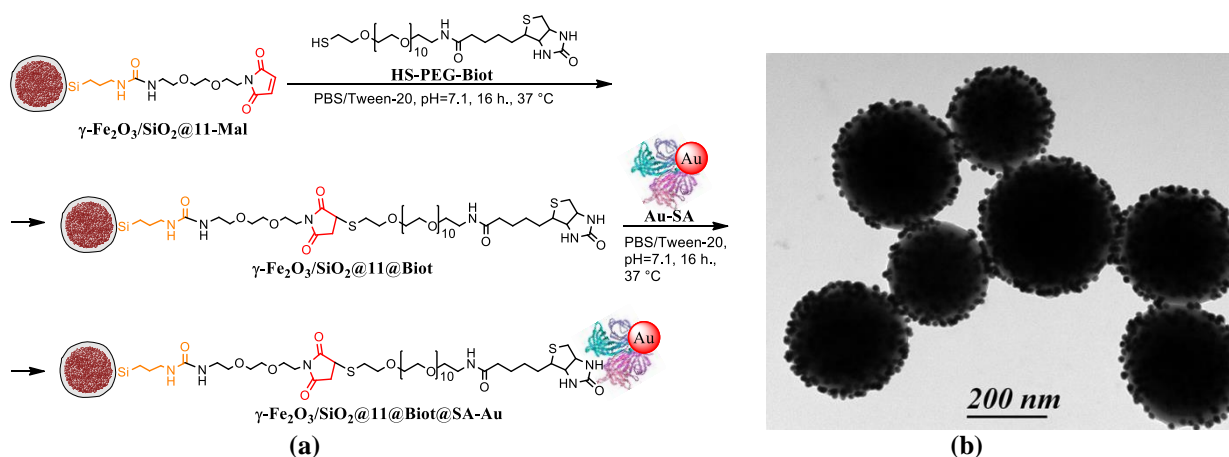


**Figure 6.** (a) Immobilisation de HS-PEG-Biot sur  $\gamma\text{-Fe}_2\text{O}_3/\text{SiO}_2@11/19/24$  suivie de l'immobilisation de SA-Au NPs par affinité Biotin-Streptavidin. (b) TEM image of  $\gamma\text{-Fe}_2\text{O}_3/\text{SiO}_2@24@BiotSA\text{-Au}$ .

Le premier test implique un couplage covalent de HS-PEG-Biot avec les groupements maléimide à la surface des MNPs ( $\gamma\text{-Fe}_2\text{O}_3/\text{SiO}_2@11/19/24$ ), ensuite la présence de la biotine sera révéler par l'immobilisation des nanoparticules d'or recouvertes de streptavidine (SA-Au NPs) disponibles dans le commerce, par l'affinité Biotin-Streptavidin. Les SA-Au NPs immobilisées ont servi de marqueur à l'échelle nanométrique en TEM (Figure 6 b) ainsi que pour la quantification en spectroscopie UV-Vis de SA-Au NPs immobilisées sur les MNPs.

Le second test implique trois étapes:

*La première étape* consiste dans l'immobilisation du HS-dT oligonucléotide sur les MNPs fonctionnalisées par un groupement maléimide. Dans *la deuxième étape*, l'hybridation de l'oligonucléotide dT immobilisé avec une séquence complémentaire d'oligo poly A conjugué à un fluorochrome (oligo-dA Alexa Fluor) a été effectuée. *La dernière étape* représente la déshybridation, conduisant au dosage de l'oligo-dA Alexa Fluor élué sur le lecteur de microplaques à fluorescence (Figure 8).

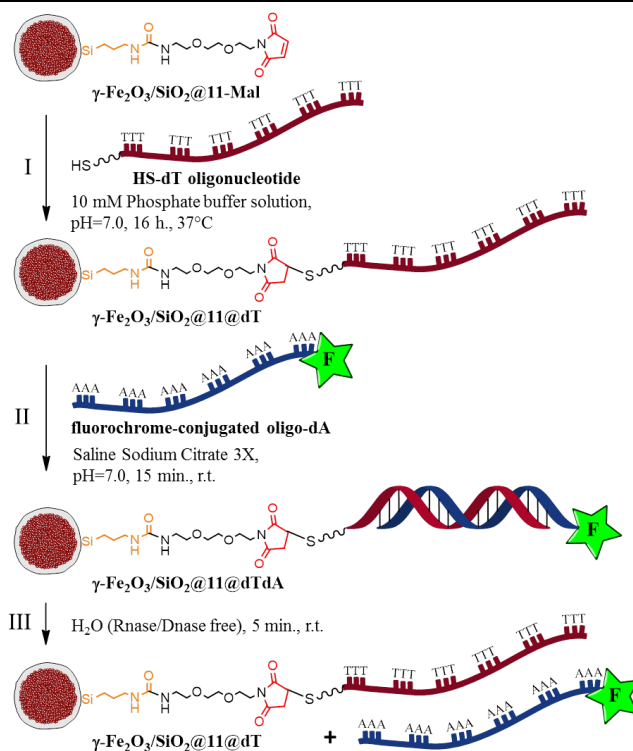


**Figure 7.** Principe d'immobilisation d'un oligonucléotide HS-dT.

Ces deux tests ont prouvé l'efficacité des MNPs ( $\gamma\text{-Fe}_2\text{O}_3/\text{SiO}_2@11/19/24$ ) pour l'immobilisation spécifique de ces biomolécules. Une excellente capacité d'immobilisation de l'oligonucléotide HS-dT a été observée (233,8 pmol/mg de particules) dans le cas des MNPs ( $\gamma\text{-Fe}_2\text{O}_3/\text{SiO}_2@24$ , Figure 8), soulignant à nouveau l'efficacité d'une fonctionnalisation dendritique de la surface des nanoparticules. De plus, les MNPs ( $\gamma\text{-Fe}_2\text{O}_3/\text{SiO}_2@11/19/24$ ) ont montré une plus grande capacité à immobiliser le PolyT-SH par rapport à leurs analogues MNPs ( $\gamma\text{-Fe}_2\text{O}_3/\text{polymer}@10/18/23$ ). En outre, il est à noter que l'optimisation des protocoles d'immobilisation pourrait conduire à une immobilisation de PolyT-SH encore plus grande.

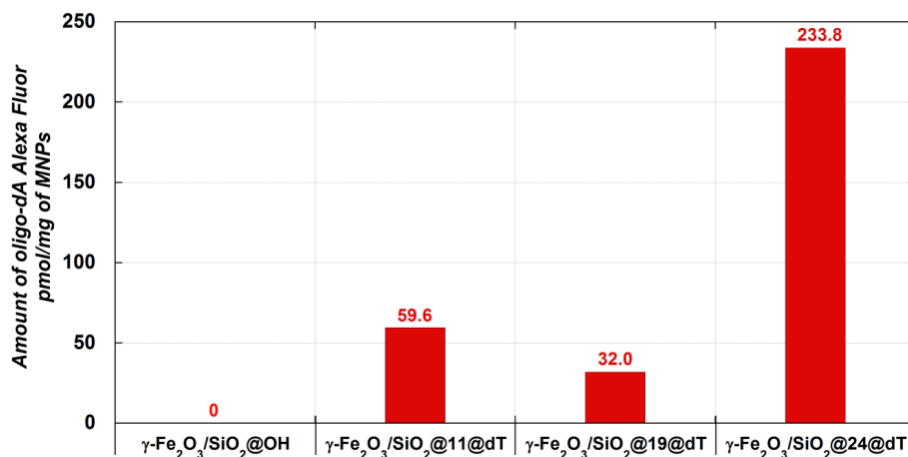


**Figure 8.** Mesure de fluorescence (Alexa Fluor) de quantification de l'oligonucléotide dA élué après deshybridation.

Pour conclure, cette étude a démontré l'intérêt de la fonctionnalisation de la surface de MNPs cœur-écorce par des structures dendritiques. Il a été déterminé que de nombreux paramètres influent sur la fonctionnalisation des MNPs, parmi eux, les trois facteurs les plus importants sont: (I) la nature de la surface (polymère ou la silice), (II) la nature des agents de couplage (linéaire ou à structure dendritique), de même que la génération de la dendron et, (III) la quantité d'agents de couplage introduit lors de l'étape de greffage.

---

**References:**

- <sup>1</sup> S. Chikazumi, S. Taketomi, M. Ukita, M. Mizukami, H. Miyajima, M. Setogawa and Y. Kurihara, *J. Magn. Magn. Mater.* **1987**, 65, 245–251.
- <sup>2</sup> (a) N. Crawley and M. Thompson, *Anal. Chem.* **2014**, 86, 130–160; (b) E. C. Wang and A. Z. Wang, *Integr. Biol.* **2014**, 6, 9–26; (c) R. M. Patil, P. B. Shete, N. D. Thorat, S. V. Otari, K. C. Barick, A. Prasad, R. S. Ningthoujam, B. M. David, *Trends in Biotechnology* **2011**, 29, 323–333 (d) K. Turcheniuk, A. V. Tarasevych, V. P. Kukhar, R. Boukherrouba and S. Szunerits, *Nanoscale*, **2013**, 5, 10729–10752; (e) L. Jézéquel, J. Loeper, and D. Pompon, *BioTechniques* **2008**, 45, 523–532; (f) W. U. Dittmer, P. de Kievit, M. W. J. Prins, J. L. M. Vissers, M. E. C. Mersch, M. F. W. C. Martens, *J. Immunol. Methods* **2008**, 338, 40–46; (g) S. Workman, S. K. Wells, C.-P. Pau, S. M. Owen, X. F. Dong, R. La Borde and T. C. Granade, *J. Virol. Methods* **2009**, 160, 14–21; (h) R. M. Patil, P. B. Shete, N. D. Thorat, S. V. Otari, K. C. Barick, A. Prasad, R. S. Ningthoujam, B. M. Tiwale and S. H. Pawar, *J. Magn. Magn. Mat.* **2014**, 355, 22–30; (i) F. Bayard, A. Raveneau, A. Letourneau, G. Joucla, C. Barbot, B. Garbay, C. Cabanne, *Anal. Biochem.* **2009**, 384, 350–352; (j) Y. Pan, X. Du, F. Zhao and B. Xu, *Chem. Soc. Rev.*, **2012**, 41, 2912–2942. (k) N. Chekina, D. Horak, P. Jendelova, M. Trchova, M. J. Benes, M. Hruby, V. Herynek, K. Turnovcova and E. Sykova, *J. Mater. Chem.* **2011**, 21, 7630–7639. (l) F. Chen, R. Shi, Y. Xue, L. Chen and Q.-H. Wan, *J. Magn. Magn. Mat.* **2010**, 322, 2439–2445; (m) A. K. Gupta and M. Gupta, *Biomaterials* **2005**, 26, 3995–4021.
- <sup>3</sup> (a) S. Krishnan and C. Walgama, *Anal. Chem.* **2013**, 85, 11420–11426; (b) S. H. Gage, B. D. Stein, L. Zh. Nikoshvili, V. G. Matveeva, M. G. Sulman, E. M. Sulman, D. Gene Morgan, E. Yu. Yuzik-Klimova, W. E. Mahmoud and L. M. Bronstein, *Langmuir* **2013**, 29, 466–473; (c) D. Rosario-Amorin, M. Gaboyard, R. Clerac, L. Vellutini, S. Nlate, and K. Heuze, *Chem. Eur. J.* **2012**, 18, 3305–3315; (d) D. Rosario-Amorin, M. Gaboyard, R. Clerac, S. Nlate and K. Heuze, *Dalton Trans.*, **2011**, 40, 44–46; (e) D. Rosario-Amorin, X. Wang, M. Gaboyard, R. Clerac, S. Nlate and K. Heuze, *Chem. Eur. J.* **2009**, 15, 12636 – 12643; (f) S. Ding, Y. Xing, M. Radosz and Y. Shen, *Macromolecules* **2006**, 39, 6399–6405.
- <sup>4</sup> A. Farrukh, A. Akram, A. Ghaffar, S. Hanif, A. Hamid, H. Duran and B. Yameen, *ACS Appl. Mater. Interfaces* **2013**, 5, 3784–3793.
- <sup>5</sup> (a) M. Colombo, S. Carregal-Romero, M. F. Casula, L. Gutierrez, M.P. Morales, I. B. Bohm, J. T. Heverhagen, D. Prospero and W. J. Parak, *Chem. Soc. Rev.*, **2012**, 41, 4306–4334; (b) A.-H. Lu, E. L. Salabas and F. Schuth, *Angew. Chem. Int. Ed.* **2007**, 46, 1222–1244.

<sup>6</sup> <http://www.ademtech.com>

<sup>7</sup> (a) K. Nakanishi, T. Sakiyama, Y. Kumada, K. Imamura and H. Imanaka, *Curr. Proteomics* **2008**, *5*, 161–175; (b) E. Ostuni, R. G. Chapman, R. E. Holmlin, S. Takayama and G. M. Whitesides, *Langmuir* **2001**, *17*, 5605–5620; (c) S. R. Benhabbour, H. Sheardown and A. Adronov, *Macromolecules* **2008**, *41*, 4817–4823; (d) S. R. Benhabbour, L. Liu, H. Sheardown and A. Adronov, *Macromolecules* **2008**, *41*, 2567–2576.





# **Contents**

---



<b>GENERAL INTRODUCTION</b> .....	1
<b>CHAPTER I. Bibliographical survey</b> .....	9
I.1. Introduction to the MNPs.....	11
I.2. Synthesis of IONPs.....	13
I.3. Stabilization, protection and functionalization of IONPs.....	14
I.3.1. Principles of colloidal stabilization.....	15
I.3.2. Surface modification with non-polymeric organic molecules.....	16
I.3.3. Polymers as stabilizers, coating and encapsulation material.....	19
I.3.4. Surface modification with dendritic structures.....	22
I.3.5. Surface modification with inorganic materials.....	25
I.4. Immobilization of biomolecules on MNPs' surface.....	26
I.4.1. Non-covalent immobilization.....	26
I.4.1.1. Physical adsorption.....	27
I.4.1.2. Biologically mediated immobilization.....	27
I.4.2. Covalent immobilization.....	29
I.4.2.1. Classical chemoligation.....	30
I.4.2.2. Site-specific chemoligation methods.....	35
I.5. Concluding remarks and motivation behind this research work.....	36
<b>CHAPTER II. Synthesis of coupling agents</b> .....	47
II.1. Choice of coupling agents.....	49
II.2. Synthesis of linear coupling agents.....	53
II.2.1. Strategy I.....	54
II.2.2. Strategy II.....	57
II.2.3. Strategy III.....	59
II.3. Synthesis of dendritic coupling agents.....	61
II.3.1. Dendrimers and dendrons.....	61
II.3.2. Synthesis of first generation (two branched) dendritic coupling agents.....	64
II.3.2.1. Strategy I.....	64
II.3.2.2. Strategy II.....	66
II.3.3. Synthesis of second generation (four branched) dendritic coupling agents.....	68
II.4. Conclusions:.....	71
<b>CHAPTER III. Functionalization of core-shell <math>\gamma</math>-Fe<sub>2</sub>O<sub>3</sub>/Polymer magnetic nanoparticles</b> .....	77
III.1. Introduction.....	79
III.2. Presentation of core-shell $\gamma$ -Fe <sub>2</sub> O <sub>3</sub> /Polymer MNPs.....	80
III.3. Surface modification chemistry of core-shell $\gamma$ -Fe <sub>2</sub> O <sub>3</sub> /Polymer MNPs.....	81
III.3.1. Grafting of linear coupling agent 10.....	82
III.3.1.1. General grafting and maleimide functional group deprotection procedures.....	82
III.3.1.2. Characterization of functionalized $\gamma$ -Fe <sub>2</sub> O <sub>3</sub> /Polymer MNPs.....	84
III.3.2. Optimization of grafting conditions.....	92
III.3.2.1. Influence of the loading in the grafting process of coupling agent 10.....	92
III.3.2.2. Influence of the loading in the grafting process of coupling agent 18.....	96
III.3.2.3. Influence of the loading in the grafting process of coupling agent 23.....	98

III.3.3. Comparative study - dendritic coupling agents versus linear coupling agent	101
III.3.3.1. Evolution of surface functionalization .....	101
III.3.3.2. Zeta potential measurements.....	103
III.3.3.3. Colloidal state of maleimide functionalized $\gamma$ -Fe <sub>2</sub> O <sub>3</sub> /Polymer MNPs in water.....	105
III.3.3.4. Covalent coupling of thiol modified biotin with maleimide functionalized $\gamma$ -Fe <sub>2</sub> O <sub>3</sub> /Polymer MNPs and consequent recognition by streptavidin coated gold NPs.....	106
III.3.3.5. Immobilization of amino functionalized gold nanoparticles on maleimide functionalized $\gamma$ -Fe <sub>2</sub> O <sub>3</sub> /Polymer MNPs.....	112
III.3.3.6. Covalent coupling of thiol modified oligonucleotide with maleimide functionalized $\gamma$ -Fe <sub>2</sub> O <sub>3</sub> /Polymer MNPs.....	114
III.4. Conclusion.....	117
<b>CHAPTER IV. Functionalization of core-shell <math>\gamma</math>-Fe<sub>2</sub>O<sub>3</sub>/SiO<sub>2</sub> magnetic nanoparticles</b> .....	123
IV.1. Introduction.....	125
IV.2. Presentation of core-shell $\gamma$ -Fe <sub>2</sub> O <sub>3</sub> /SiO <sub>2</sub> MNPs.....	125
IV.3. Surface modification chemistry of core-shell $\gamma$ -Fe <sub>2</sub> O <sub>3</sub> /SiO <sub>2</sub> MNPs.....	126
IV.3.1. General grafting and maleimide functional group deprotection procedures .....	129
IV.3.2. Characterization of functionalized $\gamma$ -Fe <sub>2</sub> O <sub>3</sub> /SiO <sub>2</sub> MNPs.....	132
IV.3.2.1. ATR FT-IR study of functionalized $\gamma$ -Fe <sub>2</sub> O <sub>3</sub> /SiO <sub>2</sub> MNPs.....	132
IV.3.2.2. TGA coupled with MS study of $\gamma$ -Fe <sub>2</sub> O <sub>3</sub> /SiO <sub>2</sub> MNPs functionalized with silylated coupling agent 11.....	138
IV.3.2.3. TEM study of maleimide functionalized $\gamma$ -Fe <sub>2</sub> O <sub>3</sub> /SiO <sub>2</sub> MNPs.....	143
IV.3.2.4. Zeta potential measurements for maleimide functionalized $\gamma$ -Fe <sub>2</sub> O <sub>3</sub> /SiO <sub>2</sub> MNPs.....	144
IV.3.2.5. Colloidal state of maleimide functionalized $\gamma$ -Fe <sub>2</sub> O <sub>3</sub> /SiO <sub>2</sub> MNPs in water.....	145
IV.4. Immobilization tests.....	146
IV.4.1. Covalent coupling of thiol modified biotin with the maleimide functionalized $\gamma$ -Fe <sub>2</sub> O <sub>3</sub> /SiO <sub>2</sub> MNPs and consequent recognition by SA-Au NPs.....	146
IV.4.2. Covalent coupling of HS-dT oligonucleotide with maleimide functionalized $\gamma$ -Fe <sub>2</sub> O <sub>3</sub> /SiO <sub>2</sub> MNPs and hybrid capture of its complementary sequence.....	149
IV.5. Conclusion.....	151
<b>GENERAL CONCLUSION</b> .....	155
<b>EXPERIMENTAL PART</b> .....	161
<b>LIST OF ABBREVIATIONS</b> .....	185

# **General introduction**



In the recent years, magnetic nanoparticles (MNPs) have become the topic of intense research in a wide range of disciplines, including the fields of magnetic fluids,<sup>1</sup> biotechnology/biomedicine,<sup>2</sup> catalysis<sup>3</sup> and environmental remediation.<sup>4</sup> All these disciplines are demanding for specific MNPs, with different geometries and physical/chemical properties. The recent improvement and development of new strategies for the synthesis of MNPs allowed a better control of their size, structure and magnetic properties. In addition, the developments made regarding the protection and stabilization techniques (coating with organic or inorganic materials/encapsulation in organic or inorganic materials) offered the possibility to disperse MNPs in aqueous and/or organic media. Moreover, the protective shells usually offer some surface functional groups, thus providing a convenient platform for the functionalization of MNPs. Therefore, the interest in designing novel MNPs continues to grow almost unabated.

Particularly, in the field of biotechnology (such as proteomics, bio-catalysis and biomaterials), the isolation, purification and controlled manipulation of biomolecules (proteins, enzymes, antibodies, peptides, lipids, nucleic acids, etc.) is of a paramount importance. Conventional protocols to achieve these goals (chromatography, electrophoresis, ultrafiltration, etc) require specific devices and are usually complicated and time consuming. Therefore, the development of highly reactive MNPs destined to the immobilization and isolation of biomolecules is in a strong demand.<sup>5</sup> In this field small MNPs are very promising materials due to their size dependent physical properties (superparamagnetism (SP)) that give the possibility to be easily concentrated under the influence of an external magnetic field (usually a simple magnet) and maintaining their colloidal stability upon field removal (Figure 1).



**Figure 1.** Picture illustrating the concentration of MNPs under the influence of a magnet (MNPs come close to the vial wall), and the dispersion of MNPs upon the field removal.

In contrast to the conventional separation procedures, the technique of magnetic separation is very simple (Figure 2).



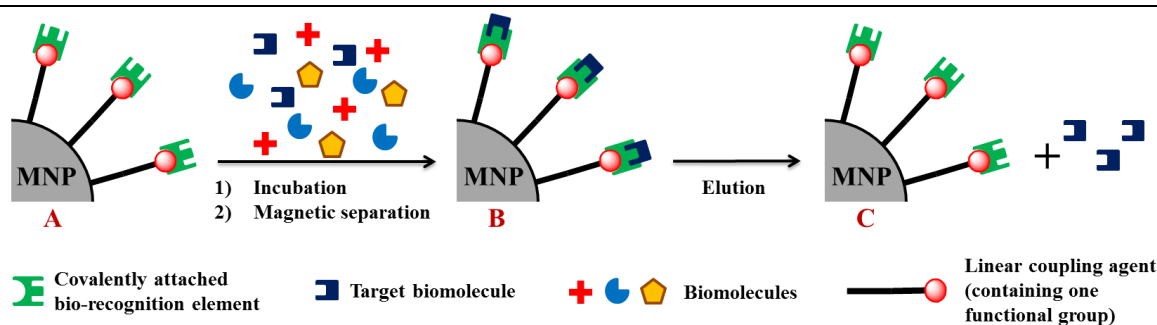


**Figure 2.** Schematic representation of the magnetic separation technique: (A) MNPs bearing a covalently attached bio-recognition element are added to a complex medium, containing the target biomolecule; (B) MNPs recognize the target biomolecule. (C) Target biomolecules are recovered via elution.

Thus, MNPs bearing a covalently attached biomolecule (containing a bio-recognition element such as affinity tag or ion-exchange groups, oligonucleotide, etc.) are added to a complex medium, containing the target biomolecule. After a suitable incubation time, the MNPs recognize the target biomolecule. Then MNPs are isolated by magnetic decantation and the contaminants washed out. Finally, the isolated target biomolecules can be recovered via their displacement, following proper elution procedures. Thus, the use of MNPs as support for biomolecules immobilization offers a fast, cheap and easy method of separation and purification.

The purpose of this work is to design stable, water-dispersible, functionalized MNPs that will ensure selective covalent immobilization of biomolecules. While, a large choice of MNPs is now commercially available, the surface modification of MNPs remains an indispensable step in the elaboration of such MNPs. A precise control over the surface functionalization of MNPs is crucial, because it governs their physicochemical properties, their colloidal stability, and their biological behaviour. In addition, the amount of covalently immobilized biomolecules is determined by the number of functional groups available on MNP's surface. Often, functionalization of MNP's provides a poor number of available functional groups that consequently leads to a poor amount of immobilized biomolecules. In this work, to overcome this problem and with the aim to increase the number of functional groups on MNPs' surfaces, it was proposed to functionalize MNPs with dendritic coupling agents, and to compare their efficiency with those functionalized with a linear analogue (Figure 3).

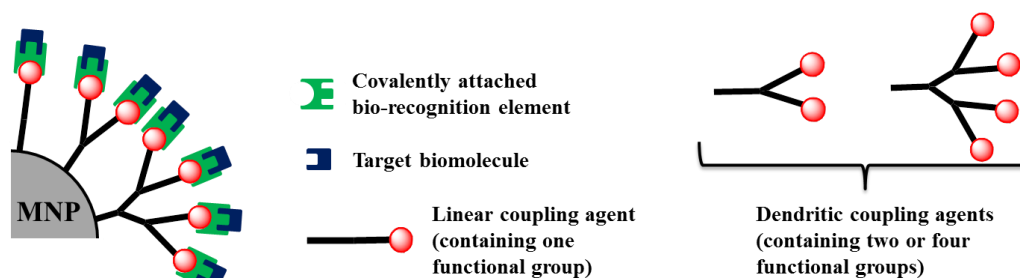


**Figure 3.** Surface functionalization with: linear coupling agent (containing one functional group); two-branched coupling agent (containing two functional groups) and four-branched dendritic coupling agent (containing four functional groups).

Moreover, it was decided to investigate the “*dendritic effect*” of the surface functionalization on two types of core-shell SP NPs: (I) with polymer and (II) with silica shell (both developed and commercialized by Ademtech SA).<sup>6</sup>

Because the surface modification chemistry was carried out on two types of core-shell MNPs, two “*families*” of coupling agents were synthesized. Each “*family*” of coupling agents possessed an *anchoring site*, capable to form covalent binding with the functional groups on the MNPs’ surface. Thus, the surface functionalization of MNPs with polymer shell was achieved by the grafting of amine containing coupling agents on carboxylic acid functional surface of MNPs (via carbodiimide chemistry). In the case of MNPs with silica shell the surface functionalization was achieved by condensation reaction of silanol groups from silica with alkoxy groups of the silyl-terminated coupling agents. In order to induce a good dispersion of the functionalized MNPs in aqueous medium, dendritic structure’s backbones were made of hydrophilic components such as poly(ethylene glycol) (PEG) chains or/and poly(amidoamine) (PAMAM) chains. In addition, the PEG chain is considered to be one of the most efficient chemical groups to limit the non-specific protein adsorption.<sup>7</sup>

This manuscript is organized into four chapters:

In the first chapter the reader can find a bibliographical survey including a brief introduction to MNPs, their synthesis, protection/stabilization and functionalization techniques. Also, chemically, physically and biologically mediated methods of biomolecules immobilization are described.

In the second chapter the synthesis of linear and dendritic coupling agents along with the reasoning of their selection is detailed. Each coupling agent comprises an *anchoring site* (amino or silane) which is capable to bind with MNP’s shell (polymer or silica) on the one side, and *functional groups* (maleimide), capable to react with biological species, on the other side. In order to investigate the “*dendritic effect*” on the surface functionalization, three types of coupling agents were designed: linear coupling agents (containing one functional group); two-branched coupling agents (containing two functional groups) and four-branched dendritic coupling agents (containing four functional groups). This chapter describes different synthetic routes of coupling agents’ synthesis as well as the difficulties met during their design.

The third chapter is dedicated to the functionalization and characterization of the core-shell MNPs with polymer shell ( $\gamma$ -Fe<sub>2</sub>O<sub>3</sub>/Polymer). Firstly, a presentation of these MNPs is performed. Next, a detailed description of the surface modification principles is illustrated, followed by the grafting procedures, as well as the adjustment of the grafting conditions for each coupling agent. These procedures take into account the parameters which can essentially influence the grafting quality, such as the choice of the dispersion medium, temperature, pH and the quantity of coupling agents. The

capacity of maleimide functionalized  $\gamma$ -Fe<sub>2</sub>O<sub>3</sub>/Polymer MNPs to immobilize biomolecules was investigated by performing a series of immobilization tests. The immobilization method is based on the formation of covalent bonds between nucleophilic residues present in biomolecules or models of biomolecules and maleimide functional groups present on the MNPs surfaces.

The fourth chapter is dedicated to the functionalization and characterization of the core-shell MNPs with silica shell ( $\gamma$ -Fe<sub>2</sub>O<sub>3</sub>/SiO<sub>2</sub>). The characteristics of core-shell  $\gamma$ -Fe<sub>2</sub>O<sub>3</sub>/SiO<sub>2</sub> MNPs are very similar to those of core-shell  $\gamma$ -Fe<sub>2</sub>O<sub>3</sub>/Polymer MNPs, while differences in the shell are discussed in the beginning of the chapter. Chemical anchoring of coupling agents onto the  $\gamma$ -Fe<sub>2</sub>O<sub>3</sub>/SiO<sub>2</sub> MNPs was achieved by hydrolysis-condensation reaction of silanol groups from silica shell with alkoxy groups of the silyl-terminated coupling agents. The capacity of maleimide functionalized  $\gamma$ -Fe<sub>2</sub>O<sub>3</sub>/SiO<sub>2</sub> MNPs to immobilize biomolecules was investigated in the same manner as those of maleimide functionalized  $\gamma$ -Fe<sub>2</sub>O<sub>3</sub>/Polymer MNPs.

**References:**

- <sup>1</sup> S. Chikazumi, S. Taketomi, M. Ukita, M. Mizukami, H. Miyajima, M. Setogawa and Y. Kurihara, *J. Magn. Magn. Mater.* **1987**, 65, 245–251.
- <sup>2</sup> (a) N. Crawley and M. Thompson, *Anal. Chem.* **2014**, 86, 130–160; (b) E. C. Wang and A. Z. Wang, *Integr. Biol.* **2014**, 6, 9–26; (c) R. M. Patil, P. B. Shete, N. D. Thorat, S. V. Otari, K. C. Barick, A. Prasad, R. S. Ningthoujam, B. M. David, *Trends in Biotechnology* **2011**, 29, 323–333 (d) K. Turcheniuk, A. V. Tarasevych, V. P. Kukhar, R. Boukherrouba and S. Szunerits, *Nanoscale*, **2013**, 5, 10729–10752; (e) L. Jézéquel, J. Loeper, and D. Pompon, *BioTechniques* **2008**, 45, 523–532; (f) W. U. Dittmer, P. de Kievit, M. W. J. Prins, J. L. M. Vissers, M. E. C. Mersch, M. F. W. C. Martens, *J. Immunol. Methods* **2008**, 338, 40–46; (g) S. Workman, S. K. Wells, C.-P. Pau, S. M. Owen, X. F. Dong, R. La Borde and T. C. Granade, *J. Virol. Methods* **2009**, 160, 14–21; (h) R. M. Patil, P. B. Shete, N. D. Thorat, S. V. Otari, K. C. Barick, A. Prasad, R. S. Ningthoujam, B. M. Tiwale and S. H. Pawar, *J. Magn. Magn. Mat.* **2014**, 355, 22–30; (i) F. Bayard, A. Raveneau, A. Letourneau, G. Joucla, C. Barbot, B. Garbay, C. Cabanne, *Anal. Biochem.* **2009**, 384, 350–352; (j) Y. Pan, X. Du, F. Zhao and B. Xu, *Chem. Soc. Rev.*, **2012**, 41, 2912–2942. (k) N. Chekina, D. Horak, P. Jendelova, M. Trchova, M. J. Benes, M. Hruby, V. Herynek, K. Turnovcova and E. Sykova, *J. Mater. Chem.* **2011**, 21, 7630–7639. (l) F. Chen, R. Shi, Y. Xue, L. Chen and Q.-H. Wan, *J. Magn. Magn. Mat.* **2010**, 322, 2439–2445; (m) A. K. Gupta and M. Gupta, *Biomaterials* **2005**, 26, 3995–4021.
- <sup>3</sup> (a) S. Krishnan and C. Walgama, *Anal. Chem.* **2013**, 85, 11420–11426; (b) S. H. Gage, B. D. Stein, L. Zh. Nikoshvili, V. G. Matveeva, M. G. Sulman, E. M. Sulman, D. Gene Morgan, E. Yu. Yuzik-Klimova, W. E. Mahmoud and L. M. Bronstein, *Langmuir* **2013**, 29, 466–473; (c) D. Rosario-Amorin, M. Gaboyard, R. Clerac, L. Vellutini, S. Nlate, and K. Heuze, *Chem. Eur. J.* **2012**, 18, 3305–3315; (d) D. Rosario-Amorin, M. Gaboyard, R. Clerac, S. Nlate and K. Heuze, *Dalton Trans.*, **2011**, 40, 44–46; (e) D. Rosario-Amorin, X. Wang, M. Gaboyard, R. Clerac, S. Nlate and K. Heuze, *Chem. Eur. J.* **2009**, 15, 12636 – 12643; (f) S. Ding, Y. Xing, M. Radosz and Y. Shen, *Macromolecules* **2006**, 39, 6399–6405.
- <sup>4</sup> A. Farrukh, A. Akram, A. Ghaffar, S. Hanif, A. Hamid, H. Duran and B. Yameen, *ACS Appl. Mater. Interfaces* **2013**, 5, 3784–3793.
- <sup>5</sup> (a) M. Colombo, S. Carregal-Romero, M. F. Casula, L. Gutierrez, M.P. Morales, I. B. Bohm, J. T. Heverhagen, D. Prospero and W. J. Parak, *Chem. Soc. Rev.*, **2012**, 41, 4306–4334; (b) A.-H. Lu, E. L. Salabas and F. Schuth, *Angew. Chem. Int. Ed.* **2007**, 46, 1222–1244.

<sup>6</sup> <http://www.ademtech.com>

<sup>7</sup> (a) K. Nakanishi, T. Sakiyama, Y. Kumada, K. Imamura and H. Imanaka, *Curr. Proteomics* **2008**, 5, 161–175; (b) E. Ostuni, R. G. Chapman, R. E. Holmlin, S. Takayama and G. M. Whitesides, *Langmuir* **2001**, 17, 5605–5620; (c) S. R. Benhabbour, H. Sheardown and A. Adronov, *Macromolecules* **2008**, 41, 4817–4823; (d) S. R. Benhabbour, L. Liu, H. Sheardown and A. Adronov, *Macromolecules* **2008**, 41, 2567–2576.

Chapter I  
**Bibliographical survey**

**Table of contents:**

I.1. Introduction to the MNPs .....	11
I.2. Synthesis of IONPs .....	13
I.3. Stabilization, protection and functionalization of IONPs.....	14
I.3.1. Principles of colloidal stabilization.....	15
I.3.2. Surface modification with non-polymeric organic molecules.....	16
I.3.3. Polymers as stabilizers, coating and encapsulation material.....	19
I.3.4. Surface modification with dendritic structures.....	22
I.3.5. Surface modification with inorganic materials.....	25
I.4. Immobilization of biomolecules on MNPs' surface .....	26
I.4.1. Non-covalent immobilization .....	26
I.4.1.1. Physical adsorption.....	27
I.4.1.2. Biologically mediated immobilization .....	27
I.4.2. Covalent immobilization .....	29
I.4.2.1. Classical chemoligation .....	30
I.4.2.2. Site-specific chemoligation methods.....	35
I.5. Concluding remarks and motivation behind this research work.....	36

## I.1. Introduction to the MNPs

Over the past decade, MNPs have demonstrated a great interest for researchers from a wide range of disciplines, including the fields of magnetic fluids,<sup>1</sup> biotechnology/biomedicine,<sup>2,3</sup> catalysis<sup>4</sup> and environmental remediation.<sup>5</sup> The development of these nanoparticle (NP) materials requires first of all a rigorous control of the NPs' size and shape, since the magnetic properties of these materials are strongly dependent on the NPs' dimensions. In this context, one of the size dependent properties is the SP. In large magnetic particles, it is well known that there is a multidomain structure, where regions of uniform magnetization are separated by domain walls.<sup>6</sup> When the size of NP is small enough (about the typical size of the magnetic domains), the energy necessary to divide itself into magnetic domains is higher than the energy needed to remain as a single magnetic domain (monodomain).<sup>6,7</sup> In this case each NP becomes a single magnetic domain. A single-domain particle is uniformly magnetized with all the spins aligned in the same direction (Figure I-1 a), and shows SP behaviour when the temperature is above the so-called blocking temperature.

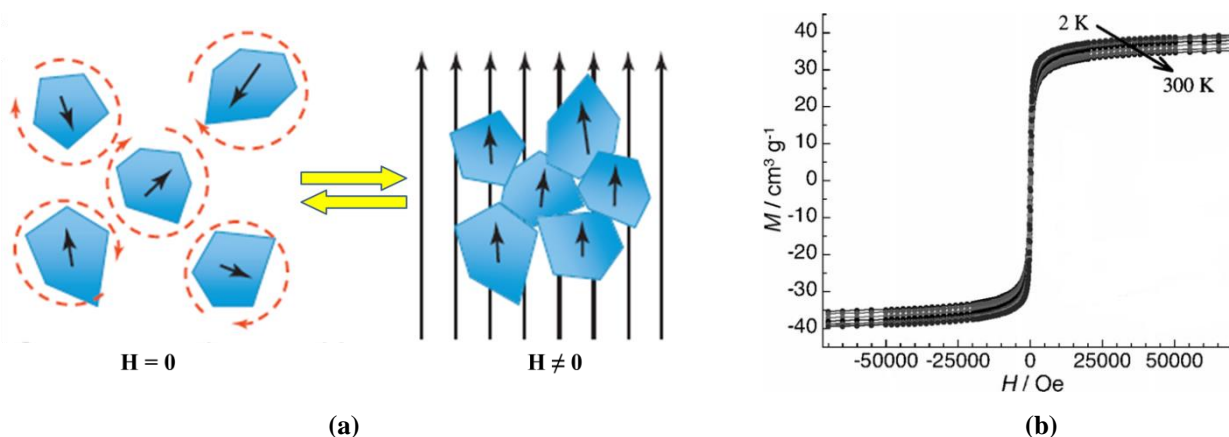


**Figure I-1.** (a) Illustration of SP NPs' response to an applied magnetic field ( $H$ ). MNPs comprise rotating crystals that align with the direction of an applied magnetic field. Crystal reorientation provides the high magnetic susceptibility and saturation magnetization. The circular dashed lines around the SP NPs on the left illustrate the randomization of their orientation, due to temperature effects, in the absence of a magnetic field;<sup>2c</sup> and (b) Typical magnetization curves of SP NPs, where  $M$  is the magnetization of the sample and  $H$  is the applied magnetic field.<sup>8</sup>

Such individual NPs have a large constant magnetic moment and behave like a giant paramagnetic atom. As a result SP NPs show a fast response to applied magnetic fields and revert to their non-magnetized state upon field removal with a null or negligible remnant magnetization (residual magnetism) and coercivity (the field required to bring the magnetization to zero).<sup>6,7</sup> The practical test for SP is the observation of anhysteretic magnetization ( $M$ ) curves as a function of the applied magnetic field ( $H$ ) over a wide range of temperatures (Figure I-1 b). This interesting property, marked by the lack of remnant magnetisation, enables the MNPs to maintain their colloidal stability



and thus avoid their aggregation, which is one of the most important conditions required in all the fields of applications.

Among the wide variety of NPs that exhibit SP behaviour, iron oxide nanoparticles (IONPs), either magnetite ( $\text{Fe}_3\text{O}_4$ ) or maghemite ( $\gamma\text{-Fe}_2\text{O}_3$ ), are the most commonly used types of NPs. This enhanced interest to IONPs in the majority of the cases is justified by their simple and low cost preparation, and not the least, due to their biocompatibility and biodegradability. In addition, iron based magnetic oxides represent the best compromise among good magnetic properties (such as saturation magnetisation) on one hand, and stability under oxidizing conditions on the other. Depending on their size, IONPs behave differently in magnetic field. The size limit for iron oxide crystals required to achieve SP is typically inferior to 20 nm. Considering this threshold, MNPs with a core larger than 20–30 nm consist of clusters of multiple smaller iron-oxide domains rather than a single large crystal.<sup>2c</sup> However, despite the increase in SP behaviour of the particles with decrease in size, a decline in the absolute saturation magnetization values occurs when the size of the particles is reduced to less than 10 nm.<sup>9</sup> Thus, the ideal diameter of IONPs exhibiting SP behaviour with the optimal saturation magnetization values, at room temperature, is between 10 and 20 nm. Such particles are small enough, so that the cooperative phenomenon of ferromagnetism is no longer observed and no permanent magnetization remains after the particles have been subject to an external magnetic field. Thereby, the SP behaviour of IONPs enables their stability and dispersion in the absence or upon removal of the magnetic field, as no residual magnetic force exists between the particles.

However, the dimension of MNPs is not the only parameter that determines the final properties of the NP material. Thus, MNPs with a proper surface coating can be dispersed into suitable solvents, forming homogeneous suspensions, called ferrofluids. The types of specific coating and their functionalization depend on the final application, and should be chosen by keeping a particular application in mind. Such MNPs can bind drugs, proteins, enzymes, antibodies, or nucleotides and can be easily manipulated using an external magnetic field. The combination of SP behaviour with the peculiar surface chemistry opens a large field of potential applications.

With the aim to improve or/and develop new applications, a careful study of the synthesis, fluid stabilization technics and surface modification chemistry of the SP IONPs is necessary, and therefore it is discussed in the following sections.

## I.2. Synthesis of IONPs

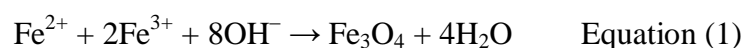
The synthesis of NPs is a complex process and hence, there is a wide range of techniques developed for the preparation of highly stable and monodisperse MNPs. The main synthesis pathways proposed for the preparation of IONPs can be divided into the three categories:<sup>3,10</sup>

(I) *Physical methods*, such as gas-phase deposition and electron beam lithography. These methods, however, suffer from their inability to control the particles' size at the nanometer scale.

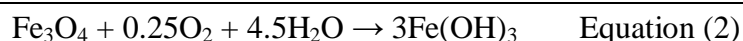
(II) *Wet chemical preparation methods*, such as sol-gel synthesis, oxidation method, chemical co-precipitation, hydrothermal reactions, flow injection synthesis, electrochemical method, aerosol/vapour phase method, sonochemical decomposition reactions, supercritical fluid method, and synthesis using nanoreactors. These routes are more tractable and more efficient with appreciable control of size, composition and sometimes even the shape of the NPs.

(III) *Microbial methods*, which are generally simple, versatile, and efficient with appreciable control over the composition and the particle geometry of the resulting material. This approach ensures high yield, good reproducibility, and good scalability, as well as low cost, but requires low temperature and low energy, contrary to the methods I and II.

The listed above synthesis pathways are detailed in several reviews.<sup>6,10,11,12</sup> Even though a large choice of synthesis techniques is available, the most common method for the production of IONPs, magnetite or maghemite remains the chemical co-precipitation technique. A widespread approach relies on the Massart's method,<sup>13</sup> where magnetite is obtained by alkaline co-precipitation of stoichiometric amounts of ferrous ( $\text{Fe}^{2+}$ ) and ferric ( $\text{Fe}^{3+}$ ) salts. Usually, for preparation of IONPs, a mixture of aqueous chloride solution of  $\text{Fe}^{2+}$  and  $\text{Fe}^{3+}$  (but other salts as sulphates, nitrates or perchlorates, can also be used as well) at a molar ratio of 1:2 is used. This reaction should proceed under inert atmosphere and can be performed at room temperature or at elevated temperature. The chemical reaction associated with the precipitation of magnetite can be written as (Equation 1):



The size, shape, and composition of the obtained magnetite MNPs depends very much on the type of salts utilized in the reaction (e.g. chlorides, sulphates, nitrates), the control and maintaining of a molar ratio of  $\text{Fe}^{3+}:\text{Fe}^{2+}$  as 2:1, the reaction temperature, the pH value and ionic strength of the media. A special attention must be paid on the maintaining of a non-oxidizing oxygen free environment, since otherwise magnetite might be oxidized according to the equation 2:<sup>3</sup>



By the chemical co-precipitation technique (Equation 1), once the synthetic conditions are fixed, the quality of the magnetite NPs is fully reproducible.<sup>6</sup> At the same time, the obtained magnetite NPs (according to the Equation 1) are not very stable under ambient conditions, and can be dissolved in an acidic medium or oxidized to maghemite according to the equation 3:<sup>12</sup>



Since maghemite is a ferrimagnet, this oxidation (Equation 3) does not present a problem, and even more, is intentionally performed. This conversion is achieved by dispersing magnetite NPs in acidic medium followed by the addition of iron (III) nitrate. The obtained maghemite particles are usually more stable in aqueous media (in alkaline and acidic medium), ensuring therefore a more durable magnetic behaviour. However, even if the magnetite particles are converted into maghemite, the experimental challenge in the synthesis of magnetite by co-precipitation method (Equation 1) lies in the control of the particle size and thus achieving a narrow particle size distribution.<sup>6</sup> The main advantage of the co-precipitation process is that a large amount of NPs can be synthesized and depending on the reaction conditions the size of obtained MNPs can range from 3 to 20 nm.<sup>2d</sup>

Independent on the synthesis method the colloidal and chemical stability of the obtained MNPs should be ensured.

### **I.3. Stabilization, protection and functionalization of IONPs**

Although, many significant developments in the synthesis of IONPs have been done, the improvement of their colloidal and chemical stability (in different media) remains an important issue, since it is a crucial requirement for any application of MNPs as well as for their storage.

In the absence of an applied magnetic field, the stability of the magnetic colloidal suspension results from the equilibrium between the attractive forces (dipole-dipole van der Waals interactions) and repulsive forces (*steric* and *electrostatic* interactions).<sup>10</sup> For magnetic suspensions, magnetic dipolar forces between two particles must be added. In the absence of surface stabilizers, magnetic IONPs have hydrophobic surfaces with a large surface area to volume ratio. Due to hydrophobic interactions between the particles they can agglomerate to form large clusters. These clusters exhibit strong magnetic dipole–dipole attractions between them, and show ferromagnetic behaviour.<sup>14</sup> When two clusters approach one another, each of them comes into the magnetic field of the neighbour and as a result each particle gets further magnetized. The adherence of remnant magnetic particles causes a

mutual magnetization, resulting in their aggregation.<sup>3</sup> Since particles are attracted magnetically, in addition to the usual flocculation due to van der Waals force, the colloidal stabilization is a necessary step. Controlling the strength of the repulsive forces (*steric* and *electrostatic*) is a key parameter to elaborate particles with good colloidal stability. In addition, the magnetic properties are very sensitive to any chemical changes that can occur on MNPs' surface and can be readily affected. Thus, ensuring the colloidal stability of MNPs as well as their chemical stabilization is indispensable. The stabilization, protection and functionalization of the MNPs are closely linked to each other, since via an appropriate surface modification all these issues (colloidal stabilization, chemical protection and availability of surface functional groups) can be achieved.

### I.3.1. Principles of colloidal stabilization

Similar to most colloidal NP suspensions, a key aspect in the preparation of IONPs is the introduction of surface stabilizers that prevent the colloidal suspension from aggregating and precipitating. These stabilizers can be introduced directly during the synthesis or immediately after formation of the initial IONP suspension. Thus, stabilizing colloidal dispersions against aggregation (irreversible coagulation or reversible flocculation) is important both during and after the synthesis of NPs. The colloidal stability of MNPs can be achieved by playing on *electrostatic* or *steric repulsion* forces depending on the stabilizers (i.e. fatty acids or amines) and the polarity of the solvent used (Figure I-2).<sup>12</sup>

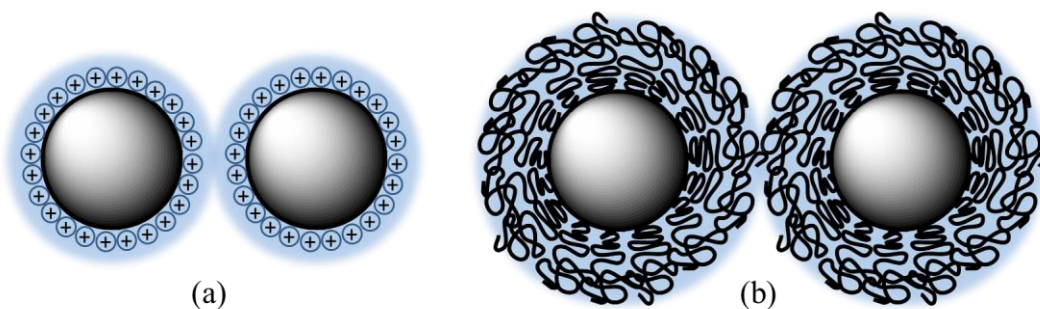


**Figure I-2.** Particles stabilized (a) by the electrostatic repulsion, and (b) by steric repulsion.

For charged colloidal particles in an electrolyte medium, the balance between the *repulsive electrostatic* and *attractive van der Waals* contributions to the total potential energy can be adjusted, so that a barrier to aggregation is created.<sup>14</sup> The repulsive force results from creation of an electric double layer around the particles, which is dependent on dispersion of the particles into a polar media, pH, concentration, and ionic strength of the suspension.<sup>15</sup> The *electrostatic repulsion* can be followed through the knowledge of the diffusion potential that may be very close to the zeta potential<sup>16</sup> and the Debye-Huckel length that mainly depends upon the ionic strength and pH of the solution. For instance,

MNPs synthesized through co-precipitation method are usually stabilized by repulsive electrostatic forces.

The *steric* force is difficult to predict and quantify but even though it is quite well-described theoretically for polymers. Among other parameters, the *steric* force is dependent upon the molecular weight of the polymer and its density.<sup>17</sup> When polymeric materials<sup>18</sup> or long-chain molecules (i.e. a long-chain fatty acid) are employed as stabilizers, their adsorption onto the MNPs confers protective *steric repulsion* and acts as a barrier against the interaction between the particles.<sup>19</sup> In other words, when the particles approach one another a repulsive force is created, as the chains interpenetrate. Such stabilization is even more efficient when using amphiphilic copolymers. The stabilizing amphiphilic copolymers typically consist of two different blocks: an anchoring block (hydrophobic segment) that enables the adhesion to the surface of IONPs and another, water-soluble block (hydrophilic segment) that renders MNPs water-dispersible. Moreover, if the polymer chains are charged, an additional *electrostatic repulsion* may occur, thus conferring a combined *electrostatic* and *steric* (*electrosteric*<sup>17</sup>) stabilization effect.

### I.3.2. Surface modification with non-polymeric organic molecules

Like most of oxide surfaces, IONPs' surface provides the hydroxyl groups (Fe–OH) allowing the attachment of several functionalities (Figure I-3). Thus, the surface modification of IONPs can be achieved using non-polymeric stabilizers, based on organic monomers, bearing functional groups like carboxylate, phosphate or sulphate (e.g. alkanesulphonic and alkanephosphonic acids,<sup>20</sup> oleic acid (OA),<sup>21,22</sup> lauric acid,<sup>22</sup> lactobionic acid,<sup>23</sup> dodecylphosphonic and hexadecylphosphonic acids,<sup>22</sup> phosphonates<sup>22</sup>). Depending on the nature of the stabilizer the colloidal dispersibility can be achieved into organic and/or aqueous media, while the functionalization of freshly prepared IONPs is mainly achieved by the reaction with organic molecules bearing diol or silane functionality (catechols<sup>24</sup> and 3-aminopropyltrimethoxysilane<sup>25</sup>).

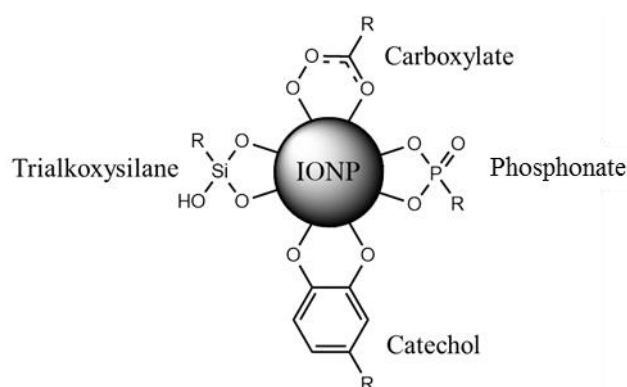


**Figure I-3.** Schematic illustration of IONPs surface modification via carboxylate, phosphonate, catechol or silane functionalities.

*Carboxylates* are often an important component in the synthesis of IONPs (when utilizing the thermal decomposition route) in organic solvents because alkyl carboxylates readily adsorb on the surface of the growing NP. For instance, by using fatty acids like OA, hydrophobic IONPs can be obtained.<sup>26</sup> However, should be noted that OA can form single or double layer on the surface of magnetite IONPs (Figure I-4).<sup>27</sup>

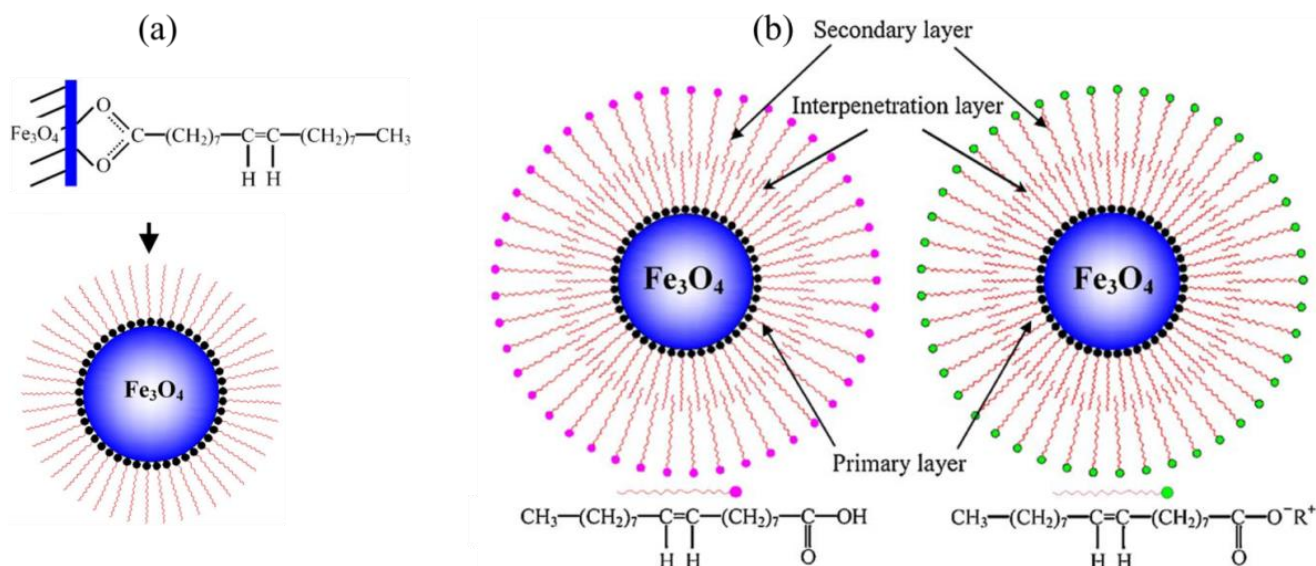


**Figure I-4.** (a) Schematic representation of single layer oleic acid-coated magnetite nanoparticles; and (b) Schematic representation of bilayer oleic acid-coated magnetite nanoparticles with either oleic acid as the secondary layer or oleate.<sup>27</sup>

For single layer oleic acid-coated magnetite NPs, oleic acid molecules are chemically adsorbed on the surface through the chemical interaction between their carboxyl groups and iron atoms. As a result, the hydrophobic tails of oleic acid molecules face outwards (Figure I-4 a) and form a nonpolar shell that makes the single layer oleic acid-coated magnetite NPs dispersed only in nonpolar carrier liquids. For bilayer oleic acid-coated magnetite NPs, the primary layer is chemically adsorbed on the surface through the chemical interaction between carboxyl groups of oleic acid and iron atoms, while the secondary layer is physically adsorbed on the primary layer by forming the interpenetration layer with the tails of the primary layer (Figure I-4 b). If the secondary layer is oleic acid, bilayer oleic acid-coated magnetite NPs can be only dispersed in nonpolar carrier liquids, while when the secondary layer evolves into the oleate from, they can be dispersed in polar carrier liquids through adjusting the pH.<sup>27</sup>

Another example is citric acid, which adsorbs on the surface of IONPs by coordinating via one or two of the carboxylate functionalities, depending upon steric necessity and the curvature of the NP surface.<sup>28</sup> This leaves at least one carboxylic acid group exposed to the solvent, which makes the surface negatively charged and hydrophilic. Thus, carboxyl group acts as an electrostatic stabilizer (Figure I-2 a) and as a result magnetite NPs can be dispersed in aqueous media. At the same time, the

remaining free carboxyl group can be used for further conjugation of the molecule of interest (i.e. biomolecule) containing amino groups via standard EDC-mediated amide bond formation.

*Phosphates* ( $\text{PO}_4^{3-}$ ) and *phosphonates* ( $\text{PO}_2^{2-}$ ) bind to IONP's surface in the same way as carboxylates.<sup>22,29,30</sup> Moreover, some experiments showed that phosphates form stronger bonds than carboxylates.<sup>22,30</sup> Thus, in the case of carboxy-alkylphosphonic acids the phosphonate moiety is bound to the IONP surface via a tridentate interaction, while the carboxylic acid remains available for conjugation.<sup>31,32</sup> It is also believed that stabilization of IONPs with alkyl phosphates or phosphonates results in the formation of bilayer-type coatings (similarly to alkyl carboxylates) that originates from hydrophobic interactions between aliphatic chains, and thus limiting their dispersibility in organic solvents.<sup>22,33</sup>

*Alcohols* and *diols* can also bind to the IONPs' surface via coordination. Simple alcohols bind weakly to IONPs' surface<sup>34</sup> while diols have showed the ability to bind stronger. Thus, variety of catechol derivatives (diols) can form very strong bidentate complexes with metal oxides<sup>35</sup> and can generate remarkably stable colloidal suspensions.<sup>36</sup> However, the catechol derivatives' affinity for the IONPs' surface is strongly dependent on the substituents nature, since the electron density of the hydroxyl groups is strictly related to the electron delocalization into the benzene ring.<sup>37</sup> Among catechol derivatives, dopamine (4-(2-aminoethyl)benzene-1,2-diol) is perhaps the most extensively utilized linker for direct conjugation of biological species to IONPs' surface.<sup>38</sup> In this case the bidentate catechol portion of the molecule binds the IONPs' surface through coordination, while the primary amine remains exposed to the surrounding environment, ensuring water dispersibility and at the same time offering a handle for direct immobilization of biomolecules or interconversion of functional groups.

One of the most successful approaches for the functionalization of oxide-based materials is the chemical grafting of organic chains via *functional organosilanes*: especially trichlorosilanes ( $\text{R-SiCl}_3$ ) or trimethoxysilanes ( $\text{R-Si(OCH}_3)_3$ ), where R represents a functional end group. This reaction, termed silanization, was derived more than 70 years ago for chromatographic applications and is now routinely used for the formation of various monolayers on different surfaces through silicon–oxygen bonds.<sup>39</sup> The use of functional organosilanes (e.g. 3-aminopropyltrimethoxysilane (APTES), mercaptopropyltrimethoxysilane, cyanoethyltriethoxysilane, etc.) allows the direct introduction of amine, thiol, cyano or other functionalities required for post-conjugation with various ligands. The versatility of silane organic functional groups makes these compounds ubiquitous for surface modification of IONPs. For example D. Li and co-workers<sup>40</sup> have functionalized IONPs with amine, aldehyde, carboxylic, epoxy, thiol, and maleimide groups through organosilane linkers and used the resulted functionalized IONPs for a conjugation with trypsin.

Thus, by an appropriate surface modification of IONPs with non-polymeric organic molecules, colloidal stabilization, chemical protection, as well as functionalization can be achieved.

### I.3.3. Polymers as stabilizers, coating and encapsulation material

In general, polymers can be chemically anchored or physically adsorbed on MNPs creating repulsive forces (mainly steric repulsion) to balance the magnetic and the van der Waals attractive forces acting on the NPs.<sup>6</sup> Thus, MNPs are stabilized in suspension by steric repulsion.

Among the most utilized polymeric stabilizers can be listed: polyethylene glycol (PEG) also known as poly(ethylene oxide) (PEO),<sup>41</sup> poly(vinyl alcohol) (PVA),<sup>42</sup> poly(ethylene imine) (PEI),<sup>43</sup> dextran,<sup>44</sup> chitosan,<sup>45</sup> etc (Figure I-5).

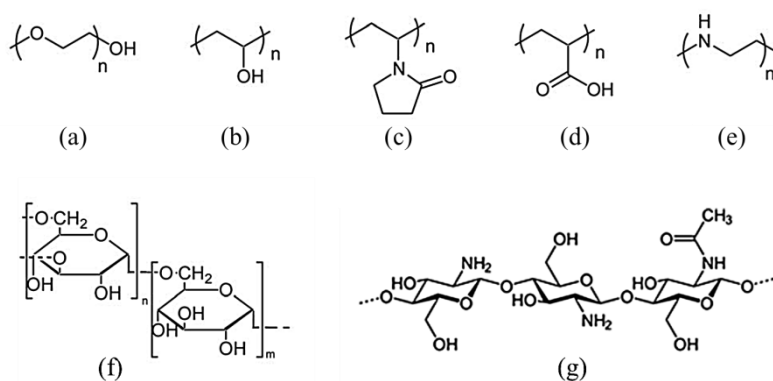


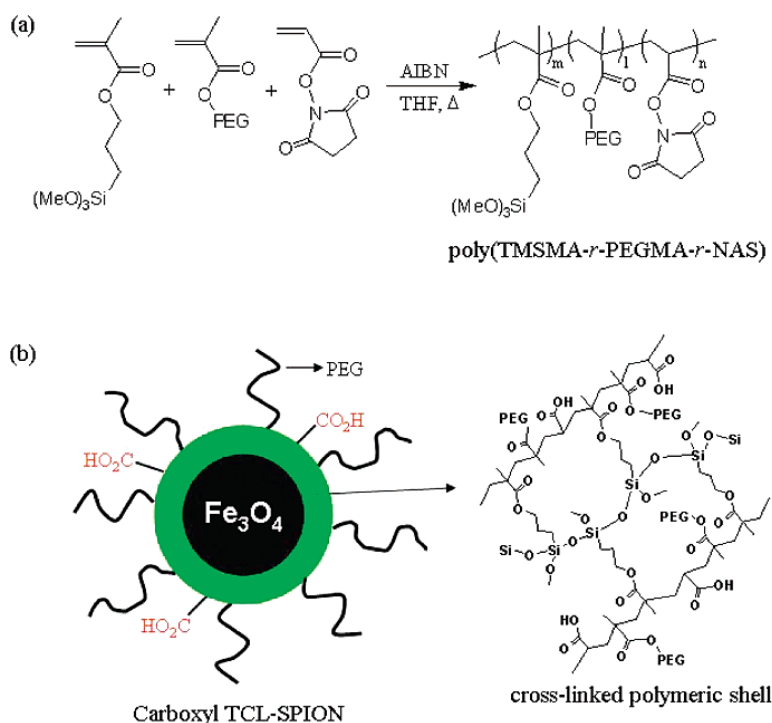
**Figure I-5.** Structures of polymers used for stabilization of NPs: (a) PEG; (b) PVA; (c) PVP; (d) PAA; (e) PEI; (f) dextran; (g) chitosan.

PEG is certainly the most extensively investigated polymer. This water soluble polymer is commonly used to enhance the aqueous solubility of hydrophobic molecules such as drugs, and in addition minimizes the non-specific adsorption.<sup>46</sup> The protein repulsion tendency of PEG does not depend on the nature of interaction between the NPs and PEG as both electrostatically and covalently attached PEG can show good protein rejection tendency. However, a covalent attachment ensures that the PEG functionality is not lost upon long term storage or in highly ionic medium.<sup>47</sup> Another widely used polymer is dextran. Dextran adsorbs onto the IONPs via hydrogen bonding between dextran hydroxyl groups and IONPs' surface. The reversible nature of the dextran adsorption onto the IONP surface is reflected by its easy removal after washing with water.<sup>44</sup> Thereby, the main limitation of using weakly attached polymers to IONPs' surface is the lack of stability, since the polymer layers can be displaced overtime, through dilution or in the presence of better surface binders.

Various strategies have been proposed for chemical (covalent) linkage of polymers (especially PEG) to MNPs, i.e. silane grafting onto the oxide surfaces.<sup>48</sup> Indeed, the development of bifunctional PEG-silanes capable to form self-assembled monolayers, allowed increasing the polymer packing onto



the NPs' surface and a better control of the polymer conformation.<sup>49</sup> Some attempts to address this issue involved cross-linking, to form cross-linked iron oxide (CLIO) particles. For example, H. Lee and co-workers<sup>50</sup> report the fabrication of thermally cross-linked SP IONPs (TCL-SPION) and their application to the dual imaging of cancer *in vivo*. Unlike dextran coated cross-linked IONPs,<sup>51</sup> TCL-SPION were prepared by thermal cross-linking method using a silanol-containing copolymer (Scheme I-1). The copolymer, poly(3-(trimethoxysilyl)propyl methacrylate-*r*-PEG methyl ether methacrylate-*r*-N-acryloxysuccinimide) [poly(TMSMA-*r*-PEGMA-*r*-NAS)], was synthesized by radical polymerization and used as a coating material for as-synthesized magnetite SPION. The polymer-coated SPION was further heated (80°C) to induce cross-linking between the silanol groups in the polymer chains, which finally generated TCL-SPION bearing a carboxyl group as a surface functional group.

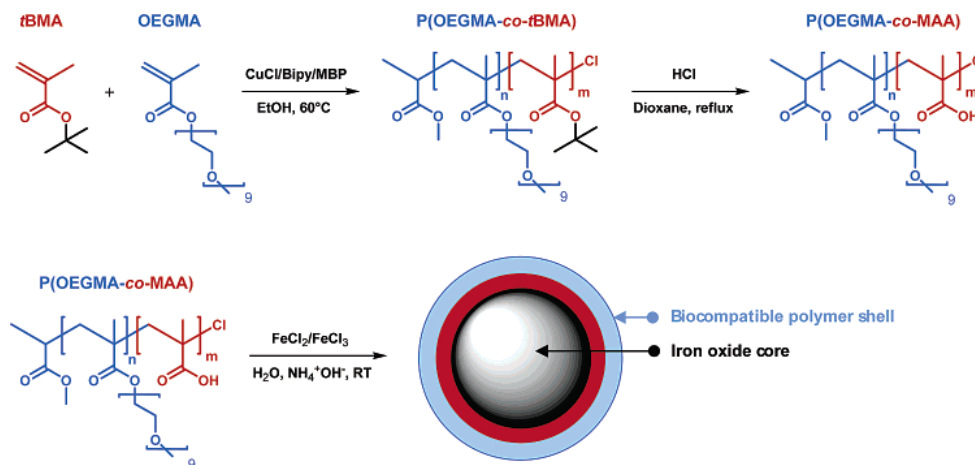


**Scheme I-1.** (a) Synthetic scheme for the production of poly(TMSMA-*r*-PEGMA-*r*-NAS). (b) Schematic illustration of carboxyl TCL-SPION showing crosslinking between polymer layers after heat treatment.<sup>50</sup>

In that example, the carboxyl TCL-SPION were converted to amine-modified TCL-SPION and then conjugated with a near-infrared dye Cy5.5 mono NHS ester. Cy5.5 dye-conjugated TCL-SPION were used for dual (magnetic resonance/optical) *in vivo* cancer imaging that was highly effective for tumour detection. Because various functional molecules, such as targeting ligands and drugs, can be attached to the TCL-SPION, they are promising material to develop multifunctional NPs for cancer imaging and therapy.

The recent development of control radical polymerization (CRP) methods (e.g. atom transfer radical polymerization (ATRP), nitroxide-mediated polymerization (NMP) or reversible addition-

fragmentation transfer polymerization (RAFT)) considerably broadened the field of macromolecular engineering.<sup>52</sup> For instance, J.-F. Lutz and co-workers<sup>53</sup> prepared well-defined poly(oligo(ethylene glycol) methacrylate-co-methacrylic acid) [P(OEGMA-co-MAA)] and used it for coating IONPs' (Scheme I-2).



**Scheme I-2.** Schematic illustration for the preparation of well-controlled POEOMA-*b*-PMAA block copolymer and polymer-coated SIONPs.<sup>53</sup>

In this model the methacrylic acid units of the copolymer interacts with the surfaces of the IONP, whereas the oligo(ethylene glycol) segments enhance the water dispersibility and the biocompatibility of the colloid.

As, shown in Scheme I-1 and Scheme I-2, coating of IONPs with polymer/copolymer shells leads to the formation of core-shell morphology that ensure a high protection of IONP core and stability over time. This type of coating (generating a shell) can be achieved either during the synthesis of IONPs or subsequently. Moreover, depending on the nature of the polymers, the shell can handle various functional groups.

As an alternative method of stabilization, protection and functionalization is encapsulation of IONPs into a polymer shell (Figure I-6). In this case, core-shell MNPs' composite may consist of either a polymer matrix (i.e., nanosphere)<sup>54</sup> or a reservoir system in which an aqueous or an oily core is surrounded by a polymeric shell (i.e., nanocapsule).<sup>55,10</sup>

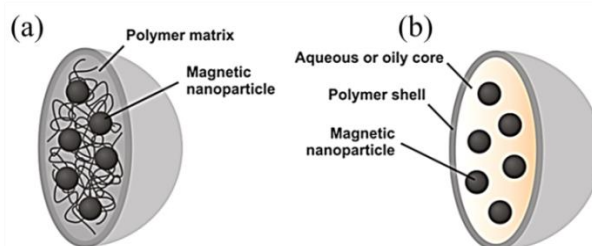


**Figure I-6.** Schematic representation of the stabilization/protection of MNPs by encapsulation into nanospheres (a) or nanocapsules (b).<sup>10</sup>

For example, C. Yang and co-workers<sup>56</sup> developed a novel swelling and thermolysis technique for the preparation of monodisperse magnetic polymer microspheres. The process involved the impregnation of ferric oleate within the swollen polymer microspheres, and subsequently the IONPs were formed within the polymer matrix by thermal decomposition of ferric oleate. More importantly, this novel method can be considered as an inexpensive way of preparing monodisperse magnetic polymer microspheres to be used in biotechnology for cell separation, enzyme immobilization and purification of proteins.

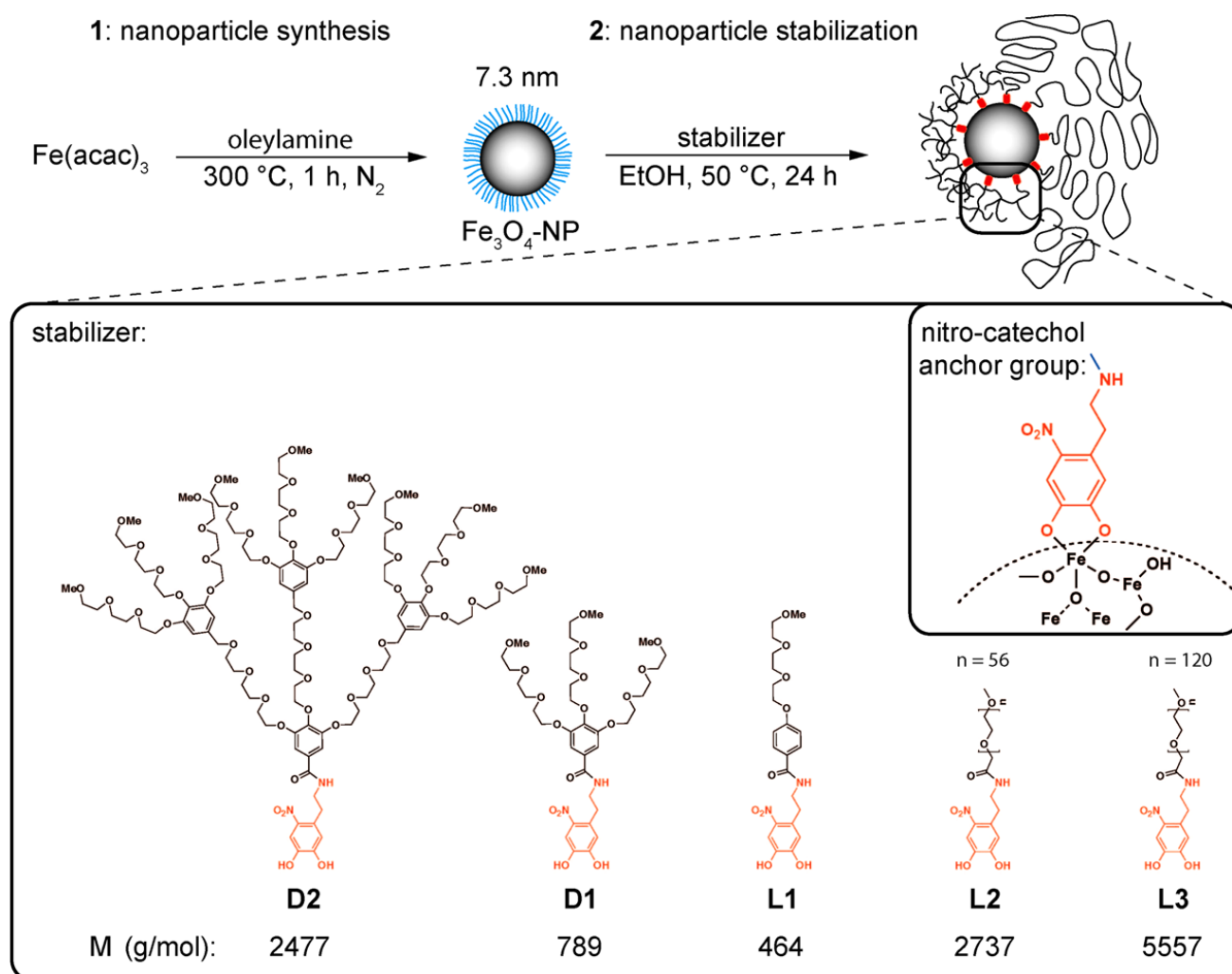
In another example, X. Y. Liu and co-workers<sup>57</sup> reported a flexible and facile synthesis of well-defined hydrophilic and biocompatible poly(styrene-co-acrylic acid) [poly(St-AA)/Fe<sub>3</sub>O<sub>4</sub>] microspheres with functional carboxyl groups on the surface and high saturation magnetization. Monodisperse cross-linked SP poly(St-AA)/Fe<sub>3</sub>O<sub>4</sub> microspheres were prepared via miniemulsion copolymerization. These magnetic microspheres provide a number of advantages, such as highly dispersive, excellent long-term stability and a high sensitivity to external magnetic field. The functional polymer shell abundant with carboxyl groups was easily covalently conjugate with various biological molecules. Therefore, these monodisperse magnetic polymer microspheres, presenting excellent SP and adsorption properties can be used in biotechnology (cell separation, enzyme immobilization and purification of proteins).

Thus, polymers can tailor not only colloidal and chemical stability of the MNPs but also bring a chemical functionality.

#### **I.3.4. Surface modification with dendritic structures**

Usually, NPs are sterically stabilized with hydrophilic polymeric matrices (*as described in the previous section I.3.3*) while the possibility of using dendritic structures (dendrons) is comparatively neglected. Despite their unique properties, very few reports on the use of dendritic molecules for the stabilization and functionalization of NPs are available up to date.

Recently, T. Gillich and co-worker<sup>58</sup> reported a comparative study regarding the stabilization of SP IONPs with dendritic and linear ethylene-glycol-based stabilizers of comparable molecular weight, achieved by varying the generation and chain length, respectively (Scheme I-3).

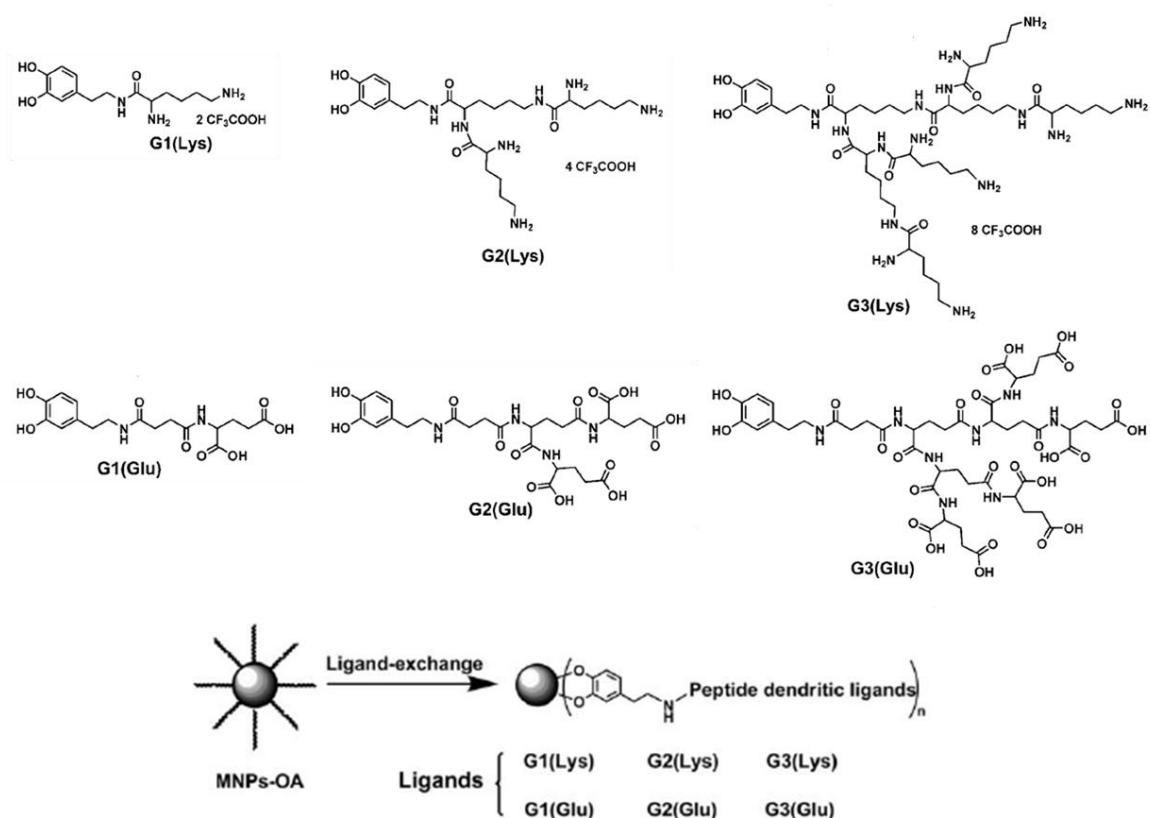


**Scheme I-3.** Illustration of NP core synthesis and stabilization with ethylene-glycol-based dispersants of linear and dendritic structure. A single nitro-catechol chelate group serves as the anchor between the macromolecular stabilizer and the iron oxide NP surface. M = molecular weight of the polymeric dispersants.<sup>58</sup>

The results demonstrated that the properties such as thermally induced aggregation and its reversibility, solubility, and colloidal stability are different when NPs are stabilized by dendrons or linear polymer chains. Dendron-stabilized NPs provided excellent colloidal stability compared to linear PEG analogues. Moreover, for the same grafting density and molecular weight of the stabilizers, oligo(ethylene glycol) (OEG) dendron-stabilized NPs show a reversible temperature-induced aggregation behaviour, in contrast to the essentially irreversible aggregation and sedimentation observed for the linear PEG analogues. These encouraging results make dendrons an attractive, well-controlled surface modifier and an alternative to the conventional linear brush systems, particularly for biooriented applications.

Also, dendritic macromolecules have been successfully investigated as ligands for surface modification of IONPs. Thus, R. Zhu and co-workers<sup>59</sup> synthesised L-Lysine- and L-glutamic acid-based peptide dendritic ligands with dopamine located at the focal points. The dendritic ligands of different generations (G1 to G3) were designed and synthesized before the functionalization and then

immobilized on the surface of oleic acid-coated hydrophobic MNPs via ligand-exchange method (Scheme I-4).



**Scheme I-4.** L-Lysine- and L-glutamic acid-based peptide dendritic ligands of different generations (G1 to G3) and their immobilized on the surface of oleic acid-coated hydrophobic MNPs via ligand-exchange method.

The modified MNPs exhibited an adjustable number of terminal functional groups and superior stability in aqueous solutions in a broad pH range. The presence of the water soluble polypeptide ligands on the MNPs' surface promoted monodispersity of the particles and led to an increased hydrodynamic diameter under 30 nm from G1 to G3. Both series of modified MNPs preserved the SP behaviour and exhibited approximate magnetization in the same generation, while the saturation magnetization of the MNPs decreased with increasing surface dendritic generation. This novel functionalization strategy provides a potential platform for designing and preparing highly stable ultrafine MNPs with high magnetization for biomedical applications.

Other dendrons were also successfully utilized for surface modification of IONPs such as poly(amidoamine) (PAMAM),<sup>60</sup> poly(ester amine) (PEA),<sup>61</sup> Simanek-type (melamine),<sup>62</sup> etc.<sup>63</sup>

Clearly, the synthesis of dendritic molecules is a more difficult and time consuming procedure than the one employed for polymers that can be one of the reasons why they are less employed. However, dendritic structures present several remarkable advantages over the polymers that make them very attractive for the surface engineering. First of all, the structure and size of dendrons can be

accurately controlled during the stepwise synthesis, allowing designing dendrons with a well-defined molecular structure, weight and number of functional groups. Due to their conical-like structure and focal points dendrons present a special interest for the surface modification of ultrasmall NPs with very high curvature, since their radial monomer density distribution is expected to decay less rapidly with distance from the NP surface. In addition, their conical-like structure can improve steric resistance to macromolecular adsorption and particle agglomeration.<sup>58</sup> Moreover, stabilization of NPs with such structures provides a relatively thin organic shell while offering high surface densities of functional groups at the periphery that is of high interest for various biological applications. Also, similar to dendrimers, small molecules such as drugs could be incorporated into the dendritic framework of dendron-stabilized/functionalized NPs, making this system attractive as a potential drug release system.<sup>64,58</sup>

### I.3.5. Surface modification with inorganic materials

IONPs can be coated with inorganic components, most often including silica<sup>65</sup> or precious metals such as Au.<sup>66</sup> Similarly to the coatings with organic molecules, inorganic coatings provide the stability of MNPs in solution and possibility for binding various ligands (including biological ligands). These MNPs have an inner IO core with an outer shell of inorganic materials, as shown in Figure I-7.

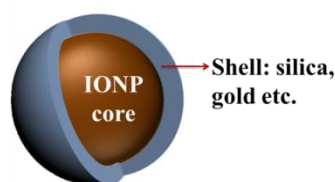


**Figure I-7.** Schematic representation of the core-shell MNPs with inorganic shell.

Coating IONPs' with gold is an efficient strategy to ensure the stability of magnetic material under acidic and neutral pH in aqueous media. Also, it provides the possibility of depositing monolayers of alcohol or carboxylic acid-terminated thiols, which further give the opportunity for surface functionalization with other ligands of interest. However, the main limitation of coating with gold is the difficulty in the formation of the uniform gold shell over the NP surface due to the chemical inertness of gold.<sup>67</sup>

Undoubtedly, silica represents the most exploited inorganic material for coating and encapsulating various types of MNPs, including IONPs. The most widely employed method for the formation of silica shell on IONPs is the Stöber synthesis (Scheme I-5) that consists in the deposition of tetraethoxysilane (tetraethyl orthosilicate or TEOS) on IONPs' surface in the alkaline media.<sup>68</sup> Moreover, the coating thickness can be tuned by varying the concentration of ammonium and the ratio of TEOS to H<sub>2</sub>O.



**Scheme I-5.** (A) Formation of silica coated IONPs (core-shell) through hydrolysis and condensation of TEOS. (B) Hydrolysis and condensation of TEOS.

Based on this method encapsulation of IONPs into silica shell is also possible.<sup>69</sup>

There are several reasons for choosing silica as coating (or matrix material) for MNPs. First of all the silica shell provides silanol surface groups which may easily be converted into a variety of functional groups (through silanization reaction), providing a convenient platform for further functionalization. At the same time, the silica shell prevents MNPs' aggregation in aqueous solutions (since the silica shell is negatively charged) and improves their chemical stability. From a technical point of view, the possibility of controlling the coating thickness and its porosity combined with the chemical inertness of the silica, its low cost of production and optical transparency make silica coated IONPs very promising nanomaterial.

## I.4. Immobilization of biomolecules on MNPs' surface

In general immobilization of biomolecules on IONPs can be attained in two ways: (I) *directly* by conjugation to the native IO surface (*following the same chemistry as described in the sections I.3.2 and I.3.3*) or (II) *indirectly*, where first the surface of the IONPs is coated with an intermediate stabilizing molecular layer/shell that is subsequently exploited for further conjugation. In fact, due to the limited chemical reactivity of the IONPs' surface, it is usually the coating and not the NP surface that is chosen as the site of chemical/biological functionalization. Chemical/biological functionalization itself will either be covalent (including covalent coupling to the IONP surface or surface coating) or non-covalent. In the following sections chemically, physically and biologically mediated methods of biomolecules immobilization are discussed.

### I.4.1. Non-covalent immobilization

The non-covalent methods of biomolecules' immobilization onto the NP surface can be roughly divided into *physical adsorption* of the biomolecule onto the NP surface (or its coating) or *biologically mediated immobilization*. The later, involves first a covalent immobilization of a small molecule (or biomolecule) on the NP surface that can then recognize and bind the biomolecule of interest.

#### **I.4.1.1. Physical adsorption**

Non-covalent methods of biomolecules' immobilization take place through the binding forces, such as electrostatic interactions, hydrogen bonds, van der Waals forces or hydrophobic interactions.<sup>70</sup> The simplest and most widely used biomolecules' immobilization approach is electrostatic attachment, because usually no reagents and only a minimum of activation steps are required. The principle of this immobilization relies on the attraction between oppositely charged species. Thus, a charged MNP will electrostatically attract an oppositely charged species. Another example is the attachment of biomolecule through weak coordination bonding. In this case the stability is determined by the equilibrium dissociation constants and therefore, such immobilization is sensitive to the concentrations of MNPs and biomolecules during the preparation and in subsequent application. Even though the non-covalent immobilization has been widely employed, the main disadvantage of this method is that biomolecule's attachment is done through weak and reversible interactions and as a result, biomolecules can leach out from the NP support. At the same time, the adsorption of biomolecules onto the MNPs surfaces often results in its conformational changes or denaturation.<sup>71</sup> Furthermore, since there is no control over the packing density of the immobilized biomolecules, their activity may be further reduced by steric congestion.<sup>72</sup>

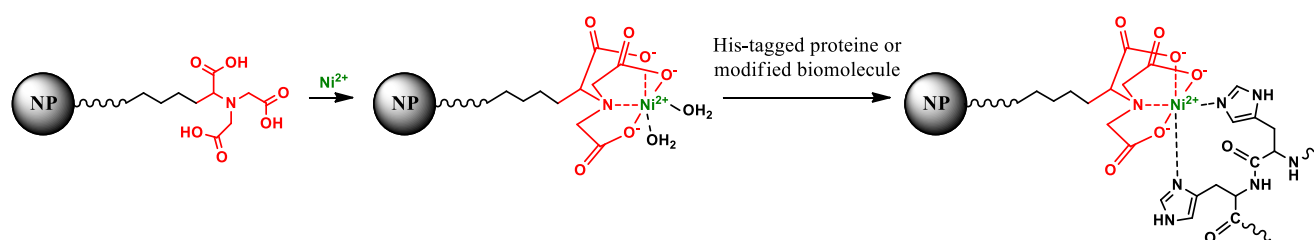
#### **I.4.1.2. Biologically mediated immobilization**

Over the years, a number of biomolecule-biomolecule and biomolecule-small molecule binding interactions (affinity) have been exploited for immobilization.<sup>70,73,74</sup> These interactions are highly selective (with respect to the identity of binding partners as well as the location on the molecules at which binding occurs) and initially were developed for protein purification by affinity chromatography. Nowadays, these affinity interactions are widely exploited in immobilization of biomolecules for the use in various other applications, since they allow a gentle oriented immobilization of biomolecules, providing an important advantage over other orienting immobilization techniques. Additionally, by this method it is also possible to release biomolecules and to use same NPs several times.<sup>75</sup>

One of the most well-known genetically encoded affinity tag is the *polyhistidine tag*. It was discovered that the histidine (His) tag (usually consisting of six sequential His residues) has an affinity for metals, such as  $\text{Cu}^{\text{II}}$ ,  $\text{Co}^{\text{II}}$ ,  $\text{Zn}^{\text{II}}$ , or  $\text{Ni}^{\text{II}}$ . In the very beginning this affinity was used for separating proteins and peptides with naturally present exposed His tags. This method was termed as immobilized metal affinity chromatography (IMAC).<sup>76</sup> Later, it was found that the optimum chromatography media was one derivatized with the nitrilotriacetic acid group (NTA) (although other chelating moiety can be used, i.e iminodiacetic acid) that binds a hexacoordinate  $\text{Ni}^{\text{II}}$  atom in a configuration that leaves two adjacent coordination sites unoccupied (Scheme I-6), creating a binding site with a strong, selective



affinity towards polyhistidine. In practice, following this strategy, NPs bearing NTA as chelating moiety are treated with a solution of  $\text{Ni}^{\text{II}}$  salt to produce Ni-activated NPs, which are then used for biomolecules immobilization through chelation with the His residues of the tag (Scheme I-6).



**Scheme I-6.** Immobilization of His-tagged modified biomolecule onto the NTA functionalized NP. The chelating NTA moiety is first “activated” with the addition of a hexacoordinate metal ion (in this example  $\text{Ni}^{2+}$ ) followed by addition of the tagged modified biomolecule. The biomolecule is immobilized on the support through chelation of the metal ion by the imidazole moieties of the Histidine residues.

Nowadays, with all the developments in genetic engineering it became possible to produce a large variety of the recombinant biomolecules such as His<sub>6</sub>-tagged fluorescent proteins, antibodies or viruses and thus broadened the field of applications.<sup>77</sup> The immobilization of His<sub>6</sub>-tagged proteins on Ni-NTA functionalized NP offers several distinct advantages over biochemical recognition elements such as antibodies systems: (1) His<sub>6</sub>-tags bound to either the C-terminus or the N-terminus are commercially available for a large number of proteins; (2) the formation of a His–Ni<sup>II</sup> complex is a fast reaction without significant alteration of the protein functionality; (3) the reaction is reversible when the surface is exposed to a stronger chelating agent (i.g. ethylenediaminetetraacetic acid (EDTA)) or when using a competitive agent (i.g. imidazole); and (4) the spatially defined attachment of His-tags on proteins or antibodies offers the opportunity for their controlled immobilization (i.e. orientation and distance) on the support.<sup>78,75</sup> However, the general selectivity level of this method is relatively low since several endogenous proteins have been recognized to be able to bind the metal ion, thus competing with the desired His<sub>6</sub>-fused protein. The strength of the binding interaction is also relatively weak, potentially leading to unwanted dissociation of immobilized protein.<sup>75,79</sup>

Certainly, the most well-known and extensively researched protein-mediated immobilization methods that exploit the affinity interaction is the *avidin-biotin* (or alternatively *streptavidin-biotin*) system.<sup>75,79</sup> The avidin-biotin system represents one of the strongest known non-covalent binding in nature, with an association constant ( $K_a$ ) of  $10^{-15}$  M.<sup>75,79</sup> The high-affinity nature of the avidin-biotin interaction has made it very popular for biorecognition applications and biosensing platforms.<sup>80</sup> Avidin (Figure I-8 a), originally discovered in egg whites but now found in a number of tissues, is a glycoprotein with a molecular weight of ~67 kDa that comprises a homotetrameric subunit structure, with each subunit is capable of binding to one biotin (Figure I-8 b).<sup>33</sup>

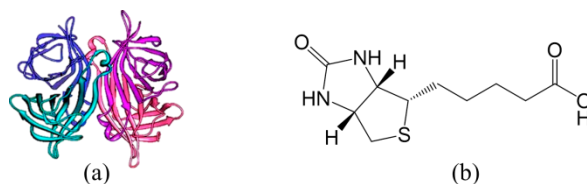


**Figure I-8.** (a) A ribbon model of tetrameric avidin, and (b) chemical structure of biotin.

Since avidin contains high carbohydrate content it has the tendency to nonspecific binding. To overcome this problem it was deglycosylated (removal of carbohydrate functionality) that has largely ameliorated nonspecific binding issues and the deglycosylated avidin is now commercially available. Streptavidin (SA), isolated from the bacteria *Streptomyces avidinii*, is a homologous tetrametric biotin binding protein that has similar to avidin affinity.<sup>81</sup> SA, like avidin, is extremely stable to a number of extreme conditions (temperature, pH etc.) and since it is not a glycoprotein it has a lower nonspecific binding. Biotin (also known as vitamin B7 or vitamin H) is a water-soluble organic compound that functions as an essential coenzyme for several carboxylase enzymes in various species including humans. These enzymes control metabolism of fatty acids, amino acids, and glucose. A large variety of biotin derivatives displaying amine, thiol, carboxyl, azide, and other functional groups are commercially available making biotinylation of NPs and biological molecules rather straightforward.<sup>33</sup>

However, in order to exploit this system, it is required first to perform a covalently immobilization biotin on the MNP surface and then use it for a specific recognition of the avidin (or SA) modified biomolecule, or vice versa. In both cases, since each avidin protein can bind up to four biotin moieties, care must be taken not to over biotinylate the NP (or biomolecule of interest), since this can induce cross-linking of the NPs and resulting in their precipitation.

An alternative route for immobilization of a biomolecules of interest is the use of *antibodies*. Antibodies can specifically recognize the biomolecule of interest due to the selectivity of their binding interactions.<sup>79,82</sup> However, the main limitation of this method is the necessity to use a well-defined monoclonal antibody (polyclonal antibodies are unsuitable because they are not a single species but a heterogeneous population of antibodies that bind their epitope in a variety of conformations).<sup>79</sup>

Finally, all these methods require first a covalent immobilization of the biomolecule that exhibit a specific affinity regarding the biomolecule of interest.

#### **I.4.2. Covalent immobilization**

The most intensely used immobilization method is definitely the formation of covalent bonds between the biomolecule of interest and the functional groups present on the surface of MNPs. The main advantage of covalent binding is that it can prevent the desorption of biomolecules from the

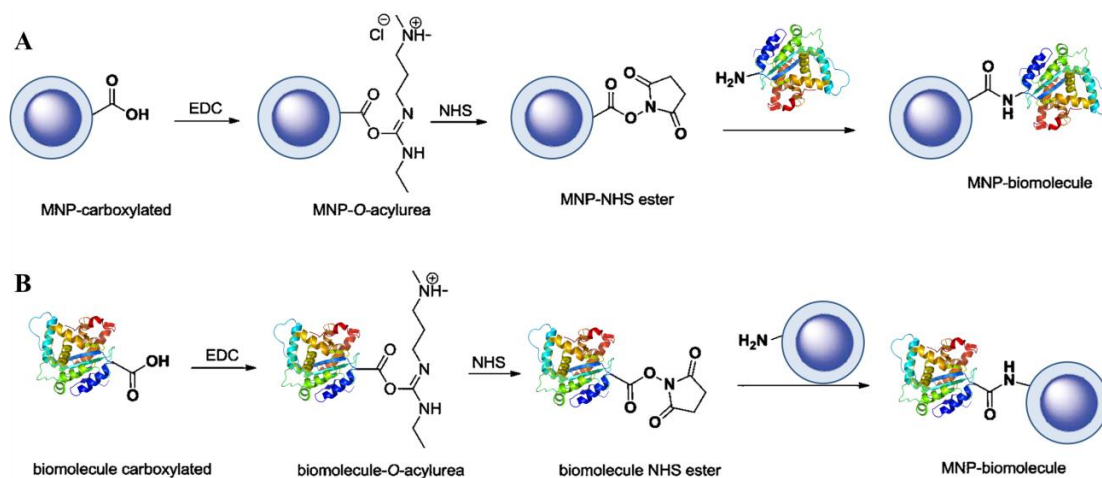
MNP surface even in the presence of substrates and solutions of high ionic strength. In addition, it can decrease the thermal movement of the biomolecule from the MNP surface at an elevated temperature. All the covalent immobilization methods relies on the formation of a covalent bound between the functional groups present on the MNP surface and the naturally present or artificially introduced functionality of biomolecule of interest.

#### **I.4.2.1. Classical chemoligation**

Classical chemoligation chemistries are mainly determined by the functional groups naturally present in biomolecules suitable for covalent binding. Thus, for example the amino acid side chains of proteins, peptides and enzymes contain: the *amino* group in Lysine and Arginine; the *thiol* group in Cysteine; the *carboxyl* groups in aspartic acid, glutamic acid or the C-terminus; the *hydroxyl* groups in Serine and Threonine; the *phenol* ring in Tyrosine; the *imidazole* group of histidine; and *indole* groups of tryptophan.<sup>83</sup> Carbohydrates and glycosylated proteins offer *hydroxyl* groups or *aldehydes* as alternative reaction sites, while nucleic acids typically provide *ribose sugars* and *phosphates* groups.<sup>83,33</sup> Therefore, the functional groups of MNPs will be mainly designed depending on the available functionality in the target biomolecule (unless it is artificially introduced). For example, a biomolecule containing available amino groups can be immobilized on the MNPs functionalized with N-hydroxysuccinimide ester (NHS), aldehyde or epoxide groups; the one containing thiol groups will be immobilized on maleimide functionalized MNPs, etc.

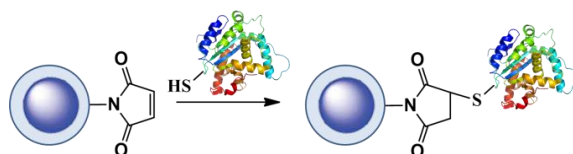
The carbodiimide mediated immobilization is a very popular and powerful chemistry that is often made to work with NPs. The method is based on the reaction between amine and carboxylic acid functions and its main advantage is that the coupling can be performed in aqueous solutions, at room temperature or even at lower temperatures (does not require harsh reaction conditions). It is a two steps reaction, involving first the activation of the carboxylic function by a carbodiimide (EDC, N-Ethyl-N'-(3-dimethylaminopropyl)carbodiimide hydrochloride) that gives rise to an O-acylurea ester, which is usually immediately transformed in to the activated ester in the presence of N-hydroxysuccinimide (NHS). For instance, even though EDC/NHS-driven coupling between aminated MNPs and carboxylated biomolecules (Scheme I-7) (or vice versa) is widely used, it is important to realize that successful use of this technique is not equivalent to controlling the display of that biomolecule on the NPs' surface. Moreover, it is often the case that the amino acid side chains of proteins contain a comparable number of carboxyl and amine functionalities, and therefore protein-protein cross-linking as a competitive reaction can occur. In addition, multiple lysine residues (amine functionalities) can also drive protein mediated MNP-MNP cross-linking.<sup>84</sup> This is why, for the success of the reaction it is important that equivalent amounts of carbodiimide to carboxylic groups are used. As a result of protein

random orientation, the properties of the immobilized proteins may be partially or even completely lost.



**Scheme I-7.** Covalent binding of biomolecules through: (A) amine or (B) carboxylic acids to IONPs via EDC/NHS coupling.

In contrast to lysine residues, cysteine (Cys) residues are usually scarce in proteins, and bioconjugate chemistries that target the reactive thiol of Cys residues can potentially ameliorate many of the liabilities associated with EDC/NHS chemistry. The most representative example is the reaction of thiols with maleimides (Scheme I-8).



**Scheme I-8.** Covalent binding of biomolecules via thiol (of cysteine residues) addition to the maleimide-functionalized MNPs.

Maleimide-thiol reaction is highly selective at nearly neutral pH (maleimide groups strongly favour conjugate addition with thiols at pH between 6.5 and 7.5, since under these conditions amines are predominantly protonated).<sup>85,2b,75,79</sup> At pH 7.0 the reaction with thiol proceeds 1000 times faster than with amines,<sup>83</sup> while at higher pH values, the addition of amino groups take place.<sup>86</sup> The high reactivity of C=C maleimides double bond can be explained by two main factors: (I) the bond angle distortion and the ring strain; and (II) the carbonyl groups being in the cis conformation. The thiol-maleimide reaction is favoured to proceed in highly polar solvents (i.e. dimethylsulfoxide (DMSO), or dimethylformamide (DMF)) as the formation of active species (i.e., the thiolate ion) is achieved due to the polarity of the solvent.<sup>87</sup>

Since proteins generally have very few surface-exposed Cys residues, it is possible to achieve site-selective immobilization.<sup>88</sup> An example of a protein in which there is a unique thiol that can be labelled is Yeast Cytochrome C. This cysteine is close to the surface of the protein, near the C-

terminus, and thus has been a viable site for labelling. Two other cysteines do exist in the protein but these are linked to the heme and thus not available for labeling.<sup>82</sup> Moreover, nowadays the biomolecules of interest (protein, peptide, oligonucleotide, oligopeptide, etc.) can be produced using recombinant engineering techniques that allows leaving of a unique cysteine residue (or synthetically inserting of a unique cysteine residue) providing a well-defined point of attachment between a biomolecule and a maleimide-activated NPs.<sup>89</sup> This, enables a certain degree of control over biomolecule orientation and largely avoids issues associated with undesirable cross-linking or other side reactions.<sup>84</sup>

Moreover, the maleimide functional group is a popular constituent of many homobifunctional cross-linkers i.e. bis-maleimidohexane (BHM) and heterobifunctional crosslinkers i.e. succinimidyl-4-(N-maleimidomethyl)cyclohexane-1-carboxylate (SMCC), sulphosuccinimidyl-4-(N-maleimidomethyl)cyclohexane-1-carboxylate (Sulpho-SMCC) and 4-(4-N-maleimidiphenyl)-butyric acid hydrazide (MPBH) (Figure I-9).

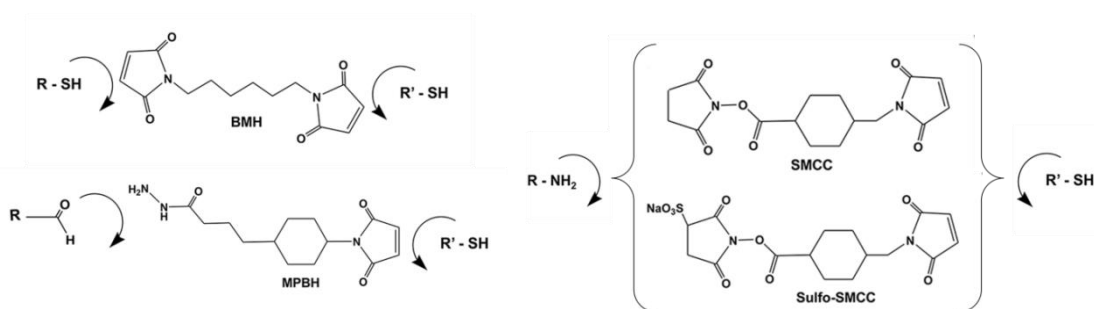


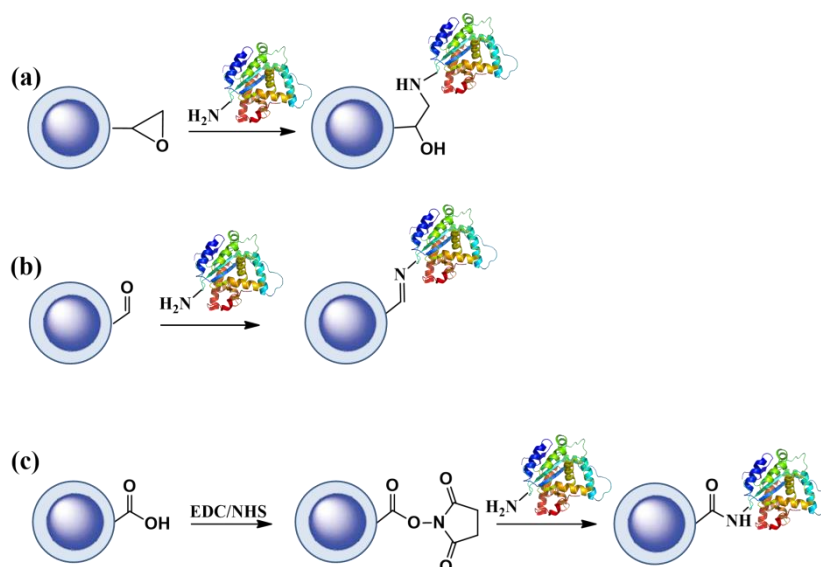
**Figure I-9.** Homobifunctional and heterobifunctional cross-linkers: bis-maleimidohexane (BHM), succinimidyl-4-(N-maleimidomethyl)cyclohexane-1-carboxylate (SMCC), sulphosuccinimidyl-4-(N-maleimidomethyl)cyclohexane-1-carboxylate (Sulpho-SMCC) and 4-(4-N-maleimidiphenyl)-butyric acid hydrazide (MPBH).

SMCC is the most popular cross-linker ever designed for protein conjugation purposes.<sup>83</sup> The reactive NHS ester end can react with primary amine groups on proteins to form stable amide bonds, while the maleimide end is specific for coupling to thiols when the reaction pH is in the range of 6.5-7.5.

The main advantages of the thiol-maleimide reaction are: the selectivity of the thiol-maleimide reaction in aqueous environments; the rapid kinetics associated with the reaction; and the stability of the thiol-maleimide product. However, a recent study show that the some succinimide thioether (generally accepted as stable) undergoes retro and exchange reactions in the presence of other thiol compounds at physiological pH and temperature, offering a novel strategy for controlled release.<sup>90</sup>

The main drawback of the maleimide group is the undergo hydrolysis to an open maleamic acid that is unreactive towards thiols, or hydrolysis of thiol-maleimide product. The speed of this ring-opening reaction typically increases with the increase of pH.<sup>83</sup>

Another method of covalent immobilization, often used for immobilization of enzymes, is via epoxide or aldehyde functionalized MNPs. S. Lin and co-workers<sup>91,92</sup> performed the immobilization of trypsin onto  $\text{Fe}_3\text{O}_4@\text{SiO}_2$  microspheres through a reaction between amino groups of trypsin with: (a) 3-glycidoxypropyltrimethoxysilane (GLYMO) modified MNPs, which provides the epoxy group as a reactive spacer; (b) glutaraldehyde (GA) modified MNPs, which provides the aldehyde functionality; and (c) carboxyl functionalized MNPs via EDC/NHS chemistry (Scheme I-9).



**Scheme I-9.** Covalent immobilization of trypsin via the reaction between amino groups of lysine residue and (a) epoxy-, (b) aldehyde-, and (c) carboxyl-functionalized MNPs.

In the abovementioned covalent enzyme immobilization methods, the highest amount of immobilized trypsin per gram of MNPs was obtained through the activation of amino group-modified MNPs by the use of GA (78–88  $\mu\text{g}/\text{mg}$ ), followed by immobilization via the interaction between amino groups of trypsin and GLYMO on MNPs (10.8–37.2  $\mu\text{g}/\text{mg}$ ). The lowest immobilization amount was achieved when MNPs were functionalized with carboxylic groups and then activated with NHS/EDAC or EDC (14.8–21  $\mu\text{g}/\text{mg}$ ). Moreover, different functionalization strategies to generate different functionalities (e.g. terminal amine, aldehyde, carboxylic, epoxy groups etc.) on MNPs' surfaces certainly have great influence on the performance of the immobilized enzyme.

Some of the most commonly utilized classical chemoligation strategies are summarized in Table I-1, showing their advantages and disadvantages respectively. Most of the classical chemoligation methods (except few specific cases, as the above given example with maleimide) suffer from the general disadvantage of generating a random orientation of the immobilized biomolecules, meaning that some of the immobilized biomolecules will be inactive. Therefore, approaches that enable covalent site-specific immobilization of selected biomolecules are highly desirable.

**Table I-1.** Summary of the most commonly utilized classical chemoligation strategies for biomolecules immobilization.<sup>75</sup>

<b>MNPs' functional group</b>	<b>Biomolecule's target group</b>	<b>Reaction description</b>	<b>(+) Advantages and (-) disadvantages</b>
N-hydroxysuccinimide (NHS) ester-functionalized MNPs	Amino groups i.g. Lysine residue	Amide bond formation	<p>(+) - Covalent attachment - Universally applicable to any protein, including native proteins - Single-step immobilization with no labelling of protein required - No coupling reagents required, "reagent-free"</p> <p>(-) - NHS esters susceptible to hydrolysis, MNPs must be carefully stored or freshly prepared prior to use - Modest immobilization yields - Random protein orientation.</p>
Amine-functionalized MNPs	Carboxyl groups i.g. aspartic acid, glutamic acid or the C-terminus	In situ formation of NHS esters on protein carboxyl sites via carbodiimide chemistry, followed by amide bond formation	<p>(+) - Covalent attachment - Universally applicable to any protein, including native proteins</p> <p>(-) - Carbodiimides and NHS esters susceptible to hydrolysis, competing hydrolysis gives poor yields - Coupling between proteins gives polymers - Random protein orientation</p>
Maleimide-functionalized MNPs	Thiol groups i.g. Cysteine residue (or amino groups, i.g. Lysine residue)	Michael addition of thiol (or amine) groups to the maleimide double bond	<p>(+) - Covalent attachment. - Universally applicable to any protein, including native proteins - Single-step immobilization, no labelling of protein required - No coupling reagents required, "reagent-free" - Selective for thiol groups (amines react slowly)</p> <p>(-) - Random protein orientation (unless only one exposed Cysteine residue)</p>
Aldehyde-functionalized MNPs	Amino groups i.g. Lysine residue	Imine formation	<p>(+) - Universally applicable to any protein, including native proteins - Single-step immobilization, no labeling of protein required - Reagent-free (unless reduced amine bond desired) - No coupling reagents required for imine formation</p> <p>(-) - Reversible covalent bond, unless converted to amine with reducing agent - Random protein orientation</p>
Epoxide-functionalized MNPs	Thiol groups i.g. Cysteine residue (or amino groups, i.g. Lysine residue)	Nucleophilic ring-opening of epoxide by amino or thiol groups	<p>(+) - Covalent attachment - Universally applicable to any protein, including native proteins - Single-step immobilization, no labelling of protein required - No coupling reagents required, "reagent-free"</p> <p>(-) - Modest immobilization yields - Slow reaction, long immobilization times required - Random protein orientation</p>

### I.4.2.2. Site-specific chemoligation methods

In order to ensure the desired biomolecules' orientation, it is necessary to expose their binding sites towards the NP surface. Therefore, different site-specific immobilization techniques have been developed in the past few years. Such approaches often require functionalization of the target biomolecules or derivatization of the NP surface, or both.

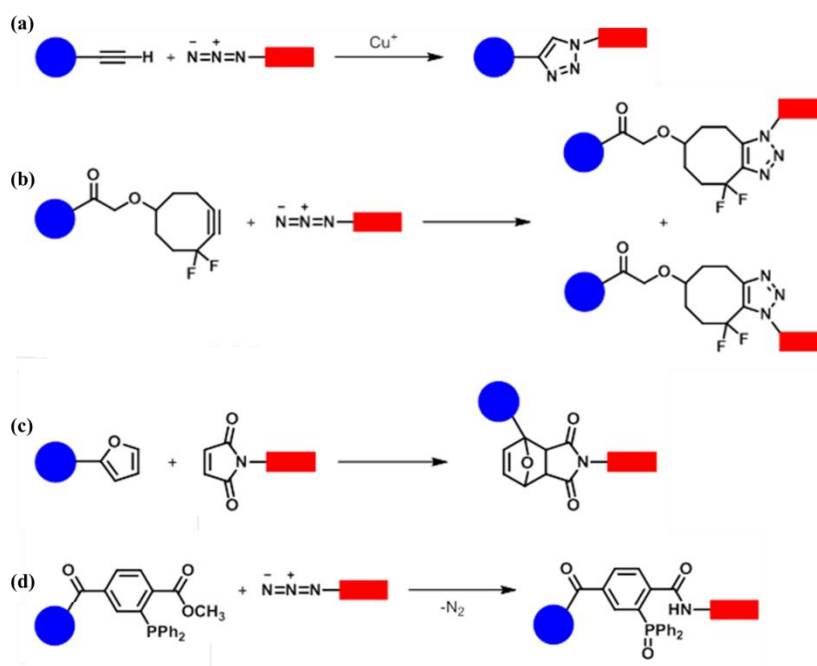
The site-specific immobilization techniques imply the use of “click chemistry” reactions.<sup>93</sup> These reactions must proceed in simple reaction conditions; involve the use of readily available starting materials and reagents; use nontoxic or no solvents; and lead to the simple product isolation. Also, click reactions provide the *orthogonal reactivity* (controlled chemical coupling between two targeted functional groups regardless of the presence of other functional groups). In addition, if the click reaction can be applied in a biological environment (where diverse biomolecular functional groups are present) without cross-reactivity, proceeds in water at or near neutral pH, between 25 and 37°C, and do not involve cytotoxic reagents or byproducts the reaction is considered *bioorthogonal* (when the two reactive functional groups are highly chemoselective and unreactive to the other functionalities present in biological systems).<sup>94,84,33</sup>

Perhaps, the most popular click reaction is the Huisgen *1,3-dipolar cycloaddition* of azides and alkynes to form 1,2,3- triazoles. In the presence of a Cu<sup>I</sup> salt, this reaction (Scheme I-10 a) is greatly accelerated, regioselective and highly efficient.<sup>95,96</sup> Cu<sup>I</sup>-mediated [3 + 2] azide–alkyne cycloaddition (CuAAC), have been widely used in drug synthesis, controlled surface modification, protein labelling and activity-based protein profiling.<sup>97</sup> As an alternative ligation route can be the strain-promoted AAC - “copper-free click chemistry” (Scheme I-10 b). This approach relies on using an alkyne in a strained geometry (such as inclusion in a cyclooctyne-based ring system) and has already been utilized in several biological studies and applications.<sup>94,98</sup> However, the main drawback of this strategy is the reduced chemoselectivity, since the alkyne moiety is intrinsically reactive toward nucleophiles. In addition, the challenges associated with its solubility and the multistep synthesis of the strained cyclooctyne structures limits the application of the copper-free AAC reaction in the preparation of NP-bioconjugates.

Another method of selective chemoligation is the *Diels–Alder cycloaddition* ([4 + 2]-cycloaddition between a diene and a dienophile). This chemistry is increasingly finding application in bio functionalizing NP materials. For example, Shi et al. have used a [4 + 2] cycloaddition reaction between a maleimide-labelled antibody and furan groups associated with the corona of poly(2-methyl-2-carboxytrimethylene-carbonate-co-D,L-lactide)-graft-poly-(ethylene glycol)-furan biodegradable micellular NPs (Scheme I-10 c).<sup>99</sup> This cycloaddition reaction is selective and efficient under mild



conditions, however to be strict bioorthogonal it requires the absence of other nontargeted thiol groups and control of pH (to prevent the undesired reaction of amines with the maleimide).



**Scheme I-10.** Examples of click chemistry reactions: (a) Cu<sup>I</sup>-mediated [3 + 2] azide–alkyne cycloaddition (CuAAC); (b) Cu-free AAC; (d) Diels–Alder cycloaddition; and (d) Staudinger ligation. The blue circle and red rectangle represent the different molecules to which these functionalities would be attached.<sup>33</sup>

A promising click reaction is the *Staudinger ligation*,<sup>100</sup> where the aza-ylide is trapped by an adjacent electrophilic carbonyl group to yield an amide bond after hydrolysis (Scheme I-10 d).<sup>101</sup> This bioorthogonal and chemoselective ligation has been extensively used for the fluorescent labelling of proteins and DNA, immobilization of proteins on surfaces and specific labelling of unnatural glycoproteins on cell surfaces.<sup>102</sup> However, there have been only a few reports of the preparation of NP-bioconjugates. The shortcoming of Staudinger ligation is the potential oxidation of phosphines under ambient conditions or by metabolic enzymes.

## I.5. Concluding remarks and motivation behind this research work

The first part of this chapter offers a general view on the recent developments regarding IONPs' synthesis and surface modification techniques (stabilization/protection and functionalization). Although, this chapter was mainly focused on the progresses of MNPs in biotechnology applications, these recent developments considerably broadened the field of MNPs' application. Since bioanalysis and biotechnological applications require the immobilization of biomolecules on solid supports, in the second part of the chapter, chemically, physically and biologically mediated methods of biomolecules

immobilization were described. All of these methods were supplied by illustrative examples for envisaged applications. Evidently, each immobilization method has some advantages and drawbacks. The choice of the immobilization chemistry will strongly depend on the desired application. However, covalent attachment of the biomolecule to the particle surface is preferred, not only to avoid the desorption from the particle surface but also to ensure a certain degree of control over the biomolecule's orientation. In this context, all the covalent immobilization methods require the introduction of the functional groups on the MNPs' surface.

The objective of this work is the development of highly reactive hybrid MNPs towards the immobilization and isolation of biomolecules. Even though the interest in designing of novel MNPs is tremendously growing up, it is also essential to devote a part of efforts to the surface modification of already existing MNPs. Therefore, this work is focused on the surface modification of two types of commercially available MNPs with functional linear and dendritic coupling agents. The choice of surface modification with functional dendritic coupling agents is justified not only by the possibility to increase the number of functional groups on MNPs' surface (positive "*dendritic effect*") but also by their ability to provide an excellent colloidal stability to the modified MNPs. Although, this approach may seem to be obvious and simple, it is still relatively undeveloped and very few examples of surface modification with dendritic structures are reported up to date.

In chapter II, the synthesis of linear and dendritic coupling agents is detailed along with the reasoning behind their selection. This chapter describes different synthetic routes of coupling agents' synthesis as well as the difficulties met during their design. The following chapters are dedicated to the functionalization and characterization of two types of core-shell MNPs. Functionalization and characterization of the MNPs with polymer shell ( $\gamma\text{-Fe}_2\text{O}_3/\text{Polymer}$ ) are discussed in Chapter III, while that of MNPs with silica shell ( $\gamma\text{-Fe}_2\text{O}_3/\text{SiO}_2$ ) in Chapter IV. In these chapters, the surface modification principles (grafting procedures) as well as the adjustment of the grafting conditions for each coupling agent are discussed. Finally, the capacity of the functionalized  $\gamma\text{-Fe}_2\text{O}_3/\text{Polymer}$  and  $\gamma\text{-Fe}_2\text{O}_3/\text{SiO}_2$  MNPs to immobilize biomolecules was investigated via a series of immobilization tests.

---

**References:**

- <sup>1</sup> S. Chikazumi, S. Taketomi, M. Ukita, M. Mizukami, H. Miyajima, M. Setogawa and Y. Kurihara, *J. Magn. Magn. Mater.* **1987**, 65, 245–251.
- <sup>2</sup> (a) N. Crawley and M. Thompson, *Anal. Chem.* **2014**, 86, 130–160; (b) E. C. Wang and A. Z. Wang, *Integr. Biol.* **2014**, 6, 9–26; (c) R. M. Patil, P. B. Shete, N. D. Thorat, S. V. Otari, K. C. Barick, A. Prasad, R. S. Ningthoujam, B. M. David, *Trends in Biotechnology* **2011**, 29, 323–333 (d) M. Colombo, S. Carregal-Romero, M. F. Casula, L. Gutierrez, M.P. Morales, I. B. Bohm, J. T. Heverhagen, D. Prospero and W. J. Parak, *Chem. Soc. Rev.*, **2012**, 41, 4306–4334; (e) L. Jézéquel, J. Loeper, and D. Pompon, *BioTechniques* **2008**, 45, 523–532; (f) W. U. Dittmer, P. de Kievit, M. W. J. Prins, J. L. M. Vissers, M. E. C. Mersch, M. F. W. C. Martens, *J. Immunol. Methods* **2008**, 338, 40–46; (g) S. Workman, S. K. Wells, C.-P. Pau, S. M. Owen, X. F. Dong, R. La Borde and T. C. Granade, *J. Virol. Methods* **2009**, 160, 14–21; (h) R. M. Patil, P. B. Shete, N. D. Thorat, S. V. Otari, K. C. Barick, A. Prasad, R. S. Ningthoujam, B. M. Tiwale and S. H. Pawar, *J. Magn. Magn. Mat.* **2014**, 355, 22–30; (i) F. Bayard, A. Raveneau, A. Letourneau, G. Joucla, C. Barbot, B. Garbay, C. Cabanne, *Anal. Biochem.* **2009**, 384, 350–352; (j) Y. Pan, X. Du, F. Zhao and B. Xu, *Chem. Soc. Rev.*, **2012**, 41, 2912–2942. (k) N. Chekina, D. Horak, P. Jendelova, M. Trchova, M. J. Benes, M. Hruby, V. Herynek, K. Turnovcova and E. Sykova, *J. Mater. Chem.* **2011**, 21, 7630–7639. (l) F. Chen, R. Shi, Y. Xue, L. Chen and Q.-H. Wan, *J. Magn. Magn. Mat.* **2010**, 322, 2439–2445; (m) K. Turcheniuk, A. V. Tarasevych, V. P. Kukhar, R. Boukherrouba and S. Szunerits, *Nanoscale*, **2013**, 5, 10729–10752.
- <sup>3</sup> A. K. Gupta and M. Gupta, *Biomaterials* **2005**, 26, 3995–4021.
- <sup>4</sup> (a) S. Krishnan and C. Walgama, *Anal. Chem.* **2013**, 85, 11420–11426; (b) S. H. Gage, B. D. Stein, L. Zh. Nikoshvili, V. G. Matveeva, M. G. Sulman, E. M. Sulman, D. Gene Morgan, E. Yu. Yuzik-Klimova, W. E. Mahmoud and L. M. Bronstein, *Langmuir* **2013**, 29, 466–473; (c) D. Rosario-Amorin, M. Gaboyard, R. Clerac, L. Vellutini, S. Nlate, and K. Heuze, *Chem. Eur. J.* **2012**, 18, 3305–3315; (d) D. Rosario-Amorin, M. Gaboyard, R. Clerac, S. Nlate and K. Heuze, *Dalton Trans.*, **2011**, 40, 44–46; (e) D. Rosario-Amorin, X. Wang, M. Gaboyard, R. Clerac, S. Nlate and K. Heuze, *Chem. Eur. J.* **2009**, 15, 12636 – 12643; (f) S. Ding, Y. Xing, M. Radosz and Y. Shen, *Macromolecules* **2006**, 39, 6399–6405.
- <sup>5</sup> A. Farrukh, A. Akram, A. Ghaffar, S. Hanif, A. Hamid, H. Duran and B. Yameen, *ACS Appl. Mater. Interfaces* **2013**, 5, 3784–3793.
- <sup>6</sup> A.-H. Lu, E. L. Salabas and F. Schuth, *Angew. Chem. Int. Ed.* **2007**, 46, 1222–1244.

- <sup>7</sup> M. Knobel, W. C. Nunes, L. M. Socolovsky, E. De Biasi, J. M. Vargas and J. C. Denardin, *J. Nanosci. Nanotechnol.* **2008**, 8, 2836–2857.
- <sup>8</sup> K. Heuze, D. Rosario-Amorin, S. Nlate, M. Gaboyard, A. Bouter and R. Clerac, *New J. Chem.*, **2008**, 32, 383–387.
- <sup>9</sup> Y. Li, P. Xiong, S. von Molnar, S. Wirth, Y. Ohno and H. Ohno, *Appl Phys Lett.* **2002**, 80, 4644–4646.
- <sup>10</sup> L. H. Reddy, J. L. Arias, J. Nicolas and P. Couvreur, *Chem. Rev.* **2012**, 112, 5818–5878.
- <sup>11</sup> R. Ladj, A. Bitar, M. Eissa, Y. Mugnier, R. Le Dantec, H. Fessia and A. Elaissari, *J. Mater. Chem. B* **2013**, 1, 1381–1396.
- <sup>12</sup> S. Laurent, D. Forge, M. Port, A. Roch, C. Robic, L. Vander Elst and R. N. Muller, *Chem. Rev.* **2008**, 108, 2064–2110.
- <sup>13</sup> Massart, R. *IEEE Trans. Magn.* **1981**, 17, 1247–1248.
- <sup>14</sup> I. W. Hamley, *Angew. Chem. Int. Ed.* **2003**, 42, 1692–1712.
- <sup>15</sup> D. K. Kim, M. Mikhaylova, Y. Zhang and M. Muhammed, *Chem. Mater.* **2003**, 15, 1617–1627.
- <sup>16</sup> M. Kobayashi, M. Skarba, P. Galletto, D. Cakara and M. Borkovec, *J. Colloid Interface Sci.* **2005**, 292, 139–147.
- <sup>17</sup> G. Fritz, V. Schadler, N. Willenbacher, and N. J. Wagner, *Langmuir* **2002**, 18, 6381–6390.
- <sup>18</sup> J. K. Oh and J. M. Park, *Progr. Polym. Sci.* **2011**, 36, 168–189.
- <sup>19</sup> J. D. G. Duran, J. L. Arias, V. Gallardo and A. V. Delgado, *J. Pharm. Sci.* **2008**, 97, 2948–2983.
- <sup>20</sup> (a) D. Portet, B. Denizot, E. Rump, J. J. Lejeune and P. J. Jallet, *Colloid Interface Sci.* 2001, 238, 37–42; (b) D. I Kreller, G. Gibson, W. Novak, G. W. Van Loon and J. H. Horton, *Colloids Surf., A* 2003, 212, 249–264. it's OK
- <sup>21</sup> (a) S. H. Sun, H. Zeng, D. B. Robinson, S. Raoux, P. M. Rice, S. X. Wang and G. X. J. Li, *Am. Chem. Soc.* **2004**, 126, 273–279; (b) E. H. Kim, H. S. Lee, B. K. Kwak and B. K. Kim, *J. Magn. Mater.* **2005**, 289, 328–330; (c) K. Woo, J. Hong and J. P. Ahn, *J. Magn. Mater.* **2005**, 293, 177–181.

- <sup>22</sup> Y. Sahoo, H. Pizem, T. Fried, D. Golodnitsky, L. Burstein, C. N. Sukenik and G. Markovich, *Langmuir* **2001**, 17, 7907–7911.
- <sup>23</sup> K. M. K. Selim, Y. S. Ha, S. J. Kim, Y. M. Chang, T. J. Kim, G. H. Lee and I. K. Kang, *Biomaterials* **2007**, 28, 710–716.
- <sup>24</sup> S. Mohapatra, N. Panda and P. Pramanik, *Mater. Sci. Eng., C* **2009**, 29, 2254–2260.
- <sup>25</sup> (a) V. Yathindranath, Z. Sun, M. Worden, L. J. Donald, J. A. Thliveris, D. W. Miller and T. Hegmann, *Langmuir* **2013**, 29, 10850–10858; (b) A. D. Angheluta, A. Dascalu, A. Fifere, A. Coroaba, L. Pricop, H. Chiriac, V. Tura, P. Pinteala and B. C. Simionescu, *J. Magn. Magn. Mater.*, **2012**, 324, 1679–1689. (c) F. Gao, B. F. Pan, W. M. Zheng, L. M. Ao and H. C. Gu, *J. Magn. Magn. Mater.*, **2005**, 293, 48–54; (d) S. Mohapatra, N. Pramanik, S. Mukherjee, S. K. Ghosh and P. Pramanik, *J. Mater. Sci.* **2007**, 42, 7566–7574.
- <sup>26</sup> L. Zhang, R. He and H.-C. Gu, *Appl. Surf. Sci.* **2006**, 253, 2611–2617.
- <sup>27</sup> K. Yang, H. Peng, Y. Wen and N. Li, *Appl. Surf. Sci.* **2010**, 256, 3093–3097.
- <sup>28</sup> Y. Sahoo, A. Goodarzi, M. T. Swihart, T. Y. Ohulchanskyy, N. Kaur, E. P. Furlani, and P. N. Prasad, *J. Phys. Chem. B* **2005**, 109, 3879–3885.
- <sup>29</sup> C. Yee, G. Kataby, A. Ulman, T. Prozorov, H. White, A. King, M. Rafailovich, J. Sokolov and A. Gedanken, *Langmuir* 1999, 15, 7111–7115.
- <sup>30</sup> (a) D. Portet, B. Denizot, E. Rump, J.-J. Lejeune, and P. Jallet, *J. Colloid Interface Sci.* **2001**, 238, 37–42; (b) .
- <sup>31</sup> M. Das, D. Mishra, T. K. Maiti, A. Basak and P. Pramanik, *Nanotechnology* **2008**, 19, 415101–415115.
- <sup>32</sup> M. Das, D. Mishra, P. Dhak, S. Gupta, T. K. Maiti, A. Basak and P. Pramanik, *Small* **2009**, 5, 2883–2893.
- <sup>33</sup> K. E. Sapsford, W. R. Algar, L. Berti, K. B. Gemmill, B. J. Casey, E. Oh, M. H. Stewart and I. L. Medintz, *Chem. Rev.* **2013**, 113, 1904–2074.
- <sup>34</sup> (a) E. H. Loeser, W. D. Harkins and S. B. Twiss, *J. Phys. Chem.* **1953**, 57, 591–597; (b) N. J. Turro, P. H. Lakshminarasimhan, S. Jockusch, S. P. O'Brien, S. G. Grancharov and F. X. Redl, *Nano Lett.* **2002**, 2, 325–328; (c) *Chem. Mater.* **2002**, 14, 2628–2636.

- <sup>35</sup> Q. Ye, F. Zhou and W. Liu, *Chem. Soc. Rev.*, **2011**, 40, 4244–4258
- <sup>36</sup> (a) H. Basti, L. Ben Tahar, L. S. Smiri, F. Herbst, M.-J. Vaulaya, F. Chaua, S. Ammar and S. Benderbous, *J. Colloid Interface Sci.* **2010**, 341, 248–254; (b) E. Amstad, T. Gillich, I. Bilecka, M. Textor and E. Reimhult, *Nano Lett.* **2009**, 9, 4042–4048.
- <sup>37</sup> E. Amstad, A. U. Gehring, H. Fischer, V. V. Nagaiyanallur, G. Hahner, M. Textor and E. Reimhult, *J. Phys. Chem. C* **2011**, 115, 683–691
- <sup>38</sup> L. X. Chen, T. Liu, M. C. Thurnauer, R. Csencsits and T. Rajh, *J. Phys. Chem. B* **2002**, 106, 8539–8546.
- <sup>39</sup> (a) R. A. Bini, R. F. C. Marques, F. J. Santos, J. A. Chaker, M. Jafelicci Jr, *J. Magn. Magn. Mater.*, **2012**, 324, 534–539; (b) S. Cousinié, M. Gressier, P. Alphons and M.-J. Menu, *Chem. Mater.* **2007**, 19, 6492–6503; (c) C. P. Tripp and M. L. Hair, *Langmuir* **1992**, 8, 1961–1967; (d) P. Silberzan, J L. Leger, D. Ausserre and J. J. Benattar, *Langmuir* **1991**, 7, 1647–1651; (e) K. Cheng and C. C. Landry, *J. Am. Chem. Soc.* **2007**, 129, 9674–9685.
- <sup>40</sup> D. Li, W. Y. Teoh, J. J. Gooding, C. Selomulya and R. Amal, *Adv. Funct. Mater.*, **2010**, 20, 1767–1777.
- <sup>41</sup> (a) B. J. Xie, C. Xu, N. Kohler, Y. Hou and S. Sun, *Adv. Mater.* **2007**, 19, 3163–3166; (b) J. V Jokerst, T. Lobovkina, R. N. Zare and S. S. Gambhir, *Nanomedicine* **2011**, 6, 715–728.
- <sup>42</sup> T.-Y. Liu, S.-H. Hu, K.-H. Liu, D.-M. Liu, and S.-Y. Chen, *Controlled Release* **2008**, 126, 228–236.
- <sup>43</sup> S. Huth, J. Lausier, S. W. Gersting, C. Rudolph, C. Plank, U. Welsch and J. Rosenecker, *J. Gene Med.* **2004**, 6, 923–936.
- <sup>44</sup> M. C. Bautista, O. Bomati-Miguel, M. del Puerto Morales, C. J. Serna and S. Veintemillas-Verdaguer, *J. Magn. Magn. Mater.* **2005**, 293, 20–27.
- <sup>45</sup> Z. Jia, W. Yujun, L. Yangcheng, M. Jingyu and L. Guangsheng, *React. Funct. Polym.* **2006**, 66, 1552–1558.
- <sup>46</sup> (a) K. Nakanishi, T. Sakiyama, Y. Kumada, K. Imamura and H. Imanaka, *Current Proteomics* **2008**, 5, 161–175; (b) E. Ostuni, R. G. Chapman, R. E. Holmlin, S. Takayama and G. M. Whitesides, *Langmuir* **2001**, 17, 5605–5620; (c) S. R. Benhabbour, H. Sheardown and A. Adronov, *Macromolecules* **2008**, 41, 4817–4823; (d) S. R. Benhabbour, L. Liu, H. Sheardown and A. Adronov,

*Macromolecules* **2008**, 41, 2567–2576; (e) H. Otsuka, Y. Nagasaki and K. Kataoka, *Adv. Drug Delivery Rev.*, **2003**, 55, 403–419.

<sup>47</sup> A. S. Karakoti, S. Das, S. Thevuthasan and S. Seal, *Angew. Chem., Int. Ed.*, **2011**, 50, 1980–1994.

<sup>48</sup> (a) M. D. Butterworth, L. Illum and S. S. Davis, *Colloids Surf. A Physicochem. Eng. Aspects*. **2001**, 179, 93–102; (b) E. K. Larsen, T. Nielsen, T. Wittenborn, H. Birkedal, T. Vorup-Jensen, M. H. Jakobsen, L. Ostergaard, M. R. Horsman, F. Besenbacher, K. A. Howard and J. Kjems, *ACS Nano* **2009**, 3, 1947–1951; (c) M. Pilloni, J. Nicolas, V. Marsaud, K. Bouchemal, F. Frongia, A. Scano, G. Ennas and C. Dubernet, *Int. J. Pharm.* **2010**, 401, 103–112.

<sup>49</sup> (a) Y. Zhang, N. Kohler and M. Zhang, *Biomaterials* **2002**, 23, 1553–1561; (b) O. Veiseh, C. Sun, J. Gunn, N. Kohler, P. Gabikian, D. Lee, N. Bhattarai, R. Ellenbogen, R. Sze, A. Hallahan, J. Olson and M. Q. Zhang, *Nano Lett.* **2005**, 5, 1003–1008.

<sup>50</sup> H. Lee, M. K. Yu, S. Park, S. Moon, J. J. Min, Y. Y. Jeong, H.-W. Kang and S. Jon, *J. Am. Chem. Soc.* **2007**, 129, 12739–12745.

<sup>51</sup> H. Cho, D. Alcantara, H. Yuan, R. A. Sheth, H. H. Chen, P. Huang, S. B. Andersson, D. E. Sosnovik, U. Mahmood and L. Josephson, *ACS Nan*, **2013**, 7, 2032–2041.

<sup>52</sup> J. K. Oh and J. M. Park, *Prog. Polym. Sci.* **2011**, 36, 168–189.

<sup>53</sup> J. F. Lutz, S. Stiller, A. Hoth, L. Kaufner, U. Pison and R. Cartier, *Biomacromolecules* **2006**, 7, 3132–3138.

<sup>54</sup> (a) J. L. Arias, M. López-Viota, E. Sáez-Fernández, M. A. Ruiz and A. V. Delgado, *Colloids Surf., A* **2011**, 384, 157–163; (b) L. Wang, T. Yang, J. Yang, Q. Li, D. Hao, J and Yang, G. Ma, *Powder Technol.* **2013**, 235, 1017–1024.

<sup>55</sup> S. Lecommandoux, O. Sandre, F. Chécot and R. Perzynski, *Prog. Solid State Chem.* **2006**, 34, 171–179.

<sup>56</sup> C. L. Yang, Q. Shao, J. He and B. W. Jiang, *Langmuir* **2010**, 26, 5179–5183.

<sup>57</sup> X. Y. Liu, S. W. Zheng, R. Y. Hong, Y. Q. Wang and W.G. Feng, *Colloids Surf., A* 2014, 443, 425–431.

<sup>58</sup> T. Gillich, C. Acikgoz, L. Isa, A. D. Schluter, N. D. Spencer and M. Textor, *ACS Nano* **2013**, 7, 316–329.

- <sup>59</sup> R. Zhu, W. Jiang, Y. Pu, K. Luo, Y. Wu, B. He and Z. Gu, *J. Mater. Chem.*, **2011**, 21, 5464–5474.
- <sup>60</sup> (a) T. Tanaka, K. Shibata, M. Hosokawa, K. Hatakeyama, A. Arakaki, H. Gomyo, T. Mogi, T. Taguchi, H. Wake, T. Tanaami and T. Matsunaga, *J. Colloid Interface Sci.* **2012**, 377, 469–475; (b) H. Liu, J. Guo, L. Jin, W. Yang and C. Wang, *J. Phys. Chem. B* **2008**, 112, 3315–3321; (c) R. Abu-Reziq, H. Alper, D. Wang and M. L. Post, *J. Am. Chem. Soc.* **2006**, 128, 5279–5282.
- <sup>61</sup> M. Li, L. Q. Xu, L. Wang, Y. P. Wu, J. Li, K.-G. Neoha and E.-T. Kang, *Polym. Chem.*, **2011**, 2, 1312–1321.
- <sup>62</sup> C. Duanmu, I. Saha, Y. Zheng, B. M. Goodson and Y. Gao, *Chem. Mater.* **2006**, 18, 5973–5981.
- <sup>63</sup> (a) X. He, X. Wu, X. Cai, S. Lin, M. Xie, X. Zhu and D. Yan, *Langmuir* **2012**, 28, 11929–11938; (b) B. Basly, D. Felder-Flesch, P. Perriat, C. Billotey, J. Taleb, G. Pourroya and S. Begin-Colin, *Chem. Commun.*, **2010**, 46, 985–987; (c) M. Kim, Y. Chen, Y. Liu and X. Peng, *Adv. Mat.* **2005**, 17, 1429–1432.
- <sup>64</sup> S. Svenson, *Eur. J. Pharm. Biopharm.* **2009**, 71, 445–462.
- <sup>65</sup> (a) C. Zhang, B. Wangler, B. Morgenstern, H. Zentgraf, M. Eisenhut, H. Untenecker, R. Kruger, R. Huss, C. Seliger, W. Semmler and F. Kiessling, *Langmuir* **2007**, 23, 1427–1434; (b) P. Tartaj, T. Gonzalez-Carreno and C. J Serna, *Langmuir* **2002**, 18, 4556–4558, (c) S. Santra, R. Tapeç, N. Theodoropoulou, J. Dobson, A. Hebard and W. Tan, *Langmuir* **2001**, 17, 2900–2906; (d) X. Liu, Z. MA, J. Xing, H. Liu, *J. Magn. Magn. Mater.*, **2004**, 270, 1–6.
- <sup>66</sup> (a) A. H. Latham and M. E. Williams, *Acc. Chem. Res.*, **2008**, 41, 411–420; (b) L. Wang, H. Y. Park, S. I. Lim, M. J. Mark, J. Schadt, D. Mott, J. Luo, X. Wang and C. J. Zhong, *J. Mater. Chem.*, **2008**, 18, 2629–2635; (c) J. Lin, W. Zhou, A. Kumbhar, J. Wiemann, J. Fang, E. E. Carpenter and C. J. O'Connor, *J. Solid State Chem.* **2001**, 159, 26–31.
- <sup>67</sup> H. Yu, M. Chen, P. M. Rice, S. X. Wang, R. L. White and S. Sun, *Nano Lett.* **2005**, 5, 379–383.
- <sup>68</sup> W. Stöber and A. Fink, *J. Coll. Interf. Sci.* **1968**, 26, 62–69.
- <sup>69</sup> P. Tartaj and J. Serna, *J. Am. Chem. Soc.*, **2003**, 125, 15754–15755.
- <sup>70</sup> F. Rusmini, Z. Zhong and J. Feijen, *Biomacromolecules* **2007**, 8, 1775–1789.
- <sup>71</sup> J. J. Gray, *Curr. Opin. Struct. Biol.* **2004**, 14, 110–115.



- <sup>72</sup> W. Kusnezow and J. D. Hoheisel, *J. Mol. Recognit.* **2003**, 16, 165–176.
- <sup>73</sup> (a) M. Hedhammar, T. Graslund and S. Hober, *Chem. Eng. Technol.* **2005**, 28, 1315–1325; (b) J. Arnau, C. Lauritzen, G. E. Petersen and J. Pedersen, *Protein Exp. Purif.* **2006**, 48, 1–13; (c) K. Terpe, *Appl. Microbiol. Biotechnol.* **2003**, 60, 523–533.
- <sup>74</sup> J. A. Camarero, *Peptide Sci.* **2008**, 90, 450–458.
- <sup>75</sup> M. Frasconi, F. Mazzei and T. Ferri, *Anal. Bioanal. Chem.* **2010**, 398, 1545–1564.
- <sup>76</sup> V. Gaberc-Porekar and V. Menart, *Chem. Eng. Technol.* **2005**, 28, 1306–1314.
- <sup>77</sup> (a) T. T. Le, C. P. Wilde, N. Grossman and A. E. G. Cass, *Phys. Chem. Chem. Phys.*, **2011**, 13, 5271–5278; (b) W. Wang, D. I. C. Wang and Z. Li, *Chem. Commun.*, **2011**, 47, 8115–8117; (c) J. Kim, H.-Y. Park, J. Kim, J. Ryu, D. Y. Kwon, R. Grailheb and R. Song, *Chem. Commun.*, **2008**, 1910–1912; (d) F. Khan, M. He and M. J. Taussig, *Anal. Chem.* **2006**, 78, 3072–3079
- <sup>78</sup> (a) E. Gizeli and J. Glad, *Anal. Chem.* **2004**, 76, 3995–4001; (b) S. Lata and J. Piehler, *Anal. Chem.* **2005**, 77, 1096–1105.
- <sup>79</sup> L. S. Wong, F. Khan and J. Micklefield, *Chem. Rev.* **2009**, 109, 4025–4053.
- <sup>80</sup> (a) O. H. Laitinen, H. R. Nordlund, V. P. Hytönen and M. S. Kulomaa, *Trends Biotechnol.* **2007**, 25, 269–281; (b) M. A. Nash, P. Yager, A. S. Hoffman and P. S. Stayton *Bioconjugate Chem.* **2010**, 21, 2197–2204; (c) X. Li and P. Kohli, *J. Phys. Chem. C* **2010**, 114, 6255–6264.
- <sup>81</sup> L. Chaiet and F. J. Wolf, *Archiv. Biochem. Biophys.* **1964**, 106, 1–5.
- <sup>82</sup> M.-E. Aubin-Tam and K. Hamad-Schifferli, *Biomed. Mater.* **2008**, 3, 1–17.
- <sup>83</sup> G. T. Hermanson, *Bioconjugate Techniques* – 2<sup>nd</sup> edition, Academic Press, San Diego, **2008**.
- <sup>84</sup> W. R. Algar, D. E. Prasuhn, M. H. Stewart, T. L. Jennings, J. B. Blanco-Canosa, P. E. Dawson and I. L. Medintz, *Bioconjugate Chem.* **2011**, 22, 825–858.
- <sup>85</sup> (a) D. G. Smith, O. O. Blumenfeld and W. Konigsberg, *Biochem. J.*, **1964**, 91, 589–595; (b) G. Gorin, P. A. Martic and G. Doughty, *Arch. Biochem. Biophys.* **1966**, 115, 593–597; (c) J. R. Heitz, C. D. Anderson and B. M. Anderson, *Arch. Biochem. Biophys.* **1968**, 127, 627–636; (d) M. D. Partis, D. G. Griffiths, G. C. Roberts and R. B. Beechey, *J. Protein. Chem.* **1983**, 2, 263–277.
- <sup>86</sup> C. F. Brewer and J. P. Riehm, *Anal. Biochem.* **1967**, 18, 248–255.

- <sup>87</sup> D. P. Nair, M. Podgórski, S. Chatani, T. Gong, W. Xi, C. R. Fenoli and C. N. Bowman, *Chem. Mater.*, **2014**, 26, 724–744.
- <sup>88</sup> Y. Kim, S. O. Ho, N. R. Gassman, Y. Korlann, E.V. Landorf, F. R. Collart and S. Weiss, *Bioconjugate Chem.* **2008**, 19, 786–791.
- <sup>89</sup> (a) C. L. Cheung, J. A. Camarero, B. W. Woods, T. Lin, J. E. Johnson, and J. J. De Yoreo, *J. Am. Chem. Soc.* **2003**, 125, 6848–6849; (b) V. E. V. Ferrero, L. Andolfi, G. Di Nardo, S. J. Sadeghi, A. Fantuzzi, S. Cannistraro and G. Gilardi, *Anal. Chem.* **2008**, 80, 8438–8446.
- <sup>90</sup> (a) A. D. Baldwin and K. L. Kiick, *Bioconjugate Chem.* **2011**, 22, 1946–1953; (b) A. D. Baldwin and K. L. Kiick, *Polym. Chem.*, **2013**, 4, 133–143.
- <sup>91</sup> Y. Li, X. Zhang and C. Deng, *Chem. Soc. Rev.*, **2013**, 42, 8517–8539.
- <sup>92</sup> (a) S. Lin, G. P. Yao, D. W. Qi, Y. Li, C. H. Deng, P. Y. Yang and X. M. Zhang, *Anal. Chem.*, **2008**, 80, 3655–3665; (b) S. Lin, Z. X. Lin, G. P. Yao, C. H. Deng, P. Y. Yang and X. M. Zhang, *Rapid Commun. Mass Spectrom.*, **2007**, 21, 3910–3918; (c) S. Lin, D. Yun, D. W. Qi, C. H. Deng, Y. Li and X. M. Zhang, *J. Proteome Res.*, **2008**, 7, 1297–1307.
- <sup>93</sup> H. C. Kolb, M. G. Finn and K. B. Sharpless, *Angew. Chem. Int. Ed.* **2001**, 40, 2004–2021.
- <sup>94</sup> (a) E. M. Sletten and C. R. Bertozzi, *Angew. Chem., Int. Ed.* **2009**, 48, 6974–6998; (b) J. C. Jewetta and C. R. Bertozzi, *Chem. Soc. Rev.*, **2010**, 39, 1272–1279.
- <sup>95</sup> C. W. Tornøe, C. Christensen and M. Meldal, *J. Org. Chem.* **2002**, 67, 3057–3064.
- <sup>96</sup> (a) J. E. Moses and A. D. Moorhouse, *Chem. Soc. Rev.*, **2007**, 36, 1249–1262; (b) V. V. Rostovtsev, L. G. Green, V. V. Fokin, and K. B. Sharpless, *Angew. Chem., Int. Ed.* **2002**, 41, 2596.
- <sup>97</sup> (a) J. E. Moses and A. D. Moorhouse, *Chem. Soc. Rev.*, **2007**, 36, 1249–1262; (b) M. Meldal and C. W. Tornøe, *Chem. Rev.* **2008**, 108, 2952–3015.
- <sup>98</sup> (a) N. J. Agard, J. A. Prescher and C. R. Bertozzi, *J. Am. Chem. Soc.* **2004**, 126, 15046–15047; (b) J. M. Baskin, J. A. Prescher, S. T. Laughlin, N. J. Agard, P. V. Chang, I. A. Miller, A. Lo, J. A. Codelli and C. R. Bertozzi, *Proc. Natl. Acad. Sci. U.S.A.* **2007**, 104, 16793–16797; (c) S. T. Laughlin, J. M. Baskin, S. L. Amacher and C. R. Bertozzi, *Science* **2008**, 320, 664–667.
- <sup>99</sup> M. Shi, J. H. Wosnick, K. Ho, A. Keating, and M. S. Shoichet, *Angew. Chem. Int. Ed.* **2007**, 46, 6126–6131.

<sup>100</sup> H. Staudinger and J. Meyer, *Helv. Chim. Acta* **1919**, 2, 635–646.

<sup>101</sup> E. Saxon and C. R. Bertozzi, *Science* **2000**, 287, 2007–2010.

<sup>102</sup> M. Kohn and R. Breinbauer, *Angew. Chem. Int. Ed.* **2004**, 43, 3106–3116.

# Chapter II

## **Synthesis of coupling agents**

**Table of contents:**

II.1. Choice of coupling agents .....	49
II.2. Synthesis of linear coupling agents.....	53
II.2.1. Strategy I .....	54
II.2.2. Strategy II.....	57
II.2.3. Strategy III.....	59
II.3. Synthesis of dendritic coupling agents.....	61
II.3.1. Dendrimers and dendrons.....	61
II.3.2. Synthesis of first generation (two branched) dendritic coupling agents .....	64
II.3.2.1. Strategy I .....	64
II.3.2.2. Strategy II .....	66
II.3.3. Synthesis of second generation (four branched) dendritic coupling agents .....	68
II.4. Conclusions: .....	71

## II.1. Choice of coupling agents

When MNPs are designed with the aim of immobilization, separation or concentration of certain species in solution, surface functionalization of MNPs is a necessary step. For this purpose, chemical modification of an organic or inorganic NP material can be achieved by grafting of a suitable coupling agent. Clearly, the choice of a coupling agent strongly depends on the desired properties of the future hybrid organic-inorganic material. In this context, NPs intended to be used for immobilization and separation of biomolecules should satisfy several criteria: (I) should exhibit a good dispersion in the incubation medium; (II) possess specificity towards the target biomolecule to immobilize; and (III) possess an ability to concentrate under the influence of a magnetic field. Consequently, the choice of coupling agents represents a crucial step in the design of MNPs for biomolecules' immobilization. The chosen coupling agent can essentially influence the properties of the future functionalized MNPs, such as their colloidal stability, selectivity towards some functionalities as well as their behaviour regarding nonspecific adsorption. In addition, the surface modification chemistry should not affect the magnetic properties of the NPs, and thereby, it is crucial to design coupling agents' structures considering all these factors.

It is obvious that the amount of covalently immobilized biomolecules is limited by the number of available functional groups on MNP's surface. Often, the number of available functional groups on NP's surface is scarce, resulting in the poor amounts of immobilized biomolecules. In this work, we aim to increase the number of functional groups on magnetic nanoparticles' surfaces, therefore functionalization with dendritic coupling agents was proposed. Dendrons have already been used for the surface modification of NPs and showed to be well-suited for these applications due to their fairly uniform structure and presence of abundant (usually flexible) terminal functional groups on the dendron's periphery (*as was previously described in Chapter I*). Therefore, functionalization of MNPs with dendritic structures can provide an increase of the number of binding sites, thus enhancing their affinity and sensitivity towards the target biomolecule.

In order to investigate the “*dendritic effect*”<sup>1</sup> of the surface functionalization, three types of coupling agents were proposed: linear coupling agents (containing one functional group); two-branched coupling agents (containing two functional groups) and four-branched dendritic coupling agents (containing four functional groups) (Figure II-1). Each coupling agent should comprise an *anchoring site* which is capable to bind with MNP's shell on the one side, and *functional groups*, capable to react with biological species, on the other side.

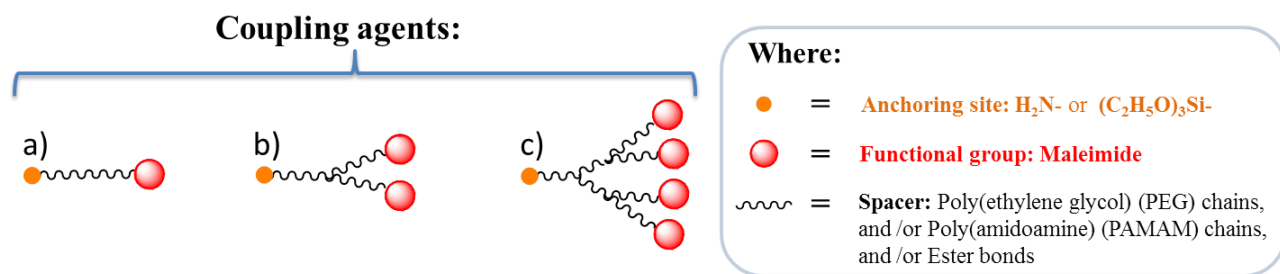


**Figure II-1.** Schematic representation of coupling agents: a) linear coupling agent; b) two-branched dendritic coupling agent (dendron of generation 1); c) four-branched dendritic coupling agent (dendron of generation 2).

The functionalization of MNPs with dendritic structures can be achieved by two major ways: (I) divergent approach<sup>2</sup> where the dendritic structure is built step by step on MNPs' surface (Figure II-2), and (II) convergent approach (Figure II-3), according to which the dendritic structures are synthesized in the first step, and grafted on MNPs' surface in the second step. Growing the dendritic structure by divergent approach can cause some structural defects (Figure II-4) because numerous reactions take place at the same time in each growth step that makes more difficult the characterization of surface chemistry. On the contrary, convergent approach allows the preparation of dendritic structures of high generations in large quantities, allowing at the same time a better control over their structure as well as their characterization before the grafting step. Therefore, it was decided to achieve the functionalization of MNPs with dendritic structures via convergent approach. For this purpose, dendritic coupling agents were synthesised by a method based on the Tomalia-type poly(amidoamine) (PAMAM) dendrimers' model.<sup>3</sup>

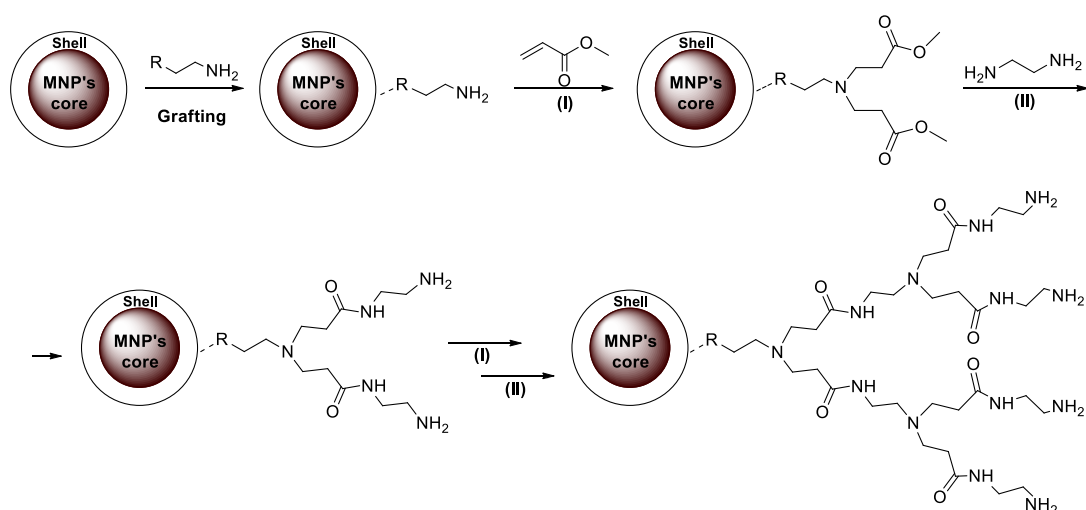


**Figure II-2.** Growth of PAMAM dendron on MNP's surface by divergent approach via successive reactions of Michael type addition (I) followed by amidation (II).

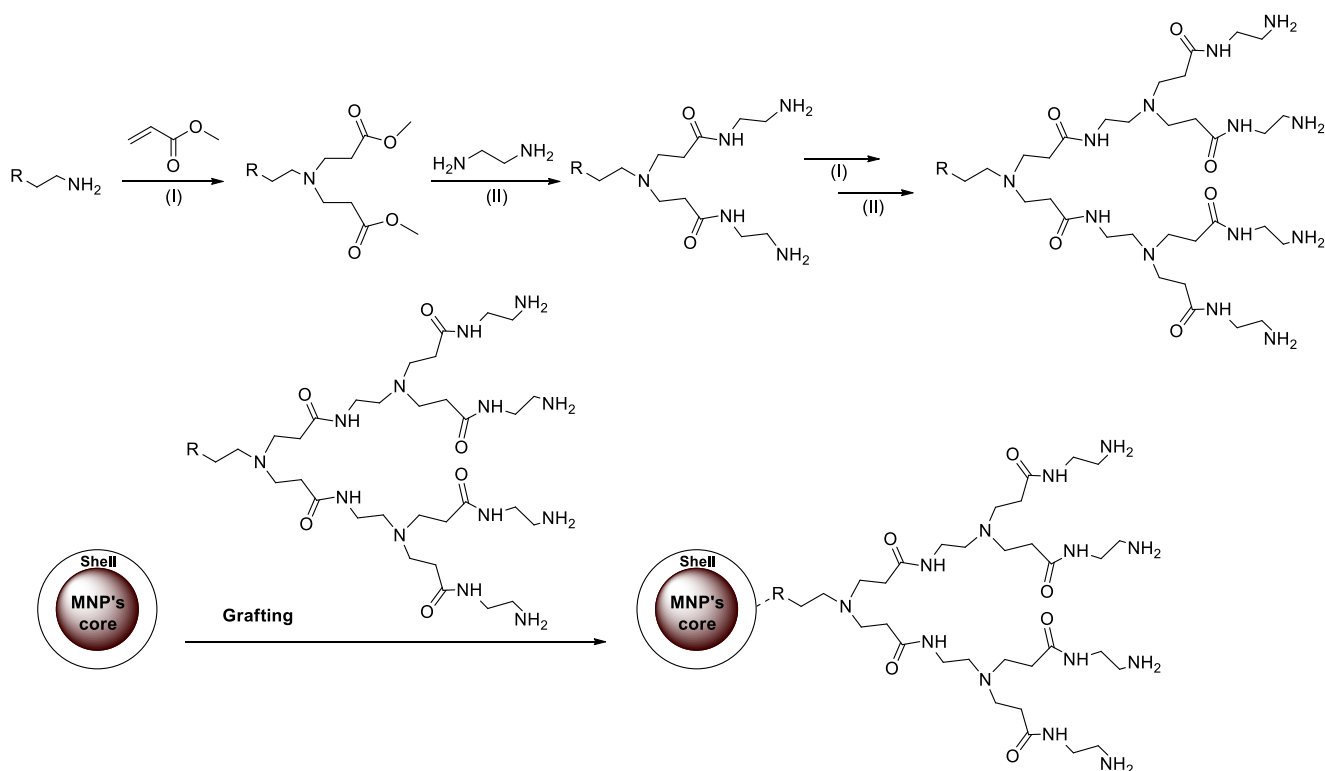


**Figure II-3.** Functionalization of MNPs with dendritic structures by convergent approach. In the first step the synthesis of a PAMAM dendron by a successive Michael type addition (I) followed by amidation (II) is performed, followed by the grafting of dendritic structure in the second step.

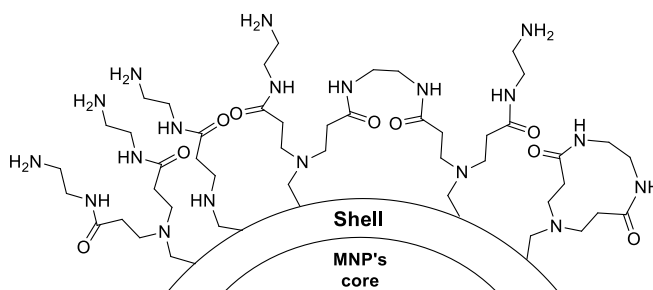


**Figure II-4.** Examples of structural defects that can occur during the functionalization of MNPs by divergent approach.

Also, it was decided to investigate the “*dendritic effect*” of the surface functionalization on two types of core-shell SP NPs: (I) with polymer and (II) with silica shell. This study was carried out to compare two completely different surfaces of MNPs towards dendritic functionalization. Although silica is in general rigid and robust material, in this work silica coated MNPs have a particularly uniform shell with controlled thickness, while polymer coated MNPs’ shell is rougher.

Because the surface modification chemistry was carried out on two types of core-shell SP NPs (with polymer or silica shell), two “*families*” of coupling agents were synthesized. Each “*family*” of coupling agents should possess an *anchoring site*, capable to form covalent binding with the functional



groups on the MNPs' surface. Thus, for the grafting on MNPs with polymer shell it was necessary to synthesize coupling agents which contain an amine as *anchoring site*, capable to bind with carboxylic acid groups present on the surface of this type of MNPs. In the case of MNPs with silica shell there was a need to synthesise coupling agents with silane *anchoring site* that can provide covalent binding with silanol groups present on the surface of these MNPs. For this purpose, organosilane reagents (R-Si(OEt)<sub>3</sub>) are often used for the grafting reaction in hydroalcoholic medium.<sup>4</sup>

Maleimide group was chosen as *functional group*, due to its high selectivity towards thiol group of cysteine residue which is naturally present in some biomolecules. The addition of thiol group to maleimide group is typically performed under mild conditions (in aqueous solutions at neutral pH and temperatures from 25°C up to 37°C), resulting in the formation of a stable thioether linkage. Taking into account that the number of cysteine residues naturally present in biomolecules is very scarce (in comparison with other functionalities: amino groups, carboxyl groups etc.), the maleimide-thiol coupling chemistry enables a certain degree of control over biomolecular orientation and at the same time allows to avoid undesirable side reactions (comparing to the EDC bioconjugate chemistry, for example, *see Chapter I*). In addition, the thiol group can be artificially inserted into the biomolecule's structure, providing a well-defined point of attachment between the biomolecule of interest and maleimide functionalized MNPs. Modifying biomolecules is now very common and allows displaying a unique cysteine residue for site-specific labelling.<sup>5,6</sup> Furthermore, biomolecules of synthetic origin (particularly peptides and nucleic acids) are far more versatile, because virtually, any functional group or chemical handle can be site-specifically introduced as needed during initial synthesis or by subsequent modification.<sup>6</sup> Also, it is important to note that the maleimide functionalized MNPs do not require any activation prior to biomolecule immobilization. For all these reasons, maleimide functional group is of high interest in the field of biomolecules' immobilization.

As the *anchoring sites* and *functional group* were chosen, a *spacer (or linker)* which will permit to link them had to be defined. The *spacer*, being a component part of the coupling agent, should promote and supplement the specific properties of the future functionalized MNPs. Spacer groups are often an essential part of polymer structures, particularly functional polymers. Many physical, chemical and biological properties strongly depend on them. In this context the spacer groups can provide flexibility in highly rigid polymers as well as accessibility of functional groups, resulting in efficient chemical reactions.<sup>7</sup> At the same time, the spacers' nature (hydrophilic, hydrophobic or amphiphilic) can essentially influence the colloidal stability of the functionalized MNPs. An imperative property of the functionalized MNPs is their colloidal stability in aqueous medium, since most of the biomolecule immobilization tests are carried out in aqueous solutions. Thus, in order to confer a good dispersion in aqueous medium, hydrophilic components such as poly(ethylene glycol)

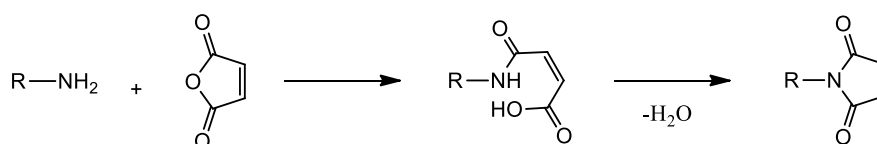
(PEG) chains and/or poly(amidoamine) (PAMAM) chains were introduced in the *linker's* backbone. The concepts of particle's surface modification with PEG have now been by far the most widely used in the variety of fields, especially in nanomedicine<sup>8</sup> due to its nontoxicity, providing a high colloidal stability.<sup>9</sup> In addition, it is considered to be one of the most efficient chemical groups that limits the non-specific adsorption of proteins.<sup>10</sup>

In the following paragraphs, different synthetic routes towards linear and dendritic coupling agents are presented.

## II.2. Synthesis of linear coupling agents

Before describing the synthetic methods of linear coupling agents' preparation, let us first have a look at a short bibliographical survey on the N-Substituted maleimides synthesis methods.

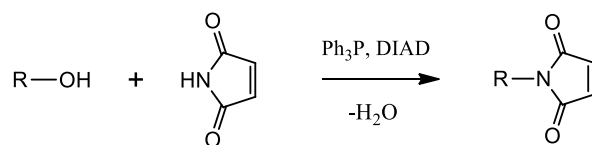
N-substituted maleimides represent an important class of organic compounds, which found applications in diverse fields, especially in biomedicine<sup>11,12</sup> and polymer chemistry.<sup>13</sup> Despite the wide applicability, available synthesis methods of N-substituted maleimides are limited. Nevertheless, several efficient methods are described in the literature.<sup>11,14</sup> Most commonly N-substituted maleimides are obtained by the reaction between a primary amine and maleic anhydride. This method of synthesis is generally accomplished in two steps as it is shown in Scheme II-1.



**Scheme II-1.** General procedure of N-substituted maleimides synthesis by the reaction between a primary amine and maleic anhydride.

*The first step* involves the generation of an N-substituted maleamic acid and, usually, occurs in quantitative yields, while the *second step* (cyclodehydration of the intermediate N-substituted maleamic acid) often occurs in poor yields. Because of the need of additional chemicals such as dehydrating agents<sup>15</sup> or catalysts<sup>16</sup> and complicated methods of purification, the last step plays the main role in the terms of the yield and final price of the product.

Another way to obtain N-substituted maleimides is via the Mitsunobu method.<sup>17</sup> This method represents a reaction between an alcohol and maleimide, as it is shown in the Scheme II-2.



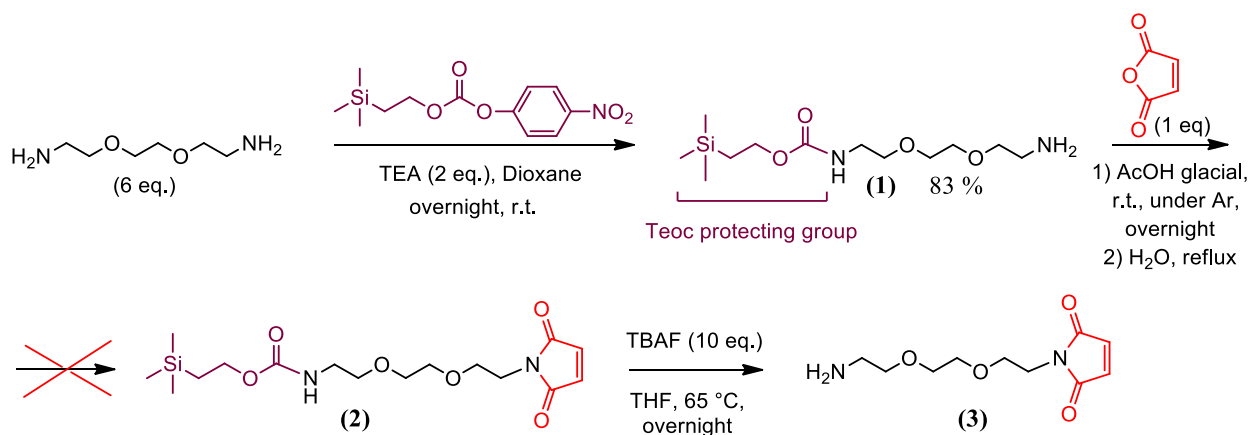
**Scheme II-2.** General procedure of N-substituted maleimides synthesis by Mitsunobu Method.

As we can see from the Scheme II-2, Mitsunobu method involves the use of triphenylphosphine ( $\text{Ph}_3\text{P}$ ) and diisopropyl azodicarboxylate (DIAD) which essentially complicate purification of the final product from the reaction mixture and usually affords from low to moderate yields (31-73%).<sup>18</sup> Also this method is limited to the use of alcohols as starting materials.

However, both methods described above are applied in the synthesis of N-substituted maleimides. In this research work, the reaction between a primary amine and maleic anhydride (Scheme II-1) for the synthesis of linear coupling agents (N-substituted maleimides) was chosen.

### II.2.1. Strategy I

In the first approach, it was proposed to synthesise the linear coupling agent **3** according to the procedure described in the Scheme II-3.



**Scheme II-3.** Synthesis of precursor **3** according to the Strategy I.

The starting material, 2,2-(ethylenedioxy)bis(ethylamine), possesses two terminal amino groups, and in order to monofunctionalize it, it was necessary to protect one of the terminal amino groups in the first step.

Numerous amino protecting groups are reported to date, including *carbamates* ( $-\text{NH}-\text{CO}_2\text{R}$ ), used for the protection of amino acids in peptide and protein synthesis, and *amides* ( $-\text{NH}-\text{COR}$ ), used more widely in synthesis of alkaloids and for the protection of the nitrogen bases (adenine, cytosine and guanine) in nucleotide synthesis.<sup>19</sup>

Among the most useful carbamates used for protection of amino group may be listed:

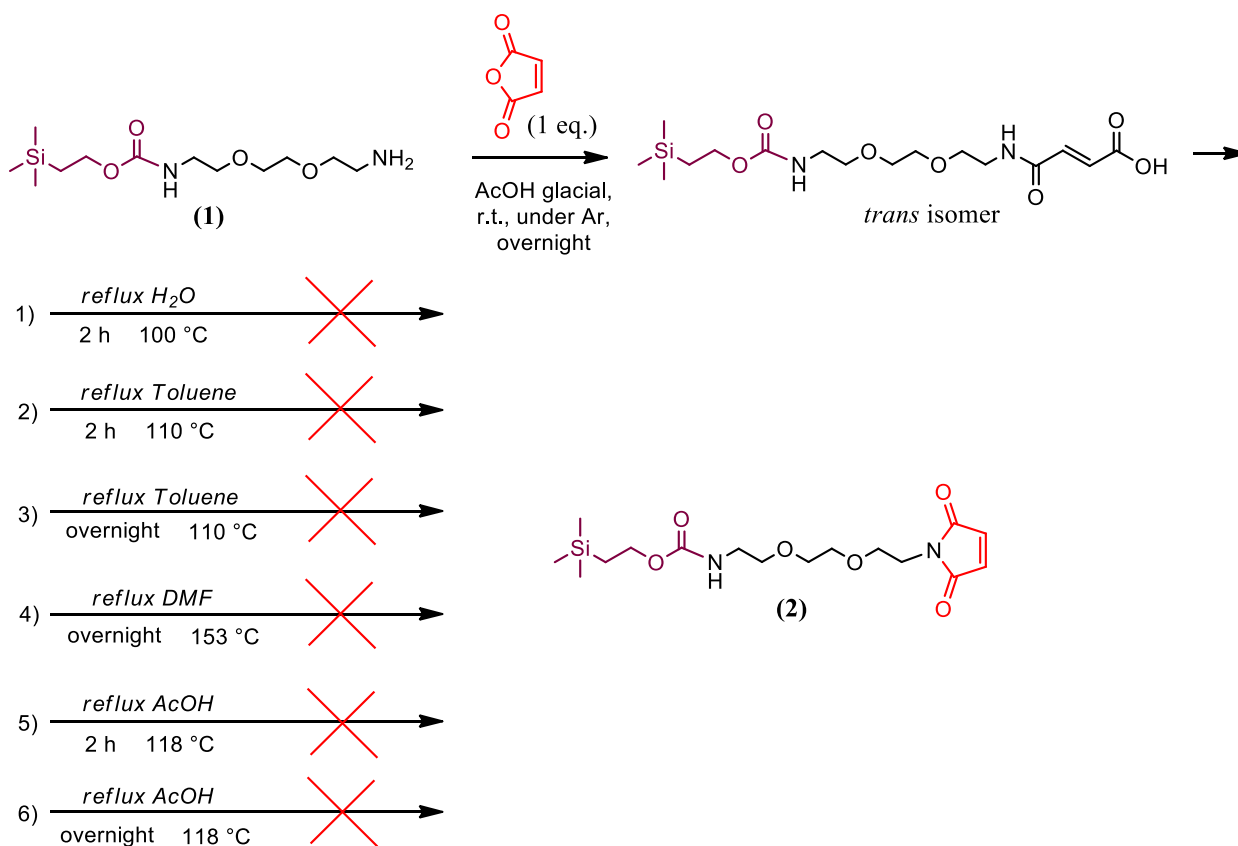
- *t*-butyl (Boc), readily cleaved by acidic hydrolysis;
- 2-(biphenyl)isopropyl, cleaved more easily than *t*-butyl carbamates by dilute acetic acid;
- benzyl (Cbz or Z), cleaved by catalytic hydrogenolysis;
- 9-fluorenylmethyl (Fmoc), cleaved by  $\beta$ -elimination with base;
- 2,2,2-trichloroethyl (Troc), cleaved by reduction with zinc in acetic acid;
- 2-trimethylsilylethyl (Teoc), readily cleaved by tetrabutylammonium fluoride in tetrahydrofuran;
- and allyl (Aloc or Alloc), readily cleaved by Pd-catalyzed isomerization.

Among amides, used for protection of amino group, probably the most useful is the phthalimide (Phth), cleaved by classical Gabriel reaction.<sup>20</sup>

As we can see, the biggest part of protecting groups are not stable in acidic conditions while one of the synthesis steps (the addition of compound **1** to maleic anhydride, Scheme II-3) should be carried out in glacial acetic acid (AcOH). Thereby, it was decided to protect one of the terminal amino groups of 2,2-(ethylenedioxy)bis(ethylamine) with 4-Nitrophenyl 2-(trimethylsilyl)ethyl carbonate (Teoc-ONp), that was chosen due to its stability in acidic conditions.

Thus, the synthesis begins with the protection of one of the terminal amino groups of 2,2-(ethylenedioxy)bis(ethylamine). The reaction between 2,2-(ethylenedioxy)bis(ethylamine) and Teoc-ONp (Scheme II-3) leads to the formation of carbamate **1** and *p*-nitrophenol which was removed by extraction in water. Thus, compound **1** was obtained in 83 % yield.

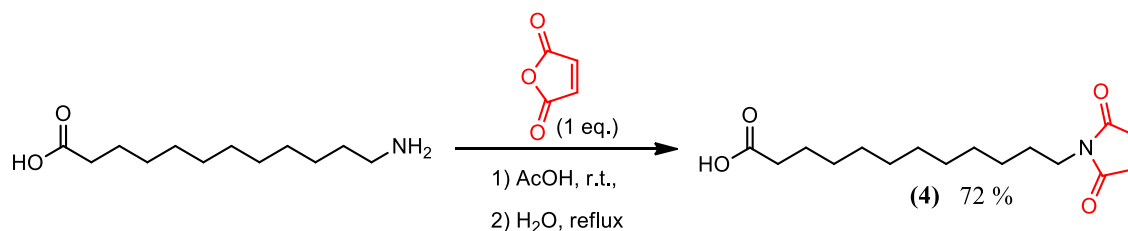
Next, the reaction between the primary amine **1** and maleic anhydride was performed. As it was previously described (Scheme II-1), this type of reactions is accomplished in two steps. Thereby, first the addition of primary amine **1** to maleic anhydride was performed in glacial AcOH, and then the cyclodehydration of the intermediate *N*-substituted maleamic acid was carried out by refluxing in water. The reaction was monitored by <sup>1</sup>H, <sup>13</sup>C, COSY, HSQC and HMBC NMR analyses, according to which, the expected product **2** was not obtained. Several of reaction conditions were modified: the use of toluene as an azeotropic dehydration solvent; the use of dimethylformamide (DMF) as a polar aprotic solvent; the use of AcOH as a reaction solvent, and the increase of the reaction time did not give better results (Scheme II-4).



**Scheme II-4.** Representation of different reactions conditions for the synthesis of compound **2**.

One explanation is probably that after the first step (formation of the corresponding maleamic acid), a *trans* isomer instead of a *cis* isomer was obtained (Scheme II-4). In this case the *trans* isomer represents a more thermodynamically stable structure than the *cis* isomer and the dehydration of this isomer requires higher temperatures. However, heating to higher temperatures and a longer reaction time increases the risk of polymerization of maleimide product, this being the reason why this strategy was abandoned.

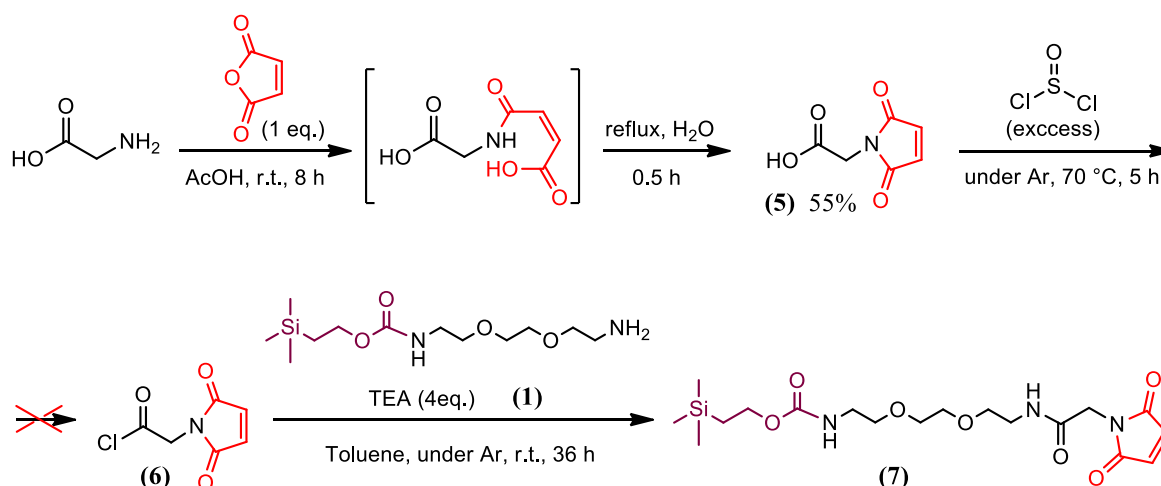
It is noteworthy that while we did not succeed to obtain compound **2** by this way, we easily obtained maleimidolauric acid **4** in a quite good yield (72 %) using the same protocol<sup>11(a)</sup> (Scheme II-5). If we compare the two starting materials (aminolauric acid and compound **1**), we can notice that one of the differences between these two molecules is the presence of the aliphatic chain in aminolauric acid and ethyleneglycol chain in compound **1**, the latter seems to interfere in this reaction.

Scheme II-5. Synthesis of 12-maleimidolauric acid **4**.

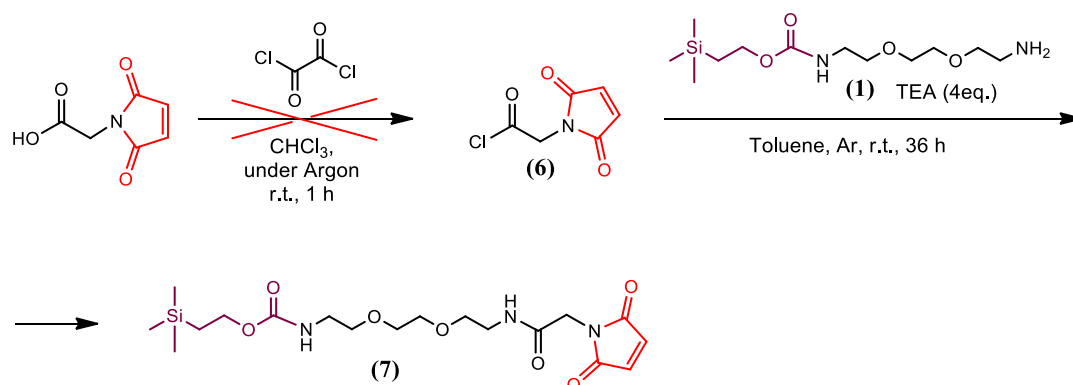
Based on this experiment, and in order to form the desired linear coupling agent decorated with maleimide functionality, it was decided to use an aliphatic amine as starting material. This synthesis is described in the next strategy.

## II.2.2. Strategy II

In the second approach it was attempted to obtain compound **7** from glycine, according to the strategy presented in the Scheme II-6.

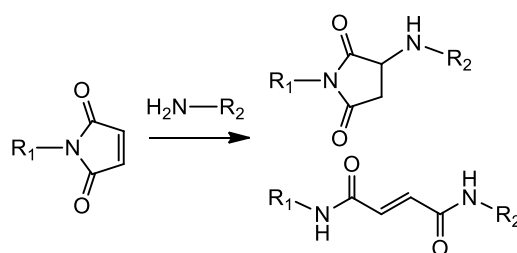
Scheme II-6. Synthesis of precursor **7** according to the Strategy II.

First, the 2-maleimidoacetic acid **5** was obtained in 55 % yield, according to the protocol<sup>11(a)</sup> used for the synthesis of maleimidolauric acid **4**. Next, in order to increase the reactivity of carboxylic acid group it was decided to transform the carboxylic acid **5** into its acyl chloride **6**. The reaction between 2-maleimidoacetic acid **5** and thionyl chloride proceeded under argon atmosphere at 70°C for 5 h, but did not yield the desired product. As a result of this reaction, the starting material (glycine) was obtained (according to <sup>1</sup>H, <sup>13</sup>C NMR analysis), that can be explained by the decomposition of 2-maleimidodiacetic acid **5** under such strong conditions. The reaction conditions were changed, thionyl chloride was replaced with oxalyl chloride and the following reactions were carried out as shown in the Scheme II-7.



**Scheme II-7.** Synthesis of precursor **7** according to the Strategy II.

N-maleimidoacetic acid **5** was dispersed in chloroform ( $\text{CHCl}_3$ ) and cooled to  $0^\circ\text{C}$ , then 1 equivalent of oxalyl chloride was added dropwise. The mixture was stirred under argon at room temperature for 1 h. Next, the solvent was evaporated to give a beige powder which was immediately dissolved in  $\text{CHCl}_3$  and added dropwise to the solution of compound **1** and triethylamine (TEA). The mixture was stirred at room temperature under argon for 36 h, then the solvent was evaporated. The residue was analysed by  $^1\text{H}$  NMR. In the  $^1\text{H}$  NMR spectrum a singlet corresponding to maleimide double bond was found at 6.02 ppm with an integration of 0.89 (instead of 2.00), and two doublets at 6.12 and 5.86 ppm with  $J=13.0$  Hz, and an integration of 0.28 and 0.26 respectively, corresponding to the formation of an asymmetric alkene ( $\text{R}_1\text{-CH}=\text{CH-R}_2$ ). This result suggests that other two reactions occur. The amino group can react with maleimide in either one of two ways (Scheme II-8): a facile Michael addition of the amine to the maleimide double bond (analogous to the addition of  $-\text{SH}$ )<sup>21</sup> or the addition of the amine to one of the carbonyl groups followed by the maleimide ring opening.<sup>22</sup>

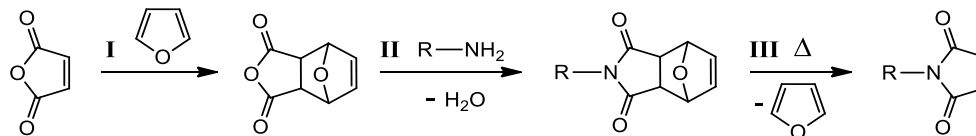


**Scheme II-8.** Possible reactions between maleimide moiety and primary amines.

To avoid any problem of competition reactions on this reactive position (maleimide double bond) this approach was abandoned and other strategy was envisaged as following.

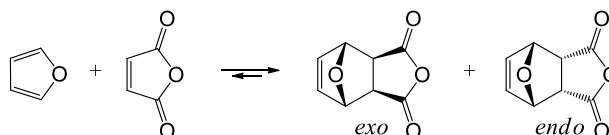
### II.2.3. Strategy III

As an alternative method of N-substituted maleimides synthesis can be considered the approach presented in the Scheme II-9,<sup>23</sup> which in addition, represents an efficient method of carbon-carbon double bonds protection.<sup>24</sup> This method includes 3 general steps:



**Scheme II-9.** I) Synthesis and protection of N-substituted maleimide by Diels-Alder addition of furan to maleic anhydride; II) Primary amine insertion into the Diels-Alder adduct; and III) retro-Diels-Alder deprotection of N-substituted maleimide group.

The *first step* represents a Diels-Alder (DA) addition of furan to maleic anhydride. This type of [4 + 2] cycloaddition occurs easily and fast, and can lead to the formation of *endo* and *exo* stereoisomers (Scheme II-10).



**Scheme II-10.** Diels-Alder [4 + 2] cycloaddition of furan with maleic anhydride to give the kinetic *endo* and thermodynamic *exo* Diels-Alder adducts.

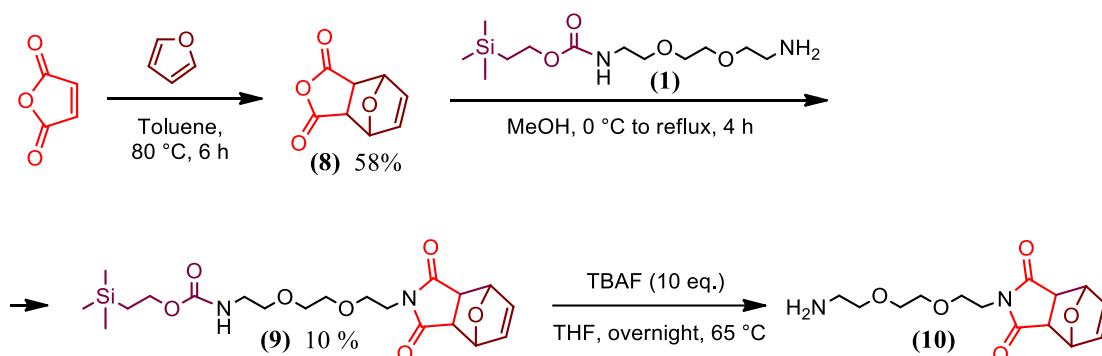
An experimental and theoretical study affirms the predominant formations of an *exo* adduct, caused by its higher thermodynamic stability, and only a very small kinetic preference for the formation of an *endo* isomer was observed.<sup>25</sup> In our work, for clarity, the stereochemistry of the obtained DA adduct will not be further indicated, since this reaction is simply used as protection method and will be cleaved later.

In the *second step* (Scheme II-9) a primary amine insertion into the DA adduct (furan protected maleic anhydride) is performed. The resulting succinimide derivative is less labile to nucleophiles than maleimides that possess two carbonyl groups conjugated to the double bond, and as the result, the highly electron poor double bond is susceptible to react with a range of nucleophiles. Suchwise, this step represents an efficient method of maleimide group protection against the addition of nucleophiles.<sup>26</sup>

The *third step* (Scheme II-9) is the retro-DA reaction. This step permits to generate the desired maleimide group, and for this reason it is sometimes called the deprotection step.

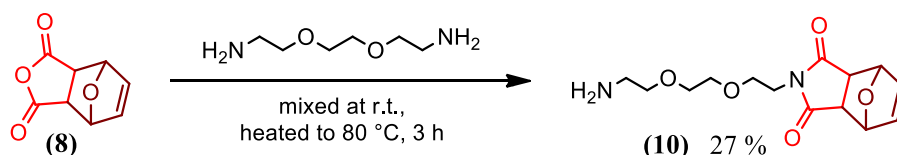
Based on the aforesaid, a new approach was developed (Scheme II-11).





**Scheme II-11.** Synthesis of precursor **10** according to the Strategy III.

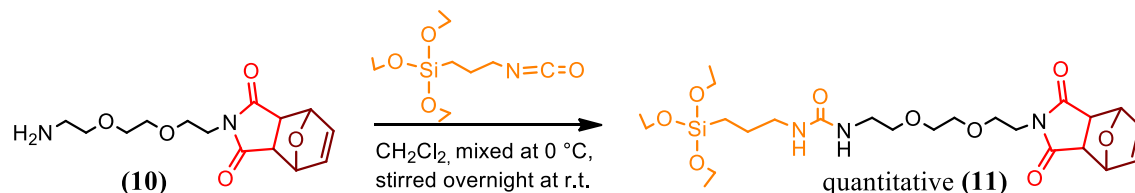
The DA cycloaddition of furan to maleic anhydride results in the formation of furan protected maleic anhydride **8** in 58 % yield.<sup>23a,b</sup> Next, the addition of the primary amine **1** to the furan protected maleic anhydride **8** was performed. This reaction leads to a 10 % yield of compound **9** after the purification by column chromatography on silica gel. Next, the cleavage of Teoc protection of amino group from compound **9** was performed. Unfortunately, compound **10** could not be isolated, mostly because of the large excess of tetrabutylammonium fluoride hydrate (TBAF) involved in the reaction process. Therefore, the procedure shown in the Scheme II-11 was considered not efficient for several reasons: poor yield of compound **9**, difficulties in the isolation of compound **10** and additional costs for the TEOC-ONp protecting group and deprotection agent (TBAF). Considering these parameters, a direct coupling between furan protected maleic anhydride **8** and 2,2-(ethylenedioxy)bis(ethylamine)<sup>27</sup> was tried as shown in Scheme II-12, despite the fact that compound **8** can react with amino groups from both sides.



**Scheme II-12.** Single step synthesis of linear coupling agent **10** that hereinafter used for the grafting on MNPs with polymer shell.

Using this approach, after the purification by column chromatography on alumina (activated, basic, Brockmann I), compound **10** was obtained in 27 % yield. Taking into account that this compound was obtained in a single step, without any protection of the terminal amino groups of the starting material, this approach was considered much more efficient in comparison with the previous one (Scheme II-11). Nevertheless, it is worthy to mention that compound **10** is not stable at room temperature and should be purified and used right after the synthesis (or kept in the freezer at  $-18^\circ\text{C}$ ). Compound **10** represents the first target linear coupling agent for the grafting on MNPs with polymer shell.

In order to obtain an analogues coupling agent, which can be grafted on MNPs with silica shell it was necessary to transform the amino-functionality of compound **10** into silane-functionality. This silane-functionality was readily introduced by reacting compound **10** with triethoxy(3-isocyanatopropyl)silane (Scheme II-13).



**Scheme II-13.** Synthesis of silylated linear coupling agent **11** hereinafter used for the grafting on MNPs with silica shell.

The reaction took place in freshly distilled DCM and led to the formation of the silylated coupling agent **11** in a quantitative yield. To avoid the hydrolysis of the ethoxy groups, silylated coupling agent **11** was grafted right after its synthesis.

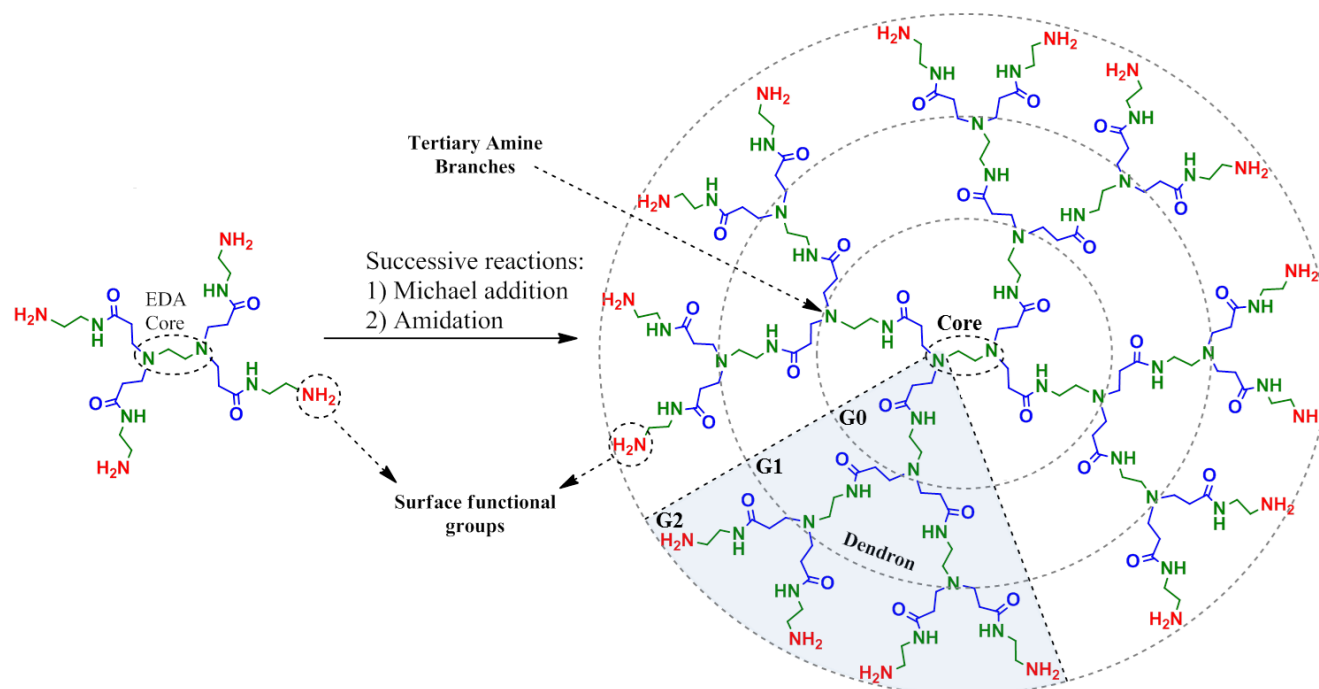
### II.3. Synthesis of dendritic coupling agents

For clarity, a brief introduction of dendrimers and dendrons is stated below. Then, the synthetic routes to obtain dendritic coupling agents will be detailed.

#### II.3.1. Dendrimers and dendrons

The name “Dendrimer” comes from the Greek word “δέντρο” that means tree, a dendrimer respectively, is a tree like (with branches) molecule. These branched molecules are produced in an iterative sequence of reaction steps, in which each additional iteration leads to a higher generation material.<sup>28</sup> The concept of iterative growth of branched molecules was first reported in 1978 by Buhleier et al.<sup>29</sup> (University of Bonn, Germany). This was followed in 1979 by the parallel and independent development of the divergent, macromolecular synthesis of poly(amidoamine) (PAMAM) dendrimers in the Tomalia group (Dow Chemical Co.).<sup>3a,b,f</sup> As early as 1984, PAMAM dendrimers were the first complete dendrimer family (Generation = 0 – 7) to be synthesized and characterized.<sup>3g</sup> The first article using the term “dendrimer” and describing the preparation of PAMAM dendrimers was published in 1985.<sup>3c</sup> In the same year a communication reported the synthesis of “arborols” systems (unimolecular micelles) by Newkome et al. (Louisiana State University).<sup>30</sup> Tomalia’s PAMAM dendrimers and Newkome’s “arborols” were the first dendritic structures that have been thoroughly investigated and fully characterized. Both dendrimers are constructed divergently, implying that the synthesis starts from a molecule’s core and grows to the periphery (on the contrary, in convergent procedures, the synthesis starts from the periphery to the core).<sup>31</sup>

Since the seminal works in this field, a large number of dendrimer structures have been developed and have become the subject of intense interdisciplinary research efforts, bringing together scientists from various fields. Based on the rapid advances in this area, PAMAM dendrimers became one of the most common classes of dendrimers suitable for materials science and biotechnology due to their architecture and their functionalities that can be modified and adapted for various fields of application.<sup>3g,32</sup> This type of dendrimers consist of a diamine core (commonly ethylenediamine (EDA) or ammonia core) and tertiary amine branches (Scheme II-14). Their synthesis is based on a repetition of two successive reactions: Michael type addition and amidation. These successive reactions create higher generations (G), and this typical “growth” pattern of dendritic molecules determines their solution properties and makes these properties deviate from those of linear molecules, especially at higher molecular weights.<sup>28</sup>

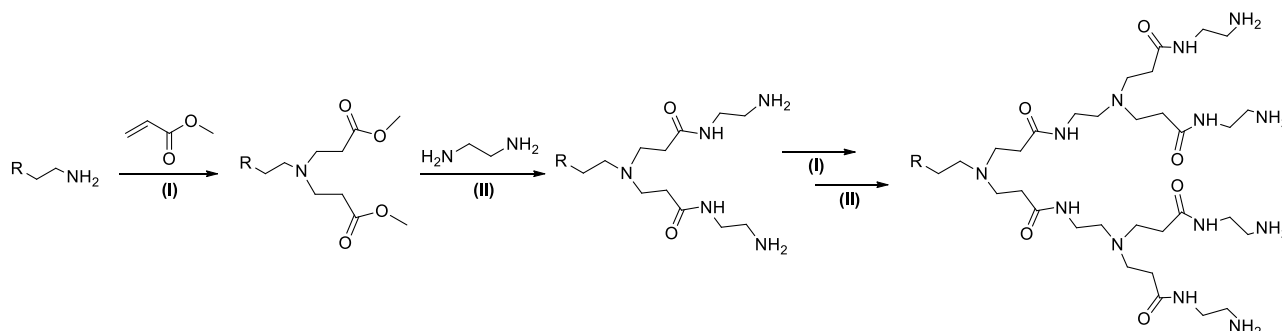


**Scheme II-14.** Schematic representation of the PAMAM dendrimers' structural components, as well as its generation's growth by divergent approach.

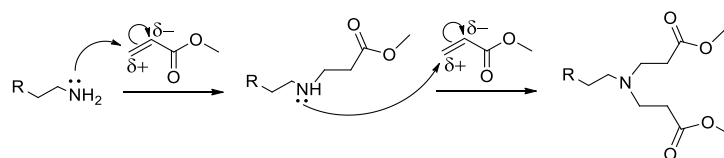
Since several years our team (C2M) is interested in the preparation of dendritic structures, namely, PAMAM dendrons, based on this type of dendrimers. A dendron, being a structural part of a dendrimer, represents a branched molecule that contains a focal point, interior branching units, and well-defined numbers of functional surface groups as a function of generation level.<sup>31a,33</sup>

The difference between dendron and dendrimer is illustrated in Scheme II-14. In this work the terms dendron and dendritic coupling agent are sometimes used interchangeably.

Similarly to PAMAM dendrimers, PAMAM dendrons are synthesized by a successive Michael type addition followed by amidation (Scheme II-15). The mechanism of a Michael type addition is shown in the Scheme II-16.



**Scheme II-15.** Synthesis of a PAMAM dendron by a successive double Michael addition (I) followed by amidation (II).



**Scheme II-16.** Mechanism of the double Michael addition.

The first attempts of PAMAM dendrons synthesis, in our team, were done during the thesis of Hakim Rahma,<sup>34</sup> who developed amino functional dendritic organosilanes of G1 and G2 (Figure II-5) for chemical modification of silica MNPs' surface. Moreover, the amino functionalized MNPs were successively transformed into carboxyl functionalized MNPs.

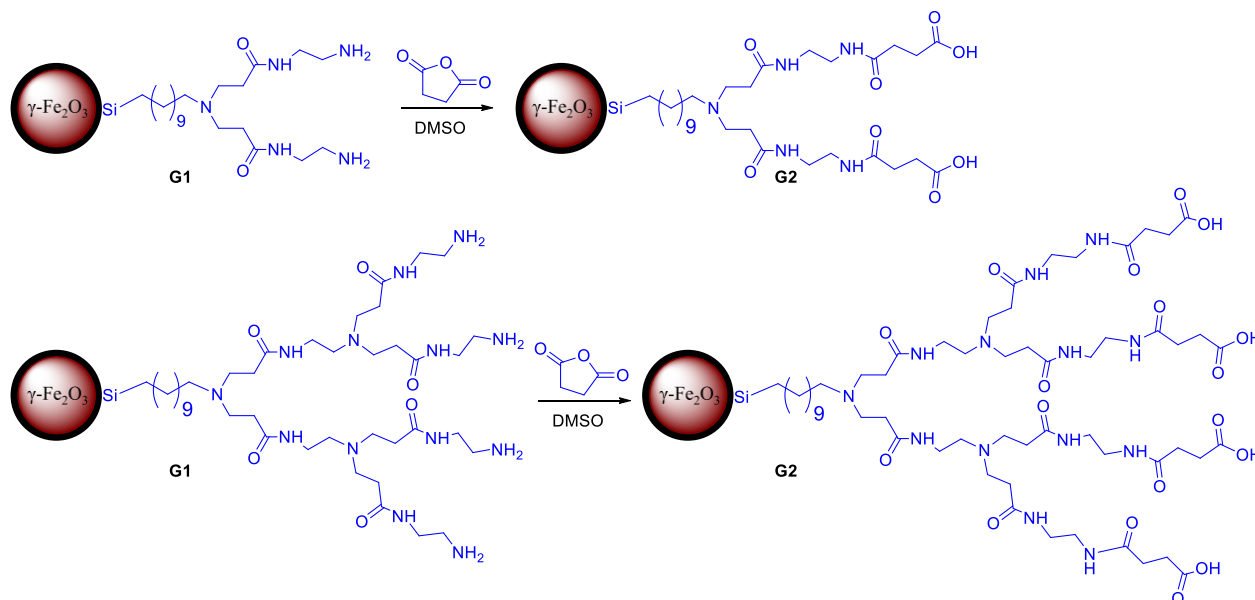


**Figure II-5.** Amino functionalized MNPs (via grafting of dendritic organosilanes G1 and G2) and their successive transformation in carboxyl functionalized MNPs.<sup>34</sup>

The carboxyl functionalized MNPs demonstrated the ability to immobilize biomolecules.<sup>34</sup> Despite these encouraging results, one of the disadvantages of these functionalized MNPs was their limited dispersion in aqueous solutions.

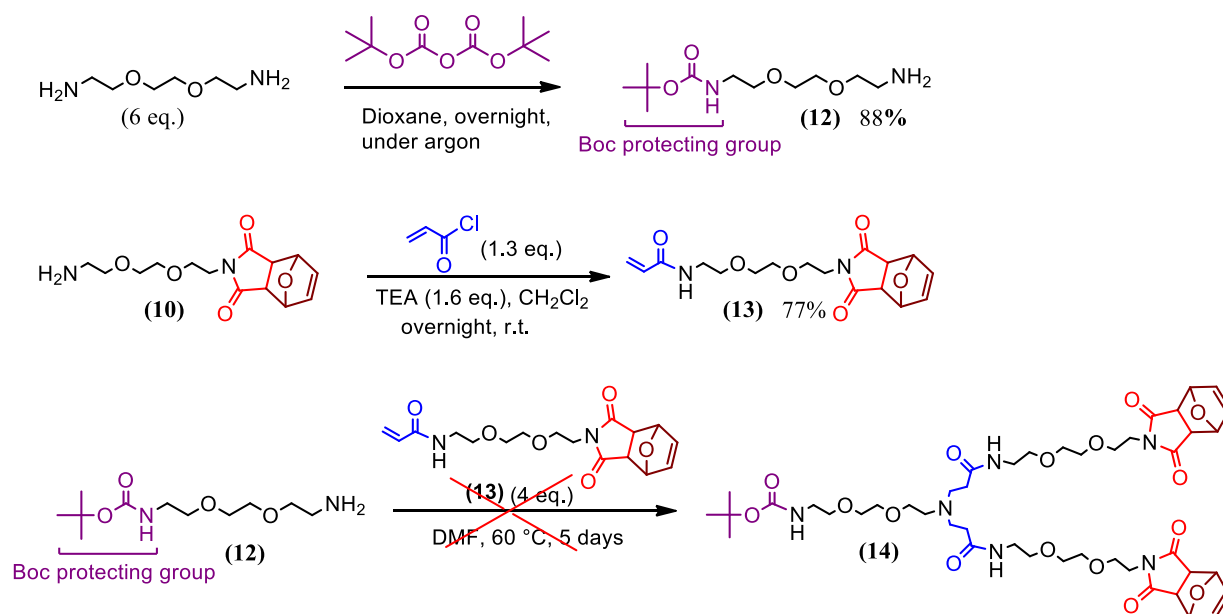
To overcome this problem, in the present work, PEG chain was introduced in the PAMAM dendron's backbone. The synthesis of maleimide decorated dendrons of G1 and G2 for chemical modification of silica and polymer coated MNPs is presented below.

### II.3.2. Synthesis of first generation (two branched) dendritic coupling agents

In the case of dendritic (branched) coupling agents' synthesis, it was decided to keep the spacers' structures similar or close to those of the linear coupling agents' structure. Thus, for the synthesis of two branched coupling agents, the procedure described below was proposed.

#### II.3.2.1. Strategy I

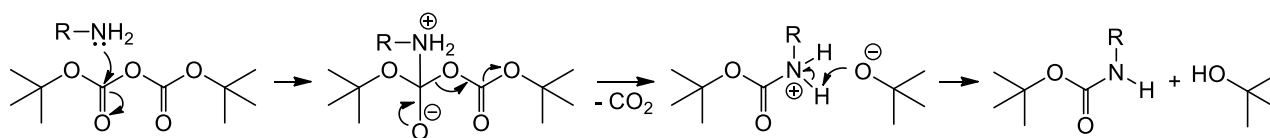
In this strategy (Scheme II-17), 2,2-(ethylenedioxy)bis(ethylamine) was used as starting material for the synthesis of two branched coupling agents **14** (dendrons of G1).



**Scheme II-17.** Synthesis of two branched structure **14**.

Following this strategy, first a monoprotection of the 2,2-(ethylenedioxy)bis(ethylamine) was performed with di-tert-butyl dicarbonate (Boc anhydride) which is extremely resistant towards basic and nucleophilic reagents and it is probably one of the most commonly used amino protecting groups in organic synthesis.<sup>19</sup> This protecting group was chosen because of the high yield in protected product and its fast and easy cleavage procedure, classically done with a strong protic acid (most commonly

with trifluoroacetic or hydrochloric acid). Thus, the reaction between di-*tert*-butyl dicarbonate and 2,2-(ethylenedioxy)bis(ethylamine), taken in excess (6 eq.), was carried out in a large amount of dioxane in order to favour the monoprotection. The reaction leads to the formation of protected amine, carbon dioxide (CO<sub>2</sub>) and *t*-butanol as side product, according to the mechanism presented in the Scheme II-18.<sup>35</sup>



**Scheme II-18.** Mechanism of a primary amine protection with di-*tert*-butyl dicarbonate.

The solvent, CO<sub>2</sub> and *t*-butanol were then eliminated under vacuum, and the excess of 2,2-(ethylenedioxy)bis(ethylamine) was removed by extraction in water. The residue was then purified by column chromatography on alumina (activated, basic, Brockmann I) to yield one side Boc protected diamine **12** in 88 % yield.

Next, the acrylamide **13** was obtained by the reaction between compound **10** and acryloyl chloride. Acryloyl chloride was added dropwise to the mixture of compound **10** and TEA, solubilised in freshly distilled DCM, and then the mixture was stirred at room temperature overnight under argon atmosphere. The solvent, excess of acryloyl chloride and TEA were evaporated and the triethylamine hydrochloride (TEA•HCl) salt was removed by extraction in water. Thus, acrylamide **13** was obtained in 77 % yield. Nevertheless, it should be noted that compound **13** is not stable. The formation of very long needles (of around 4 cm) is observed whilst the solubilisation of compound **13** in DCM (Figure II-6).



**Figure II-6.** Needles formed during the solubilization of compound **13** in DCM.

These needles are not soluble (at room temperature and on heating) in H<sub>2</sub>O, MeOH, DMF, DMSO, Acetonitrile, EtOH, Acetone, AcOEt, THF, CHCl<sub>3</sub>, DCM, Et<sub>2</sub>O, Toluene and Pentane. This being the reason why these needles could not be analysed and the process that take place identified. It

was supposed that this happening can be explained by acrylamide polymerization and in order to stop it, 100 ppm (0.01 %) of Hydroquinone monomethyl ether (MEHQ) was added. MEHQ is often used as an inhibitor and stabilizer in vinyl and acrylic monomers, acrylonitriles, and various polymers especially for finished products. This considerably diminished this happening and allowed the storage of compound **13** for long period of time.

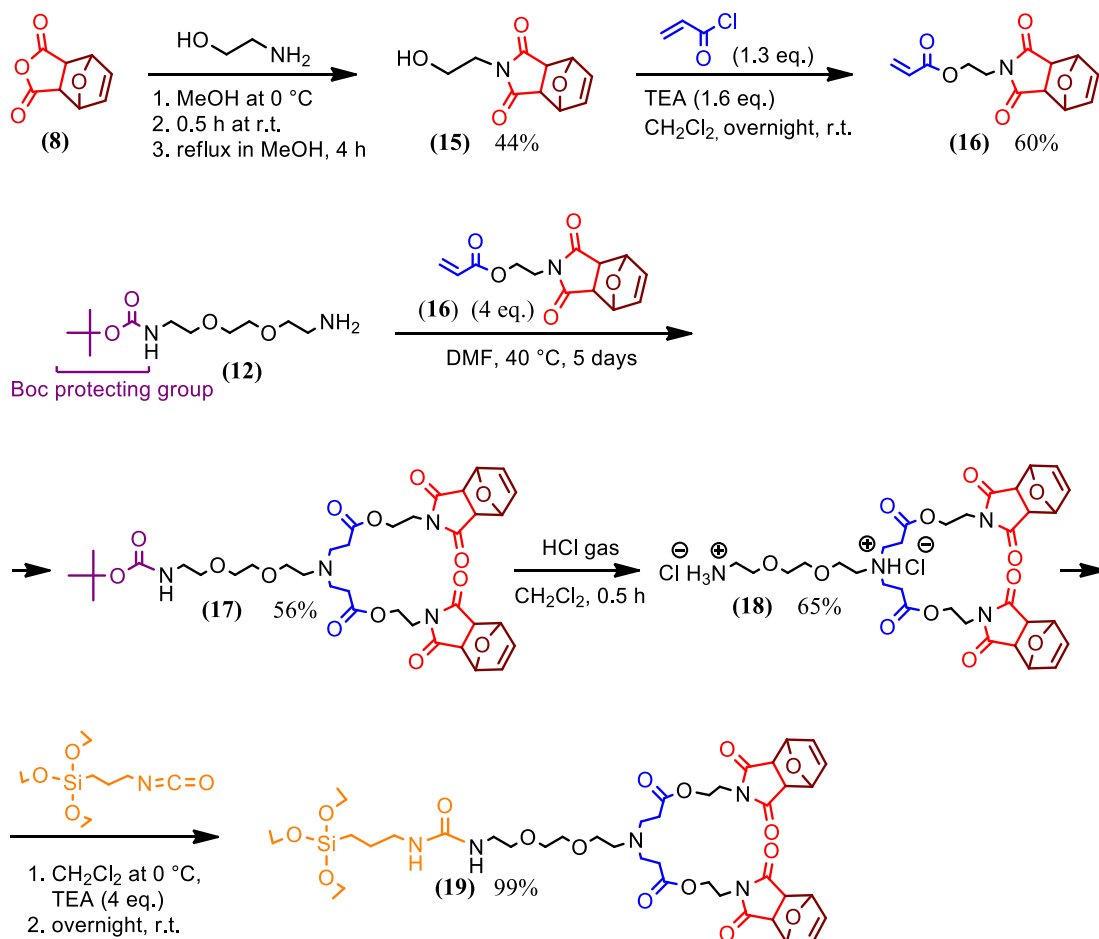
The next step of the synthesis (Scheme II-17) represents the step of the double Michael addition of precursors **12** to the acrylamide **13**. The reaction was carried out in DMF during 5 days. At the end of reaction, the obtained mixture was analysed by NMR ( $^1\text{H}$ ,  $^{13}\text{C}$ , HSQC, DEPT). According to the results, both starting materials remained present in the reaction mixture and there was no evidence of the expected dendritic structure **14** formation. The reaction proceeded for 6 weeks and the NMR analyses ( $^1\text{H}$ ,  $^{13}\text{C}$ , HSQC, DEPT) were repeated. These analyses showed that the amount of acrylamide **13** has diminished and could be caused by the addition of amino group from compound **12** to the acrylamide **13** double bound. In order to check if the compound **14** was formed, a mass analysis was carried out by two technics: Electrospray Ionization (ESI) and Field Desorption (FD). The mass (MS [ $\text{MH}^+$ ] calc = 949.48 g/mol,) corresponding to the expected compound **14** was not found while the mass corresponding to the formation of a compound with only one ramification (MS [ $\text{MH}^+$ ] calc = 599.31 g/mol) was detected.

Consequently, the synthesis according to this strategy (Scheme II-17) was stopped at the step of double Michael addition of precursors **12** to the acrylamide **13**, since the desired two branched structure **14** was not obtained.

### II.3.2.2. Strategy II

This strategy, similarly to the previous one, relies on the synthesis of an acrylate decorated with the furan protected maleimide functionality (Scheme II-19).

The synthesis starts with a reaction between the furan protected maleic anhydride **8** and ethanolamine. This reaction was carried out according to the literature procedure<sup>23a,b</sup> leading to the formation of compound **15** in 44 % yield. The alcohol **15** has a good stability contrary to the amine **10**.

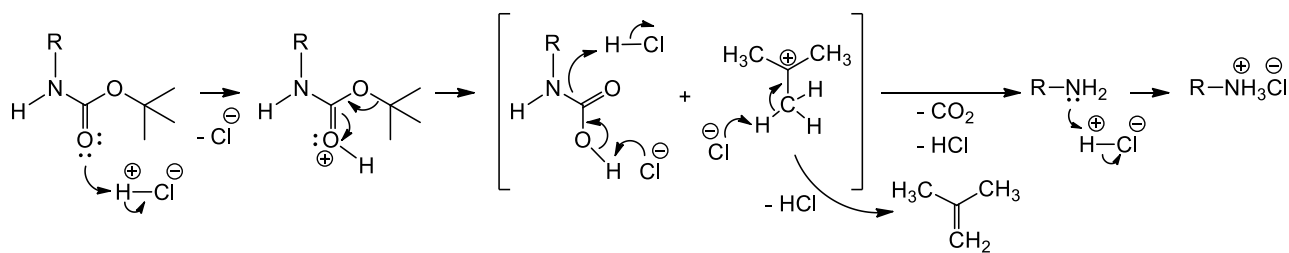
Scheme II-19. Synthesis of two branched coupling agents **18** and **19**.

Next, a reaction between the alcohol **15** and acryloyl chloride was performed. Acryloyl chloride was added dropwise to the mixture of compound **15** and TEA (added in excess) solubilized in freshly distilled DCM that was preliminarily cooled to  $0^\circ\text{C}$ . The mixture was stirred at room temperature overnight under argon atmosphere. The solvent, excess of acryloyl chloride and TEA were evaporated under vacuum. The obtained residue was solubilized in DCM and the TEA•HCl salt was removed by extraction in water. The organic phase was dried under vacuum and purified by column chromatography on silica allowing to obtain compound **16** in 60 % yield. The acrylate **16** possesses a better stability in comparison with acrylamide **13** and can be stored for months.

Afterwards, a Michael type addition of the primary amine **12** to the acrylate **16** was performed. The reaction proceeded in anhydrous dimethylformamide, at  $40^\circ\text{C}$  during 5 days. The two branched structure **17** was then purified by column chromatography on silica gel giving compound **17** in 56 % yield.

The next step of the synthesis is the deprotection of the amino group from compound **17**. Boc protecting group was cleaved by bubbling gaseous hydrogen chloride through the DCM solution of compound **17** during 30 minutes, according to the following mechanism (Scheme II-20):<sup>36</sup>





**Scheme II-20.** Mechanism of Boc protecting group cleavage with gaseous hydrogen chloride.<sup>36</sup>

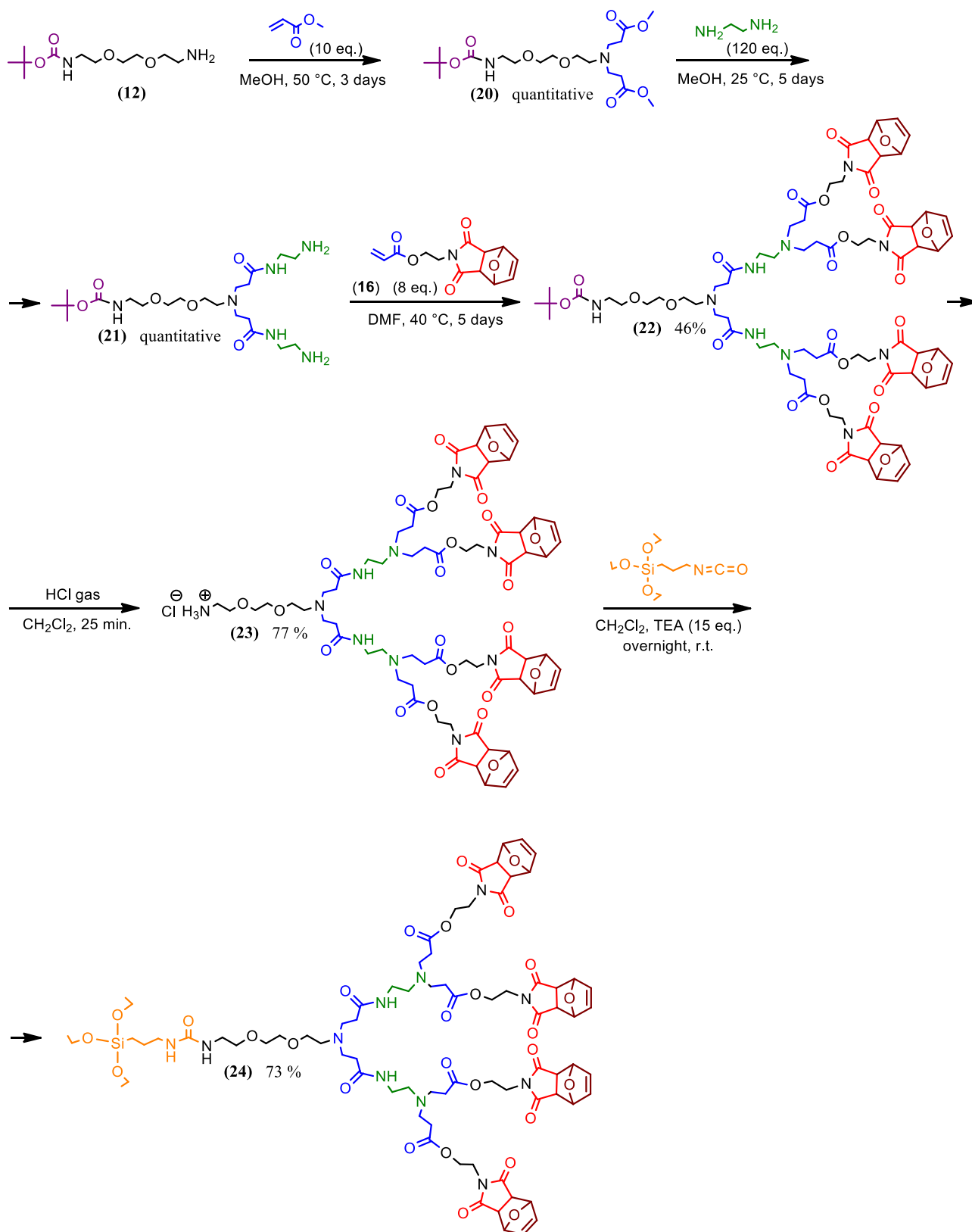
As a result, compound **18** was obtained as an ammonium salt, in 65 % yield (after the purification step). This compound represents the target two branched coupling agent that will be further used for the grafting on MNPs with polymer shell.

To obtaining the analogous silylated two branched coupling agent **19** (for the grafting on MNPs with silica shell) it was necessary to transform the amino-functionality of compound **18** into a silane-functionality. This silane-functionality, was introduced by using triethoxy(3-isocyanatopropyl)silane, similarly as was done to obtain the linear silylated coupling agent **11**. The reaction between triethoxy(3-isocyanatopropyl)silane and compound **18** took place in freshly distilled DCM, in the presence of TEA (taken in excess), since compound **18** was obtained in the protonated form (as an ammonium salt and otherwise it is not soluble in DCM).

Triethoxy(3-isocyanatopropyl)silane was added dropwise to the DCM mixture of compound **18** and TEA (4 eq.) that was preliminarily cooled to 0°C, then the mixture was stirred at room temperature overnight under argon atmosphere. Afterwards, the solvent and the excess of TEA were evaporated. The residue was solubilized in tetrahydrofuran (THF) and the precipitated out TEA•HCl salt was removed by filtration. The solution was concentrated under vacuum to afford the silylated two branched coupling agent **19** in 99 % yield. Compound **19** is hereinafter used for the grafting on MNPs with silica shell.

### II.3.3. Synthesis of second generation (four branched) dendritic coupling agents

In order to keep the structures of four branched dendritic coupling agents very similar to those of the two branched coupling agents' structures, an approach showed in Scheme II-21 was proposed. It was decided to use as a starting materials compound **12**, and the same acrylate **16** for introducing furan protected maleimide functionality at the peripheral sides of the four branched coupling agents' structures. According to this approach, first, it was necessary to synthesize a two branched structure, with two amino groups at the one side and one Boc protected amino group at the other side (compound **21**).



**Scheme II-21.** Synthesis of the four branched dendritic coupling agents **23** and **24**.

The synthesis begins with a double Michael type addition of the primary amine **12** to methyl acrylate. This reaction was carried out in methanol at 50°C during 3 days. At the end of reaction, the

excess of methyl acrylate as well as the reaction solvent were evaporated and compound **20** was obtained in quantitative yield.

Next, the synthesis was followed by the amidation of methyl ester terminal groups from compound **20**. This reaction was carried out in methanol, in the presence of a large excess of ethylenediamine, at 50°C during 5 days. At the end of reaction, the excess of ethylenediamine as well as the solvent were evaporated, affording the two branched structure **21** in quantitative yield.

Afterwards, a Michael type addition of the primary amine **21** to the acrylate **16** was performed. The reaction temperature was lowered to 40°C in order to avoid undesirable retro-DA deprotection of maleimide group. The reaction proceeded in DMF during 5 days. At the end of reaction, the solvent was evaporated and the residue was purified relying on the difference of solubility of the mixture in Toluene. The compound **22** is not soluble in Toluene while the starting material **16** (added in a large excess) is. Based on this difference of solubility, the residue was solubilized in minimum of DCM and added dropwise in a large volume of toluene, and then the solution volume was reduced twice. After several days the precipitated out gluey mass was separated from the solution by decantation and the procedure was repeated again at least four times. By this procedure compound **22** was obtained in 46 % yield.

Next, Boc protecting group was cleaved by bubbling gaseous hydrogen chloride through the compound **22** solubilized in DCM. After several minutes (5 – 10 min.) the product **23** began to precipitate out from the solution. The deprotection was carried out for not more than 25 minutes, since increasing the reaction time can lead to acid hydrolysis (of ester groups) side reaction. The deprotected compound **23** was separated from compound **22** by extraction in water. As a result, compound **23** was obtained as an ammonium salt, in 77 % yield. This compound represents the target four branched coupling agent (dendron of G2) that will be further used for the grafting on MNPs with polymer shell.

The last step of the synthesis represents the transformation of the amino-functionality of compound **23** into its silane analogue **24** that hereinafter is used for the grafting on MNPs with silica shell. The silane-functionality, was introduced by using triethoxy(3-isocyanatopropyl)silane, similarly as was done to obtain the two branched silylated coupling agent **19**.

Compound **23** was dispersed in freshly distilled DCM and 15 equivalents of TEA were added. After few seconds compound **23** solubilized, the solution was cooled to 0°C and isocyanato propyl tri-(etoxy)silane was added dropwise. The reaction proceeded at room temperature, under argon atmosphere, overnight. Afterwards the solvent and the excess of TEA were evaporated, and the residue was purified by gel permeation chromatography. Three successive size exclusion columns with Biorad

S-X3 beads swelled with DCM allowed yielding the four branched silylated coupling agent **24** (dendron of G2) in 73 %.

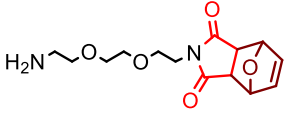
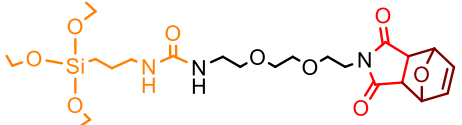
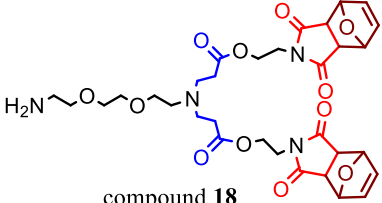
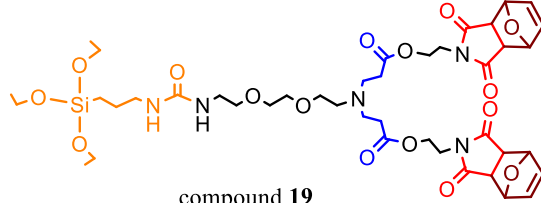
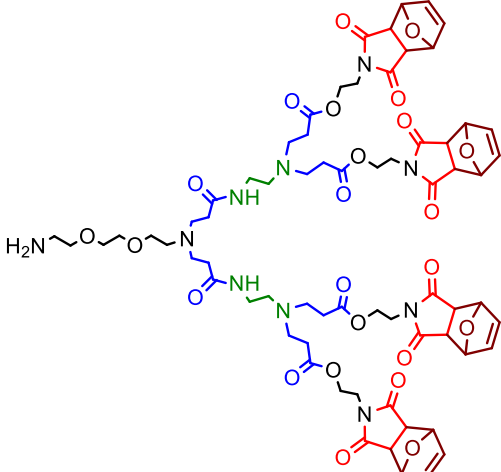
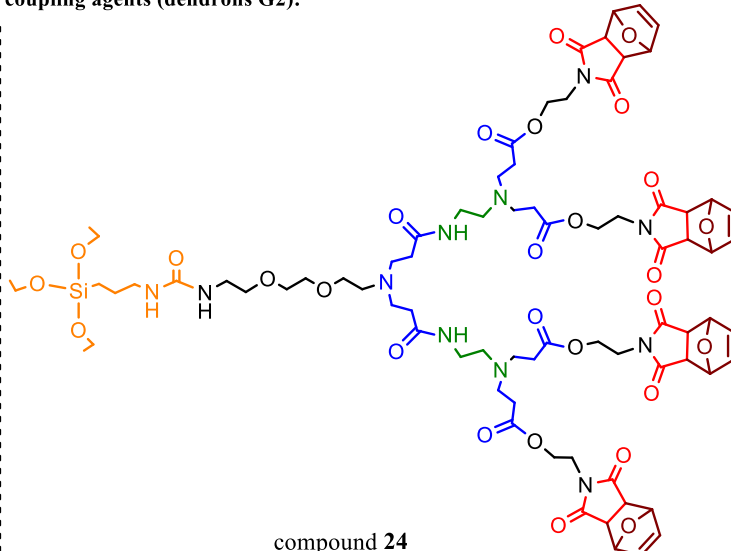
## II.4. Conclusions:

The strategies towards synthesis of linear and dendritic coupling agents of G1 and G2 decorated with maleimide group (protected form) were developed. According to these strategies the protection of maleimide functionality was achieved via Diels-Alder cycloaddition of furan to maleic anhydride followed by a primary amine insertion into the formed Diels-Alder adduct. The resulting succinimide derivative being less labile to nucleophiles than maleimides allowed an efficient protection of maleimide functionality during all the steps of the multistep synthesis, as well as during their grafting on MNPs' surface. The growth of the dendritic generations was performed based on the example of PAMAM denrimers, leading to the dendrons with a well-defined number of functional groups.

Both “*families*” of coupling agents, amino and silane-based coupling agents (Table II-1), were successfully synthesized and characterized. Coupling agents obtained for the grafting on MNPs with polymer shell (linear **10**, two-branched **18** and four-branched **23**) showed a high solubility in water, and it was presumed that they will provide a good dispersion in aqueous solutions after their grafting on MNPs, that is one of the main objectives to achieve. Coupling agents for the grafting on MNPs with silica shell (linear **11**, two-branched **19** and four-branched **24**) are also soluble in water.

The grafting of amino and silane-based coupling agents is described in *Chapter III* and *IV* respectively. Once grafted the maleimide functional group is easily generated via retro-Diels-Alder reaction and represents the final step of the synthesis.

**Table II-1.** Presentation of coupling agents' "families" designed for chemical modification of core-shell MNPs with polymer or silica shell.

The "family" of coupling agents designed for chemical modification of MNPs with polymer shell	The "family" of silylated coupling agents designed for chemical modification of MNPs with silica shell
<p style="text-align: center;"><b>linear coupling agents:</b></p>  <p style="text-align: center;">compound 10</p>	 <p style="text-align: center;">compound 11</p>
<p style="text-align: center;"><b>two-branched coupling agents (dendrons G1):</b></p>  <p style="text-align: center;">compound 18</p>	 <p style="text-align: center;">compound 19</p>
<p style="text-align: center;"><b>four-branched coupling agents (dendrons G2):</b></p>  <p style="text-align: center;">compound 23</p>	 <p style="text-align: center;">compound 24</p>

**References:**

- <sup>1</sup> (a) K. Heuze, D. Rosario-Amorin, S. Nlate, M. Gaboyard, A. Bouter and R. Clerac, *New J. Chem.* **2008**, 32, 383–387.
- <sup>2</sup> (a) J. Bu, R. Li, C. W. Quah and K. J. Carpenter, *Macromolecules* **2004**, 37, 6687–6694; (b) M. Li, L. Q. Xu, L. Wang, Y. P. Wu, J. Li, K.-G. Neoha and E.-T. Kang, *Polym. Chem.* **2011**, 2, 1312–1321.
- <sup>3</sup> (a) D. A. Tomalia, *Sci. Am.* **1995**, 272, 62–66; (b) D. A. Tomalia, J. M. J. Frechet, *J. Polym. Sci. Part A: Polym. Chem.* **2002**, 40, 2719–2728; (c) D. A. Tomalia, H. Baker, J. Dewald, M. Hall, G. Kallos, S. Martin, J. Roeck, J. Ryder and P. Smith, *Polym. J.* **1985**, 17, 117–132; (d) D. A. Tomalia, H. Baker, J. Dewald, M. Hall, G. Kallos, S. Martin, J. Roeck, J. Ryder and P. Smith, *Macromolecules* **1986**, 19, 2466–2468; (e) D. A. Tomalia, M. Hall and D. Hedstrand, *Macromolecules* **1987**, 20, 1164–1167; (f) R. Esfand and D. A. Tomalia, *Drug Discovery Today* **2001**, 6, 427–436; (g) S. Svenson, D. A. Tomalia, *Adv. Drug Delivery Reviews* **2005**, 57, 2106–2129.
- <sup>4</sup> M. Colombo, S. Carregal-Romero, M. F. Casula, L. Gutierrez, M. P. Morales, I. B. Bohm, J. T. Heverhagen, D. Prospero and W. J. Parak, *Chem. Soc. Rev.* **2012**, 41, 4306–4334.
- <sup>5</sup> (a) R. M. De Lorimier, J. J. Smith, M. A. Dwyer, L. L. Looger, K. M. Sali, C. D. Paavola, S. S. Rizk, S. Sadigov, D. W. Conrad, L. Loew, H. W. Hellinga, *Protein Sci.* **2002**, 11, 2655–2675; (b) I. L. Medintz, E. R. Goldman, M. E. Lassman, A. Hayhurst, A.W. Kusterbeck, and J. R. Deschamps, *Anal. Chem.* **2005**, 77, 365–372.
- <sup>6</sup> K. E. Sapsford, W. R. Algar, L. Berti, K. B. Gemmill, B. J. Casey, E. Oh, M. H. Stewart and I. L. Medintz, *Chem. Rev.* **2013**, 113, 1904–2074.
- <sup>7</sup> Z. Janović, A. Jukić, O. Vogl, *Polimeri* **2010**, 31, 14–21
- <sup>8</sup> (a) R. Gref, M. Lück, P. Quellec, M. Marchand, E. Dellacherie, S. Harnisch, T. Blunk, R. H. Müller, *Colloids Surf., B* **2000**, 18, 301–313; (b) H. Shang, W. S. Chang, S. Kan, S. A. Majetich, G. Lee, *Langmuir* **2006**, 22, 2516–2522.
- <sup>9</sup> M. D. Butterworth, L. Illum, S. S. Davis, *Colloids Surf., A* **2001**, 179, 93–102
- <sup>10</sup> (a) K. Nakanishi, T. Sakiyama, Y. Kumada, K. Imamura and H. Imanaka, *Curr. Proteomics* **2008**, 5, 161–175; (b) E. Ostuni, R. G. Chapman, R. E. Holmlin, S. Takayama and G. M. Whitesides, *Langmuir* **2001**, 17, 5605–5620; (c) S. R. Benhabbour, H. Sheardown and A. Adronov, *Macromolecules* **2008**,

41, 4817-4823; (d) S. R. Benhabbour, L. Liu, H. Sheardown and A. Adronov, *Macromolecules* **2008**, 41, 2567–2576.

<sup>11</sup> (a) H. Y. Song, M. H. Ngai, Z. Y. Song, P. A. MacAry, J. Hobley and M. J. Lear, *Org. Biomol. Chem.* **2009**, 7, 3400–3406; (b) J. Zhu, C. Waengler, R. B. Lennox and R. Schirrmacher, *Langmuir* **2012**, 28, 5508–5512; (c) Y. Pan, M. J. C. Long, X. Li, J. Shi, L. Hedstrom and B. Xu, *Chem. Sci.* **2011**, 2, 945–948; (d) N. Matuszak, G. G. Muccioli, G. Labar and D. M. Lambert, *J. Med. Chem.* **2009**, 52, 7410–7420; (e) A. Warnecke, I. Fichtner, D. Garmann, U. Jaehde and F. Kratz, *Bioconjugate Chem.* **2004**, 15, 1349–1359; (f) L. X. Wang, J. Ni and S. Singh, *Bioorg. Med. Chem.* **2003**, 11, 159–166; (g) J. Ni, S. Singh and L. X. Wang, *Bioconjugate Chem.* **2003**, 14, 232–238; (h) A. Szczepanska, J. L. Espartero, A. J. Moreno-Vargas, A. T. Carmona and I. Robina, *J. Org. Chem.* **2007**, 72, 6776–6785; (i) C. Peifer, T. Stoiber, E. Unger, F. Totzke, C. Schachtele, D. Marme, R. Brenk, G. Klebe, D. Schollmeyer and G. Dannhardt, *J. Med. Chem.* **2006**, 49, 1271–1281.

<sup>12</sup> (a) F. Meyer-Losic, J. Quinonero, V. Dubois, B. Alluis, M. Dechambre, M. Michel, F. Cailler, A.-M. Fernandez, A. Trouet and J. Kearsley, *J. Med. Chem.* **2006**, 49, 6908–6916; (b) L. Torrance, A. Ziegler, H. Pittman, M. Paterson, R. Tothb and I. Eggleston, *J. Virol. Methods* **2006**, 134, 164–170.

<sup>13</sup> T. Oishi, H. Nagata and H. Tsutsumi, *Polymer* **1989**, 39, 4135–4146.

<sup>14</sup> (a) P. Y. Reddy, S. Kondo, T. Toru and Y. Ueno, *J. Org. Chem.* **1997**, 62, 2652–2654; (b) W. J. Shu, J. C. Ho and L. H. Perng, *Eur. Polym. J.* **2005**, 41, 149–156.

<sup>15</sup> C. K. Sauers, *J. Org. Chem.* **1969**, 34, 2275–2279.

<sup>16</sup> K. Li, C. Yuan, S. Zheng, Q. Fang, *Tetrahedron Lett.* **2012**, 53, 4245–4247.

<sup>17</sup> (a) O. Mitsunobu and M. Yamada, *Bull. Chem. Soc. Jpn.* **1967**, 40, 2380–2382; (b) O. Mitsunobu, *Synthesis* **1981**, 1, 1–28.

<sup>18</sup> (a) M. A. Walker, *Tetrahedron Lett.* **1994**, 35, 665–668; (b) M. A. Walker, *J. Org. Chem.* **1995**, 60, 5352–5355.

<sup>19</sup> (a) Ph. J. Kocienski, *Protecting Groups*, Foundation of Organic Chemistry Series, G. Thieme V. Stuttgart, New York **1994**; (b) Th. W. Green and P. G. M. Wuts, *Protective Groups in Organic Synthesis* 3<sup>rd</sup> edition, John Wiley & Sons, New York **1999**; (c) A. Isidro-Llobet, M. Alvarez, F. Albericio, *Chem. Rev.* **2009**, 109, 2455–2504.

- <sup>20</sup> (a) <http://www.name-reaction.com/gabriel-synthesis>; (b) S. Gabriel, *Ber. Dtsch. Chem. Ges.* **1887**, 20, 2224–2236.
- <sup>21</sup> (a) S. Billiet, W. V. Camp, X. K.D. Hillewaere, H. Rahier, F. E. Du Prez, *Polymer* **2012**, 53, 2320–2326; (b) T. Dispinar, W. Van Camp, L. J. De Cock, B. G. De Geest, F. E. Du Prez, *Macromol. Biosci.* **2012**, 12, 383–394; (c) B. D. Mather, K. Viswanathan, K. M. Miller, T. E. Long, *Prog. Polym. Sci.* **2006**, 31, 487–531; (d) S. Okumoto, *J. Org. Chem.* **2000**, 65, 1544–1548
- <sup>22</sup> (a) Y. Bi, L. Bailly, F. Marsais, V. Levacher, C. Papamicael and G. Dupas, *Tetrahedron: Asymmetry* **2004**, 15, 3703–3706; (b) G. Shen, A. Horgan, R. Levicky, *Colloids Surf., B: Biointerfaces* **2004**, 35, 59–65.
- <sup>23</sup> (a) G. Mantovani, F. Lecolley, L. Tao, D. M. Haddleton, J. Clerx, J. J. L. M. Cornelissen and K. Velonia, *J. Am. Chem. Soc.* **2005**, 127, 2966–2973; (b) W. H. Heath, F. Palmieri, J. R. Adams, B. K. Long, J. Chute, T. W. Holcombe, S. Zieren, M. J. Truitt, J. L. White and C. G. Willson, *Macromolecules* **2008**, 41, 719–726; (c) T. Dispinar, R. Sanyal and A. Sanyal, *J. Polym. Sci., A: Polym. Chem.* **2007**, 45, 4545–4551; (d) T. Engel and G. Kickelbick, *Chem. Mater.* **2013**, 25, 149–157.
- <sup>24</sup> (a) M. B. Smith, J. March, *March's Advanced organic chemistry: Reactions, Mechanisms, and Structure* – 5<sup>th</sup> edition, John Wiley & Sons, New York **2001**, 1066; (b) A. Ichihara, *Synthesis* **1987**, 207–222; (c) M. Lasne, J. L. Ripoll, *Synthesis* **1985**, 121–143; (d) J. L. Ripoll, A. Rouessac, F. Rouessac, *Tetrahedron* **1978**, 34, 19–40; (e) R. F. C. Brown, *Pyrolytic Methods in Organic Chemistry*, Academic Press, New York **1980**, 259; (f) H. Kwart, K. King, *Chem. Rev.* **1968**, 68, 415–447.
- <sup>25</sup> L. Rulisek, P. Sebek, Z. Havlas, R. Hrabal, P. Capek, and A. Svatos, *J. Org. Chem.* **2005**, 70, 6295–6302.
- <sup>26</sup> (a) A. Sanchez, E. Pedroso and A. Grandas, *Org. Lett.* **2011**, 13, 4364–4367; (b) M. M. Kose, S. Onbulak, I. I. Yilmaz and A. Sanyal, *Macromolecules* **2011**, 44, 2707–2714; (c) L. Billiet, O. Gok, A. P. Dove, A. Sanyal, L.-T. T. Nguyen and F. E. D. Prez, *Macromolecules* **2011**, 44, 7874–7878.
- <sup>27</sup> (a) B. Chen and H. F. Sleiman, *Macromolecules* **2004**, 37, 5866–5872; (b) N. B. Sankaran, A. Z. Rys, R. Nassif, M. K. Nayak, K. Metera, B. Chen, H. S. Bazzi and H. F. Sleiman, *Macromolecules* **2010**, 43, 5530–5537.
- <sup>28</sup> A. W. Bosman, H. M. Janssen, E. W. Meijer, *Chem. Rev.*, **1999**, 99, 1665–1688.
- <sup>29</sup> E. Buhleier, W. Wehner, F. Vogtle, *Synthesis* **1978**, 155–158.
-



- <sup>30</sup> G. R. Newkome, Z.-Q. Yao, G. R. Baker, V. K. Gupta, *J. Org. Chem.* **1985**, 50, 2003–2004.
- <sup>31</sup> (a) A. Calmark, Craig Hawaker, A. Hult, M. Malkoch, *Chem. Soc. Rev.*, **2009**, 38, 352–362; (b) S. M. Grayson and J. M. J. Fréchet, *Chem. Rev.* **2001**, 101, 3819–3867.
- <sup>32</sup> (a) J. Satija, V. V. R. Sai and S. Mukherji, *J. Mater. Chem.* **2011**, 21, 14367–14386; (b) L. Tao, J. Geng, G. Chen, Y. Xu, V. Ladmiral, G. Mantovania and D. M. Haddleton, *Chem. Commun.* **2007**, 3441–3443; (c) S-E. Striba, H. Frey and R. Haag, *Angew. Chem. Int. Ed.* **2002**, 41, 1329–1334. (d) D. Astruc, E. Boisselier, and C. Ornelas, *Chem. Rev.* **2010**, 110, 1857–1959 (e) Y. Wei, Y. Li, N. Zhang, G. Shi, L. Jin, *Ultrasonics Sonochemistry* **2010**, 17, 17–20; (f) G. Navarro, G. Maiwald, R. Haase, A. L. Rogach, E. Wagner, C. Tros de Ilarduya, M. Ogris, *J. Controlled Release* **2010**, 146, 99–105; (g) Y. Cheng, H. Qu, M. Ma, Z. Xu, P. Xu, Y. Fang, T. Xu, *Eur. J. Med. Chem.* **2007**, 42, 1032–1038; (h) M. Ma, Y. Cheng, Z. Xu, P. Xu, H. Qu, Y. Fang, T. Xu, L. Wen, *Eur. J. Med. Chem.* **2007**, 42, 93–98; (i) K. C. Liu and Y. Yeo, *Mol. Pharmaceutics* **2013**, 10, 1695–1704 (j) M. Pohl, N. Michaelis, F. Meister, and Th. Heinze, *Biomacromolecules* **2009**, 10, 382–389.
- <sup>33</sup> (a) J. I. Paez, M. Martinelli, V. Brunetti, M. C. Strumia, *Polymers* **2012**, 4, 355–395; (b) G. R. Newkome, C. N. Moorefield, F. Vögtle, *Dendrimers and dendrons, concept, Syntheses and applications*, **2002**, Wiley-VCH.
- <sup>34</sup> Hakim Rahma Thesis, *Universite de Bordeaux I* **2012**, N° d'ordre: 4393.
- <sup>35</sup> [www.commonorganicchemistry.com/Rxn\\_Pages/Boc\\_Protection/Boc\\_Protection\\_Mech.htm](http://www.commonorganicchemistry.com/Rxn_Pages/Boc_Protection/Boc_Protection_Mech.htm)
- <sup>36</sup> (a) I. W. Ashworth, B. G. Cox and B. Meyrick, *J. Org. Chem.* **2010**, 75, 8117–8125; (b) [www.commonorganicchemistry.com/Rxn\\_Pages/Boc\\_Protection/Boc\\_Protection\\_HCl\\_Mech.htm](http://www.commonorganicchemistry.com/Rxn_Pages/Boc_Protection/Boc_Protection_HCl_Mech.htm)

Chapter III

**Functionalization of core-shell**

**$\gamma$ -Fe<sub>2</sub>O<sub>3</sub>/Polymer**

**magnetic nanoparticles**

**Table of contents:**

III.1. Introduction .....	79
III.2. Presentation of core-shell $\gamma$ -Fe <sub>2</sub> O <sub>3</sub> /Polymer MNPs .....	80
III.3. Surface modification chemistry of core-shell $\gamma$ -Fe <sub>2</sub> O <sub>3</sub> /Polymer MNPs .....	81
III.3.1. Grafting of linear coupling agent 10.....	82
III.3.1.1. General grafting and maleimide functional group deprotection procedures.....	82
III.3.1.2. Characterization of functionalized $\gamma$ -Fe <sub>2</sub> O <sub>3</sub> /Polymer MNPs.....	84
III.3.2. Optimization of grafting conditions.....	92
III.3.2.1. Influence of the loading in the grafting process of coupling agent 10.....	92
III.3.2.2. Influence of the loading in the grafting process of coupling agent 18.....	96
III.3.2.3. Influence of the loading in the grafting process of coupling agent 23.....	98
III.3.3. Comparative study - dendritic coupling agents versus linear coupling agent.....	101
III.3.3.1. Evolution of surface functionalization .....	101
III.3.3.2. Zeta potential measurements .....	103
III.3.3.3. Colloidal state of maleimide functionalized $\gamma$ -Fe <sub>2</sub> O <sub>3</sub> /Polymer MNPs in water .....	105
III.3.3.4. Covalent coupling of thiol modified biotin with maleimide functionalized $\gamma$ -Fe <sub>2</sub> O <sub>3</sub> /Polymer MNPs and consequent recognition by streptavidin coated gold NPs .....	106
III.3.3.5. Immobilization of amino functionalized gold nanoparticles on maleimide functionalized $\gamma$ -Fe <sub>2</sub> O <sub>3</sub> /Polymer MNPs.....	112
III.3.3.6. Covalent coupling of thiol modified oligonucleotide with maleimide functionalized $\gamma$ -Fe <sub>2</sub> O <sub>3</sub> /Polymer MNPs.....	114
III.4. Conclusion.....	117

### III.1. Introduction

In the recent years, considerable efforts have been dedicated to the development of highly reactive NP materials for biomolecules immobilization.<sup>1,2</sup> In this context, a major focus of research in chemical biology is directed towards creating a NP material that would covalently bind a biomolecule (without perturbing its structure or functional groups) and, at the same time, would limit the nonspecific adsorption. Thus, the development of a novel NP material for biomolecules immobilization continues to be at the forefront of NPs' chemistry.

Among the wide variety of NPs<sup>1</sup>, IONPs can be listed between the most extensively used types of NPs in this area. This intense interest is mainly justified by their unique size dependent properties that make IONPs very attractive for various applications in biomedical and materials engineering.<sup>2</sup> One of these specific size-dependent properties is SP. The SP phenomenon appears when the ferromagnetic NP is smaller than the typical size of the magnetic domains.<sup>3</sup> In this case, NPs are characterized by paramagnetic behaviour. As a result SP NPs are prone to elevated magnetization when subjected to a magnetic field and revert to their non-magnetized state upon field removal with a null or negligible remnant magnetization. This interesting property avoids NPs aggregation and consequently results in their colloidal stability in the absence of magnetic field.

Combining the SP behaviour of NPs with their rational functionalization allows creating a powerful tool that is in strong demand in various fields of biotechnology. The usefulness of such material in biotechnology consists in the possibility to be easily manipulated using an external magnetic field (a simple magnet) minimizing the number of separation and purification steps that usually present additional drawbacks.

This chapter is dedicated to the functionalization and characterization of the IO core-shell MNPs ( $\gamma$ -Fe<sub>2</sub>O<sub>3</sub>/polymer) developed and commercialized by Ademtech SA.<sup>4</sup> In the beginning of this chapter a brief description of MNPs with polymer shell is presented, with the support of a transmission electron microscopy (TEM) image of the particles and their schematical representation. Next, a detailed description of the surface modification principles is illustrated, followed by the grafting procedures, as well as the adjustment of the grafting conditions for each coupling agent. These procedures take into account the parameters which can essentially influence the grafting quality, such as the choice of the dispersion medium, temperature, pH and the quantity of coupling agents.

The surface modification chemistry has been mainly controlled via Fourier Transformed Infrared Spectrometry (FT-IR) in Attenuated Total Reflectance (ATR) mode. The surface modification of MNPs functionalized with linear coupling agent **10** was also investigated using Thermogravimetric

Analyses (TGA) coupled with Mass Spectrometry (MS). The integrity of the maleimide functionalized MNPs has been monitored by TEM. The colloidal state of final maleimide functionalized MNPs dispersed in water was observed via Transmitted Light Microscopy. The surface charge of the final maleimide functionalized MNPs was estimated by Zeta Potential ( $\zeta$ ) measurements in a range of pH from 3.6 to 8.0, that also gives an indication of the stability of the colloidal system. The combination of these technics gave the possibility to fully characterize the functionalization of MNPs.

Finally, the efficiency of maleimide functionalized MNPs was studied by performing a series of immobilization tests.

### III.2. Presentation of core-shell $\gamma\text{-Fe}_2\text{O}_3$ /Polymer MNPs

In this work, the surface modification chemistry was carried out on 300 nm core-shell MNPs. These MNPs consist of the maghemite ( $\gamma\text{-Fe}_2\text{O}_3$ ) ferrofluid core, coated with a polymer shell based on highly cross-linked functional polystyrene (Figure III-1).

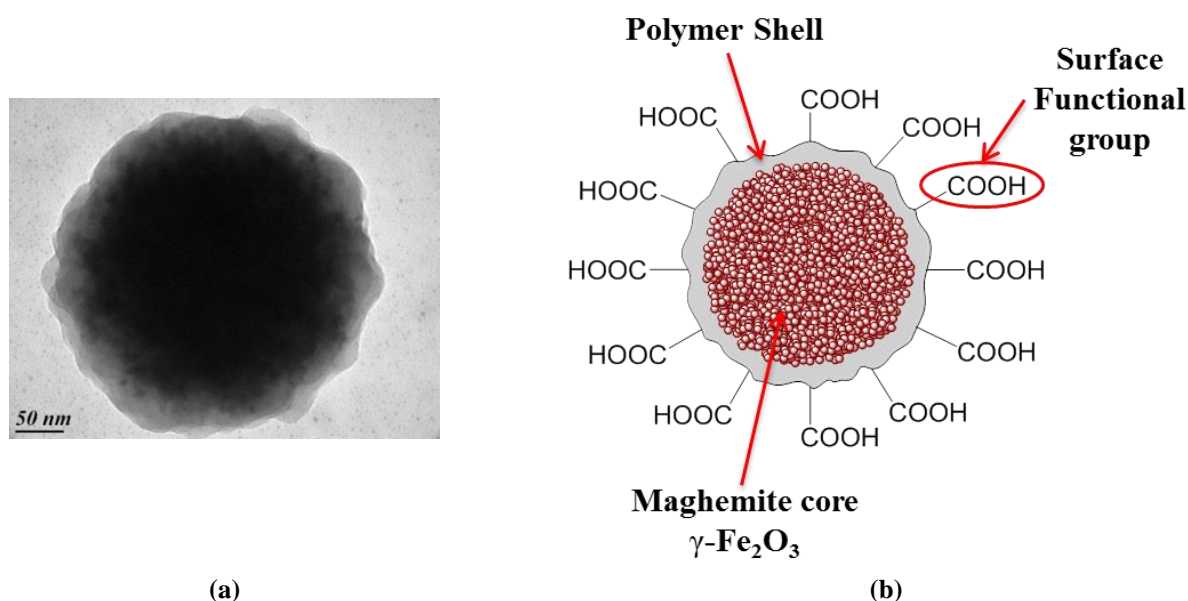


**Figure III-1.** (a) TEM image of the core-shell  $\gamma\text{-Fe}_2\text{O}_3$ /Polymer MNPs; (b) Schematic representation of the core-shell  $\gamma\text{-Fe}_2\text{O}_3$ /Polymer MNPs.

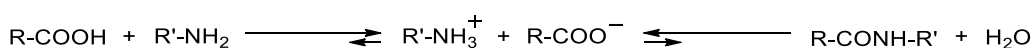
This ferrofluid is composed of nano-sized particles (diameter  $\leq 10$  nm, that are smaller or below the typical size of magnetic domains) which are stabilized in a fluid (surfactants). These are magnetically independent preserving the SP behaviour of the entire MNP. In other words, they exhibit paramagnetic properties only when placed within a magnetic field and show no residual magnetization when removed from this field. Specifically, due to the high magnetic content (70 %) of the SP IONPs these 300 nm MNPs manifest a fast and high answer to an external magnetic field (Magnetization at

saturation: approx. 40 cm<sup>3</sup>/g at 300 K), therefore offering a fast, easy and cheap method of separation from the reaction medium (superior to 99 % in 1 min.). It is noteworthy that smaller core-shell MNPs usually hold a smaller magnetic content and consequently need more time for magnetization, while increasing the MNPs' size affects their colloidal stability. Thereby this size (300 nm) of core-shell MNPs is more appropriate for envisaged applications in immobilization and separation of biomolecules. These  $\gamma$ -Fe<sub>2</sub>O<sub>3</sub>/Polymer MNPs have already been successfully used in our group (C2M) in the field of catalysis,<sup>5</sup> and in the field of biotechnology in other groups.<sup>6</sup>

The hydrophilic polymer coating holds the ferrofluid in the centre of the particle ensuring at the same time several functions: (I) it protects the core ( $\gamma$ -Fe<sub>2</sub>O<sub>3</sub>) against the degradation and isolates it from the reaction medium (for example in biological applications IONPs can interfere with some enzymatic reactions); (II) stabilizes MNPs by preventing aggregation and provides their excellent dispersion abilities; (III) ensures low non-specific binding; and (IV), the most important, offers an efficient surface for functionalization. These core-shell ( $\gamma$ -Fe<sub>2</sub>O<sub>3</sub>/Polymer) MNPs have a high surface area available for specific coupling (15 m<sup>2</sup>/g) bearing as surface functional group carboxylic acid functionality in a high density (COOH density: > 350  $\mu$ mol/g) that offer the possibility of various surface modifications via carbodiimide chemistry. Ademtech has developed simple and reproducible protocols for coupling proteins onto nanoparticles, yielding high binding capacities while keeping non-specific binding low and ensuring long-term stability. Nevertheless, it is still in strong demand to extend protocols involving modification of functional groups on MNPs' surface for each coupling agent apart.

### III.3. Surface modification chemistry of core-shell $\gamma$ -Fe<sub>2</sub>O<sub>3</sub>/Polymer MNPs

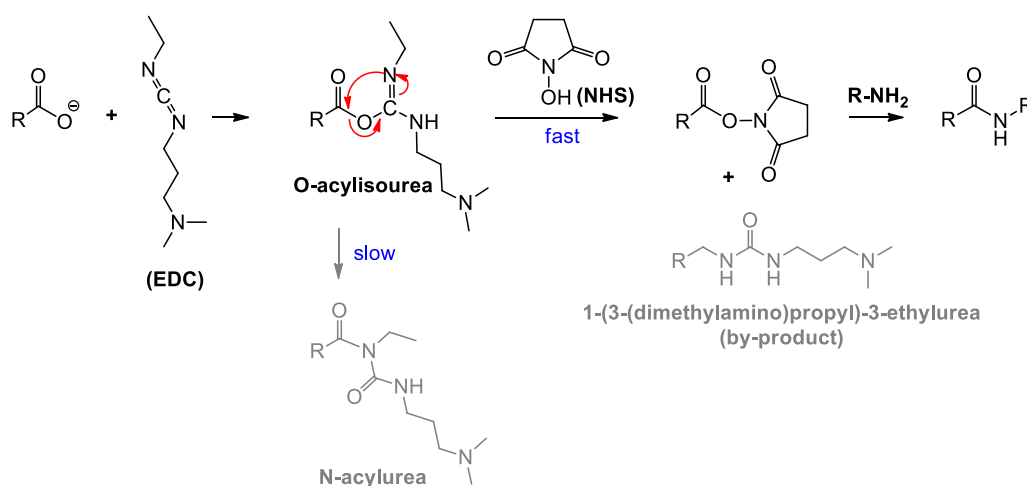
As aforesaid, the surface of  $\gamma$ -Fe<sub>2</sub>O<sub>3</sub>/Polymer MNPs bears carboxylic acid functionalities. It is known that on mixing of a carboxylic acid with an amine, an acid – base reaction occurs first to form a stable salt. Thus, the amide bond formation has to fight against the adverse thermodynamics as the equilibrium shown in the Scheme III-1.<sup>7</sup>



**Scheme III-1.** Schematic representation of amide bond formation.<sup>7</sup>

Therefore, the activation of the carboxylic groups is necessary to allow the attack by the amino group. For this purpose carbodiimides are often used as a carboxyl activating agents to yield amide bonds formation. The most commonly used carbodiimides are the water-soluble EDC

(*N*-Ethyl-*N'*-(3-dimethylaminopropyl)carbodiimide) for aqueous crosslinking and the water-insoluble DCC (N,N'-Dicyclohexylcarbodiimide) for non-aqueous organic synthesis methods. The carbodiimide reacts with the carboxylic acid to form the *O*-acylisourea mixed anhydride, which can then directly react with the amine to yield the desired amide and the urea by-product. However, a more complex mechanism might co-exist. The *O*-acylisourea intermediate is unstable in aqueous solutions and instead of reacting with an amine it can hydrolyse, thus regenerating the carboxylic acid and releasing an unreactive *N*-acylurea (see Scheme III-2).<sup>7,8</sup> This side reaction can be considerably decreased by adding of a nucleophile that reacts faster than the competing acyl transfer and generates a more reactive amine-product to couple with the amine. Among such nucleophiles, the most widely used for the amide (or ester) bond formation are DMAP (4-Dimethylaminopyridine), NHS (N-hydroxysuccinimide) and its water-soluble analogue Sulfo-NHS or HOBt (hydroxybenzotriazole).



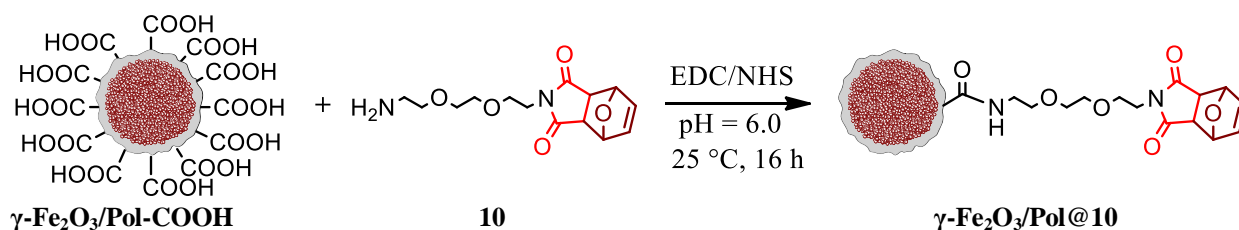
**Scheme III-2.** Schematic representation of EDC/NHS coupling, where EDC activates the carboxylate and NHS increases the coupling efficiency and decreases the side reactions.

This well-known and efficient synthetic approach was successfully applied in the following work for the surface modifications of  $\gamma$ -Fe<sub>2</sub>O<sub>3</sub>/Polymer MNPs with the amino functional coupling agents reported in Chapter II.

### III.3.1. Grafting of linear coupling agent 10

#### III.3.1.1. General grafting and maleimide functional group deprotection procedures

The first attempts of functional groups modification on the surface of  $\gamma$ -Fe<sub>2</sub>O<sub>3</sub>/Polymer MNPs were done by grafting the linear coupling agent **10** (Scheme III-3). The protocol of the grafting proceeds via EDC/NHS chemistry (Scheme III-2) based on the protocol developed by our group in the frame of the PhD thesis of D. Rosario-Amorin.<sup>9</sup>

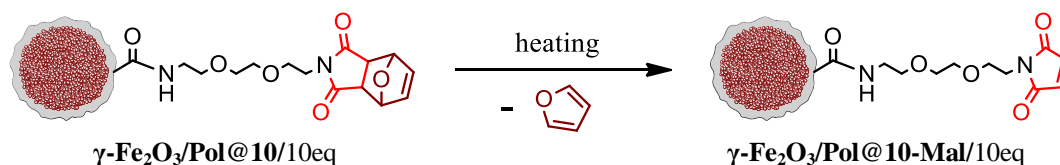


**Scheme III-3.** Grafting of linear coupling agent **10** on  $\gamma\text{-Fe}_2\text{O}_3$ /Polymer MNPs. The maleimide functionality of linear coupling agent **10** is in a protected form.

The colloidal stability of  $\gamma\text{-Fe}_2\text{O}_3$ /Polymer MNPs was ensured by employing Pluronic F-127 (PF) surfactant. This surfactant acts at the same time as an antifoaming agent, since foaming can occur during sample sonication. Solubilisation of this surfactant in water, however, leads to a decrease of the pH of solution. Therefore, the pH of solution was adjusted to 6.0 (suitable for the EDC/NHS coupling) by adding 4-Morpholineethanesulfonic acid (MES).

Assuming that polymer coated  $\gamma\text{-Fe}_2\text{O}_3$  MNPs contain around 350  $\mu\text{mol}$  of carboxylic groups per 1 g of particles, for the first grafting experiment 10 equivalents of linear coupling agent **10** (per equivalent of COOH groups) were loaded. During the grafting reaction, the particles remained well dispersed and no sedimentation or aggregation was observed, proving that the colloidal stability was not affected. At the end of the grafting reaction, MNPs were separated from the reaction mixture by magnetic decantation and the supernatant was carefully pipetted off. Next, the resulting MNPs ( $\gamma\text{-Fe}_2\text{O}_3/\text{Pol@10}/10\text{eq}$ ) were analysed by TEM, FT-IR spectroscopy and TGA coupled with MS, and the results are discussed in the following paragraphs.

Once the coupling agent **10** is grafted, the maleimide protection must be cleaved, thus generating maleimide functionalized MNPs ( $\gamma\text{-Fe}_2\text{O}_3/\text{Pol@10-Mal}/10\text{eq}$ ). The cleavage of *furan* protection represents a retro Diels-Alder reaction that can be achieved by simply heating of MNPs up to temperatures around  $100^\circ\text{C}$  (Scheme III-4).



**Scheme III-4.** Deprotection of maleimide functional group with release of furan after heating the sample at temperatures of around  $100^\circ\text{C}$ .

Several procedures to perform the retro-Diels-Alder reaction are described in the literature, most often the deprotection is achieved by refluxing in toluene.<sup>10</sup> Also, it can be performed by microwave irradiation<sup>11</sup> or by simply heating under vacuum.<sup>12</sup> In our case, none of these procedures are convenient: the reflux in toluene cannot be carried out because of the bad dispersion of MNPs in



toluene; the deprotection by microwave irradiation cannot be done due to the IO core of MNPs; and finally, the deprotection by heating under vacuum is not possible because of the absence of a device which will ensure at the same time the heating, vacuum and mechanical stirring. Thus, the deprotection of maleimide group on  $\gamma\text{-Fe}_2\text{O}_3/\text{Pol}@10/10\text{eq}$  was performed by heating the particles dispersed in a polar aprotic solvent (DMSO anhydrous) under mechanical stirring, according to the Scheme III-4.

### III.3.1.2. Characterization of functionalized $\gamma\text{-Fe}_2\text{O}_3$ /Polymer MNPs

#### a) Transmission Electron Microscopy

TEM allows investigating the morphological changes (size, shape etc.) that can occur on the MNPs' surface upon the surface modification chemistry and provides direct information about the particles' integrity. Therefore, the native MNPs ( $\gamma\text{-Fe}_2\text{O}_3/\text{Pol-COOH}$ ), MNPs obtained after the grafting of linear coupling agent **10** ( $\gamma\text{-Fe}_2\text{O}_3/\text{Pol}@10/10\text{eq}$ ) as well as MNPs obtained after the deprotection step ( $\gamma\text{-Fe}_2\text{O}_3/\text{Pol}@10\text{-Mal}/10\text{eq}$ ) were analysed by TEM (Figure III-2).

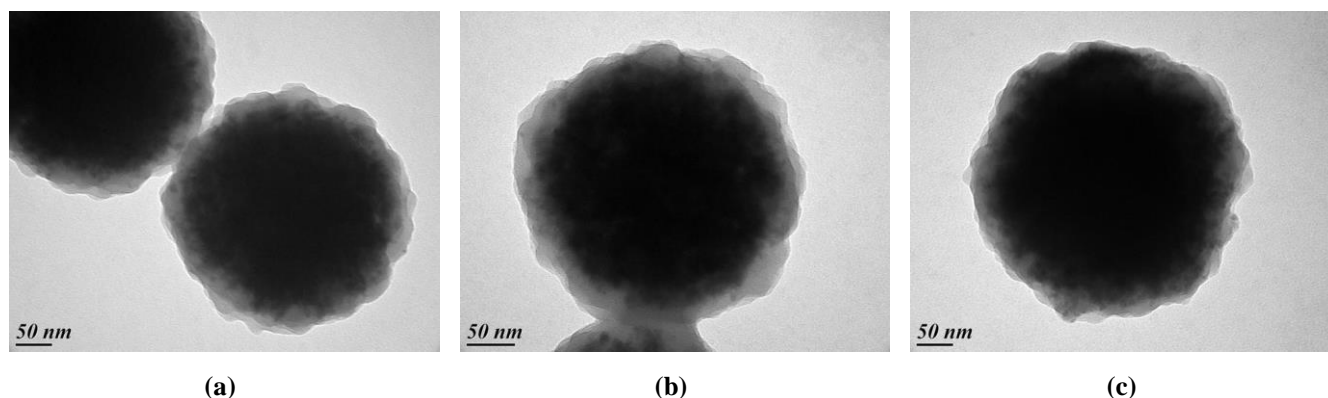


**Figure III-2.** TEM images of (a) native  $\gamma\text{-Fe}_2\text{O}_3/\text{Pol-COOH}$  MNPs; (b) MNPs obtained after the grafting of linear coupling agent **10** ( $\gamma\text{-Fe}_2\text{O}_3/\text{Pol}@10/10\text{eq}$ ); and (c) MNPs obtained after the deprotection step ( $\gamma\text{-Fe}_2\text{O}_3/\text{Pol}@10\text{-Mal}/10\text{eq}$ ).

As observed from TEM images (Figure III-2) the general aspect of MNPs did not show any significant differences after the surface modification. The shape and size of modified MNPs remained comparable with that of native  $\gamma\text{-Fe}_2\text{O}_3$ /Polymer MNPs. It should be noted that for these particles the change of the shell size cannot be measured precisely from TEM image due to the high rugosity of polymer coating. Also, these results confirm that the experimental conditions of the deprotection step (DMSO, 99°C, 5 h.) do not affect the integrity of MNPs.

#### b) Infrared Spectroscopy Study

The surface modification chemistry of MNPs has been followed by FT-IR spectrometry. The FT-IR spectra were recorded using an ATR accessory that allows direct comparison of samples due to the fixed penetration depth of the IR radiation on the sample. Thus, the relative intensity of the

coupling agent's absorption bands can be directly related to the amount of grafted compound on MNP's surface.

With the aim to analyse the characteristic IR bands for linear coupling agent **10**, the FT-IR spectrum of the organic molecule was first recorded (Figure III-3).

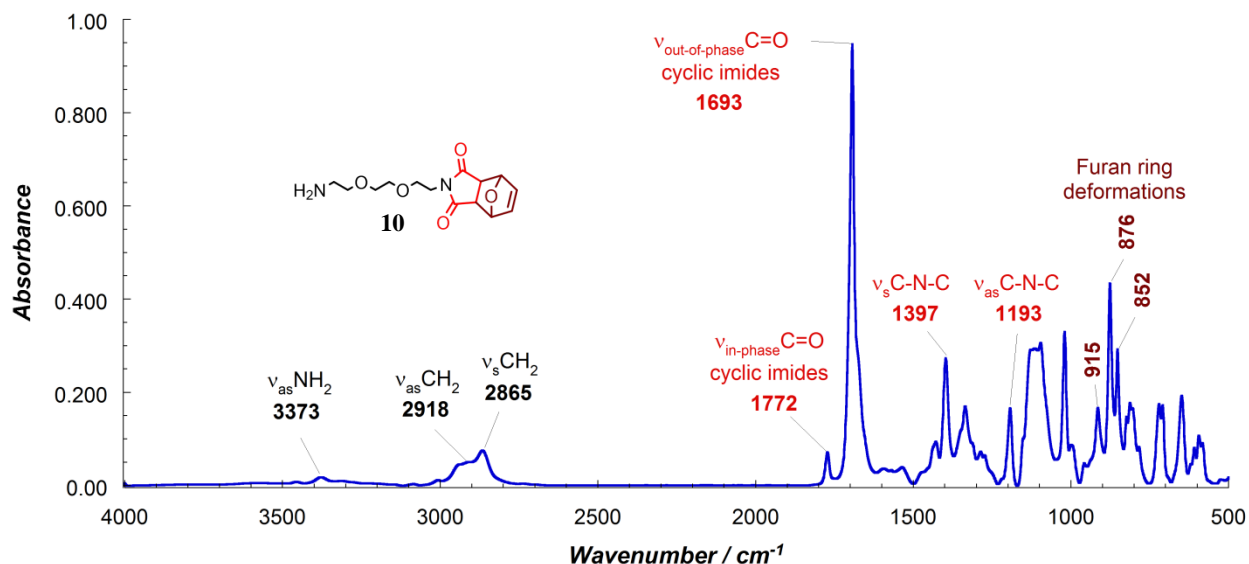


**Figure III-3.** ATR FT-IR spectrum of coupling agent **10**.

In the high energy infrared region, the spectrum of linear coupling agent **10** showed the presence of a very weak peak at  $3373\text{ cm}^{-1}$  characteristic to the antisymmetric  $\text{NH}_2$  stretching vibration, and two peaks at  $2918\text{ cm}^{-1}$  and  $2865\text{ cm}^{-1}$  characteristic to the antisymmetric and symmetric CH stretching vibrations of  $-\text{O}-\text{CH}_2$  groups.<sup>13</sup>

In the carbonyl region, two peaks are present, at  $1772\text{ cm}^{-1}$  (weak) and at  $1693\text{ cm}^{-1}$  (strong). These two peaks are characteristic to the in-phase ( $1772\text{ cm}^{-1}$ ) and out-of-phase ( $1693\text{ cm}^{-1}$ ) stretching vibrations of the two  $\text{C}=\text{O}$  groups present in five membered cyclic imide rings, such as maleimides, succinimides and phthalimides.<sup>13,14</sup>

At lower wavenumbers, several other characteristic peaks are observed, such as the bands at  $1397\text{ cm}^{-1}$  and  $1193\text{ cm}^{-1}$  that involve symmetric and antisymmetric C-N-C stretch,<sup>15</sup> as well as several bands at  $915\text{ cm}^{-1}$ ,  $876\text{ cm}^{-1}$  and  $852\text{ cm}^{-1}$ , characteristic to the furan ring deformation.<sup>13,16</sup>

The out-of-phase  $\text{C}=\text{O}$  band seen at  $1693\text{ cm}^{-1}$  represents the strongest absorption band in the whole spectrum, and therefore represents a powerful tool for investigating the efficiency of the grafting reaction.

The ATR spectra of native MNPs ( $\gamma\text{-Fe}_2\text{O}_3$ /Pol-COOH), MNPs resulted after the grafting reaction ( $\gamma\text{-Fe}_2\text{O}_3$ /Pol@10/10eq) and MNPs obtained after the deprotection step ( $\gamma\text{-Fe}_2\text{O}_3$ /Pol@10-Mal/10eq) are presented in Figure III-4.

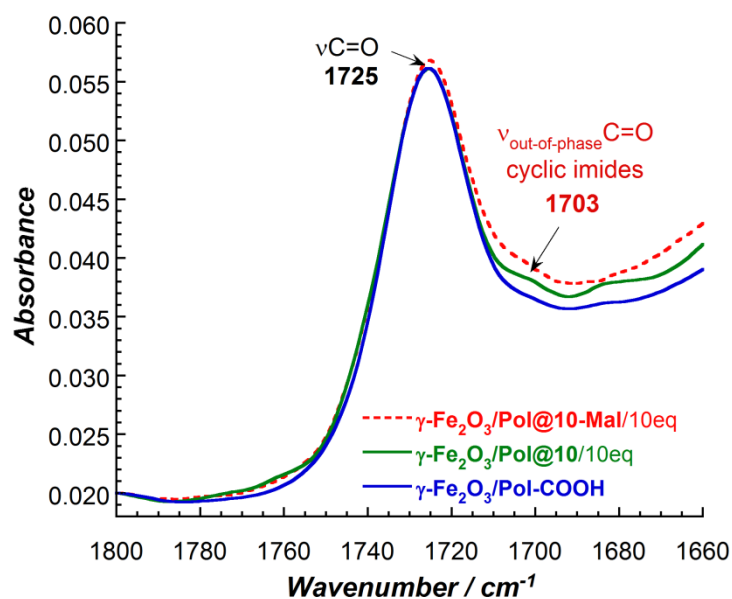


**Figure III-4.** ATR FT-IR spectra of native MNPs ( $\gamma\text{-Fe}_2\text{O}_3$ /Pol-COOH) in blue; MNPs resulted after the grafting reaction ( $\gamma\text{-Fe}_2\text{O}_3$ /Pol@10/10eq) in green; and MNPs obtained after the deprotection step ( $\gamma\text{-Fe}_2\text{O}_3$ /Pol@10-Mal/10eq) in red.

The spectrum of native  $\gamma\text{-Fe}_2\text{O}_3$ /Polymer MNPs (in blue) shows a strong band at  $1725\text{ cm}^{-1}$  assigned to the carboxyl groups resulting from the polymer coating. The intensity of this band remains nearly constant after the grafting of linear coupling agent **10**, since most of the carbonyl groups are immersed in the polymer matrix and are not available for the surface modification chemistry.

The efficiency of grafting reaction was estimated by monitoring the strongest IR band of linear coupling agent **10**, namely, the out-of-phase C=O band (observed for compound **10** at  $1693\text{ cm}^{-1}$ , Figure III-3). The spectrum of  $\gamma\text{-Fe}_2\text{O}_3$ /Pol@10/10eq (Figure III-4, in green) showed that after the grafting of coupling agent **10**, this band has slightly shifted from  $1693\text{ cm}^{-1}$  to  $1703\text{ cm}^{-1}$ . However, the intensity of this band showed to be very weak, suggesting a very low surface coverage. The spectrum of  $\gamma\text{-Fe}_2\text{O}_3$ /Pol@10-Mal/10eq (Figure III-4, in red) did not show any evident changes comparing to the spectrum of  $\gamma\text{-Fe}_2\text{O}_3$ /Pol@10/10eq (Figure III-4, in green). Therefore, at this stage the cleavage of furan protection remained unconfirmed.

To conclude, the FT-IR spectroscopy investigation confirmed the presence of the organic molecule **10** on MNPs' surface. However, the grafting of compound **10** in these reaction conditions showed a very low surface coverage. Moreover, this study did not confirm the deprotection step of the maleimide group.

## c) Thermogravimetric Analysis coupled with Mass Spectrometry

The surface coverage of the modified MNPs was then characterized by TGA coupled with MS. TG analysis on its own can provide direct information about the quantity of organic components present on MNPs' surface. Also it allows performing a study regarding the thermal stability of the sample as well as the determination of the thermal decomposition steps. The Mass Spectrometer, on its turn, ionizes the molecules which are eliminated in the process of thermal decomposition (during the same experiment) and then detects the mass of formed ions. Therefore, the combination of these techniques affords the possibility to associate the mass loss observed in TGA with the corresponding key fragment ion detected via MS at the given range of temperatures. Particularly, in our case, the combination of these techniques allowed to confirm the presence of the grafted coupling agent by monitoring in MS, the molecular fragment ion of *furan*. *Furan* represents a component part of the grafted coupling agent **10** and is responsible for the protection of the maleimide functional group. Since, the TG analysis involves heating of the sample up to high temperatures, the deprotection reaction (Scheme III-4) will naturally occur during the experiment, generating the release of *furan* that can be detected in MS ( $m/z = 68.06$ ).

With the aim to investigate the thermal decomposition processes of the modified MNPs, three TG analyses coupled with MS were performed for: native MNPs ( $\gamma$ -Fe<sub>2</sub>O<sub>3</sub>/Pol-COOH); MNPs after the grafting of linear coupling agent **10** ( $\gamma$ -Fe<sub>2</sub>O<sub>3</sub>/Pol@**10**/10eq); and MNPs after the deprotection of maleimide functional group ( $\gamma$ -Fe<sub>2</sub>O<sub>3</sub>/Pol@**10**-Mal/10eq).

In the case of  $\gamma$ -Fe<sub>2</sub>O<sub>3</sub>/Pol-COOH sample, the total mass loss estimated from TGA after heating the sample to 600°C constitutes 35.78 % (Figure III-5). This mass loss represents the mass of organic components (polymer coating of MNPs and adsorbed water and/or solvents) present on MNPs.

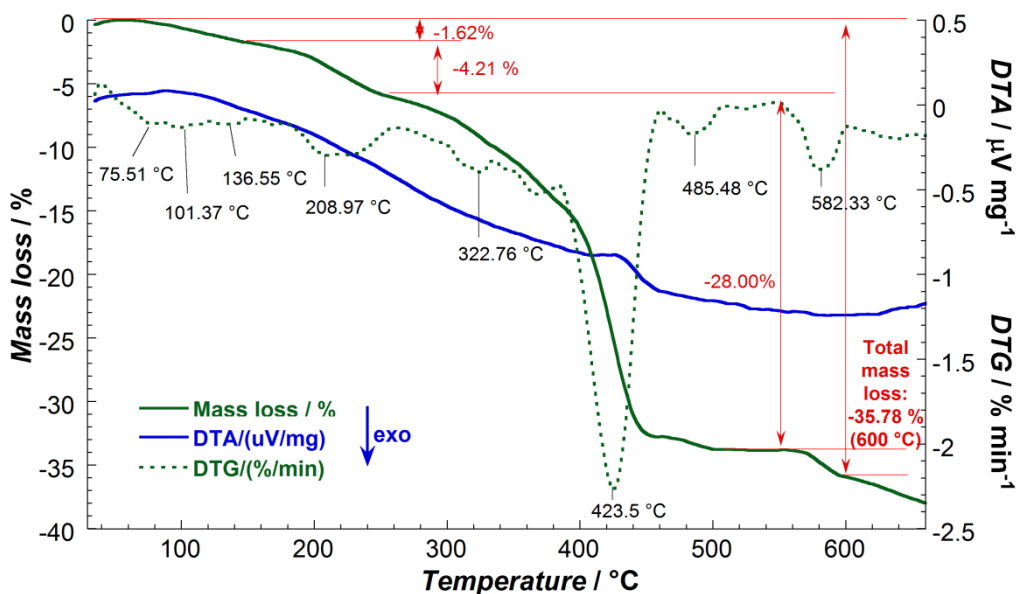
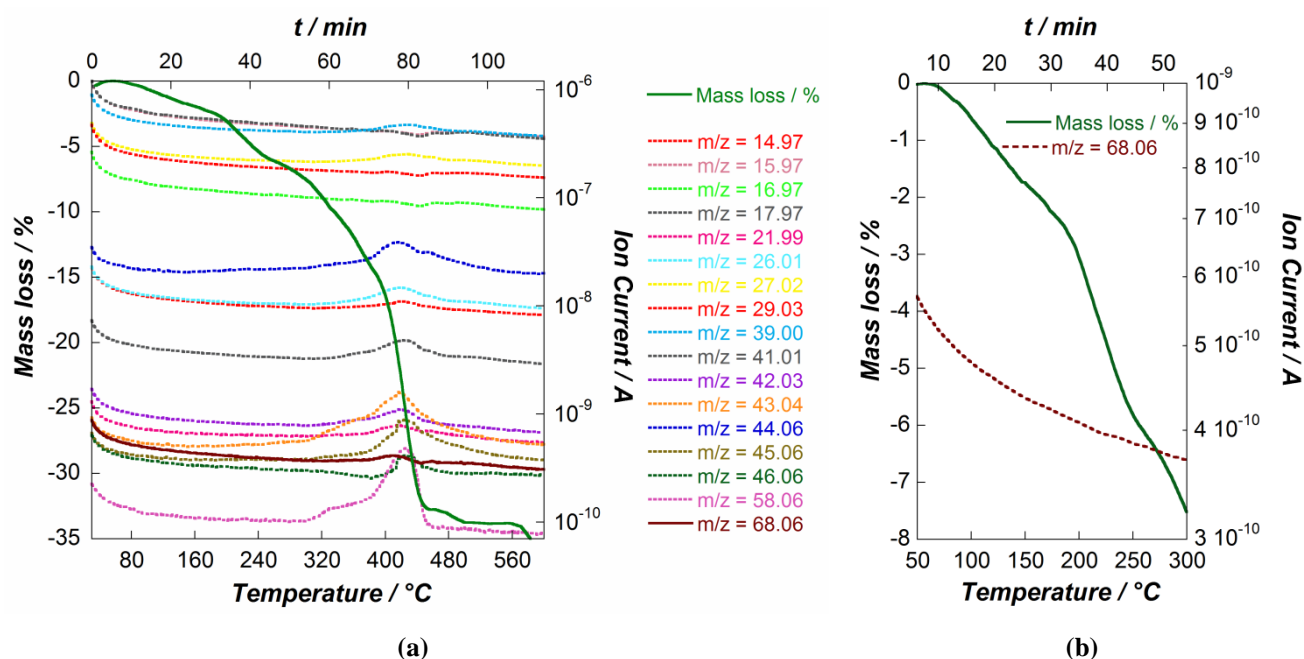


Figure III-5. TG measurement of native MNPs ( $\gamma$ -Fe<sub>2</sub>O<sub>3</sub>/Pol-COOH).

The temperature dependent mass loss of  $\gamma$ -Fe<sub>2</sub>O<sub>3</sub>/Pol-COOH (Figure III-5) revealed three discernible steps: first from 30°C to 150°C; second from 150°C to 240°C and third from 240°C to 600°C. In the derivative of the thermogravimetric curve (DTG), several well-defined peaks corresponding to the occurring thermal decomposition processes are observed. These thermal decomposition processes were explained by combining the mass loss curve from TGA with the corresponding key ion currents detected in MS at the given range of temperatures (Figure III-6 a). Each detected ion current corresponds to a key fragment that can be associated to a probable parent molecule (see Table 1 from reference 17).<sup>17</sup>

In the first step (30°C – 150°C) the release of adsorbed water and ethanol onto MNPs' surface is observed. This mass loss constitutes around 1.62 % of total mass loss. The second step (150°C – 240°C) mainly corresponds to the continued release of ethanol and represents 4.21 % of the total mass loss. The third step (240°C to 600°C) showed an intense emission of acetone, ethanol, carbon dioxide, carbon monoxide, water and other molecular fragments and represents the thermal decomposition of polymer coating. This step constitutes 28.00 % of the total mass loss.

According to the MS (Figure III-6 b), no ion current with  $m/z = 68.06$  was detected in the range of temperatures from 50°C to 250°C (correspond to the range of temperatures when the retro Diels-Alder reaction occurs). The absence of this ion current is of high importance since it allows verifying the cleavage of furan protection (retro Diels-Alder reaction) on modified MNPs ( $\gamma$ -Fe<sub>2</sub>O<sub>3</sub>/Pol@10/10eq).



**Figure III-6.** (a) Combination of the mass loss curve from TGA for native MNPs ( $\gamma$ -Fe<sub>2</sub>O<sub>3</sub>/Pol-COOH) with the corresponding ion currents detected in MS in the range of temperatures between 30°C and 600°C; and (b) Combination of the mass loss curve from TGA for  $\gamma$ -Fe<sub>2</sub>O<sub>3</sub>/Pol-COOH with the ion current corresponding to  $m/z = 68.06$  in the range of temperatures between 50°C and 300°C.

TG curve of the second sample ( $\gamma\text{-Fe}_2\text{O}_3/\text{Pol@10/10eq}$ ), corresponding to the *furan* protected maleimide functionalized MNPs, is showed in the Figure III-7.

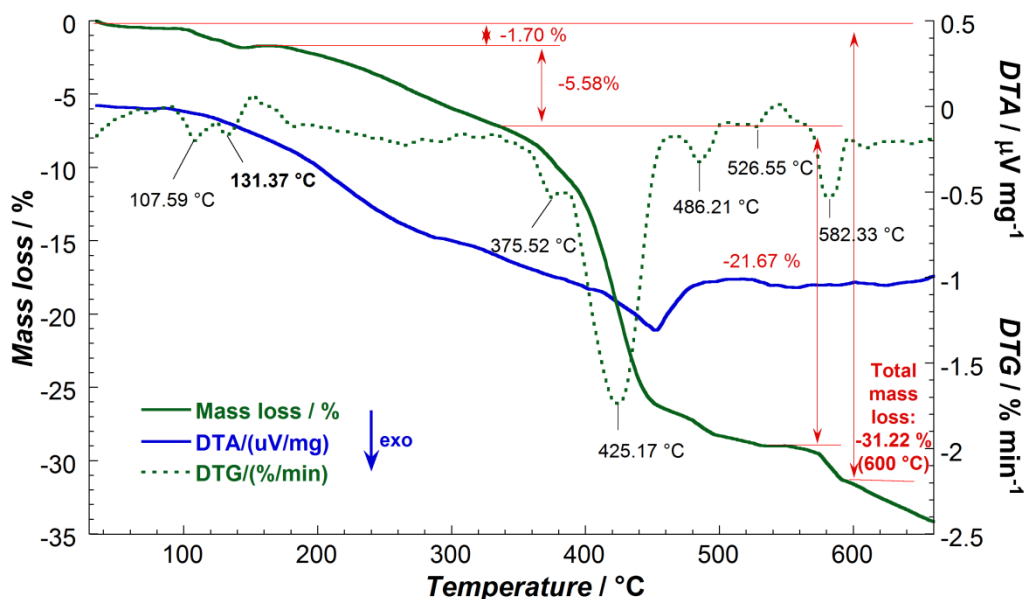


**Figure III-7.** TG measurement for MNPs after the grafting of linear coupling agent **10** added in 10 equivalents ( $\gamma\text{-Fe}_2\text{O}_3/\text{Pol@10/10eq}$ ).

Similarly to the native MNPs ( $\gamma\text{-Fe}_2\text{O}_3/\text{Pol-COOH}$ ), this temperature dependent mass loss revealed three discernible steps: first from 30°C to 150°C, second from 150°C to 320°C and third from 320°C to 600°C. Also, the DTG curve has a similar shape as that for  $\gamma\text{-Fe}_2\text{O}_3/\text{Pol-COOH}$ , except the peak at 131.37°C. The new peak was related to the ion currents with  $m/z = 68.06$ , in the range of temperatures 50°C – 250°C (Figure III-8 a, b), corresponding to the molecular mass of *furan* group.

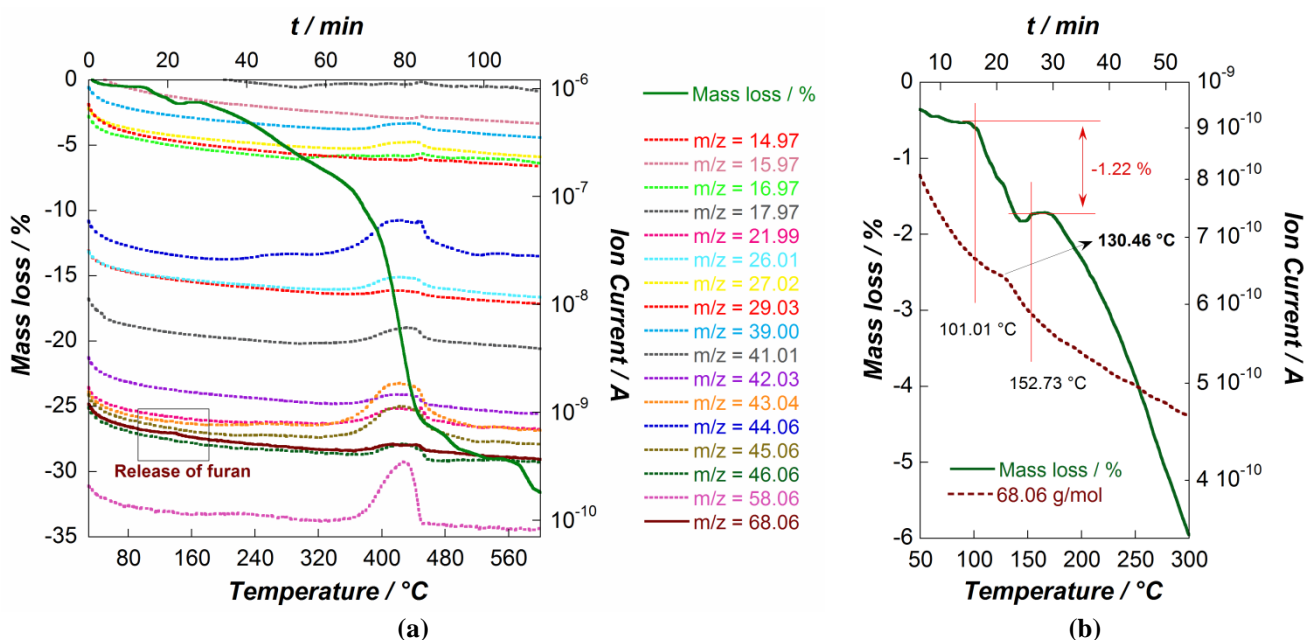


**Figure III-8.** (a) Combination of the mass loss curve from TGA for MNPs after the grafting of linear coupling agent **10** added in 10 eq. ( $\gamma\text{-Fe}_2\text{O}_3/\text{Pol@10/10eq}$ ) with the corresponding fragment ion currents detected in MS in the range of temperatures between 30°C and 600°C, and (b) Combination of the mass loss curve from TGA for  $\gamma\text{-Fe}_2\text{O}_3/\text{Pol@10/10eq}$  with the detected ion of *furan* ( $m/z = 68.06$ ) in the range of temperatures between 50°C and 300°C.

As expected, the release of *furan* (Figure III-8 b) begins around 101°C with the maximum at 131°C and finishes around 153°C. The range of temperatures where the *furan* release was detected is coherent with the literature values: thus, the *furan* release starts around 120°C in case of several *furan* protected maleimide functional polymers;<sup>12a</sup> in the case of *furan* protected copoly(urethane-urea), the *furan* release begins around 125°C;<sup>12b</sup> in the case of silica NPs functionalized with *furan* protected N – ((3-triethoxysilyl)propyl maleimide, the maximum release of *furan* from the sample was detected at 135°C;<sup>18</sup> while in the case of Au NPs functionalized with *furan* protected maleimide-PEG-thiol, the mass loss of *furan* begins at 100°C.<sup>10c</sup> The release of *furan* explains the apparition of the additional peak in the DTG curve at 131.37°C. Unfortunately, the corresponding mass loss of 1.22 % found in this range of temperatures (Figure III-8 b) cannot be attributed exclusively to the *furan* mass, since the elimination of *furan* takes place at the same time with the elimination of the water and ethanol adsorbed on the MNPs' surface. Therefore, the mass of grafted coupling agent cannot be estimated directly from these measurements.

The second step (150°C – 320°C) corresponds to the release of ethanol, acetone, beginning of release of ammonia (at 300°C) and other molecular fragments, pointing to the thermal decomposition of the coupling agent.

The third step (320°C – 600°C) showed a massive release of acetone, carbon dioxide, carbon monoxide, water and other molecular fragments that corresponds to the thermal decomposition of the polymer coating. The mass loss in this step represents 21.67 %. The total mass loss (0°C – 600°C) for this sample ( $\gamma$ -Fe<sub>2</sub>O<sub>3</sub>/Pol@10/10eq) was estimated to be 31.22 %.

The results of TGA performed for the maleimide functionalized MNPs ( $\gamma$ -Fe<sub>2</sub>O<sub>3</sub>/Pol@10-Mal/10eq) are shown in the Figure III-9. Similarly to the two previous samples, the temperature dependent mass loss displayed three steps: first from 30°C to 150°C, second from 150°C to 320°C and third from 320°C to 600°C. The DTG curve has a similar shape as for  $\gamma$ -Fe<sub>2</sub>O<sub>3</sub>/Pol-COOH, and as expected, no peak at 131.37°C (corresponding to the maximum of *furan* release) was detected.

The first step (30°C – 150°C) is related to the release of adsorbed water and ethanol onto MNPs' surface (see Figure III-10 a). The mass loss for this step constitutes 1.80 %. The second step (150°C – 320°C) corresponds to the release of ethanol, ammonia, acetone and other molecular fragments that can be assigned to the thermal decomposition of the maleimide functionality as well as that of the coupling agent, representing 5.39 % of the total mass loss. The third step (320°C to 600°C) showed the emission in a large amount of acetone, ethanol, carbon dioxide, carbon monoxide, water and other molecular fragments and represents the thermal decomposition of polymer coating. This step constitutes 22.62 % of mass loss. Finally, the total mass loss estimated for  $\gamma$ -Fe<sub>2</sub>O<sub>3</sub>/Pol@10-Mal/10eq

after heating the sample to 600°C constitutes 32.16 %, which is comparable with the results obtained for two other samples.

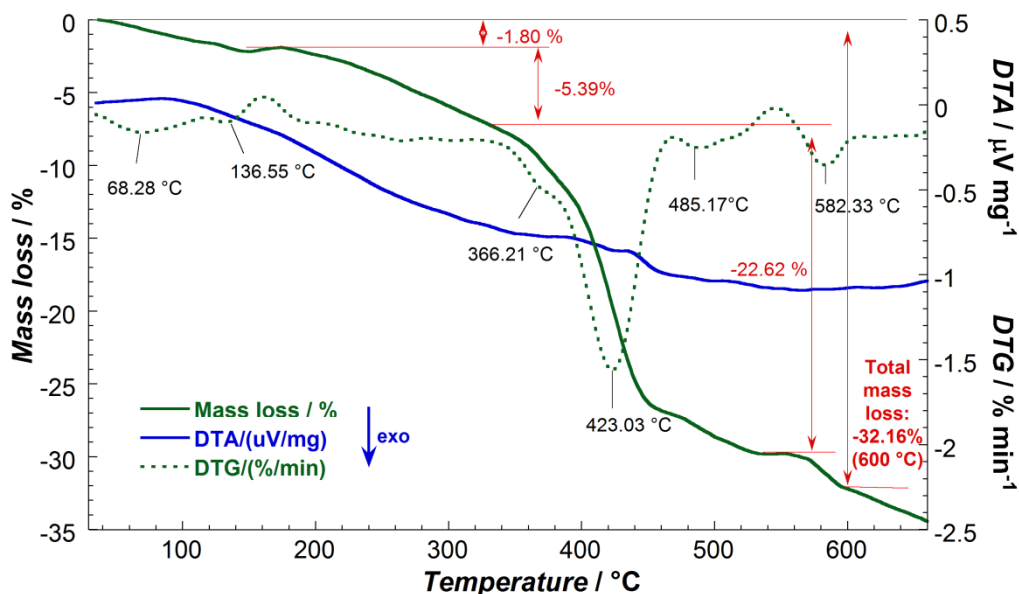


**Figure III-9.** TG measurement for MNPs after the deprotection of maleimide functionality ( $\gamma\text{-Fe}_2\text{O}_3/\text{Pol}@10\text{-Mal}/10\text{eq}$ ).

It is noteworthy that as expected, the *furan* ion current ( $m/z = 68.06$ ) was not identified in the range of temperatures between 50°C and 250°C (Figure III-10 b), thus confirming the successful formation of maleimide functionality in the deprotection step.

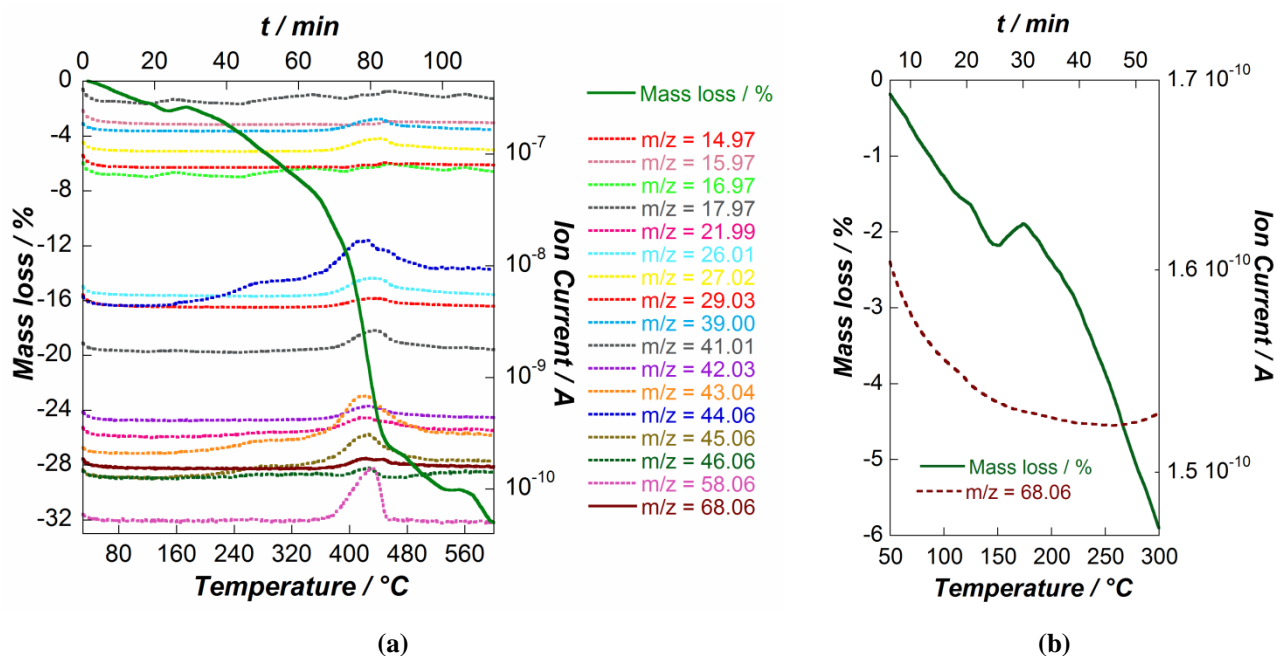


**Figure III-10.** (a) Combination of the mass loss curve from TGA for maleimide functionalized MNPs ( $\gamma\text{-Fe}_2\text{O}_3/\text{Pol}@10\text{-Mal}/10\text{eq}$ ) with the corresponding fragment ion currents detected in MS in the range of temperatures between 30 °C and 600 °C, and (b) Combination of the mass loss curve from TGA for  $\gamma\text{-Fe}_2\text{O}_3/\text{Pol}@10\text{-Mal}/10\text{eq}$  with the ion current corresponding to  $m/z = 68.06$ , in the range of temperatures between 50 °C and 300 °C.



Thus, TGA coupled with MS proved that the maleimide deprotection (Scheme III-4) carried out on MNPs' surface is complete. Unfortunately, these techniques cannot provide any information about the quantity of grafted molecules. In addition, TGA represents a destructive high mass consuming technique (10 – 20 mg of MNPs). Therefore, the TGA coupled with MS technique will not be further utilized for the characterization of functionalized  $\gamma$ -Fe<sub>2</sub>O<sub>3</sub>/Polymer MNPs.

To conclude, the grafting of linear coupling agent **10** on  $\gamma$ -Fe<sub>2</sub>O<sub>3</sub>/Polymer MNPs was confirmed by two techniques: FT-IR spectroscopy and TGA coupled with MS. The integrity of the maleimide functionalized MNPs was monitored by TEM imaging, according to which the surface modification does not affect the MNPs' integrity. However, the ATR spectrum of  $\gamma$ -Fe<sub>2</sub>O<sub>3</sub>/Pol@10/10eq points out a low surface coverage, while TGA coupled with MS showed that the grafted quantity of linear coupling agent **10** is sufficient to be detected.

### III.3.2. Optimization of grafting conditions

#### III.3.2.1. Influence of the loading in the grafting process of coupling agent **10**

The surface coverage may be improved by increasing the quantity of coupling agent **10** loaded in the grafting reaction. With the aim to increase the quantity of grafted compound, it was decided to perform several grafting experiments, varying the quantity (number of equivalents) of coupling agent **10** employed in the grafting step and keeping the other reaction parameters unchanged.

Thus, 10, 25, 35, 50 or 100 molar equivalents of coupling agent **10** (per equivalent of COOH groups) were loaded in the grafting reaction, and the resulting MNPs (corresponding to 5 grafting experiments:  $\gamma$ -Fe<sub>2</sub>O<sub>3</sub>/Pol@10/10eq,  $\gamma$ -Fe<sub>2</sub>O<sub>3</sub>/Pol@10/25eq,  $\gamma$ -Fe<sub>2</sub>O<sub>3</sub>/Pol@10/35eq,  $\gamma$ -Fe<sub>2</sub>O<sub>3</sub>/Pol@10/50eq and  $\gamma$ -Fe<sub>2</sub>O<sub>3</sub>/Pol@10/100eq) were analysed by TEM and FT-IR spectroscopy.

TEM images of  $\gamma$ -Fe<sub>2</sub>O<sub>3</sub>/Pol@10/10eq,  $\gamma$ -Fe<sub>2</sub>O<sub>3</sub>/Pol@10/25eq,  $\gamma$ -Fe<sub>2</sub>O<sub>3</sub>/Pol@10/35eq,  $\gamma$ -Fe<sub>2</sub>O<sub>3</sub>/Pol@10/50eq and  $\gamma$ -Fe<sub>2</sub>O<sub>3</sub>/Pol@10/100eq are presented in the Figure III-11. These images clearly showed that regardless the quantity of the grafted compound the surface modification step does not affect the size and shape of MNPs in comparison with the native  $\gamma$ -Fe<sub>2</sub>O<sub>3</sub>/Polymer MNPs. Also, it is noteworthy that modified MNPs do not form aggregates, this being a very important parameter that can essentially influence the colloidal stability.

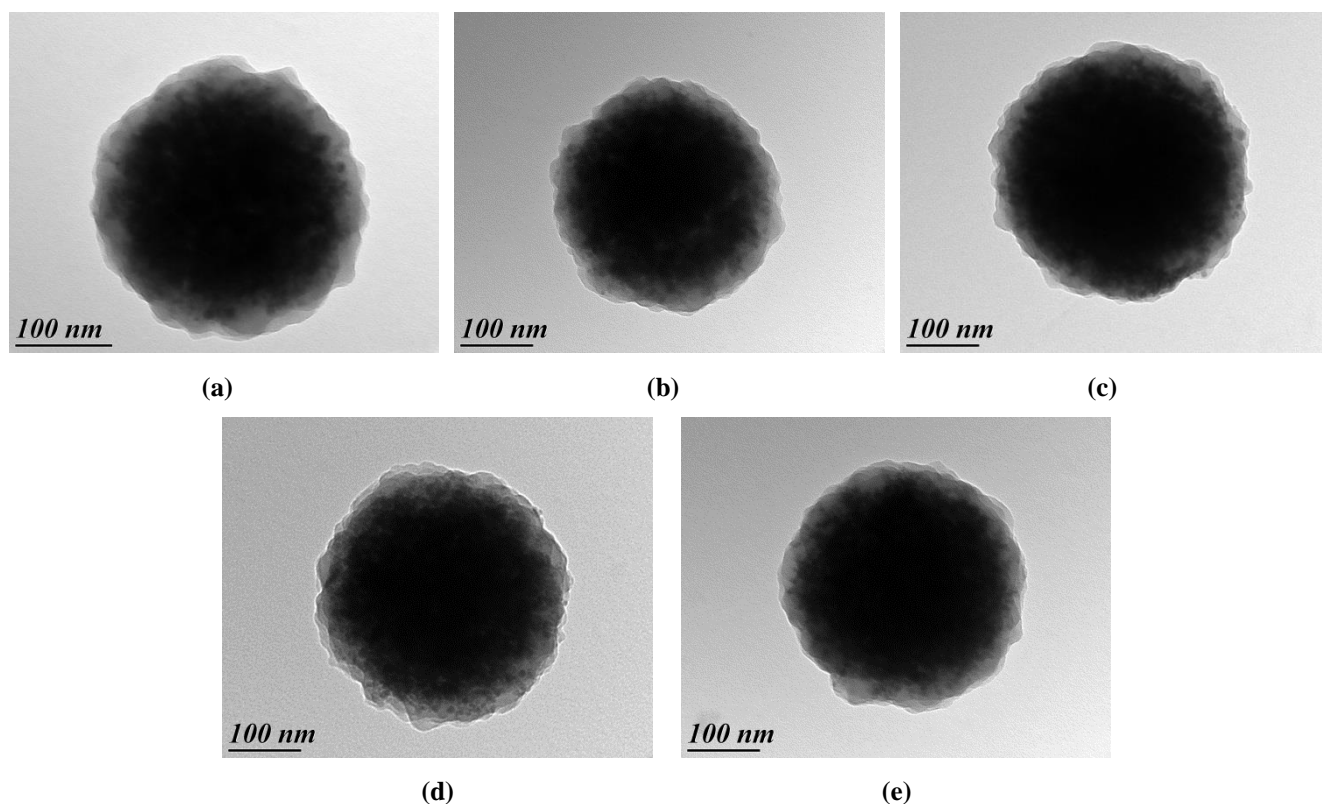


**Figure III-11.** TEM images of: (a)  $\gamma\text{-Fe}_2\text{O}_3/\text{Pol}@10/10\text{eq}$ ; (b)  $\gamma\text{-Fe}_2\text{O}_3/\text{Pol}@10/25\text{eq}$ ; (c)  $\gamma\text{-Fe}_2\text{O}_3/\text{Pol}@10/35\text{eq}$ ; (d)  $\gamma\text{-Fe}_2\text{O}_3/\text{Pol}@10/50\text{eq}$  and (e)  $\gamma\text{-Fe}_2\text{O}_3/\text{Pol}@10/100\text{eq}$ .

The IR spectra of native  $\gamma\text{-Fe}_2\text{O}_3$ /Polymer MNPs ( $\gamma\text{-Fe}_2\text{O}_3/\text{Pol-COOH}$ ) and MNPs obtained after the grafting of linear coupling agent **10**, are showed in Figure III-12 a. The efficiency of the grafting reactions was estimated by monitoring the intensity of the absorption bands in the carbonyl region.

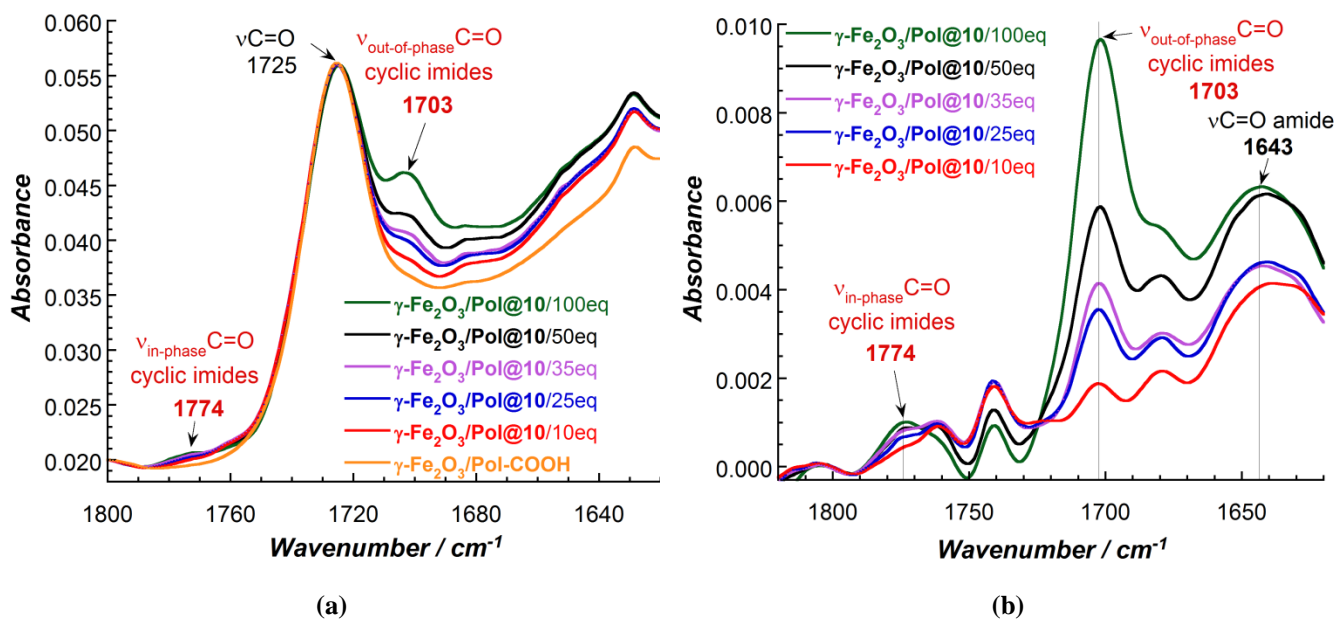


**Figure III-12.** (a) ATR spectra of obtained MNPs after the five different grafting procedures:  $\gamma\text{-Fe}_2\text{O}_3/\text{Pol}@10/10\text{eq}$ ,  $\gamma\text{-Fe}_2\text{O}_3/\text{Pol}@10/25\text{eq}$ ,  $\gamma\text{-Fe}_2\text{O}_3/\text{Pol}@10/35\text{eq}$ ,  $\gamma\text{-Fe}_2\text{O}_3/\text{Pol}@10/50\text{eq}$  and  $\gamma\text{-Fe}_2\text{O}_3/\text{Pol}@10/100\text{eq}$ ; (b) Subtraction of native polymer coated MNPs' spectrum from the obtained spectra of functionalized MNPs (corresponding to five grafting experiments).

As expected, all the samples showed the presence of the characteristic absorption band of the out-phase C=O stretching vibration at 1703 cm<sup>-1</sup> (Figure III-12 a). In addition, even a very weak band at 1774 cm<sup>-1</sup> assigned to the in-phase C=O stretching vibration is also distinguishable (Figure III-12 a). The subtraction of the native  $\gamma$ -Fe<sub>2</sub>O<sub>3</sub>/Polymer MNPs' spectrum from the spectra of functionalized MNPs (Figure III-12 b) allowed an easier observation of the spectral changings occurring as a result of grafting reaction. Therefore, all the spectra discussed further on are examined in spectral subtraction mode. Thus, the presence of the broad band at 1643 cm<sup>-1</sup> (Figure III-12 b), corresponding to the C=O amide I mode, proved the amide bond formation and thus confirmed the covalent linkage of coupling agent **10** onto MNP's surface. However, this band could be partially generated by the H-O-H bending vibration of water molecules adsorbed on MNPs' surface.<sup>19</sup> Since all the spectra showed in Figure III-12 b represent a subtraction of native MNPs ( $\gamma$ -Fe<sub>2</sub>O<sub>3</sub>/Pol-COOH) from the functionalized MNPs ( $\gamma$ -Fe<sub>2</sub>O<sub>3</sub>/Pol@**10**/10–100eq) and all the samples were dried in the same conditions, it was considered that native MNPs as well as functionalized MNPs contained the same amount of adsorbed water on MNPs' surface, and consequently the water amount was subtracted.

To conclude, this study showed that the grafting efficiency is directly proportional to the quantity of compound employed in the grafting reaction.

Next, the cleavage of furan protection was performed and the resulting maleimide functionalized MNPs ( $\gamma$ -Fe<sub>2</sub>O<sub>3</sub>/Pol@**10**-Mal/10eq,  $\gamma$ -Fe<sub>2</sub>O<sub>3</sub>/Pol@**10**-Mal/25eq,  $\gamma$ -Fe<sub>2</sub>O<sub>3</sub>/Pol@**10**-Mal/35eq,  $\gamma$ -Fe<sub>2</sub>O<sub>3</sub>/Pol@**10**-Mal/50eq and  $\gamma$ -Fe<sub>2</sub>O<sub>3</sub>/Pol@**10**-Mal/100eq) were investigated via IR spectroscopy and TEM. The IR spectra obtained after the subtraction of native  $\gamma$ -Fe<sub>2</sub>O<sub>3</sub>/Polymer MNPs are presented in Figure III-13.

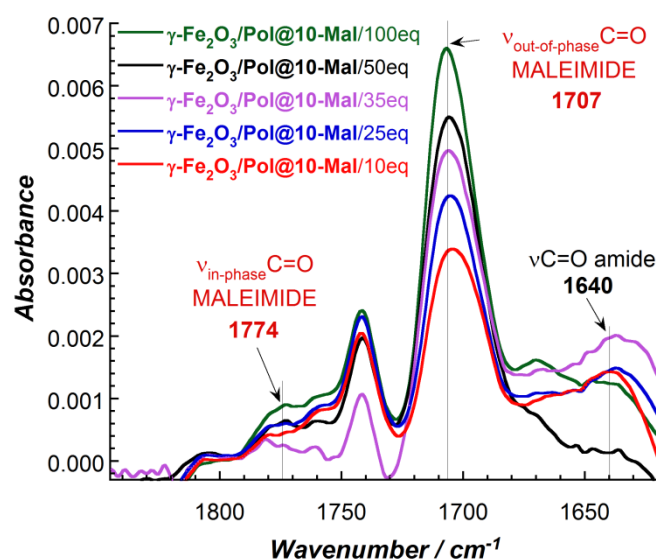


**Figure III-13.** Spectral subtraction results for:  $\gamma$ -Fe<sub>2</sub>O<sub>3</sub>/Pol@**10**-Mal/10eq;  $\gamma$ -Fe<sub>2</sub>O<sub>3</sub>/Pol@**10**-Mal/25eq;  $\gamma$ -Fe<sub>2</sub>O<sub>3</sub>/Pol@**10**-Mal/35eq;  $\gamma$ -Fe<sub>2</sub>O<sub>3</sub>/Pol@**10**-Mal/50eq and  $\gamma$ -Fe<sub>2</sub>O<sub>3</sub>/Pol@**10**-Mal/100eq.

All the spectral subtractions of maleimide functionalized MNPs confirmed the disappearance of the band at  $1703\text{ cm}^{-1}$  characteristic for out-of-phase C=O stretching vibration of cyclic imides and showed the appearance of a new band at  $1707\text{ cm}^{-1}$  characteristic to the out-of-phase C=O stretching vibration of the maleimide functionality. Thus, these spectra confirmed the deprotection step (previously proved by TGA coupled with MS, *see III.3.1.2.*). Band shift at  $1640\text{ cm}^{-1}$  attributed to the C=O amide I mode was also present in all the spectra, confirming the preservation of the grafted compound after the deprotection step.

MNPs after the deprotection step were also analysed by TEM. TEM images of  $\gamma\text{-Fe}_2\text{O}_3/\text{Pol@10-Mal}/25\text{eq}$ ,  $\gamma\text{-Fe}_2\text{O}_3/\text{Pol@10-Mal}/35\text{eq}$ ,  $\gamma\text{-Fe}_2\text{O}_3/\text{Pol@10-Mal}/50\text{eq}$  and  $\gamma\text{-Fe}_2\text{O}_3/\text{Pol@10-Mal}/100\text{eq}$  are presented in Figure III-14 (TEM image of  $\gamma\text{-Fe}_2\text{O}_3/\text{Pol@10-Mal}/10\text{eq}$  was previously showed in Figure III-2 c).

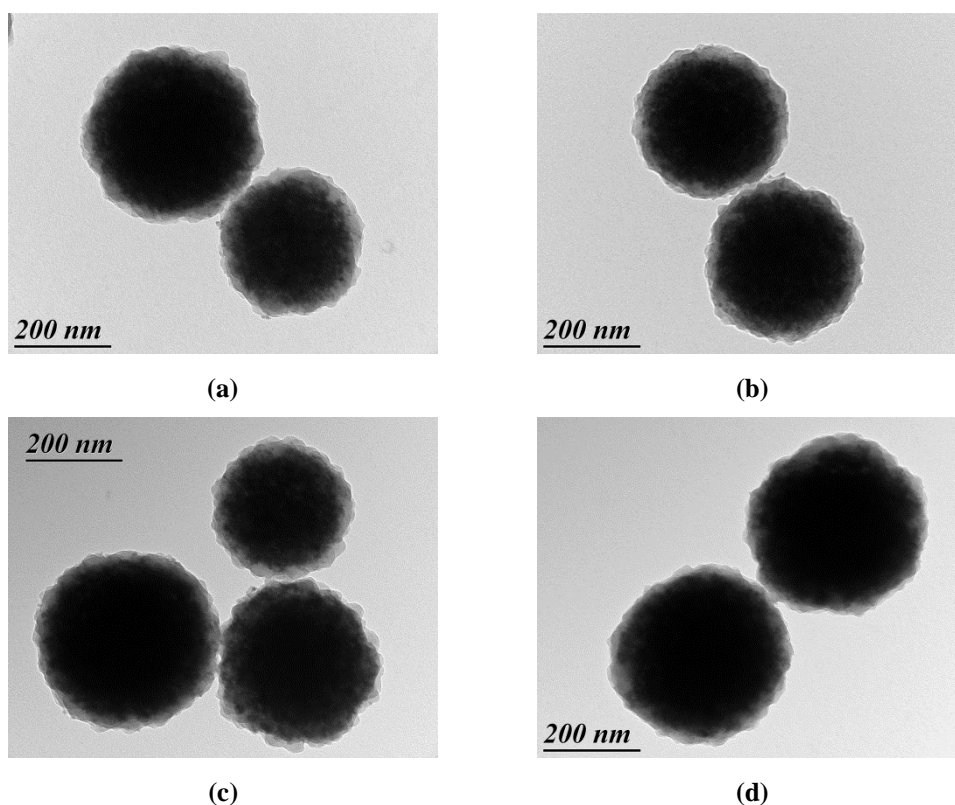


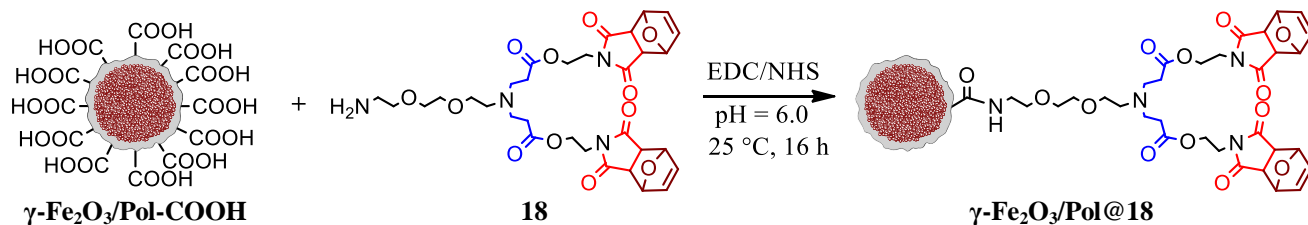
**Figure III-14.** TEM images of: (a)  $\gamma\text{-Fe}_2\text{O}_3/\text{Pol@10-Mal}/25\text{eq}$ ; (b)  $\gamma\text{-Fe}_2\text{O}_3/\text{Pol@10-Mal}/35\text{eq}$ ; (c)  $\gamma\text{-Fe}_2\text{O}_3/\text{Pol@10-Mal}/50\text{eq}$  and (d)  $\gamma\text{-Fe}_2\text{O}_3/\text{Pol@10-Mal}/100\text{eq}$ .

TEM images proved that particles' integrity is not affected after the deprotection step.

To conclude, the FT-IR study clearly showed that the grafting efficiency is directly proportional to the quantity of compound **10** introduced for the grafting reaction. The highest amount of grafted coupling agent **10** was obtained when 100 equivalents of organic molecules were loaded in the grafting reaction.

### III.3.2.2. Influence of the loading in the grafting process of coupling agent 18

Similarly to the coupling agent **10**, with the aim to find the best grafting conditions for two-branched coupling agent **18**, five grafting experiments using different amount of compound **18** were performed according to the Scheme III-5 (see also *Experimental part*).



**Scheme III-5.** Grafting of two-branched coupling agent **18** on  $\gamma$ -Fe<sub>2</sub>O<sub>3</sub>/Polymer MNPs.

Thus, 10, 25, 35, 50 or 100 molar equivalents of coupling agent **18** (per equivalent of COOH groups) were loaded in the grafting reaction.

TEM images of  $\gamma$ -Fe<sub>2</sub>O<sub>3</sub>/Pol@18/10eq,  $\gamma$ -Fe<sub>2</sub>O<sub>3</sub>/Pol@18/25eq,  $\gamma$ -Fe<sub>2</sub>O<sub>3</sub>/Pol@18/35eq,  $\gamma$ -Fe<sub>2</sub>O<sub>3</sub>/Pol@18/50eq and  $\gamma$ -Fe<sub>2</sub>O<sub>3</sub>/Pol@18/100eq are shown in Figure III-15. These images showed that the surface modification of  $\gamma$ -Fe<sub>2</sub>O<sub>3</sub>/Polymer MNPs does not affect the size and shape of the particles. Also, the observations of colloidal suspensions of all these samples in water showed that MNPs do not form aggregates, this being an important parameter regarding the targeted applications.

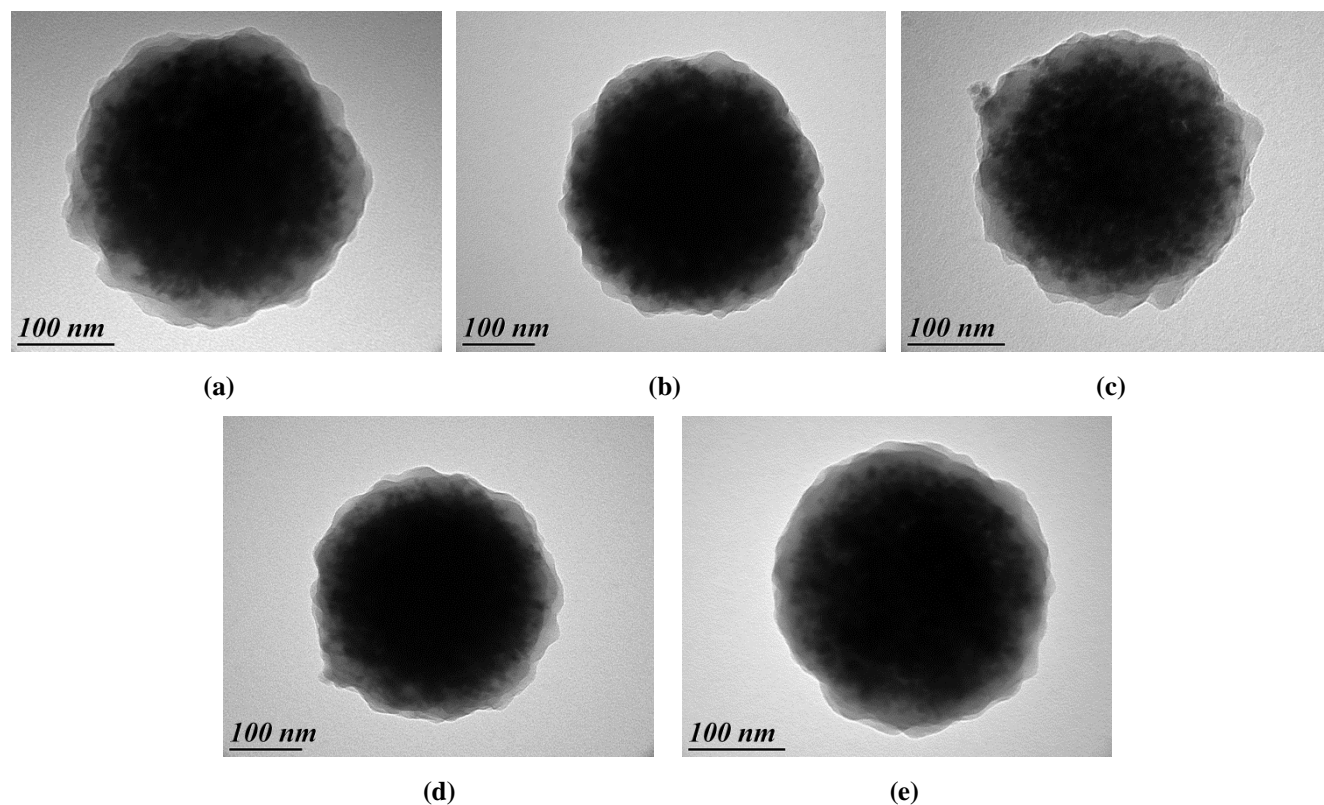


**Figure III-15.** TEM images of: (a)  $\gamma$ -Fe<sub>2</sub>O<sub>3</sub>/Pol@18/10eq; (b)  $\gamma$ -Fe<sub>2</sub>O<sub>3</sub>/Pol@18/25eq; (c)  $\gamma$ -Fe<sub>2</sub>O<sub>3</sub>/Pol@18/35eq; (d)  $\gamma$ -Fe<sub>2</sub>O<sub>3</sub>/Pol@18/50eq and (e)  $\gamma$ -Fe<sub>2</sub>O<sub>3</sub>/Pol@18/100eq.

With the aim to analyse the characteristic IR bands for two-branched coupling agent **18**, the IR spectrum was recorded (Figure III-16).

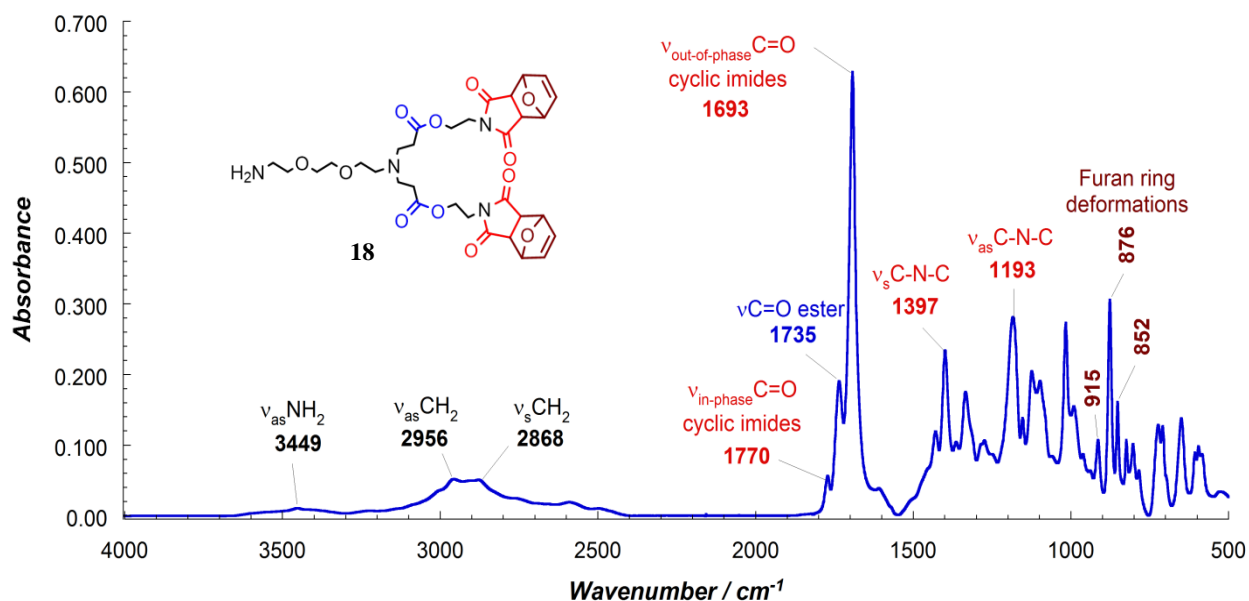


**Figure III-16.** ATR FT-IR spectrum of coupling agent **18**.

Similarly to the coupling agent **10**, the FT-IR spectrum of coupling agent **18** showed the presence of several characteristic absorption bands: a very weak absorbance band around  $3449\text{ cm}^{-1}$  assigned to the antisymmetric stretching vibration of  $\text{NH}_2$  groups; two bands at  $2956\text{ cm}^{-1}$  and  $2868\text{ cm}^{-1}$  characteristic to the antisymmetric and symmetric CH stretching vibrations of  $-\text{O}-\text{CH}_2$  groups; two peaks at  $1770\text{ cm}^{-1}$  (weak) and at  $1693\text{ cm}^{-1}$  (strong) corresponding to the in-phase and out-of-phase stretching vibrations of the two  $\text{C}=\text{O}$  groups present in five membered cyclic imide rings; the bands at  $1397\text{ cm}^{-1}$  and  $1193\text{ cm}^{-1}$  that involve the symmetric and antisymmetric C-N-C stretch; and the bands at  $914\text{ cm}^{-1}$ ,  $876\text{ cm}^{-1}$  and  $852\text{ cm}^{-1}$  characteristic to the furan ring deformation. Additionally, the absorption band at  $1735\text{ cm}^{-1}$  attributed to the  $\text{C}=\text{O}$  stretching of ester groups has appeared.<sup>13</sup>

Next, FT-IR spectra of  $\gamma\text{-Fe}_2\text{O}_3/\text{Pol@18}/10\text{eq}$ ,  $\gamma\text{-Fe}_2\text{O}_3/\text{Pol@18}/25\text{eq}$ ,  $\gamma\text{-Fe}_2\text{O}_3/\text{Pol@18}/35\text{eq}$ ,  $\gamma\text{-Fe}_2\text{O}_3/\text{Pol@18}/50\text{eq}$  and  $\gamma\text{-Fe}_2\text{O}_3/\text{Pol@18}/100\text{eq}$  were recorded, and are presented in spectral subtraction mode in Figure III-17.

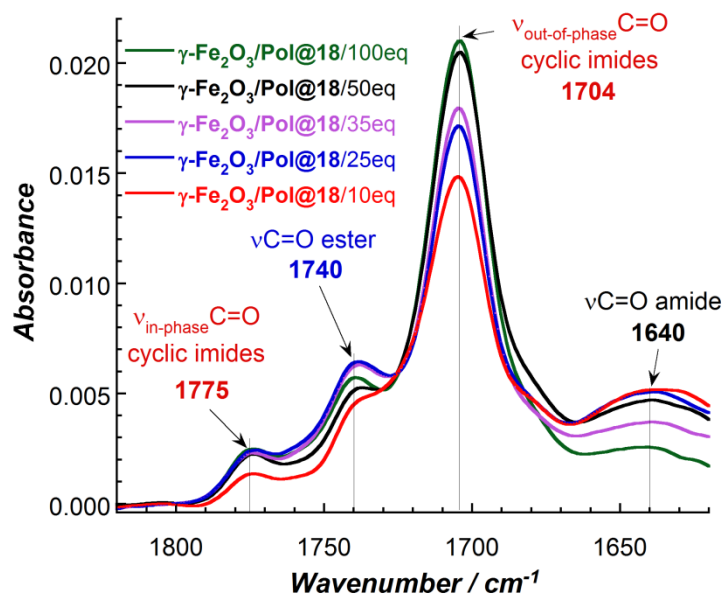


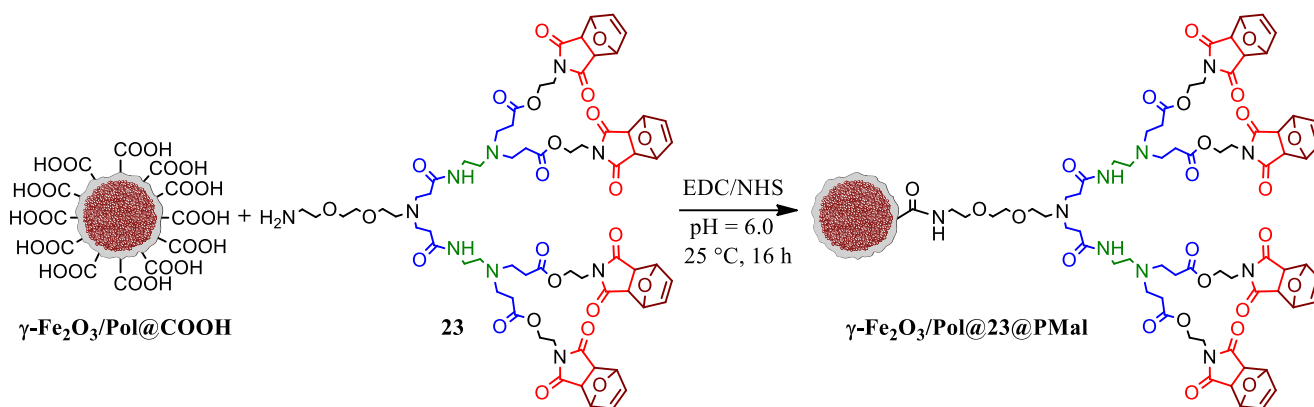
**Figure III-17.** Subtraction of native polymer coated MNPs' spectrum from the spectra of MNPs functionalized with two-branched coupling agent **18** (corresponding to 5 grafting experiments).

All the spectral subtractions (Figure III-17) showed the appearance of the characteristic strong out-of-phase C=O band at  $1704\text{ cm}^{-1}$  and the weak in-phase C=O band at  $1775\text{ cm}^{-1}$ . Also, the characteristic C=O stretching band of ester groups is observed at  $1740\text{ cm}^{-1}$ . The broad band around  $1640\text{ cm}^{-1}$  is assigned to the C=O amide I mode<sup>13</sup> and provides the direct evidence of the amide bond formation, confirming the covalent linkage of coupling agent **18** to MNP's surface.

Similarly to the grafting of coupling agent **10**, the efficiency of coupling agent **18** grafting is related to the quantity of organic coupling agent involved in the grafting reaction. However, no notable difference was observed for grafting involving 50 or 100 equivalents of compound **18**. Therefore, the highest amount of grafted two-branched coupling agent **18** can be achieved by adding *50 equivalents* of compound while for an efficient grafting of linear coupling agent **10**, *100 equivalents* of compound are necessary. In addition, the characteristic absorption bands for the grafting of two-branched coupling agent **18** are more intense than for the grafting of the linear coupling agent **10**.

### III.3.2.3. Influence of the loading in the grafting process of coupling agent **23**

Similarly to the coupling agents **10** and **18**, the grafting of coupling agent **23** (10, 25, 35, 50 or 100 equivalents) on MNPs was performed, and is schematically represented in Scheme III-6 (*see also experimental part*). The resulting MNPs ( $\gamma\text{-Fe}_2\text{O}_3/\text{Pol}@23/10\text{eq}$ ,  $\gamma\text{-Fe}_2\text{O}_3/\text{Pol}@23/25\text{eq}$ ,  $\gamma\text{-Fe}_2\text{O}_3/\text{Pol}@23/35\text{eq}$ ,  $\gamma\text{-Fe}_2\text{O}_3/\text{Pol}@23/50\text{eq}$  and  $\gamma\text{-Fe}_2\text{O}_3/\text{Pol}@23/100\text{eq}$ ) were investigated by TEM and IR spectroscopy.



**Scheme III-6.** Grafting of four-branched coupling agent **23** on  $\gamma\text{-Fe}_2\text{O}_3$ /Polymer MNPs.

Similarly to the grafting of coupling agents **10** and **18**, TEM of  $\gamma\text{-Fe}_2\text{O}_3$ /Pol@**23**/10eq,  $\gamma\text{-Fe}_2\text{O}_3$ /Pol@**23**/25eq,  $\gamma\text{-Fe}_2\text{O}_3$ /Pol@**23**/35eq,  $\gamma\text{-Fe}_2\text{O}_3$ /Pol@**23**/50eq and  $\gamma\text{-Fe}_2\text{O}_3$ /Pol@**23**/100eq (Figure III-18) showed that the surface modification does not change the particles morphology, independently on the loading of coupling agent.

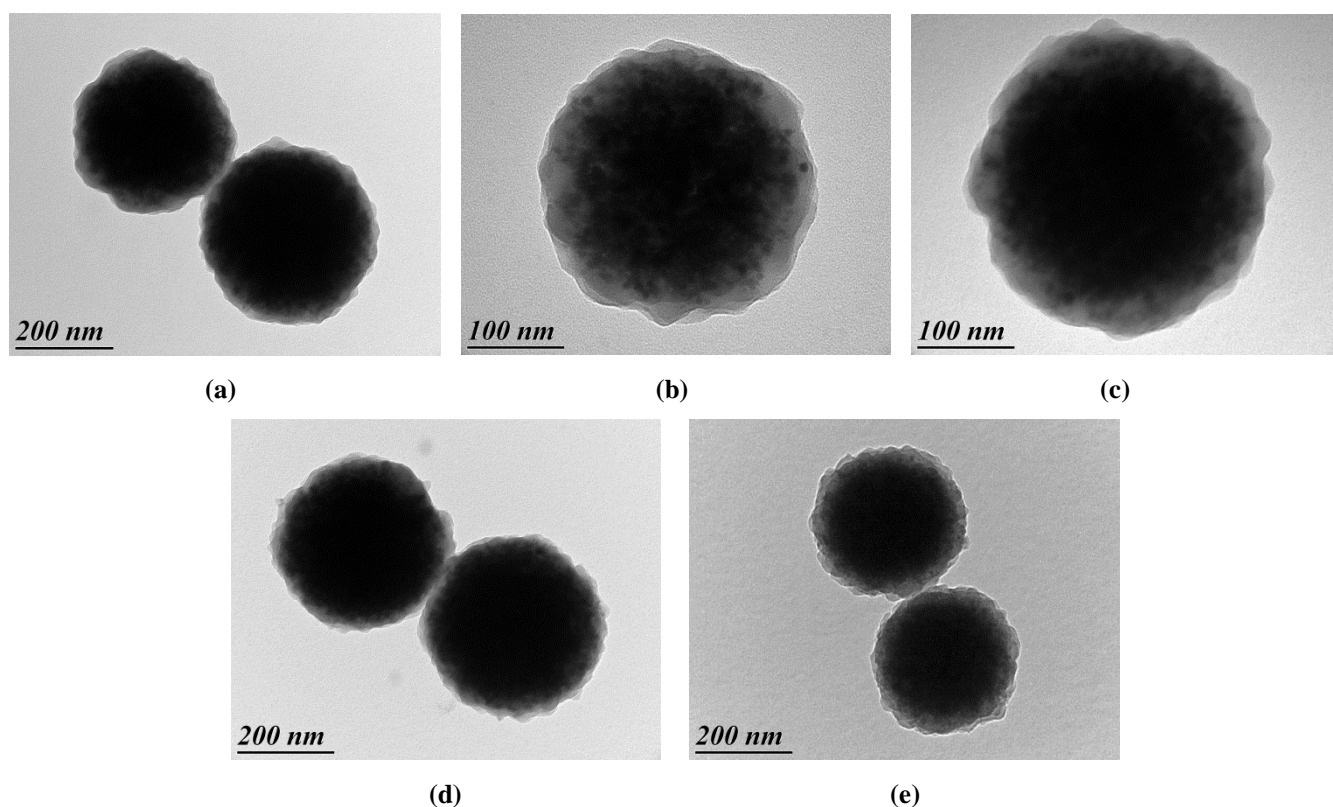


**Figure III-18.** TEM images of (a)  $\gamma\text{-Fe}_2\text{O}_3$ /Pol@**23**/10eq; (b)  $\gamma\text{-Fe}_2\text{O}_3$ /Pol@**23**/25eq; (c)  $\gamma\text{-Fe}_2\text{O}_3$ /Pol@**23**/35eq; (d)  $\gamma\text{-Fe}_2\text{O}_3$ /Pol@**23**/50eq and (e)  $\gamma\text{-Fe}_2\text{O}_3$ /Pol@**23**/100eq.

Next, FT-IR spectrum of coupling agent **23** was recorded (Figure III-19).



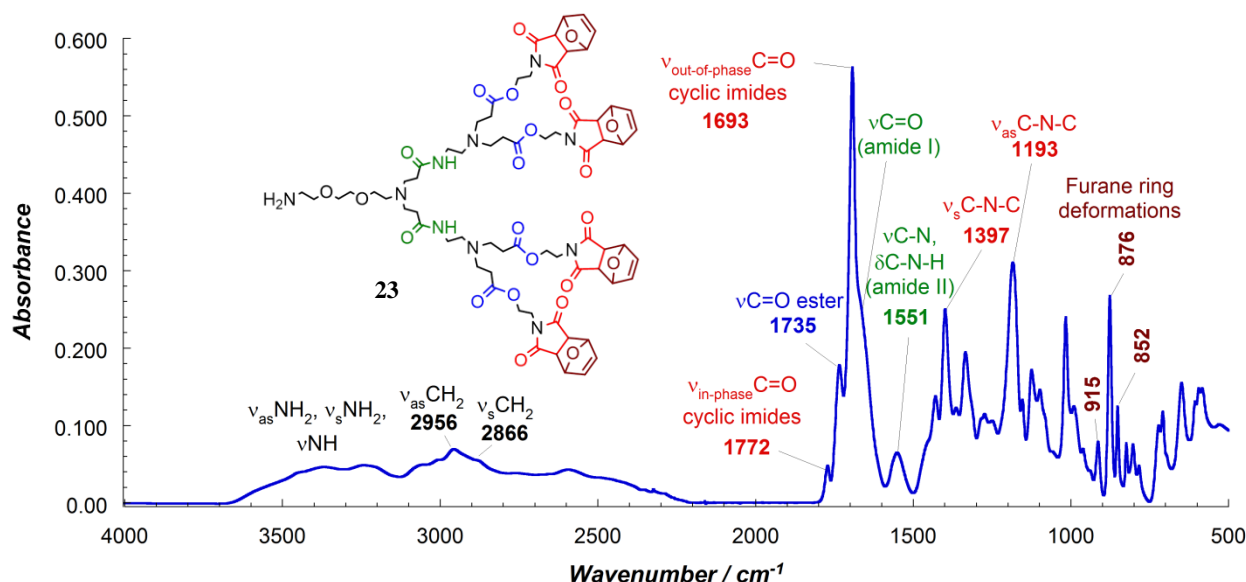


**Figure III-19.** ATR FT-IR spectrum of four-branched coupling agent **23**.

Additionally to the peaks observed for coupling agents **10** and **18** (see sections III.3.2.1 and III.3.2.2), the spectrum of dendron **23** showed the appearance of a broad band in the region between 3670  $\text{cm}^{-1}$  and 3150  $\text{cm}^{-1}$  that comprise antisymmetric and symmetric stretching vibrations of  $\text{NH}_2$  groups and N-H stretching vibrations characteristic for secondary amides. Also, a shoulder on the out-of-phase C=O stretching band (at 1693  $\text{cm}^{-1}$ ) was observed around 1668  $\text{cm}^{-1}$ . This shoulder is caused by the C=O stretching band characteristic for monosubstituted amides<sup>13</sup> and it is usually called amide I. The absorption band at 1551  $\text{cm}^{-1}$  involves both C-N stretching and C-N-H bending vibrations, and is usually called amide II.<sup>13</sup>

FT-IR spectra of the surface modified MNPs ( $\gamma$ -Fe<sub>2</sub>O<sub>3</sub>/Pol@**23**/10eq,  $\gamma$ -Fe<sub>2</sub>O<sub>3</sub>/Pol@**23**/25eq,  $\gamma$ -Fe<sub>2</sub>O<sub>3</sub>/Pol@**23**/35eq,  $\gamma$ -Fe<sub>2</sub>O<sub>3</sub>/Pol@**23**/50eq and  $\gamma$ -Fe<sub>2</sub>O<sub>3</sub>/Pol@**23**/100eq) were recorded and the subtraction of native polymer coated MNPs' spectrum was performed (Figure III-20).

The spectral subtractions (Figure III-20) showed the presence of all the bands characteristic to carbonyl groups in compound **23**: in-phase C=O band at 1775  $\text{cm}^{-1}$ , out-of-phase C=O band at 1703  $\text{cm}^{-1}$ , C=O stretching band of ester groups at 1740  $\text{cm}^{-1}$  and a broad shoulder in the 1680-1630  $\text{cm}^{-1}$  region that arises from the C=O amide stretch.

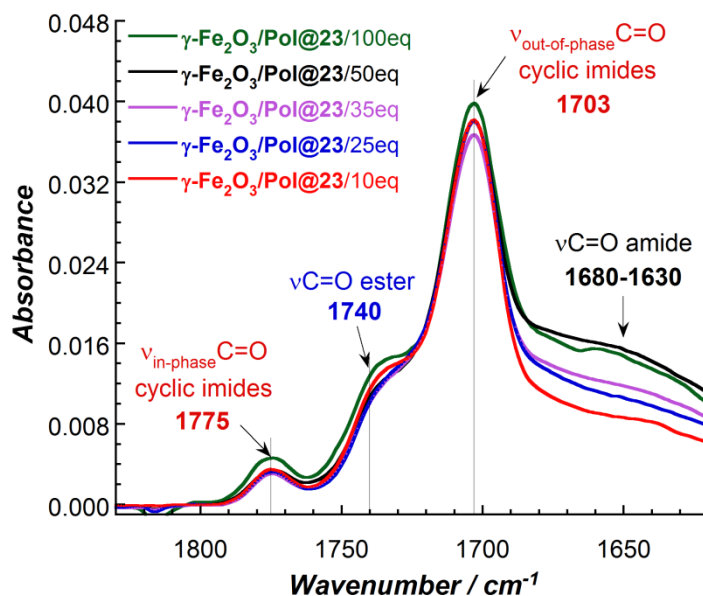


**Figure III-20.** Subtraction of native polymer coated MNPs' spectrum from the spectra of MNPs functionalized with four-branched coupling agent **23** (corresponding to 5 grafting experiments).

Obviously, the FT-IR spectroscopy study confirmed the presence of four-branched coupling agent **23** on MNPs' surface. Surprisingly, and contrary to the results obtained for the grafting of the linear coupling agent **10** and two-branched coupling agent **18**, the grafting of four-branched coupling agent **23** seems to be independent of the amount of coupling agent introduced in the grafting reaction. All the FT-IR spectra showed approximately the same intensity of the out-of-phase C=O band at  $1703\text{ cm}^{-1}$  which is much more intense comparing to the one obtained for the functionalization of MNPs with two-branched coupling agent **18**. Also, it is noteworthy that this high grafting rate was achieved by employing only *10 equivalents* of coupling agent in the grafting reaction.

To highlight the differences obtained for grafting of linear (**10**) and dendritic structures (**18** and **23**), the following comparative study was performed.

### III.3.3. Comparative study - dendritic coupling agents versus linear coupling agent

This study has the goal to monitor the effect of dendritic coupling agents' generation on the grafting reaction quality as well as on the efficiency of the functionalized MNPs in the immobilization of biomolecules, what is meant by the term “*dendritic effect*”.

#### III.3.3.1. Evolution of surface functionalization

In the previous paragraph (III.3.2), it has already been observed that the grafting of linear and dendritic coupling agents does not follow the same rules. The best way to highlight this difference is the representation of the FT-IR spectral subtractions data obtained for the grafting series (10, 25, 35,

50 or 100 equivalents) of each coupling agent (**10**, **18**, **23**) (Figure III-13, Figure III-17 and Figure III-20) on a graph, representing the dependence of the absorption band intensity at  $1703\text{ cm}^{-1}$  (the maximum of out-of-phase C=O band of cyclic imides in five membered ring) as the function of the number of equivalents of coupling agent (Figure III-21).

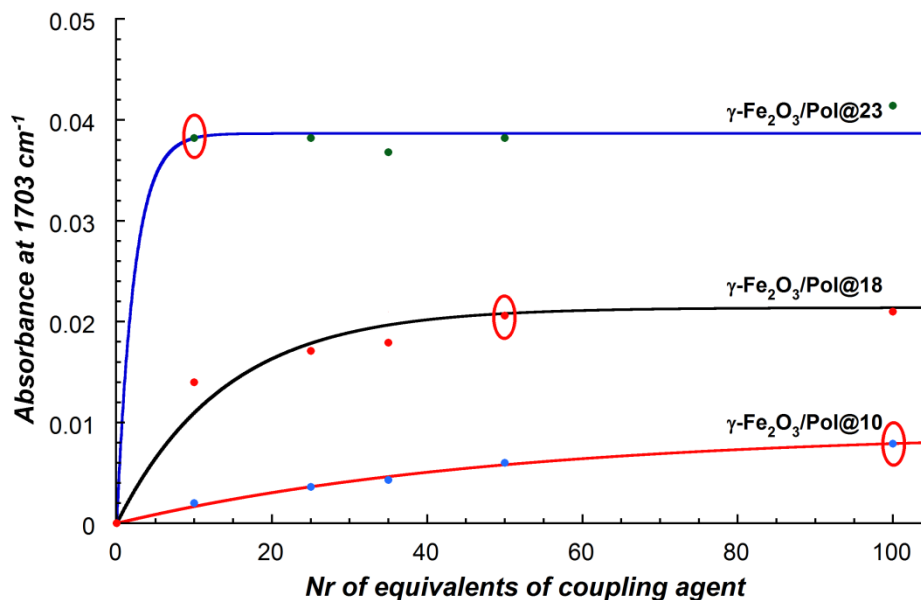


**Figure III-21.** Evolution of surface functionalization with linear coupling agent **10** (red line); two-branched coupling agent **18** (dendron G1) showed with black line; and four-branched coupling agent **23** (dendron G2) (blue line).

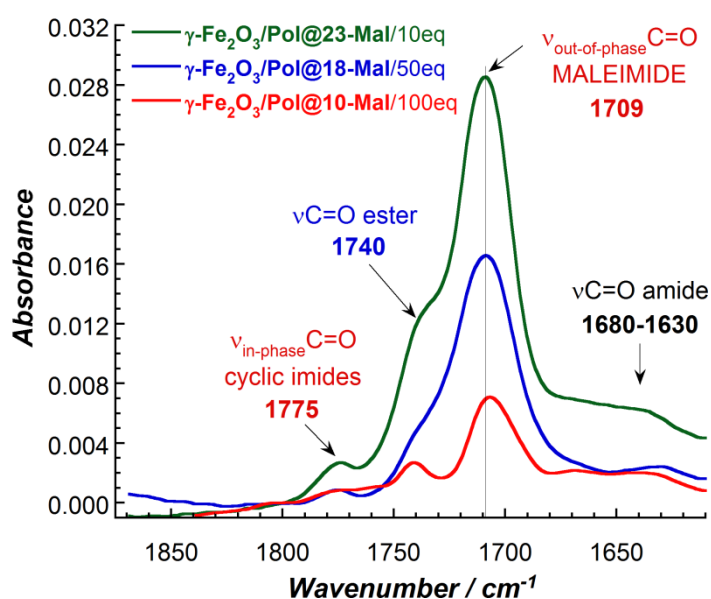
It is worthy to mention, that the series of grafting experiments (10, 25, 35, 50 or 100 equivalents) for each coupling agent (**10**, **18**, **23**) followed by their deprotection step were repeated at least 2 times and the recorded spectra were reproducible.

Figure III-21 clearly showed that under the identical conditions of the grafting reaction, the linear coupling agent **10** (red line) achieves the maximal absorbance intensity of about  $0.01$ , two-branched coupling agent **18** (black line) achieves the maximal absorbance intensity around  $0.02$  while the four-branched coupling agent **23** (blue line) achieves the maximal absorbance intensity of approximately  $0.04$ . Moreover, the ratio of the absorption bands' intensity (1:2:4) is directly proportional to the number of functional groups present on MNPs' surface that, which is provided by the growth of dendron generation. Thereby, the amount of functional groups increases with the dendron's generation, highlighting a positive "dendritic effect" on the surface functionalization.

At the same time, the amount of coupling agent necessary for achieving the maximum of surface functionalization is different for each coupling agent. Thus, the maximum of surface functionalization can be achieved when  $100$  equivalents of coupling agent are employed in the case of linear coupling agent **10**,  $50$  equivalents in the case of two-branched coupling agent **18** (dendron G1), and only  $10$

equivalents in the case of four-branched coupling agent **23** (dendron G2). Eventually, these results reinforce the positive “*dendritic effect*” on the surface functionalization.

The optimal grafting conditions (loading of coupling agents) were employed in functionalization of MNPs at a larger scale followed by deprotection of maleimide functionalities according to the previously described procedure (DMSO, 99°C, 5 h., mechanical stirring). The spectral subtractions of the obtained MNPs:  $\gamma\text{-Fe}_2\text{O}_3$ /Pol@10-Mal/100eq,  $\gamma\text{-Fe}_2\text{O}_3$ /Pol@18-Mal/50eq and  $\gamma\text{-Fe}_2\text{O}_3$ /Pol@23-Mal/10eq are presented in Figure III-22.

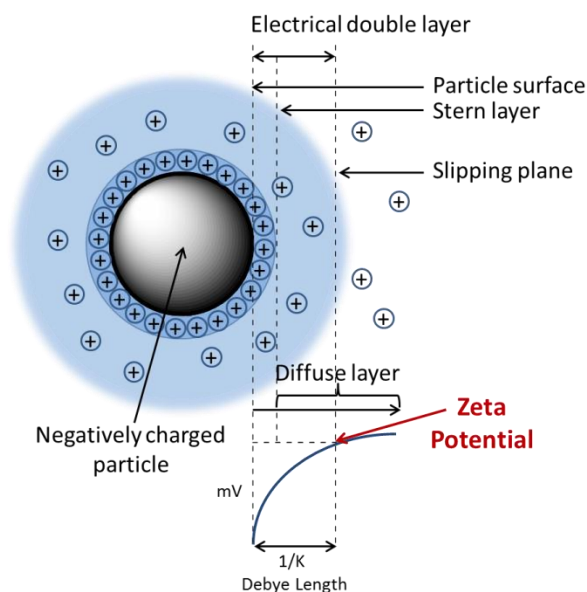


**Figure III-22.** Spectral subtraction results:  $\gamma\text{-Fe}_2\text{O}_3$ /Pol@10-Mal/100eq,  $\gamma\text{-Fe}_2\text{O}_3$ /Pol@18-Mal/50eq and  $\gamma\text{-Fe}_2\text{O}_3$ /Pol@23-Mal/10eq.

This figure confirms that the amount of grafted coupling agent does not change after the deprotection step, respecting the same ratio between the peaks intensity of 1:2:4 as before deprotection. For simplicity the number of compound's equivalents employed in the grafting reaction, will not be further indicated in the name of modified MNPs.

### III.3.3.2. Zeta potential measurements

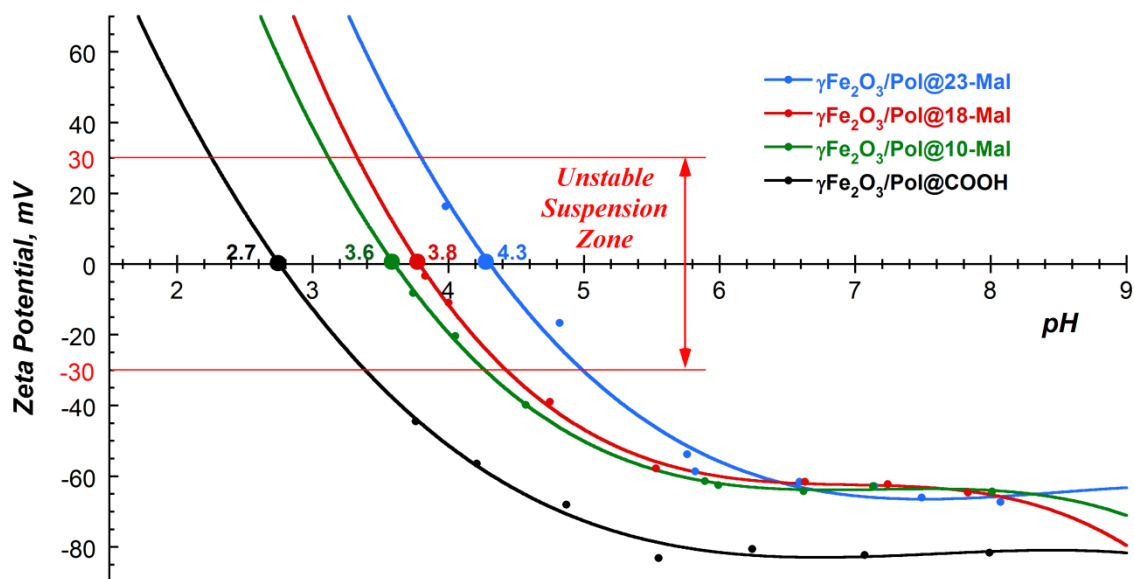
Zeta potential measurements represent an efficient technique to assess the change of the surface charge and the colloidal stability of the system. Zeta potential is a physical property exhibited by particles in suspension. Nanoparticles have a surface charge that attracts a thin layer of ions of opposite charge to the nanoparticle surface. The layer surrounding the particle exists in two parts: an inner region (Stern layer) where the ions are strongly bound and an outer layer (diffuse) region where they are less firmly associated (Figure III-23).



**Figure III-23.** Electrical double layer model.

Zeta potential is defined as the potential measured in mV at the slipping plane distance from the particle surface (for technical details on the experimental measurements see reference).<sup>20</sup> Zeta potential values typically range from +100 mV to -100 mV and can be used as an indicator of dispersion stability. Generally, particles with a zeta potential more positive than +30 or more negative than -30 mV are considered to represent stable suspensions. Suspensions with a low zeta potential value or about zero (isoelectric point) will eventually aggregate due to van der Waal inter-particle attractions.<sup>20,21</sup>

In aqueous media the pH of the sample is one of the most important factors that affect its zeta potential. Thereby, zeta potential is usually measured as a function of pH. To investigate the effect of pH on the surface charge of native and functionalized MNPs, zeta potential measurements of diluted aqueous suspensions of MNPs were performed at 25°C by varying pH from 3.6 to 8.0 (Figure III-24). The pH of the samples was adjusted by adding 0.01 M solution of hydrochloric acid or 0.01 M sodium hydroxide solution.



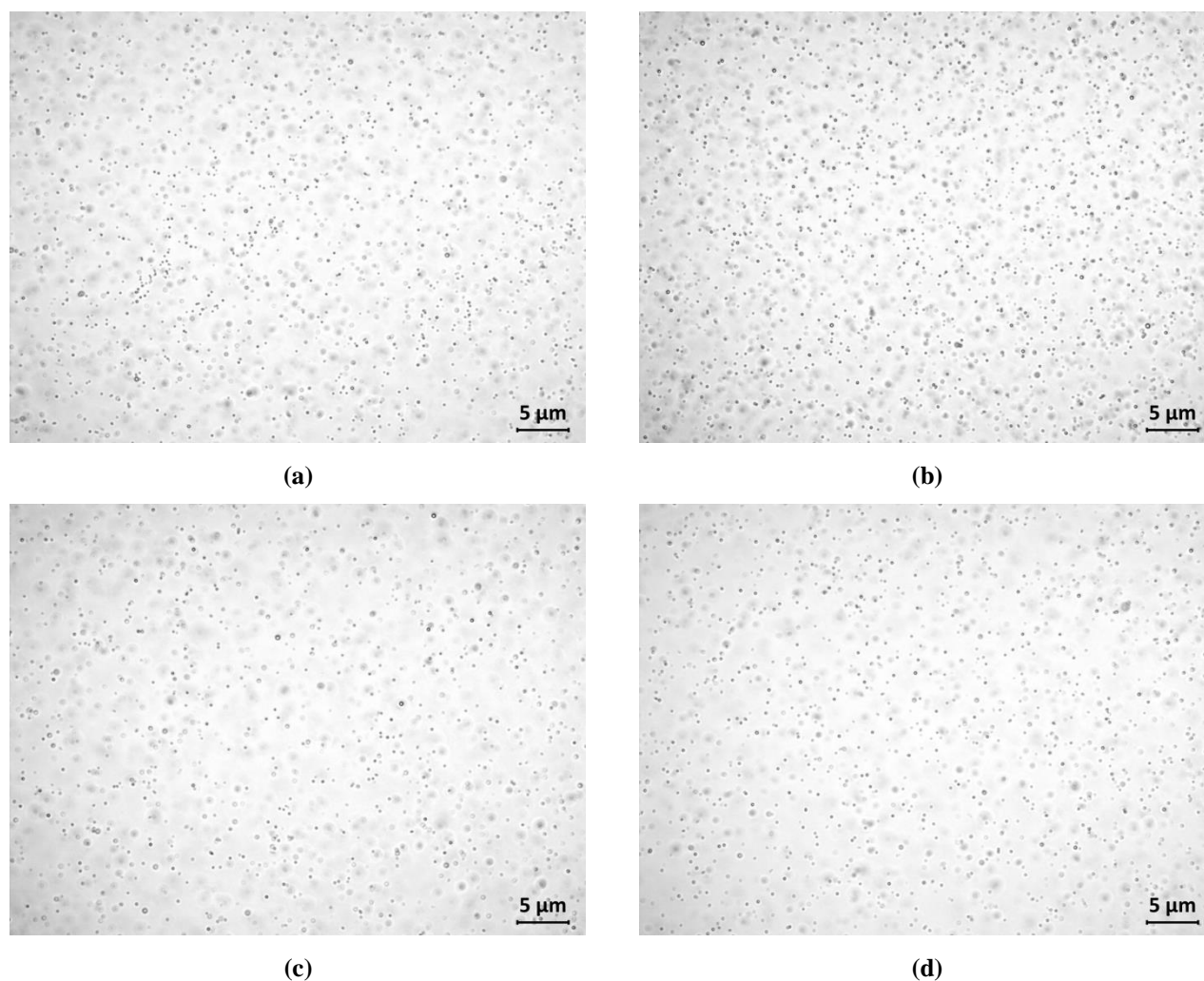
**Figure III-24.** Effect of pH on the surface charge of functionalized and initial MNPs:  $\gamma\text{-Fe}_2\text{O}_3/\text{Pol-COOH}$ ;  $\gamma\text{-Fe}_2\text{O}_3/\text{Pol@10-Mal}$ ;  $\gamma\text{-Fe}_2\text{O}_3/\text{Pol@18-Mal}$  and  $\gamma\text{-Fe}_2\text{O}_3/\text{Pol@23-Mal}$ .

Figure III-24 showed that the isoelectric point for the modified MNPs has shifted towards higher values of pH values and represents: 2.7 for native MNPs, 3.6 for  $\gamma\text{-Fe}_2\text{O}_3/\text{Pol@10-Mal}$ ; 3.8 for  $\gamma\text{-Fe}_2\text{O}_3/\text{Pol@18-Mal}$ ; and 4.3 for  $\gamma\text{-Fe}_2\text{O}_3/\text{Pol@23-Mal}$ . The shift of isoelectric point value points out the change of the surface charge of the modified MNPs, which occurred upon the surface modification chemistry. Also, zeta potential measurements allows predicting that the colloidal state of the modified MNPs will be stable in ultrapure water medium at pH values where zeta potential is more positive than +30 or more negative than -30 mV.

### III.3.3.3. Colloidal state of maleimide functionalized $\gamma\text{-Fe}_2\text{O}_3$ /Polymer MNPs in water

Colloidal state of native ( $\gamma\text{-Fe}_2\text{O}_3/\text{Pol-COOH}$ ) and maleimide functionalized MNPs ( $\gamma\text{-Fe}_2\text{O}_3/\text{Pol@10-Mal}$ ,  $\gamma\text{-Fe}_2\text{O}_3/\text{Pol@18-Mal}$  and  $\gamma\text{-Fe}_2\text{O}_3/\text{Pol@23-Mal}$ ) in ultrapure water was examined by Transmitted Light Microscopy (Figure III-25).

In accordance with zeta potential measurements, in this medium, all the analysed MNPs are well dispersed, pointing out the absence of a chemical aggregation. The absence of aggregates represents an important parameter that demonstrates the colloidal stability of the sample, resulting in a good dispersion. However, one should not forget, that particles' colloidal stability is strongly dependent on the nature of dispersant (polarity, density, etc). In the following paragraphs, concerning the ability of the modified MNPs to immobilize biomolecules or models of biomolecules, the colloidal stability will be strongly followed and optimized when necessary.



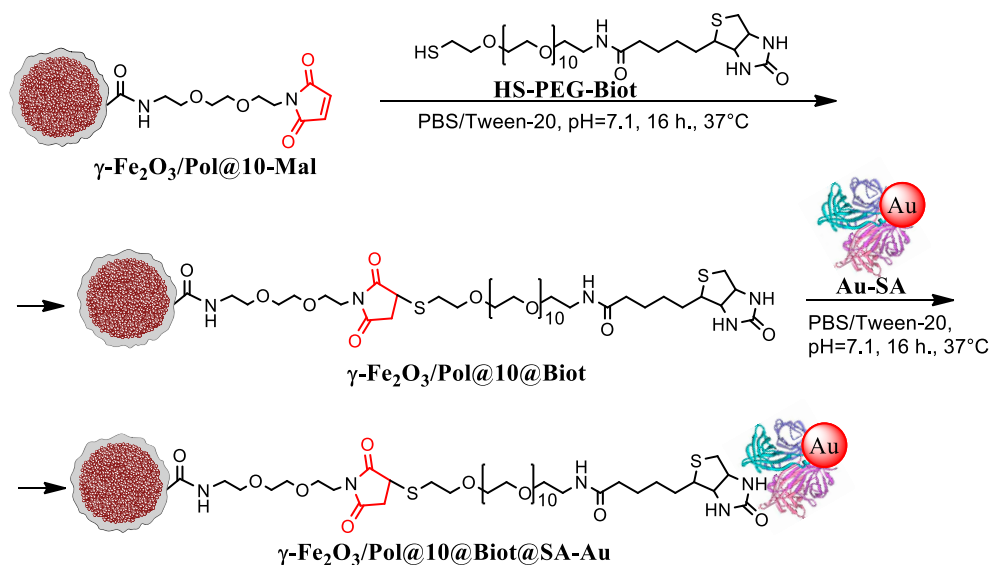
**Figure III-25.** Transmitted Light Microscopy images of (a)  $\gamma$ -Fe<sub>2</sub>O<sub>3</sub>/Pol-COOH; (b)  $\gamma$ -Fe<sub>2</sub>O<sub>3</sub>/Pol@10-Mal; (c)  $\gamma$ -Fe<sub>2</sub>O<sub>3</sub>/Pol@18-Mal and (d)  $\gamma$ -Fe<sub>2</sub>O<sub>3</sub>/Pol@23-Mal) dispersed in ultrapure water.

#### III.3.3.4. Covalent coupling of thiol modified biotin with maleimide functionalized $\gamma$ -Fe<sub>2</sub>O<sub>3</sub>/Polymer MNPs and consequent recognition by streptavidin coated gold NPs

As a model for testing the labelling efficiency of maleimide functionalized MNPs the strategy presented in Scheme III-7 was proposed.

This strategy involved first a covalent coupling of commercially available thiol modified biotin (HS-PEG-Biot) with maleimide functionalized MNPs ( $\gamma$ -Fe<sub>2</sub>O<sub>3</sub>/Pol@10-Mal,  $\gamma$ -Fe<sub>2</sub>O<sub>3</sub>/Pol@18-Mal or  $\gamma$ -Fe<sub>2</sub>O<sub>3</sub>/Pol@23-Mal) to give  $\gamma$ -Fe<sub>2</sub>O<sub>3</sub>/Pol@10@Biot,  $\gamma$ -Fe<sub>2</sub>O<sub>3</sub>/Pol@18@Biot and  $\gamma$ -Fe<sub>2</sub>O<sub>3</sub>/Pol@23@Biot respectively. Then commercially available 15 nm streptavidin coated gold NPs (SA-Au NPs) were immobilized on the resulting biotin functionalized MNPs ( $\gamma$ -Fe<sub>2</sub>O<sub>3</sub>/Pol@10@Biot,  $\gamma$ -Fe<sub>2</sub>O<sub>3</sub>/Pol@18@Biot and  $\gamma$ -Fe<sub>2</sub>O<sub>3</sub>/Pol@23@Biot) via Biotin-Streptavidin affinity to give  $\gamma$ -Fe<sub>2</sub>O<sub>3</sub>/Pol@10@Biot@SA-Au,  $\gamma$ -Fe<sub>2</sub>O<sub>3</sub>/Pol@18@Biot@SA-Au and  $\gamma$ -Fe<sub>2</sub>O<sub>3</sub>/Pol@23@Biot@SA-Au respectively. The immobilized SA-Au NPs served as a nanoscale

marker, and allowed both: their observation by TEM as well as the quantification of the immobilized SA-Au NPs amount by UV-Vis spectroscopy.



**Scheme III-7.** Schematic representation of covalent coupling of thiol modified biotin with  $\gamma\text{Fe}_2\text{O}_3/\text{Pol}@10\text{-Mal}$  followed by the immobilization of 15 nm SA-Au NPs via Biotin-Streptavidin affinity.

For this purpose, 0.05 mg of each type of biotin functionalized MNPs ( $\gamma\text{-Fe}_2\text{O}_3/\text{Pol}@10\text{@Biot}$ ,  $\gamma\text{-Fe}_2\text{O}_3/\text{Pol}@18\text{Biot}$  and  $\gamma\text{-Fe}_2\text{O}_3/\text{Pol}@23\text{@Biot}$ ) were incubated with  $2.00 \times 10^{11}$  SA-Au NPs ( $4.0 \times 10^{12}$  SA-Au NPs per 1mg of functionalized MNPs). During the immobilization reaction, no sedimentation or aggregation was observed. The solutions of 15 nm SA-Au NPs recovered after this immobilization were analysed by UV-Vis Spectroscopy for quantitative study while the resulting MNPs were examined by TEM.

TEM images of  $\gamma\text{-Fe}_2\text{O}_3/\text{Pol}@10\text{@Biot}@SA\text{-Au}$ ,  $\gamma\text{-Fe}_2\text{O}_3/\text{Pol}@18\text{@Biot}@SA\text{-Au}$  and  $\gamma\text{-Fe}_2\text{O}_3/\text{Pol}@23\text{@Biot}@SA\text{-Au}$  (Figure III-26, Figure III-27 and Figure III-28 respectively) clearly showed that MNPs functionalized with dendritic structures **18** and **23** immobilise a higher quantities of SA-Au NPs than those functionalized with a linear coupling agent **10**. At this stage, no difference was noticed between  $\gamma\text{-Fe}_2\text{O}_3/\text{Pol}@18\text{@Biot}@SA\text{-Au}$  and  $\gamma\text{-Fe}_2\text{O}_3/\text{Pol}@23\text{@Biot}@SA\text{-Au}$ , since in both cases a compact covering of functionalized MNPs with 15 nm SA-Au NPs was observed. It is worthy to mention that free SA-Au NPs were not observed in any of the samples, pointing out the efficiency of the washing procedure.



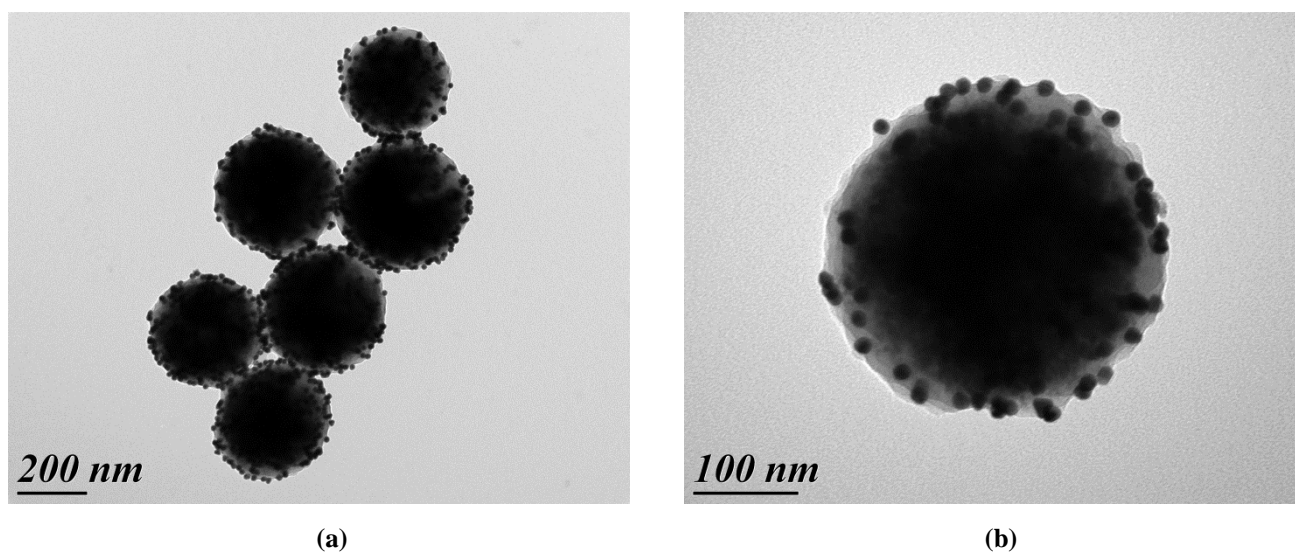


Figure III-26. (a) and (b) TEM of  $\gamma\text{-Fe}_2\text{O}_3$ /Pol@10@Biot@SA-Au.

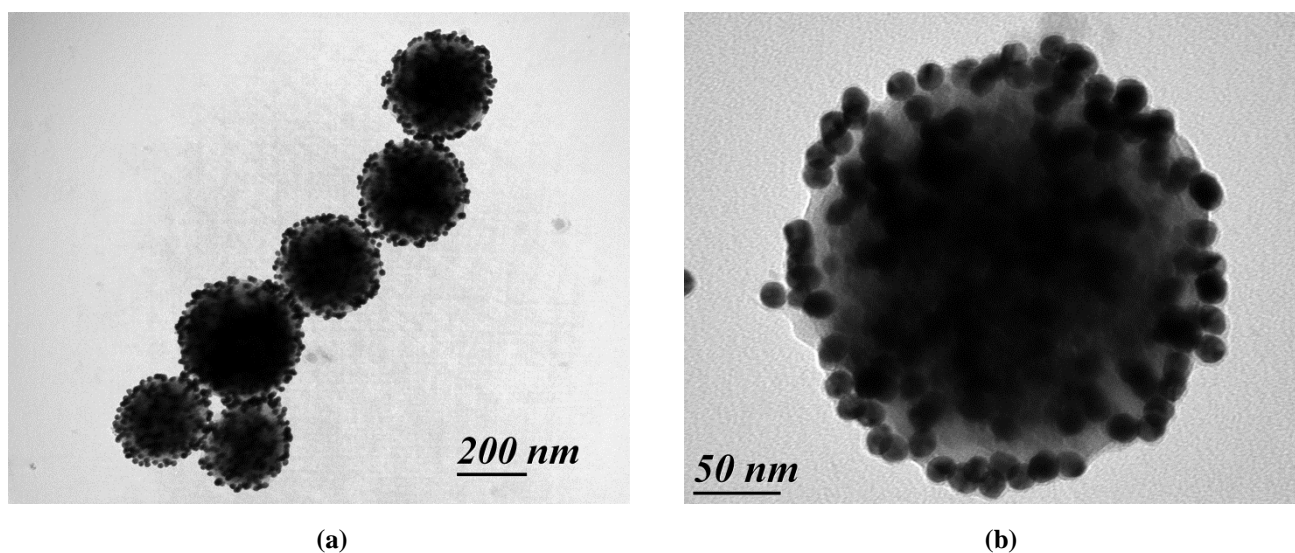


Figure III-27. (a) and (b) TEM of  $\gamma\text{-Fe}_2\text{O}_3$ /Pol@18@Biot@SA-Au.

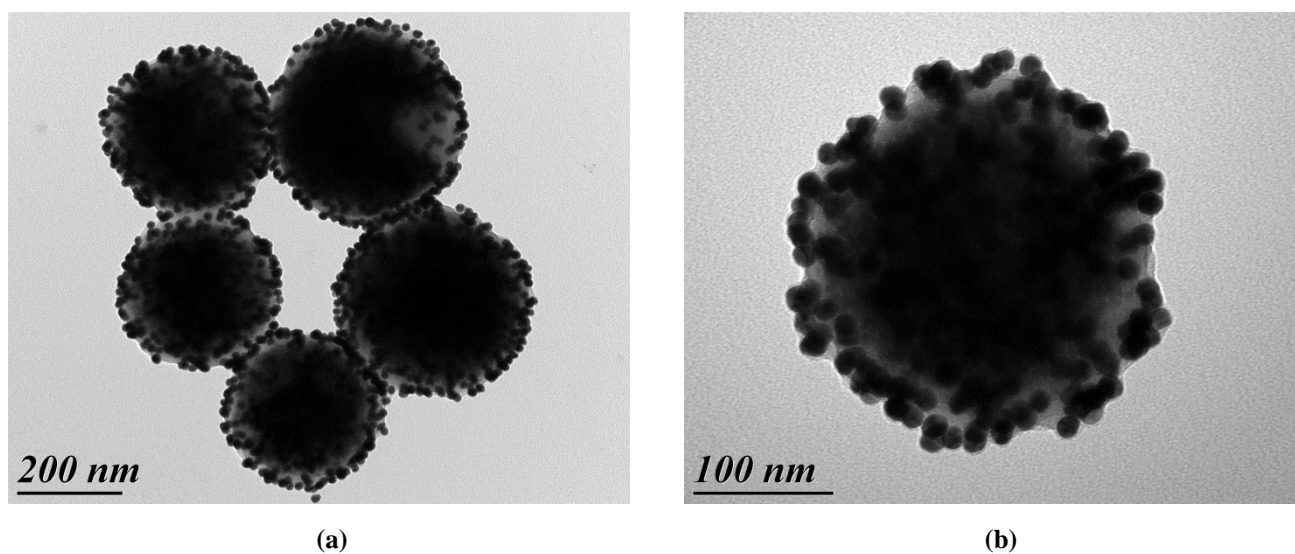


Figure III-28. (a) and (b) TEM of  $\gamma\text{-Fe}_2\text{O}_3$ /Pol@23@Biot@SA-Au.

UV-Vis absorption spectroscopy measurements of the solutions of 15 nm SA-Au NPs recovered after the immobilization reactions were performed, since Au NPs with diameter between 12 and 41 nm are strongly absorbent in the UV-Vis region 520 – 530 nm and when the size of gold nanoparticle is constant, the absorbance is proportional to the concentration of gold.<sup>22</sup> The quantitative analysis can be performed based on the Bouguer–Beer–Lambert law, commonly called Beer’s law. This law can be expressed as:

$$A = \varepsilon \cdot c \cdot l,$$

where  $A$  is the measured absorbance of the sample at a given wavelength,  $\varepsilon$  is the molecular absorptivity (or molar absorption coefficient) at a certain wavelength,  $l$  (in cm) is the path length of source beam in the sample or the thickness of the cuvette, and  $c$  is the molar concentration of the sample. This law basically states that the intensities of absorption bands are linearly proportional to the concentration of each component in a homogeneous mixture or solution.

In analogy to this law, in the case of NPs, the intensities of absorption bands are linearly proportional to the number of nanoparticles ( $N_{NP}$ ) in a homogeneous mixture. Normally, the concentration of SA-Au NPs in the sample should be expressed in  $N_{NP}/\text{mL}$ , but in our case the change in absorbance was monitored as a function of the nanoparticles number (in the sample) since the volume of all measured samples remained constant (0.2 mL). Such data representation simplifies the calculations of SA-Au NPs number in the sample. The cuvette thickness ( $l$ ) was also constant and constituted 0.1 cm in all measurements. Therefore, all said above can be expressed as:

$$A = k \cdot N_{NP},$$

where  $A$  is the measured absorbance of a sample at a given wavelength,  $k$  is a constant and  $N_{NP}$  is the number of nanoparticles in 0.2 mL.

Thus, a calibration plot was firstly recorded, in which the absorbance of 15 nm SA-Au NPs’ solutions of known concentrations was measured (Figure III-29 a). The dependence of the absorption band intensity at 526 nm as the function of number of particles represents the calibration curve (Figure III-29 b) that was used to determine number of SA-Au NPs left in solution after the immobilizations step.

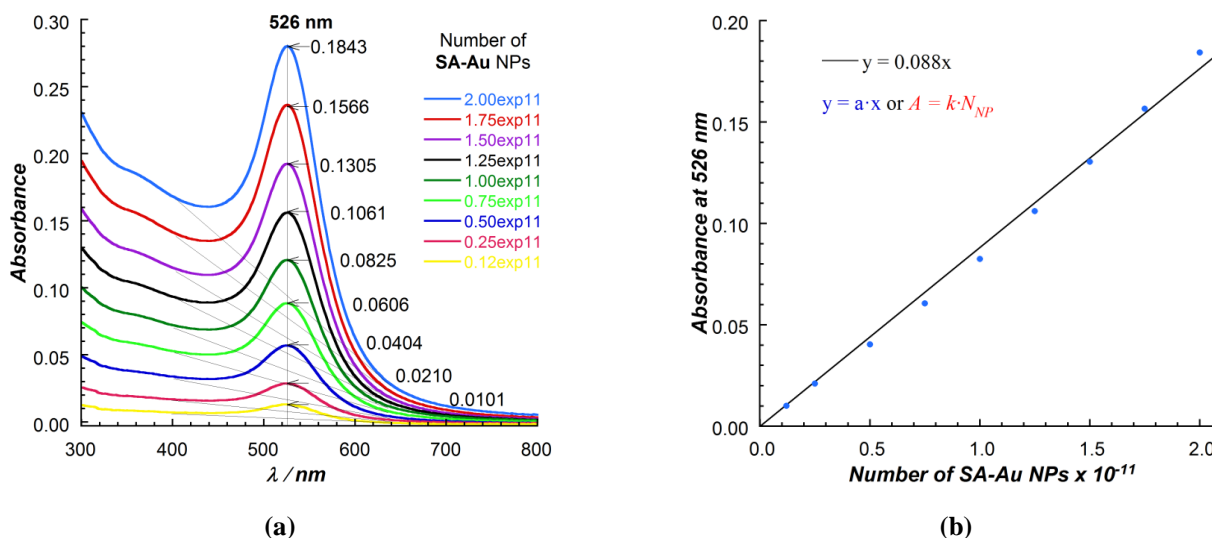


Figure III-29. (a) Calibration plot of 15 nm SA-Au NPs and (b) calibration curve.

Absorption spectra of the 15 nm SA-Au NPs' solutions, recovered after the immobilization reactions, are shown in Figure III-30 a. The measured absorbance at 526 nm was used to calculate the amount of SA-Au NPs left in solution after the immobilization reactions and respectively that of immobilized SA-Au NPs (Figure III-30 b).

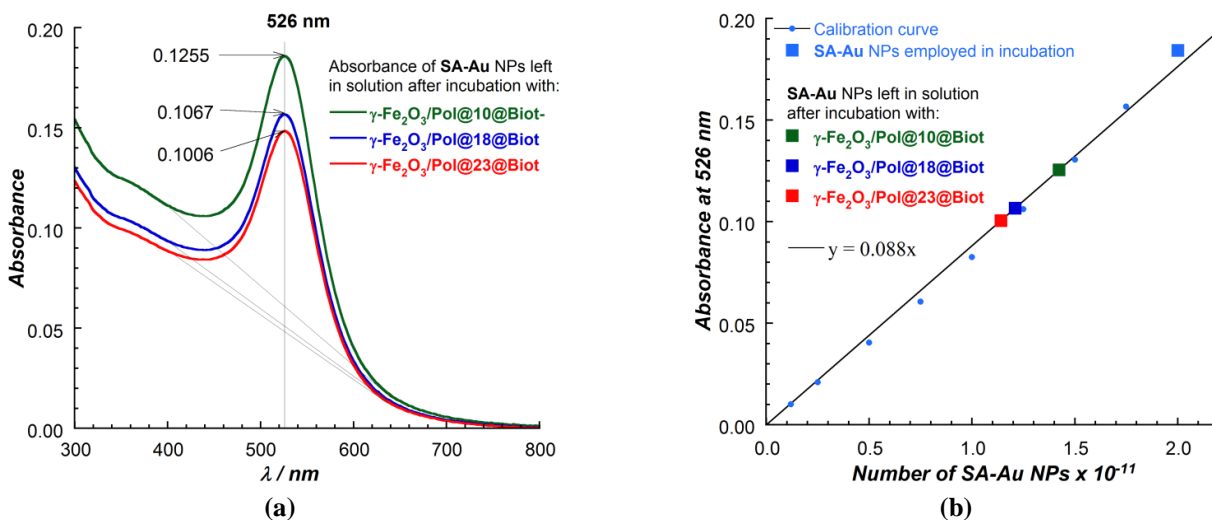
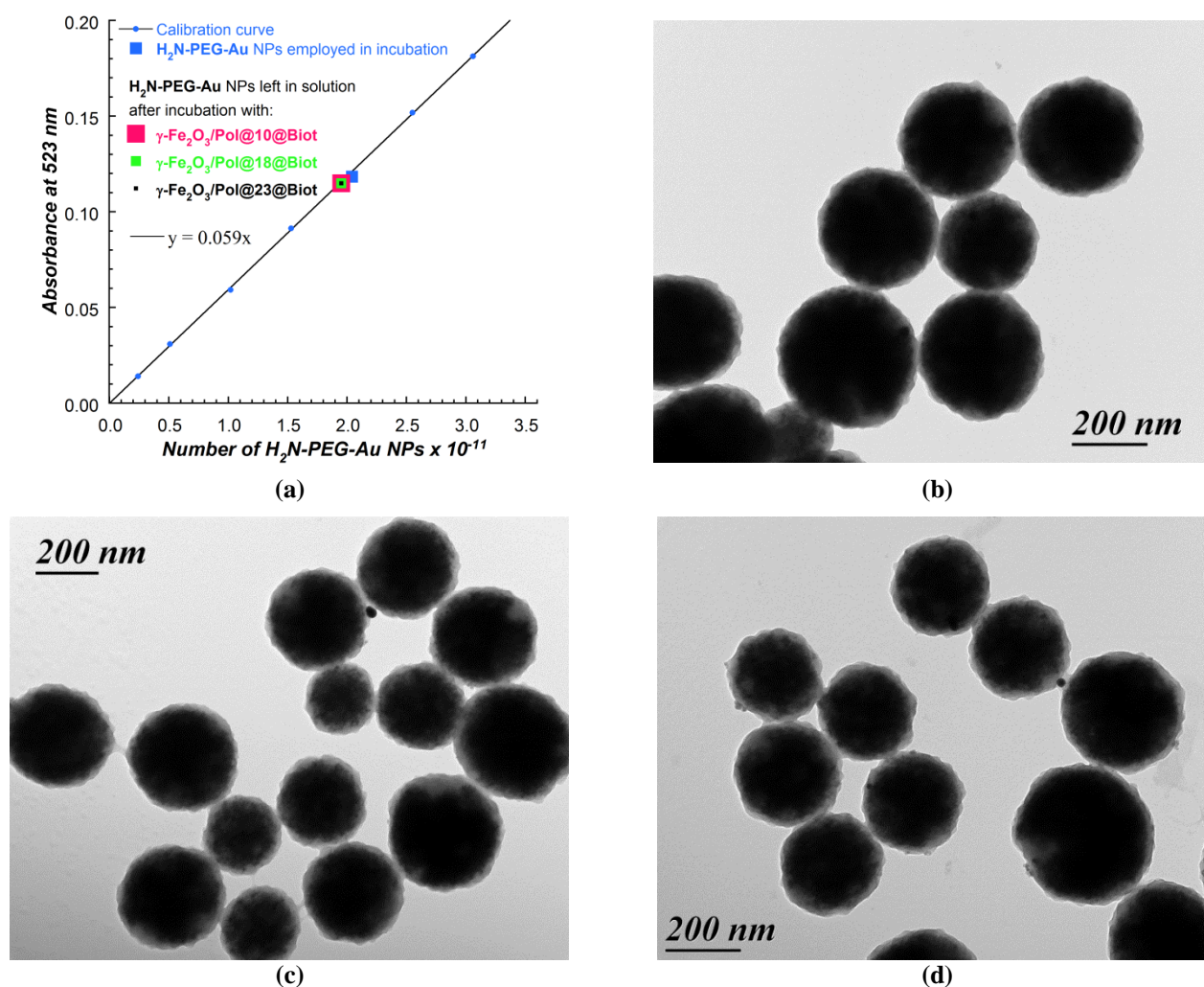


Figure III-30. (a) Dependence  $A=f(\lambda)$  of the solutions of 15 nm SA-Au NPs recovered after the immobilization reaction, and (b) Dependence of Absorbance at 526 nm as function of 15 nm SA-Au NPs number left in solution after the immobilization reaction.

According to the calculations,  $\gamma\text{-Fe}_2\text{O}_3/\text{Pol}@10@\text{Biot}$  immobilized 29 % of added SA-Au NPs ( $0.58 \times 10^{11}$  of SA-Au NPs on 0.05 mg of  $\gamma\text{-Fe}_2\text{O}_3/\text{Pol}@10@\text{Biot}$  or  $1.16 \times 10^{12}$  of SA-Au NPs per 1mg of  $\gamma\text{-Fe}_2\text{O}_3/\text{Pol}@10@\text{Biot}$ );  $\gamma\text{-Fe}_2\text{O}_3/\text{Pol}@18@\text{Biot}$  immobilized 40 % of added SA-Au NPs ( $0.79 \times 10^{11}$  of SA-Au NPs on 0.05 mg of  $\gamma\text{-Fe}_2\text{O}_3/\text{Pol}@18@\text{Biot}$  or  $1.58 \times 10^{12}$  of SA-Au NPs per 1mg of  $\gamma\text{-Fe}_2\text{O}_3/\text{Pol}@18@\text{Biot}$ ) and  $\gamma\text{-Fe}_2\text{O}_3/\text{Pol}@23@\text{Biot}$  immobilized 43 % of added SA-Au NPs ( $0.86 \times 10^{11}$  of SA-Au NPs on 0.05 mg of  $\gamma\text{-Fe}_2\text{O}_3/\text{Pol}@23@\text{Biot}$  or  $1.72 \times 10^{12}$  of SA-Au NPs per 1mg of  $\gamma\text{-Fe}_2\text{O}_3/\text{Pol}@23@\text{Biot}$ ). These results are in a good coherence with those seen by TEM

(Figure III-26-28) and highlight the positive “*dendritic effect*” on the surface functionalization. The higher is the dendron generation, the higher is the ability of maleimide functionalized MNPs to immobilize thiol containing biomolecules.

In order to check the specificity of the immobilization, biotin functionalized MNPs ( $\gamma\text{-Fe}_2\text{O}_3/\text{Pol}@10\text{@Biot}$ ,  $\gamma\text{-Fe}_2\text{O}_3/\text{MNP-Pol}@18\text{@Biot}$  and  $\gamma\text{-Fe}_2\text{O}_3/\text{Pol}@23\text{@Biot}$ ) were incubated with commercial 20 nm amino PEGylated gold nanoparticles ( $\text{H}_2\text{N-PEG-Au}$  NPs) respecting the same experimental conditions as for immobilization of SA-Au NPs ( $2.00 \times 10^{11}$  of  $\text{H}_2\text{N-PEG-Au}$  NPs per 0.05 mg of each type of MNPs). Since biotin functionalized MNPs do not possess any functionality capable to covalently react with the amino groups of  $\text{H}_2\text{N-PEG-Au}$  NPs, this model allows monitoring the specificity of biotin functionalized MNPs. UV-Vis absorption spectroscopy measurements of 20 nm  $\text{H}_2\text{N-PEG-Au}$  NPs’ solutions recovered after the incubations were performed (by recording firstly a calibration curve, similarly as it was done for SA-Au NPs) and are presented in Figure III-31a, while MNPs that were incubated with 20 nm  $\text{H}_2\text{N-PEG-Au}$  NPs were analysed in TEM (Figure III-31b, c, d).



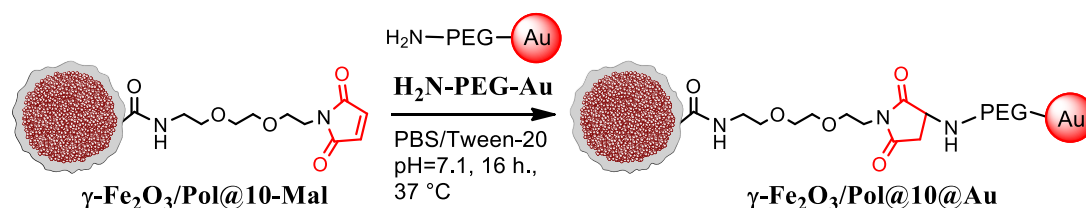
**Figure III-31.** (a) Dependence of Absorbance at 523 nm as function of 20 nm  $\text{H}_2\text{N-PEG-Au}$  NPs number left in solution after the incubation reaction; (b)  $\gamma\text{-Fe}_2\text{O}_3/\text{Pol}@10\text{@Biot}$  incubated with 20 nm  $\text{H}_2\text{N-PEG-Au}$  NPs; (c)  $\gamma\text{-Fe}_2\text{O}_3/\text{Pol}@18\text{@Biot}$  incubated with 20 nm  $\text{H}_2\text{N-PEG-Au}$  NPs; (d)  $\gamma\text{-Fe}_2\text{O}_3/\text{Pol}@23\text{@Biot}$  incubated with 20 nm  $\text{H}_2\text{N-PEG-Au}$  NPs.

As expected, Figure III-31 (a) showed that all the samples of MNPs ( $\gamma\text{-Fe}_2\text{O}_3/\text{Pol}@10\text{@Biot}$ ,  $\gamma\text{-Fe}_2\text{O}_3/\text{Pol}@18\text{@Biot}$  and  $\gamma\text{-Fe}_2\text{O}_3/\text{Pol}@23\text{@Biot}$ ) have similar behaviour regarding their incubation with 20 nm  $\text{H}_2\text{N-PEG-Au}$  NPs. Indeed, according to the calculations, the quantity of 20 nm  $\text{H}_2\text{N-PEG-Au}$  NPs that was non-specifically immobilized on biotin functionalized MNPs represent around 4 % for all the samples. These results are in a good coherence with those seen in TEM (Figure III-31 b, c, d).

To conclude, this strategy offered the possibility to indirectly quantify (via Biotin-SA affinity) the ability of maleimide functionalized MNPs to immobilize a thiol tagged biomolecule. Moreover, the test of biotin functionalized MNPs incubation with  $\text{H}_2\text{N-PEG-Au}$  NPs proved the high covering of MNPs with maleimide functionality. All these results indirectly confirm the successful functionalization of MNPs and the positive “*dendritic effect*” on the surface functionalization.

### III.3.3.5. Immobilization of amino functionalized gold nanoparticles on maleimide functionalized $\gamma\text{-Fe}_2\text{O}_3$ /Polymer MNPs

It is known that maleimide group reacts specifically with thiol groups when the pH of the reaction mixture is between 6.5 and 7.5, while at pH higher than 8.0, maleimides will favour a reaction with primary amines (like Lysine and Arginine side chains) over thiols.<sup>23,24</sup> This study aims to monitor the reactivity of maleimide functionalized MNPs towards amino group in the typical reaction conditions used for immobilization of thiols (see III.3.3.4 and III.3.3.6). For this purpose maleimide functionalized MNPs ( $\gamma\text{-Fe}_2\text{O}_3/\text{Pol}@10\text{-Mal}$ ,  $\gamma\text{-Fe}_2\text{O}_3/\text{Pol}@18\text{-Mal}$ ,  $\gamma\text{-Fe}_2\text{O}_3/\text{Pol}@23\text{-Mal}$ ) were incubated with 20 nm  $\text{H}_2\text{N-PEG-Au}$  NPs as shown in the Scheme III-8, ( $2.00 \times 10^{11}$  of  $\text{H}_2\text{N-PEG-Au}$  NPs per 0.05 mg of each type of maleimide functionalized MNPs). In this model  $\text{H}_2\text{N-PEG-Au}$  NPs were used in order to imitate the amino containing biomolecule.



**Scheme III-8.** Schematic representation of  $\text{H}_2\text{N-PEG-Au}$  NPs immobilization on  $\gamma\text{Fe}_2\text{O}_3/\text{Pol}@10\text{-Mal}$ .

As a blank sample,  $\gamma\text{-Fe}_2\text{O}_3/\text{Pol-COOH}$  were also incubated with 20 nm  $\text{H}_2\text{N-PEG-Au}$  NPs in the same conditions (carboxylic acid groups were not activated). The resulted MNPs were analysed by TEM (Figure III-32) while the 20 nm  $\text{H}_2\text{N-PEG-Au}$  NPs' solutions recovered after the performed immobilization were analysed by UV-Vis Spectroscopy (Figure III-33).

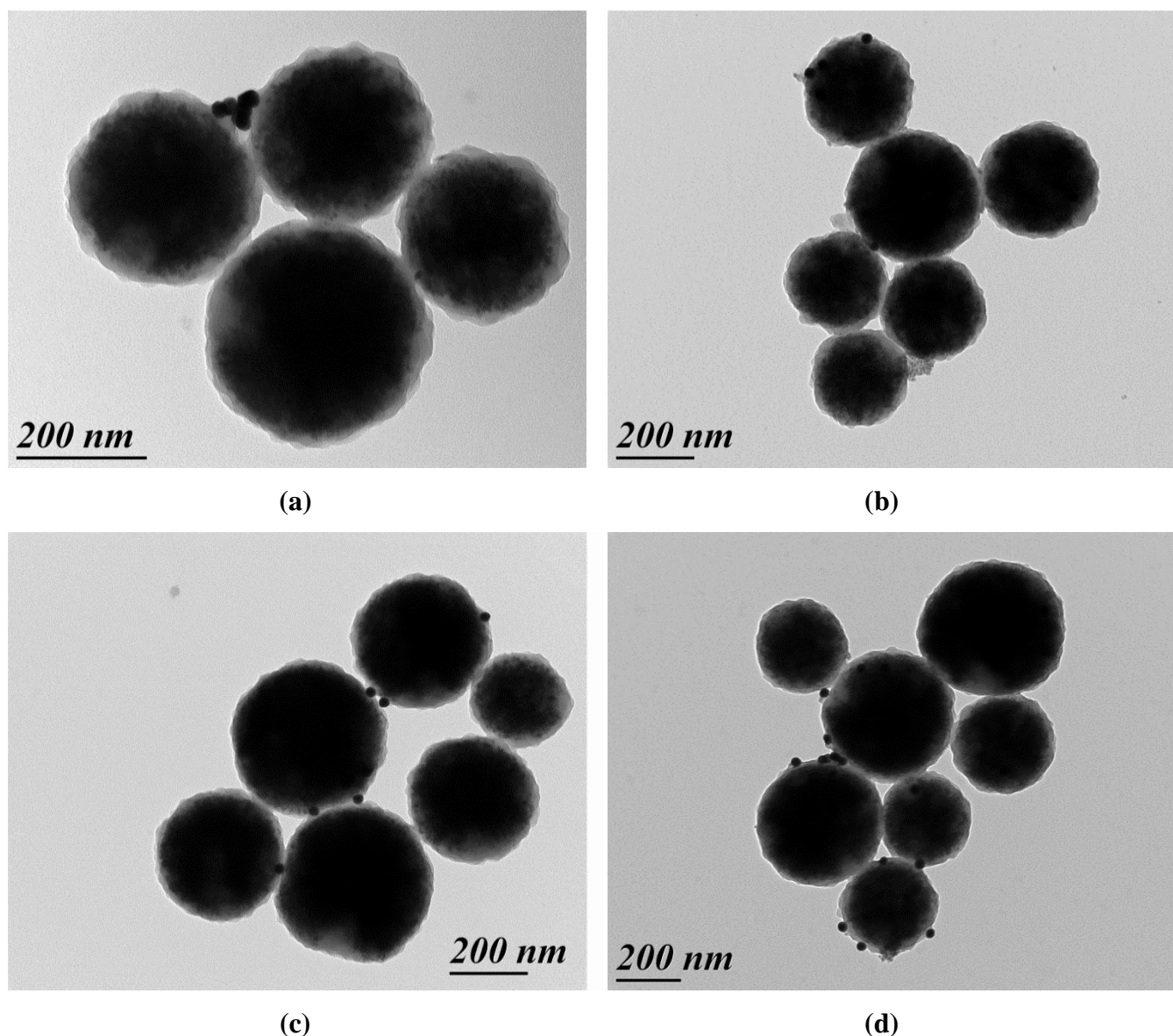


**Figure III-32.** (a)  $\gamma\text{-Fe}_2\text{O}_3/\text{Pol-COOH}$  incubated with 20 nm  $\text{H}_2\text{N-PEG-Au}$  NPs; (b)  $\gamma\text{-Fe}_2\text{O}_3/\text{Pol@10-Mal}$  incubated with 20 nm  $\text{H}_2\text{N-PEG-Au}$  NPs; (c)  $\gamma\text{-Fe}_2\text{O}_3/\text{Pol@18-Mal}$  incubated with 20 nm  $\text{H}_2\text{N-PEG-Au}$  NPs; (d)  $\gamma\text{-Fe}_2\text{O}_3/\text{Pol@23-Mal}$  incubated with 20 nm  $\text{H}_2\text{N-PEG-Au}$  NPs.

TEM revealed a relatively poor number of immobilized 20 nm  $\text{H}_2\text{N-PEG-Au}$  NPs regardless the sample (comparing to that seen in Figure III-31 b, c and d). At the same time, we can note that the amount of immobilized 20 nm  $\text{H}_2\text{N-PEG-Au}$  NPs increases with increasing the number of functional groups present on MNPs' surface, pointing out on the addition of amino group to maleimide double bond. This hypothesis is also supported by the fact that  $\gamma\text{-Fe}_2\text{O}_3/\text{Pol-COOH}$  immobilized a smaller number of 20 nm  $\text{H}_2\text{N-PEG-Au}$  NPs than maleimide functionalized MNPs and, consequently, confirms that the immobilization of  $\text{H}_2\text{N-PEG-Au}$  NPs on maleimide functionalized MNPs is due to the addition of amino group to maleimide double bond and not due to the reaction between the amino group and free carboxylic acid groups left on MNPs' surface.

The analysis of the 20 nm  $\text{H}_2\text{N-PEG-Au}$  NPs' solutions recovered after the immobilization by UV-Vis Spectroscopy (Figure III-33) afforded estimation of the percentage of immobilized  $\text{H}_2\text{N-PEG-Au}$  NPs.

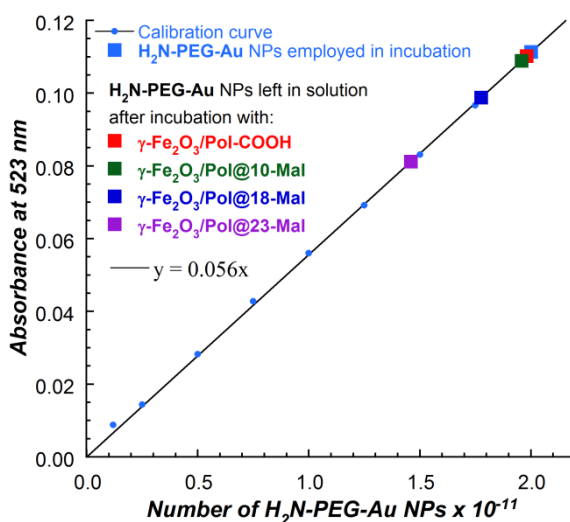


**Figure III-33.** Dependence of Absorbance at 523 nm as function of  $\text{H}_2\text{N-PEG-Au}$  NPs' number left in solution after the incubation reaction.

Thus, according to the calculations, the quantity of 20 nm  $\text{H}_2\text{N-PEG-Au}$  NPs that was immobilized on  $\gamma\text{-Fe}_2\text{O}_3/\text{Pol-COOH}$  represents 1 %, on  $\gamma\text{-Fe}_2\text{O}_3/\text{Pol}@10\text{-Mal}$  – 2 %, on  $\gamma\text{-Fe}_2\text{O}_3/\text{Pol}@18\text{-Mal}$  – 11 % and on  $\gamma\text{-Fe}_2\text{O}_3/\text{Pol}@23\text{-Mal}$  – 27 %. These results are in a good coherence with those observed in TEM images and additionally point out on the increase of the amount of immobilized 20 nm  $\text{H}_2\text{N-PEG-Au}$  NPs with the increase of the number of maleimide functional groups present on MNPs' surface.

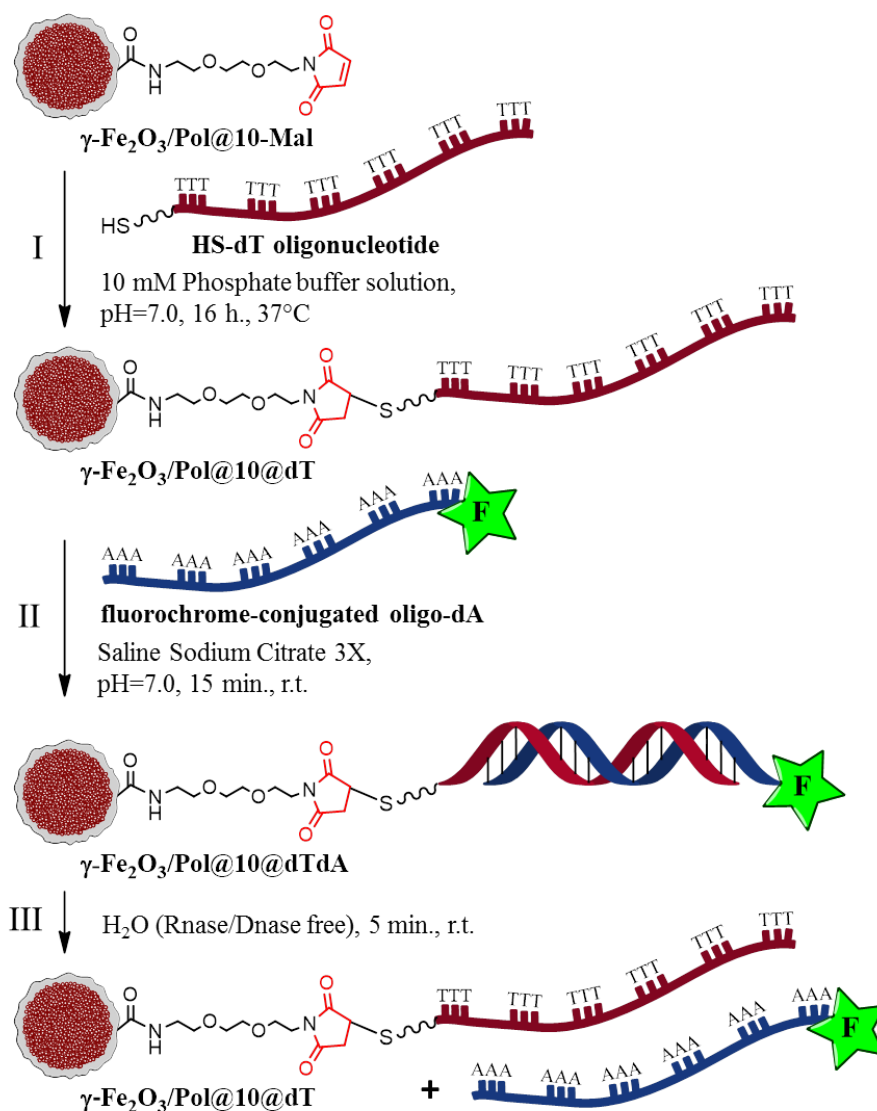
To conclude, despite the fact that this experiment showed the possibility of amino group addition, in these reaction conditions (that actually are optimized for thiol addition), the quantity of  $\text{H}_2\text{N-PEG-Au}$  NPs immobilized on maleimide functionalized MNPs remains not significant comparing to the quantities of thiol containing “objects” that can be immobilized, since the reaction with thiols takes place 1000 times faster than with amines.<sup>25</sup> Thus, the specificity of maleimide functionalized MNPs towards thiol groups was confirmed.

### III.3.3.6. Covalent coupling of thiol modified oligonucleotide with maleimide functionalized $\gamma\text{-Fe}_2\text{O}_3$ /Polymer MNPs

Oligonucleotides are short, single-stranded deoxyribonucleic acids (ssDNA) or ribonucleic acids (ssRNA). A particular property of these molecules is that they can readily bind, in a sequence-specific manner (hybridization), to their respective complementary oligonucleotides, DNA, or RNA. This property served as a foundation for their use as probes for detecting or separating DNA or RNA.<sup>26</sup>

Thus, oligonucleotides have found application in various fields of biotechnology, especially in DNA microarrays, fluorescent in situ hybridization (FISH) and the synthesis of artificial genes.

Immobilization of oligonucleotides on MNPs is of a great interest for many bioanalytical biotechnological applications due to the advantage of the magnetic separation. In view of these challenges, the covalent immobilization is of particular importance, since it gives the possibility to fully preserve the biological activity of ssDNA, including its functions of hybridization and bioaffinity. Many different approaches of covalent immobilization on different solid supports have been reported, however the number of reports on immobilization of oligonucleotides on MNPs is scarce.<sup>27</sup> In this work we report simple and effective method of oligonucleotide immobilization via thiol-maleimide reaction. Moreover the performance of oligonucleotide modified MNPs in hybrid capture of a complementary fluorescent labelled oligonucleotide was investigated. Scheme III-9 illustrates the steps of this strategy (on the example of  $\gamma\text{-Fe}_2\text{O}_3$ /Pol@10-Mal).



**Scheme III-9.** I) Covalent coupling of thiol modified oligonucleotide (HS-dT) with maleimide functionalized MNPs ( $\gamma\text{-Fe}_2\text{O}_3$ /Pol@10-Mal); II) Hybrid capture of a complementary sequence oligo poly A (fluoroconjugated oligo-dA Alexa Fluor) on oligonucleotide-modified MNP ( $\gamma\text{-Fe}_2\text{O}_3$ /Pol@10@dT); and III) Dehybridization.



In the first step the thiol modified oligonucleotide, namely 3' thiol modified oligonucleotide poly T: TTT-TTT-TTT-TTT-TTT-TTT (HS-dT oligonucleotide) was covalently immobilized on maleimide functionalized MNPs. In the second step, the hybridization of the immobilized oligonucleotide dT with a complementary sequence oligo poly A of fluorochrome-conjugated oligo-dA Alexa Fluor was performed. The last step represents the dehybridization, and the eluted in this step fluorochrome-conjugated oligo-dA was quantified on fluorescence microplate reader (Figure III-34). A control experiment was also performed on  $\gamma\text{-Fe}_2\text{O}_3$ /Pol-COOH. The hybridization, dehybridization and quantification of oligo-dA were performed by Ademtech SA.<sup>4</sup> The quantity of oligo-dA Alexa Fluor detected in Figure III-34 is directly related to the quantity of HS-dT oligonucleotide immobilized on maleimide functionalized MNPs.

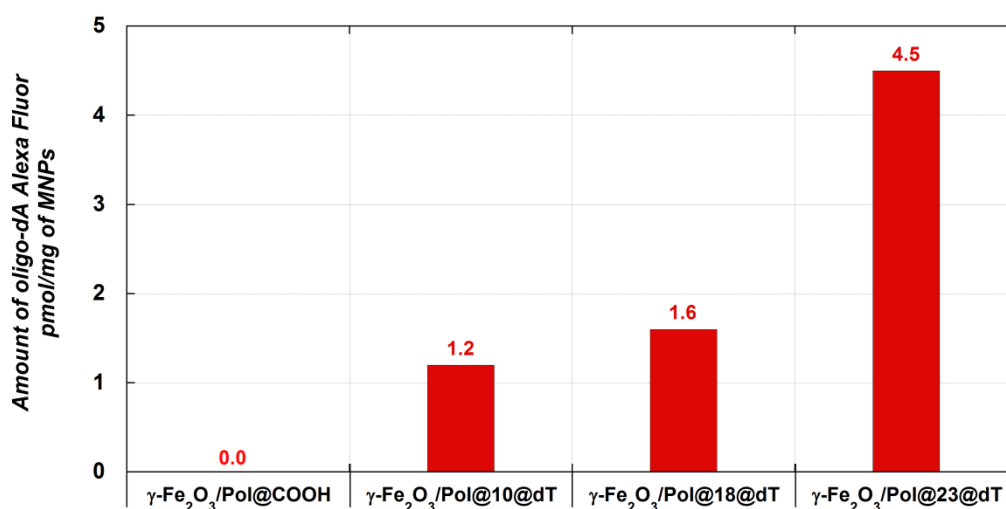


**Figure III-34.** Results of the fluorescent quantification of the oligo-dA Alexa Fluor eluted after the dehybridization.

The results showed that all the maleimide modified  $\gamma\text{-Fe}_2\text{O}_3$ /Polymer MNPs immobilize the target biomolecule. Thus,  $\gamma\text{-Fe}_2\text{O}_3/\text{Pol@10-Mal}$  immobilized 1.2 pmol/mg of HS-dT oligonucleotide;  $\gamma\text{-Fe}_2\text{O}_3/\text{Pol@18-Mal}$  – 1.6 pmol/mg and  $\gamma\text{-Fe}_2\text{O}_3/\text{Pol@23}$  – 4.5 pmol/mg. In contrast, that native  $\gamma\text{-Fe}_2\text{O}_3$ /Polymer MNPs ( $\gamma\text{-Fe}_2\text{O}_3/\text{Pol-COOH}$ , that do not possess maleimide groups) do not immobilize the any HS-dT oligonucleotide (0.0 pmol/mg), pointing out the specificity of the reaction of thiol with maleimide group. Also, these results highlights that the immobilized oligonucleotide preserved its functions of hybridization. Moreover, the results proved the positive “*dendritic effect*” on the thiol modified oligonucleotide immobilization.

For comparison, A. del Campo and co-workers<sup>28</sup> performed a similar study, in which the amino modified oligonucleotide was immobilized on aldehyde modified magnetite NPs (30 – 100 nm) and subsequently used for the capture of the complementary fluorescent labelled oligonucleotide. They showed that the amount of immobilized oligonucleotide was directly influenced by the density of the

functional groups on the NPs' surface. The maximum amount of immobilized oligonucleotide was 0.145 nmol/mg.

Thus, the amounts of immobilized oligonucleotide on the maleimide modified  $\gamma$ -Fe<sub>2</sub>O<sub>3</sub>/Polymer MNPs ( $\gamma$ -Fe<sub>2</sub>O<sub>3</sub>/Pol@10-Mal,  $\gamma$ -Fe<sub>2</sub>O<sub>3</sub>/Pol@18-Mal and  $\gamma$ -Fe<sub>2</sub>O<sub>3</sub>/Pol@23) are encouraging and can be improved by modifying the immobilization reaction conditions.

### III.4. Conclusion

In this chapter maleimide functionalization of  $\gamma$ -Fe<sub>2</sub>O<sub>3</sub>/Polymer MNPs was investigated. The chemical modification of core-shell  $\gamma$ -Fe<sub>2</sub>O<sub>3</sub>/Polymer MNPs was achieved via covalent attachment of previously synthesised coupling agents (*see Chapter II*): linear coupling agent **10** (containing one functional group); two-branched coupling agent **18** (containing two functional groups) and four-branched dendritic coupling agent **23** (containing four functional groups).

The surface modification chemistry has been controlled via FT-IR spectroscopy that proved to be an efficient technique to monitor the grafting process. It was observed that the grafting efficiency is strongly dependent on the quantity of coupling agents employed into the grafting process and had to be adjusted particularly for each molecule. Thus, the maximum of surface functionalization with linear coupling agent **10** can be achieved by adding *100 equivalents* of compound; with two-branched coupling agent **18** (dendron G1) *50 equivalents* of compound are necessary; while four-branched coupling agent **23** (dendron G2) allows achieving the maximum of surface functionalization by adding only *10 equivalents* of compound. These results clearly showed that functionalization with dendritic coupling agents **18** and **23** is more efficient than functionalization with linear coupling agent **10**. Moreover, the amount of functional groups on MNPs' surface increases with the growth of dendron's generation and according to the FT-IR studies it is directly proportional to the number of functional groups in the structure of the grafted coupling agent. This study showed that functionalizing MNPs with dendritic structures is more advantageous than functionalizing with linear structures and despite the fact that synthesis of dendritic coupling agents is more complicated, the quantities necessary for an efficient functionalization fully justifies their synthesis.

The surface modification chemistry was also proved by TGA coupled with MS analyses and zeta potential measurements. The functionalized MNPs preserved their integrity as well as their colloidal stability, possessing a good dispersion in aqueous solutions and polar solvents.

The ability of maleimide functionalized MNPs to immobilize biomolecules or a model of biomolecules was studied by performing a series of immobilization tests. In the first strategy, the covalent immobilization of a thiol modified biotin (HS-PEG-Biot) on maleimide functionalized MNPs was performed, and was controlled via Biotin-SA affinity recognition. This study clearly showed the positive “*dendritic effect*”, since MNPs functionalized with dendritic structures immobilise higher quantities of SA-Au NPs than those functionalized with linear coupling agent ( $\gamma$ -Fe<sub>2</sub>O<sub>3</sub>/Pol@10@Biot immobilized 29 % of added SA-Au NPs,  $\gamma$ -Fe<sub>2</sub>O<sub>3</sub>/Pol@18@Biot immobilized 40 % of added SA-Au NPs and  $\gamma$ -Fe<sub>2</sub>O<sub>3</sub>/Pol@23@Biot immobilized 43 % of added SA-Au NPs). Moreover, the specificity of this immobilization was confirmed.

The reactivity of maleimide functionalized MNPs towards amino group, in the typical reaction conditions used for immobilization of thiols, was monitored by incubating maleimide functionalized MNPs with H<sub>2</sub>N-PEG-Au NPs. This study revealed the specificity of the maleimide functionalized MNPs towards thiol group, since a relatively poor number of H<sub>2</sub>N-PEG-Au NPs was immobilized. Despite the fact that this experiment showed the possibility of amino group addition, in these reaction conditions (that are actually optimized for thiol addition), the quantity of H<sub>2</sub>N-PEG-Au NPs immobilized on maleimide functionalized MNPs remains non-significant comparing to the quantities of thiol containing “*objects*” that can be immobilized, since the reaction with thiols takes place much more faster than that with amines.

Finally, 3' thiol modified oligonucleotide poly T (HS-dT oligonucleotide) was successfully immobilized on maleimide functionalized MNPs and subsequently quantified. The quantities of the immobilized HS-dT oligonucleotide are encouraging, but still can be improved. As expected, an increase of the immobilized HS-dT oligonucleotide amount with the increase of the functional groups number was observed, highlighting the positive “*dendritic effect*” on the surface functionalization.

## References:

- <sup>1</sup> (a) K. E. Sapsford, W. R. Algar, L. Berti, K. B. Gemmill, B. J. Casey, E. Oh, M. H. Stewart and I. L. Medintz, *Chem. Rev.* **2013**, 113, 1904–2074; (b) E. C. Wang and A. Z. Wang, *Integr. Biol.* **2014**, 6, 9–26; (c) W. R. Algar, D. E. Prasuhn, M. H. Stewart, T. L. Jennings, J. B. Blanco-Canosa, P. E. Dawson and I. L. Medintz, *Bioconjugate Chem.* **2011**, 22, 825–858; (d) N. T. K. Thanh and L. A. W. Green, *Nano Today* **2010**, 5, 213–230; (e) M. Agrawal, S. Gupta and M. Stamm, *J. Mater. Chem.* **2011**, 21, 615–627; (f) D. Kozlova, S. Chernousova, T. Knuschke, J. Buer, A. M. Westendorf and M. Epple, *J. Mater. Chem.* **2012**, 22, 396–404; (g) R. Ladj, A. Bitar, M. Eissa, Y. Mugnier, R. Le Dantec, H. Fessia and A. Elaissari, *J. Mater. Chem. B* **2013**, 1, 1381–1396;
- <sup>2</sup> (a) Y. Li, X. Zhang and C. Deng, *Chem. Soc. Rev.*, **2013**, 42, 8517–8539; (b) L. H. Reddy, J. L. Arias, J. Nicolas and P. Couvreur, *Chem. Rev.* **2012**, 112, 5818–5878; (c) Y. Pan, X. Du, F. Zhao and B. Xu, *Chem. Soc. Rev.*, **2012**, 41, 2912–2942; (d) M. Colombo, S. Carregal-Romero, M. F. Casula, L. Gutierrez, M.P. Morales, I. B. Bohm, J. T. Heverhagen, D. Prospero and W. J. Parak, *Chem. Soc. Rev.*, **2012**, 41, 4306–4334; (e) N. Chekina, D. Horak, P. Jendelova, M. Trchova, M. J. Benes, M. Hruby, V. Herynek, K. Turnovcova and E. Sykova, *J. Mater. Chem.* **2011**, 21, 7630–7639; (f) A. K. Gupta and M. Gupta, *Biomaterials* **2005**, 26, 3995–4021.
- <sup>3</sup> M. Knobel, W. C. Nunes, L. M. Socolovsky, E. De Biasi, J. M. Vargas and J. C. Denardin, *J. Nanosci. Nanotechnol.* **2008**, 8, 2836–2857.
- <sup>4</sup> <http://www.ademtech.com>
- <sup>5</sup> (a) K. Heuze, D. Rosario-Amorin, S. Nlate, M. Gaboyard, A. Bouter and R. Clerac, *New J. Chem.* **2008**, 32, 383–387; (b) D. Rosario-Amorin, X. Wang, M. Gaboyard, R. Clerac, S. Nlate and K. Heuze, *Chem. Eur. J.* **2009**, 15, 12636–12643; (c) D. Rosario-Amorin, M. Gaboyard, R. Clerac, S. Nlate and K. Heuze, *Dalton Trans.*, **2011**, 40, 44–46; (d) D. Rosario-Amorin, M. Gaboyard, R. Clerac, L. Vellutini, S. Nlate, and K. Heuze, *Chem. Eur. J.* **2012**, 18, 3305–3315.
- <sup>6</sup> (a) F. Bayard, A. Raveneau, A. Letourneau, G. Joucla, C. Barbot, B. Garbay, C. Cabanne, *Anal. Biochem.* **2009**, 384, 350–352; (b) L. Jézéquel, J. Loeper, and D. Pompon, *BioTechniques* **2008**, 45, 523–532; (c) W. U. Dittmer, P. de Kievit, M. W. J. Prins, J. L. M. Vissers, M. E. C. Mersch, M. F. W. C. Martens, *J. Immunol. Methods* **2008**, 338, 40–46; (d) S. Workman, S. K. Wells, C.-P. Pau, S. M. Owen, X. F. Dong, R. La Borde and T. C. Granade, *J. Virol. Methods* **2009**, 160, 14–21.
- <sup>7</sup> C. A. G. N. Montalbetti and V. Falque, *Tetrahedron* **2005**, 61, 10827–10852.

- <sup>8</sup> L. H. H. Damink, P. J. Dijkstra, M. J. A. Luyn, P. B. van Wachem, P. Nieuwenhuis, J. Feijen, *Biomaterials*, **1996**, 17, 765–773.
- <sup>9</sup> D. Rosario-Amorin, *PhD Thesis*, University of Bordeaux 1, **2009**.
- <sup>10</sup> (a) M. M. Kose, S. Onbulak, I. I. Yilmaz and A. Sanyal, *Macromolecules* **2011**, 44, 2707–2714; (b) W. H. Heath, F. Palmieri, J. R. Adams, B. K. Long, J. Chute, T. W. Holcombe, S. Zieren, M. J. Truitt, J. L. White and C. G. Willson, *Macromolecules* **2008**, 41, 719–726; (c) J. Zhu, C. Waengler, R. B. Lennox, and R. Schirrmacher, *Langmuir* **2012**, 28, 5508–5512; (d) I. Kosif, E. Park, R. Sanyal and A. Sanyal, *Macromolecules* **2010**, 43, 4140–4148; (e) Z. Lu, R. Weber and R. J. Twieg, *Tetrahedron Letters* **2006**, 47, 7213–7217.
- <sup>11</sup> A. Sanchez, E. Pedroso and A. Grandas, *Org. Lett.* **2011**, 13, 16, 4364–4367.
- <sup>12</sup> (a) T. Dispinar, R. Sanyal and A. Sanyal, *J. Polym. Sci., A: Polym. Chem.* **2007**, 45, 4545–4551; (b) L. Billiet, O. Gok, A. P. Dove, A. Sanyal, L.-T. T. Nguyen and F. E. D. Prez, *Macromolecules* **2011**, 44, 7874–7878.
- <sup>13</sup> D. Lin-Vien, N. B. Colthup, W. G. Fateley, J. G. Grasselli, *The Handbook of infrared and Raman characteristic frequencies of organic molecules*, Academic Press **1991**.
- <sup>14</sup> R. A. Nyquist and S. L. Fiedler, *Vib. Spectrosc.* **1995**, 8, 365–386.
- <sup>15</sup> (b) E. C. Aguiar, J. B. P. da Silva, M. N. Ramos, *J. Mol. Struct.* **2011**, 993, 431–434; (b) E. C. Aguiar, J. B. P. da Silva, M. N. Ramos, *Spectrochim. Acta, Part A* **2008**, 71, 5–9.
- <sup>16</sup> C. Gousse, A. Gandini and P. Hodge, *Macromolecules* **1998**, 31, 314–321.

<sup>17</sup> **Table 1.** A partial list of common key fragment ions.

Mass Number, m/z	Key fragment ion	Probable parent molecule	Additional Mass Number, m/z
15	CH <sub>3</sub> <sup>+</sup>	C <sub>x</sub> H <sub>y</sub>	12, 13, 14, 26, 27
	NH <sup>+</sup>	NH <sub>3</sub>	14, 16, 17
16	O <sup>+</sup>	O <sub>2</sub>	32, 34
	O <sup>+</sup>	H <sub>2</sub> O	17, 18
	CH <sub>4</sub> <sup>+</sup>	CH <sub>4</sub>	12, 13, 14, 15
	NH <sub>2</sub> <sup>+</sup>	NH <sub>3</sub>	14, 15, 17
17	OH <sup>+</sup>	H <sub>2</sub> O	16, 18
	NH <sub>3</sub> <sup>+</sup>	NH <sub>3</sub>	14, 15, 17
18	H <sub>2</sub> O <sup>+</sup>	H <sub>2</sub> O	16, 17
22	CO <sub>2</sub> <sup>++</sup>	CO <sub>2</sub>	6, 12, 28, 29, 44
26	C <sub>2</sub> H <sub>2</sub> <sup>+</sup>	C <sub>x</sub> H <sub>y</sub>	12, 13, 14, 24, 27
27	C <sub>2</sub> H <sub>3</sub> <sup>+</sup>	C <sub>x</sub> H <sub>y</sub>	12, 13, 14, 24, 26
29	C <sub>2</sub> H <sub>5</sub> <sup>+</sup>	C <sub>x</sub> H <sub>y</sub>	12, 13, 14, 24, 26, 27, 28
	<sup>14</sup> N <sup>15</sup> N <sup>+</sup>	N <sub>2</sub>	7, 14, 28
39	C <sub>3</sub> H <sub>3</sub> <sup>+</sup>	C <sub>x</sub> H <sub>y</sub>	12, 13, 14, 24, 26, 27, 28, 38
41	C <sub>3</sub> H <sub>5</sub> <sup>+</sup>	C <sub>x</sub> H <sub>y</sub>	12, 13, 14, 24, 26, 27, 28, 38, 39
42	C <sub>3</sub> H <sub>6</sub> <sup>+</sup>	C <sub>x</sub> H <sub>y</sub>	12, 13, 14, 24, 26, 27, 28, 38, 39
43	C <sub>3</sub> H <sub>7</sub> <sup>+</sup>	C <sub>x</sub> H <sub>y</sub>	12, 13, 14, 24, 26, 27, 28, 38, 39
	C <sub>2</sub> H <sub>3</sub> O <sup>+</sup>	C <sub>2</sub> H <sub>5</sub> OH (ethanol)	31, 44, 45, 46
44	C <sub>3</sub> H <sub>8</sub> <sup>+</sup>	C <sub>3</sub> H <sub>8</sub>	41, 42, 43
	CO <sub>2</sub> <sup>+</sup>	CO <sub>2</sub>	6, 12, 28, 29
	C <sub>2</sub> H <sub>4</sub> O <sup>+</sup>	C <sub>2</sub> H <sub>5</sub> OH (ethanol)	31, 43, 45, 46
	N <sub>2</sub> O <sup>+</sup>	N <sub>2</sub> O	14, 16, 18
45	C <sub>2</sub> H <sub>5</sub> O <sup>+</sup>	C <sub>2</sub> H <sub>5</sub> OH (ethanol)	31, 43, 44, 46
	<sup>13</sup> CO <sub>2</sub> <sup>+</sup>	CO <sub>2</sub>	6, 12, 28, 29, 44
46	NO <sub>2</sub> <sup>+</sup>	NO <sub>2</sub>	14, 16
	CH <sub>5</sub> OH <sup>+</sup>	C <sub>2</sub> H <sub>5</sub> OH (ethanol)	31, 43, 44, 46
58	(CH <sub>3</sub> ) <sub>2</sub> CO <sup>+</sup>	C <sub>3</sub> H <sub>6</sub> O (acetone)	43
68	C <sub>4</sub> H <sub>4</sub> O <sup>+</sup>	C <sub>4</sub> H <sub>4</sub> O (furan)	39

<sup>18</sup> T. Engel and G. Kickelbick, *Chem. Mater.* **2013**, 25, 149–157.

<sup>19</sup> (a) R. Wagner, S. Benz, O. Mo1hler, H. Saathoff, M. Schnaiter, and U. Schurath, *J. Phys. Chem. A* **2005**, 109, 7099–7112; (b) E. Mendelovici, R. Villalba, A. Sagarzazu and O. Carias, *Clay Minerals*, **1995**, 30, 307–313.

<sup>20</sup> (a) <http://www.horiba.com/scientific/products/particle-characterization/technology/zeta-potential/>;  
(b) <http://www.horiba.com/scientific/products/particle-characterization/zeta-potential-analysis/details/sz-100-7245/>.

<sup>21</sup> T. Doane, C. H. Chuang, R. J. Hill, C. Burda, *Acc. Chem. Res.*, **2012**, 45, 317–326.

<sup>22</sup> Y. Q. He, S. P. Liu, L. Kong and Z. F. Liu, *Spectrochim. Acta, Part A* **2005**, 61, 2861–2866.

<sup>23</sup> (a) D. G. Smith, O. O. Blumenfeld and W. Konigsberg, *Biochem. J.*, **1964**, 91, 589–595; (b) G. Gorin, P. A. Martic and G. Doughty, *Arch. Biochem. Biophys.* **1966**, 115, 593–597; (c) J. R. Heitz, C.

D. Anderson and B. M. Anderson, *Arch. Biochem. Biophys.* **1968**, 127, 627–636; (d) M. D. Partis, D. G. Griffiths, G. C. Roberts and R. B. Beechey, *J. Protein. Chem.* **1983**, 2, 263–277.

<sup>24</sup> (a) M. Frascioni, F. Mazzei and T. Ferri, *Anal. Bioanal. Chem.* **2010**, 398, 1545–1564; (b) L. S. Wong, F. Khan and J. Micklefield, *Chem. Rev.* **2009**, 109, 4025–4053.

<sup>25</sup> G. T. Hermanson, *Bioconjugate Techniques* – 2<sup>nd</sup> edition, Academic Press, San Diego, **2008**.

<sup>26</sup> (a) M. Uhlen, *Nature* **1989**, 340, 733–734; (a) T. Tanaka, R. Sakai, R. Kobayashi, K. Hatakeyama, and T. Matsunaga, *Langmuir* **2009**, 25, 2956–2961.

<sup>27</sup> V. Singh, M. Zharnikov, A. Gulinoc and T. Gupta, *J. Mater. Chem.*, **2011**, 21, 10602–10618.

<sup>28</sup> A. del Campo, T. Sena, J.-P. Lellouchec and I. J. Bruce, *J. Magn. Magn. Mat.* **2005**, 293, 33–40.

Chapter IV  
**Functionalization of core-shell  
 $\gamma$ -Fe<sub>2</sub>O<sub>3</sub>/SiO<sub>2</sub>  
magnetic nanoparticles**



**Table of contents:**

IV.1. Introduction .....	125
IV.2. Presentation of core-shell $\gamma$ -Fe <sub>2</sub> O <sub>3</sub> /SiO <sub>2</sub> MNPs.....	125
IV.3. Surface modification chemistry of core-shell $\gamma$ -Fe <sub>2</sub> O <sub>3</sub> /SiO <sub>2</sub> MNPs .....	126
IV.3.1. General grafting and maleimide functional group deprotection procedures .....	129
IV.3.2. Characterization of functionalized $\gamma$ -Fe <sub>2</sub> O <sub>3</sub> /SiO <sub>2</sub> MNPs .....	132
IV.3.2.1. ATR FT-IR study of functionalized $\gamma$ -Fe <sub>2</sub> O <sub>3</sub> /SiO <sub>2</sub> MNPs .....	132
IV.3.2.2. TGA coupled with MS study of $\gamma$ -Fe <sub>2</sub> O <sub>3</sub> /SiO <sub>2</sub> MNPs functionalized with silylated coupling agent 11 .....	138
IV.3.2.3. TEM study of maleimide functionalized $\gamma$ -Fe <sub>2</sub> O <sub>3</sub> /SiO <sub>2</sub> MNPs .....	143
IV.3.2.4. Zeta potential measurements for maleimide functionalized $\gamma$ -Fe <sub>2</sub> O <sub>3</sub> /SiO <sub>2</sub> MNPs ...	144
IV.3.2.5. Colloidal state of maleimide functionalized $\gamma$ -Fe <sub>2</sub> O <sub>3</sub> /SiO <sub>2</sub> MNPs in water.....	145
IV.4. Immobilization tests.....	146
IV.4.1. Covalent coupling of thiol modified biotin with the maleimide functionalized $\gamma$ -Fe <sub>2</sub> O <sub>3</sub> /SiO <sub>2</sub> MNPs and consequent recognition by SA-Au NPs .....	147
IV.4.2. Covalent coupling of HS-dT oligonucleotide with maleimide functionalized $\gamma$ -Fe <sub>2</sub> O <sub>3</sub> /SiO <sub>2</sub> MNPs and hybrid capture of its complementary sequence .....	149
IV.5. Conclusion.....	151

## IV.1. Introduction

This chapter is dedicated to the functionalization of the core-shell  $\gamma\text{-Fe}_2\text{O}_3/\text{SiO}_2$  MNPs with maleimide functional group and their characterization. The characteristics of core-shell  $\gamma\text{-Fe}_2\text{O}_3/\text{SiO}_2$  MNPs are very similar to those of core-shell  $\gamma\text{-Fe}_2\text{O}_3/\text{Polymer}$  MNPs (see Chapter III),<sup>1</sup> while differences in the shell are discussed in the beginning of this chapter. Chemical anchoring of coupling agents' layer onto the silica surface was achieved by the hydrolysis condensation reaction of silanol groups from silica with alkoxy groups of the linear and dendritic functional silyl-terminated coupling agents **11**, **19** and **24** (see Chapter II).

The obtained maleimide functionalized  $\gamma\text{-Fe}_2\text{O}_3/\text{SiO}_2$  MNPs have been characterized by FT-IR spectroscopy, TGA coupled with MS, TEM, Transmitted Light Microscopy and Zeta Potential measurements. Also, the labelling efficiency of maleimide functionalized  $\gamma\text{-Fe}_2\text{O}_3/\text{SiO}_2$  MNPs was studied by performing a series of immobilization tests.

## IV.2. Presentation of core-shell $\gamma\text{-Fe}_2\text{O}_3/\text{SiO}_2$ MNPs

The core-shell  $\gamma\text{-Fe}_2\text{O}_3/\text{SiO}_2$  MNPs utilized as support for the surface modification chemistry in this chapter are presented in Figure IV-1. These  $\gamma\text{-Fe}_2\text{O}_3/\text{SiO}_2$  MNPs have size of 300 nm and similarly to  $\gamma\text{-Fe}_2\text{O}_3/\text{Polymer}$  MNPs (discussed in Chapter III) possess ferrofluid maghemite core and same magnetic characteristics (SPIONPs content: around 70 %; magnetization at saturation: approx. 40  $\text{cm}^3/\text{g}$  at 300 K). The only difference between these core-shell MNPs consists in their shell.

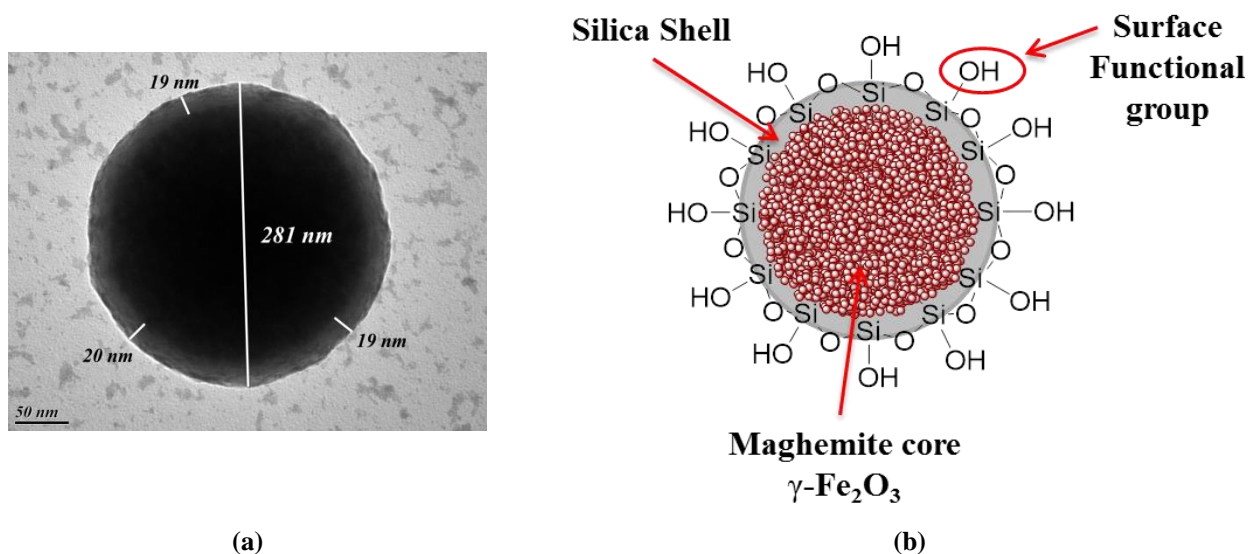


**Figure IV-1.** (a) TEM image of core-shell  $\gamma\text{-Fe}_2\text{O}_3/\text{SiO}_2$  magnetic nanoparticle; (b) Schematic representation of core-shell  $\gamma\text{-Fe}_2\text{O}_3/\text{SiO}_2$  magnetic nanoparticle.

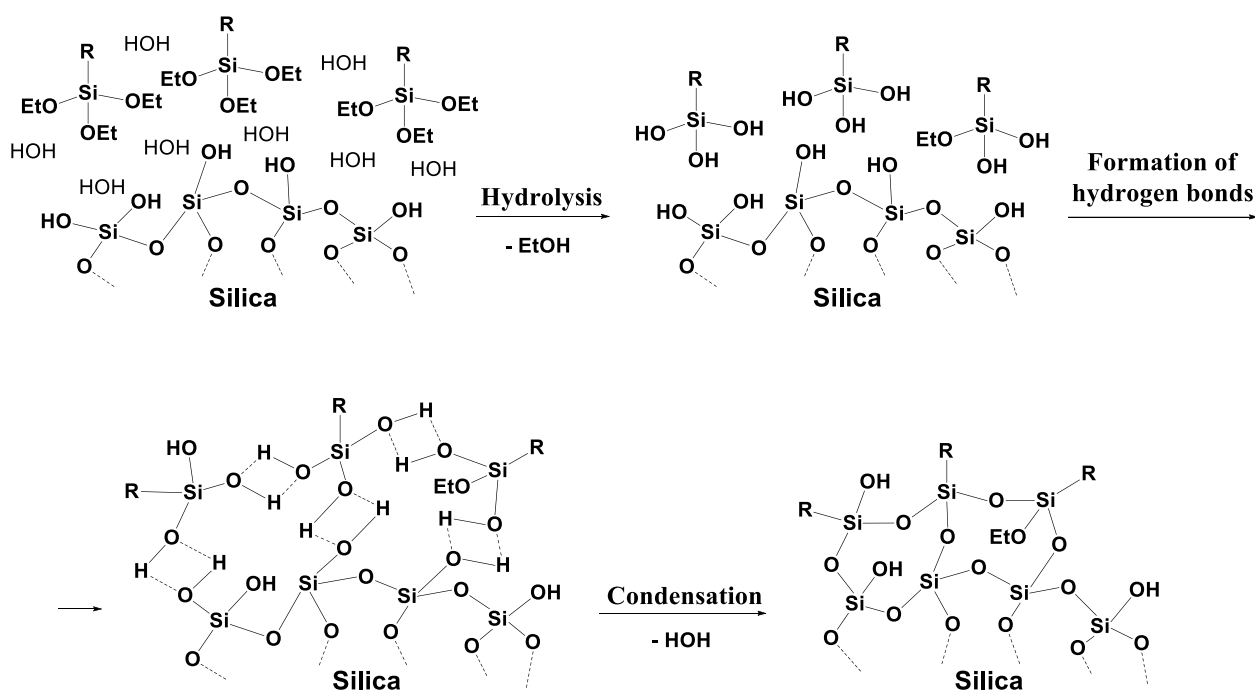
These  $\gamma$ -Fe<sub>2</sub>O<sub>3</sub>/SiO<sub>2</sub> MNPs have a uniform non-porous silica shell with controlled thickness (around 20 nm). Also, silica shell is chemically and thermally stable material. The silica shell contains two types of silicon atoms: the siloxane bridges (Si-O-Si) and silanol groups (Si-OH). Thus, silica surface modification can occur via the reaction of a particular molecule with either the siloxane (by nucleophilic substitution at the silicon atom) or silanol (direct reaction with the hydroxyl group) functions, although it is generally accepted that it is the reaction with the silanol function that constitutes the main modification pathway.<sup>2</sup> The reactivity of siloxane and silanol groups is strongly dependent on the reaction conditions. Thus, in aqueous solutions, specifically silanol groups represent the active sites for the covalent anchorage of the functional organosilane moieties onto the  $\gamma$ -Fe<sub>2</sub>O<sub>3</sub>/SiO<sub>2</sub> MNPs' surface. On the contrary, under anhydrous conditions, these are the siloxane bridges who are responsible for the chemical modification.<sup>3</sup>

When the aim of the work is creating of MNP material with a uniform and optimal surface functionalization, understanding of the involved surface modification mechanisms is essential. For this purpose, possible mechanisms of silica surface modifications as well as the influence of some parameters on the grafting efficiency are discussed in the following section.

### IV.3. Surface modification chemistry of core-shell $\gamma$ -Fe<sub>2</sub>O<sub>3</sub>/SiO<sub>2</sub> MNPs

Commonly the surface modification of silica-based hybrid materials is achieved by silanization of surface sites, relying on the formation of strong siloxane bonds.<sup>4</sup> This modification approach involves the use of functional silylated coupling agents (organosilanes), which are organic compounds with chloro- or methoxy- or ethoxysilyl anchor groups that can attack either siloxane or the silanol surface functions.<sup>5</sup> The particularity of organosilanes, is that the silane reactive groups are typically unreactive towards organic molecules, but can covalently couple to certain inorganic substrates. The reactivity of the trichloro- or trialkoxy-organosilanes increases in the following order: R-Si(OC<sub>2</sub>H<sub>5</sub>)<sub>3</sub> < R-Si(OCH<sub>3</sub>)<sub>3</sub> < R-SiCl<sub>3</sub>. Since the organosilanes with chloro- or methoxy- anchor groups are very reactive, difficulties may occur to obtain a uniform grafting. In addition, trichlorosilanes are corrosive (elimination of HCl) and can damage or even destroy MNPs, while trimethoxysilanes evolve the elimination of MeOH (toxic). In this work, the silanization was performed by using functional silylated coupling agents with ethoxy anchoring groups (*synthesized as described in Chapter II*) and therefore the further introduction to silanization chemistry is focused on the use of silanes with alcoxysilyl anchor groups. The terms silanes, organosilanes, silane coupling agents and silylated coupling agents are used interchangeably.

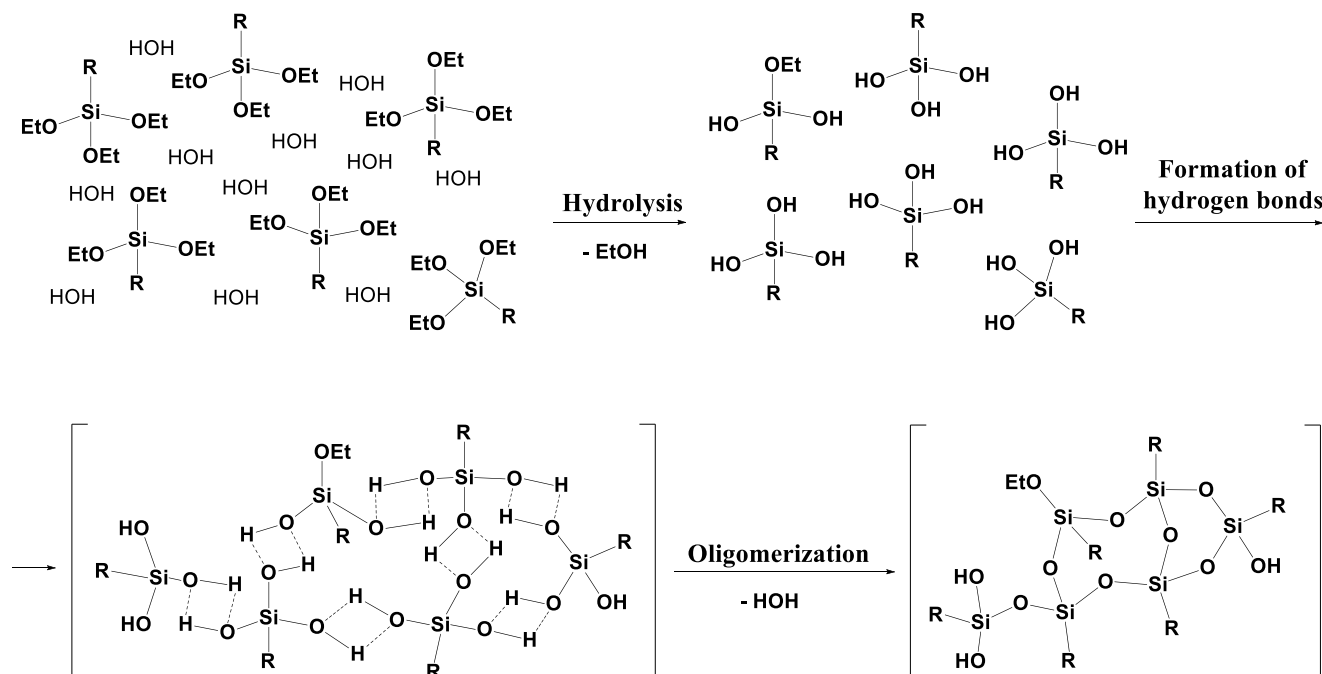
Generally, silylated coupling agents can be employed in surface modification chemistry either in organic solvents or in aqueous solutions, and in some cases even in the absence of solvents the chemical vapour deposition of the silane is possible.<sup>6</sup> Nevertheless, the silanization performed in solution remains the most common approach and the choice of the reaction solvent is mostly justified by the solubility of coupling agents. In our case, all the synthesised silylated coupling agents has a limited solubility in nonpolar solvents and are well soluble in polar solvents such as ethanol for example. Therefore, the grafting of silylated coupling agents **11**, **19** and **34** was performed in hydro-alcoholic basic medium according to a conventional method originally described by Stober.<sup>7,8</sup> In this context, hydrophilic and protic solvents (like alcohols) usually accelerate the hydrolysis of silanes and consequently increase the condensation reaction kinetics.<sup>9,10</sup> In addition, the presence of water in the reaction media is desirable for the silanization reaction to occur, since it is responsible for the hydrolysis of the alcoxysilyl anchor groups necessary for the further condensation reaction as shown in Scheme IV-1.<sup>11</sup>



**Scheme IV-1.** Simplified mechanism of silanization process (employing a functional triethoxysilane coupling agent, where R is the desired functional group) in the presence of water.

As the quantity of present free hydroxyl groups on the silica surfaces is often too low to form more than one siloxane group on the surface (for example, no more than 4 hydroxyl groups per  $\text{nm}^2$  for glass),<sup>12</sup> crosslinking between the coupling agents occurs via the left unreacted silanol groups, resulting in an even stronger attachment of the layer on the substrate surface (*see* Figure IV-4, *Condensation step*).

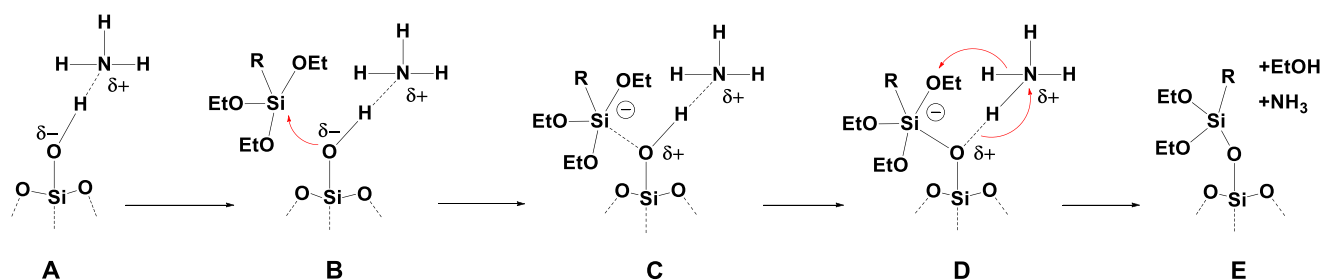
However, when the silanization reaction is performed in aqueous solutions, a special attention must be paid on the choice of the reaction conditions, since a competing reaction can occur in solution during the silanization, namely the polycondensation of the organosilane (oligomerization). This reaction leads to the formation of silane aggregates, as it is illustrated in Scheme IV-2.<sup>13</sup>



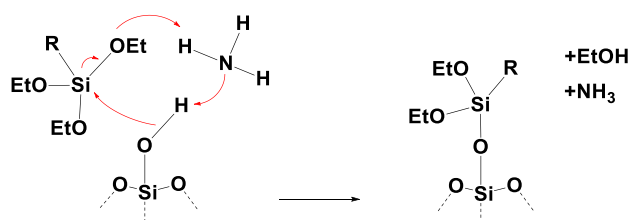
**Scheme IV-2.** Schematic representation of a possible oligomerization reaction.

The formed oligomers are still able to react with the MNPs' surface through the unreacted silanol groups and if the oligomerization reaction goes too far, large aggregates will be immobilized on the MNPs' surface. The kinetics of these processes depends on the experimental parameters used in the surface modification reaction (reaction time and temperature, chosen solvent, water concentration, etc.) and, as a consequence, the properties of the final MNP material are also dependent on these parameters. Thus, for example, raising the reaction temperature accelerates the hydrolysis and condensation kinetics, both in solution and onto the surface. The reaction time is strongly dependent on the silane reactivity and can vary from several minutes to several hours. Also, the slower silane introduction is, the more efficient the surface coverage is.<sup>14</sup> Often, not enough consideration is given to these factors.

Adding of small quantities of base or nucleophiles, especially, amines with exchangeable protons (i.e. ethylamine, diethylamine, and ammonia) in the silanization process can catalyze both, the hydrolysis and condensation reactions on the silica surface, thus promoting the surface modification process.<sup>15</sup> To explain the amines catalytic effect two mechanisms were proposed by J. P. Blitz and coworkers, as shown in Scheme IV-3 and Scheme IV-4.<sup>16</sup>



**Scheme IV-3.** General mechanistic description of amine catalysis of silanization reaction: (A) adsorption of ammonia onto a silanol site, (B) nucleophilic attack of the silicon atom of the silylated coupling agent by the oxygen atom of the silica surface, (C) pentacoordinated intermediate resulting from attack, (D) proton abstraction by ethoxy leaving group with electrophilic assistance by ammonia, and (E) silylated surface with generation of ethanol and release of ammonia.<sup>16a</sup>



**Scheme IV-4.** General mechanistic description of amine catalysis of silylation reaction involving concerted bond breaking and bond formation.<sup>16a</sup>

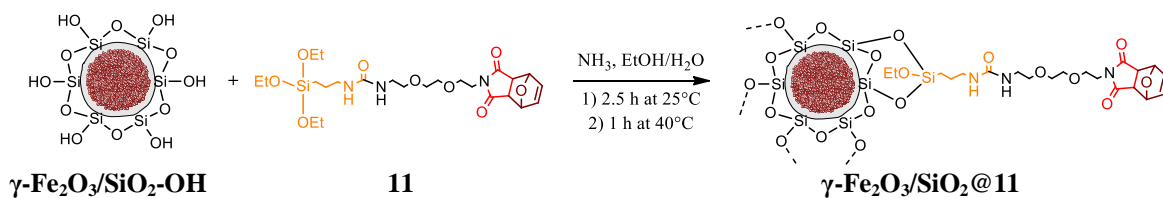
Thus, the silanization process is strongly dependent on the reaction conditions such as the choice of solvent, reaction temperature, reaction time, as well as on the nature of organosilane and catalyst concentrations involved into reaction. Several studies were performed to reveal the ways in which these parameters influence the surface modification process, but still there is no a unique protocol which will ensure maximal silanization efficiency, since the parameter that influences the reaction are various and the occurring mechanisms are complicated.<sup>9,17</sup>

Moreover, MNPs can cross-link between them through siloxane bridges as a consequence of uncontrolled reaction conditions. Also, issues such as the homogeneity of the MNPs' coating and the density of functional groups may be crucial for the final performance of the modified material.<sup>9</sup> Therefore, all these parameters should be kept in mind while choosing the grafting reaction conditions.

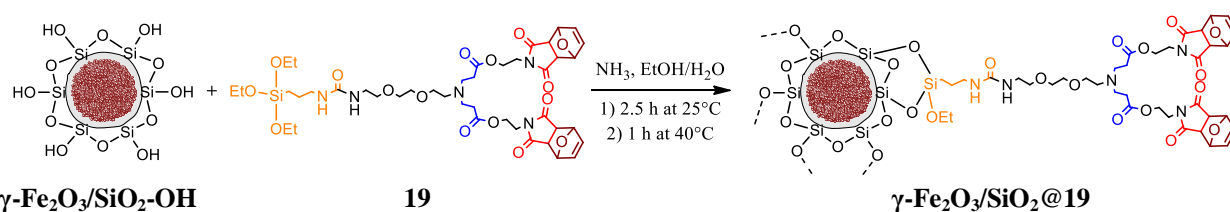
### IV.3.1. General grafting and maleimide functional group deprotection procedures

The silanization reaction (called further grafting) was performed in hydro-alcoholic solution, in the presence of ammonia catalyst. The choice of this reaction solvent is conditioned by both: the high solubility of coupling agents as well as good dispersion of  $\gamma\text{-Fe}_2\text{O}_3/\text{SiO}_2$  MNPs in polar solvents. Additionally, in order to ensure the maximal colloidal stability of  $\gamma\text{-Fe}_2\text{O}_3/\text{SiO}_2$  MNPs during the grafting procedure, polyethylene glycol tert-octylphenyl ether (Triton X-405 or Tx) surfactant was employed. The grafting of functional silylated coupling agents **11**, **19** and **24** on core-shell

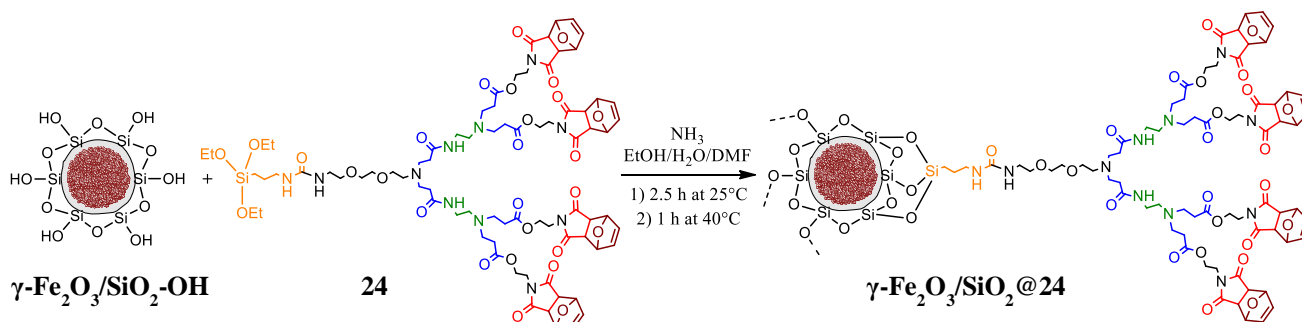
$\gamma\text{-Fe}_2\text{O}_3/\text{SiO}_2$  MNPs was performed according to the procedure described in the experimental part (respecting the same reaction conditions for the grafting of coupling agents **11**, **19** and **24**) and is illustrated in Scheme IV-5, Scheme IV-6 and Scheme IV-7.



**Scheme IV-5.** Grafting of silylated coupling agent **11** on core-shell  $\gamma\text{-Fe}_2\text{O}_3/\text{SiO}_2$  MNPs.

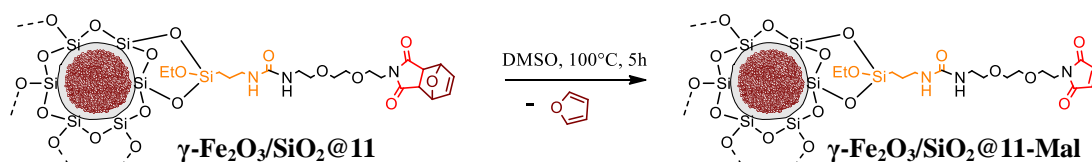


**Scheme IV-6.** Grafting of silylated coupling agent **19** on core-shell  $\gamma\text{-Fe}_2\text{O}_3/\text{SiO}_2$  MNPs.

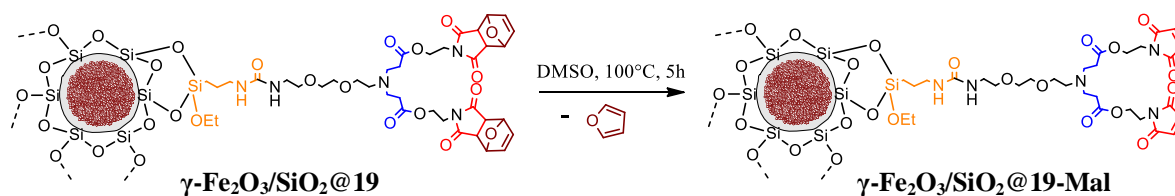
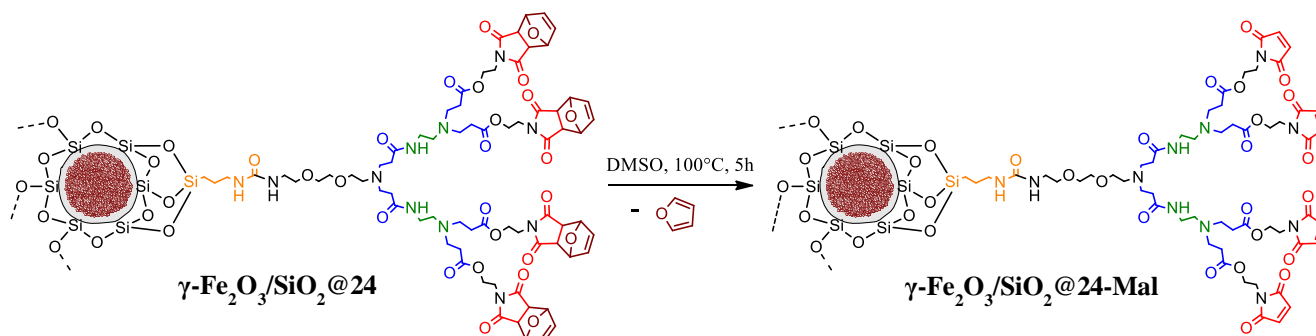


**Scheme IV-7.** Grafting of silylated coupling agent **24** on core-shell  $\gamma\text{-Fe}_2\text{O}_3/\text{SiO}_2$  MNPs.

Next, the deprotection of maleimide group on  $\gamma\text{-Fe}_2\text{O}_3/\text{SiO}_2\text{@11}$ ,  $\gamma\text{-Fe}_2\text{O}_3/\text{SiO}_2\text{@19}$ , and  $\gamma\text{-Fe}_2\text{O}_3/\text{SiO}_2\text{@24}$  was performed, as shown in Scheme IV-8, Scheme IV-9 and Scheme IV-10 respectively.

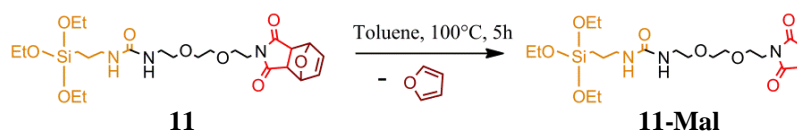
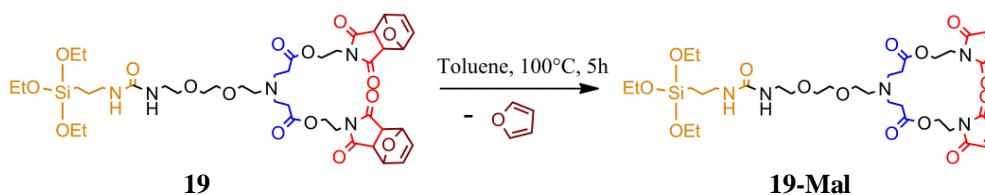


**Scheme IV-8.** Deprotection of maleimide functional group on  $\gamma\text{-Fe}_2\text{O}_3/\text{SiO}_2\text{@11}$ .

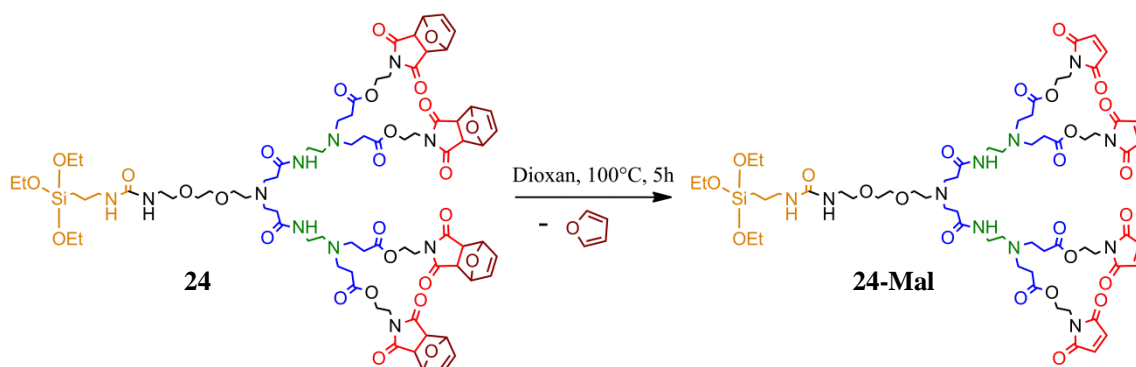
Scheme IV-9. Deprotection of maleimide functional group on  $\gamma\text{-Fe}_2\text{O}_3/\text{SiO}_2@19$ .Scheme IV-10. Deprotection of maleimide functional group on  $\gamma\text{-Fe}_2\text{O}_3/\text{SiO}_2@24$ .

All the samples of maleimide functionalized  $\gamma\text{-Fe}_2\text{O}_3/\text{SiO}_2$  MNPs, in its protected ( $\gamma\text{-Fe}_2\text{O}_3/\text{SiO}_2@11$ ,  $\gamma\text{-Fe}_2\text{O}_3/\text{SiO}_2@19$ , and  $\gamma\text{-Fe}_2\text{O}_3/\text{SiO}_2@24$ ) and deprotected form ( $\gamma\text{-Fe}_2\text{O}_3/\text{SiO}_2@11\text{-Mal}$ ,  $\gamma\text{-Fe}_2\text{O}_3/\text{SiO}_2@19\text{-Mal}$ , and  $\gamma\text{-Fe}_2\text{O}_3/\text{SiO}_2@24\text{-Mal}$ ) were submitted to analyses and are discussed in the following paragraph.

In parallel, the deprotection of maleimide functional group was performed directly on the silylated coupling agents **11**, **19** and **24**, which was not possible on the coupling agents with amino anchor group **10**, **18** and **23** (discussed in Chapter III), due to the polymerization side reaction between the amino group and maleimide double bond. The deprotection of maleimide functional group of silanes **11**, **19** and **24** was performed as illustrated in Scheme IV-11, Scheme IV-12 and Scheme IV-13 respectively.

Scheme IV-11. Deprotection of maleimide functional group on silylated coupling agent **11**.Scheme IV-12. Deprotection of maleimide functional group on silylated coupling agent **19**.





**Scheme IV-13.** Deprotection of maleimide functional group on silylated coupling agent **24**.

Recording the IR spectra of the maleimide functional silanes **11-Mal**, **19-Mal** and **24-Mal** provides direct information about the maleimide characteristic absorption bands, and thus significantly simplifies the interpretation of IR spectra of the functionalized MNPs.

### IV.3.2. Characterization of functionalized $\gamma$ -Fe<sub>2</sub>O<sub>3</sub>/SiO<sub>2</sub> MNPs

#### IV.3.2.1. ATR FT-IR study of functionalized $\gamma$ -Fe<sub>2</sub>O<sub>3</sub>/SiO<sub>2</sub> MNPs

The FT-IR spectra of the silylated coupling agents **11**, **19** and **24**, as well as those of the corresponding maleimide functional silanes **11-Mal**, **19-Mal** and **24-Mal** were recorded (Figure IV-2 and Figure IV-3), highlighting the changes of the characteristic absorption bands frequencies caused by furan cleavage. Thus, after the deprotection step, the characteristic out-of-phase C=O stretching band of cyclic imides shifted from 1698 cm<sup>-1</sup> to 1706 cm<sup>-1</sup> in the case of maleimide functional silanes **11-Mal** and **19-Mal**, and from 1696 cm<sup>-1</sup> to 1702 cm<sup>-1</sup> in the case of maleimide functional silane **24-Mal**. The furan ring deformations at 916 cm<sup>-1</sup>, 878 cm<sup>-1</sup>, and 854 cm<sup>-1</sup> completely disappeared. In the case of silane **24-Mal**, a band at 873 cm<sup>-1</sup> was observed. This absorption band was not observed in silane **24** since it was completely covered by the furan ring deformation at 878 cm<sup>-1</sup>. All the spectra showed the apparition of a new peak at 695 cm<sup>-1</sup>. This vibration seems characteristic for five-membered heterocyclic ring systems, and was observed at 697 cm<sup>-1</sup> in the maleic anhydride and at 696 cm<sup>-1</sup> in N-((3-Triethoxysilyl)propyl)maleimide.<sup>18,19</sup> Therefore, it was assigned to the maleimide ring deformation. The obtained frequencies values (cm<sup>-1</sup>) of the silanes **11**, **11-Mal**, **19**, **19-Mal**, **24** and **24-Mal** absorption bands, were used as references for interpretation of the functionalized MNPs' FT-IR spectra.

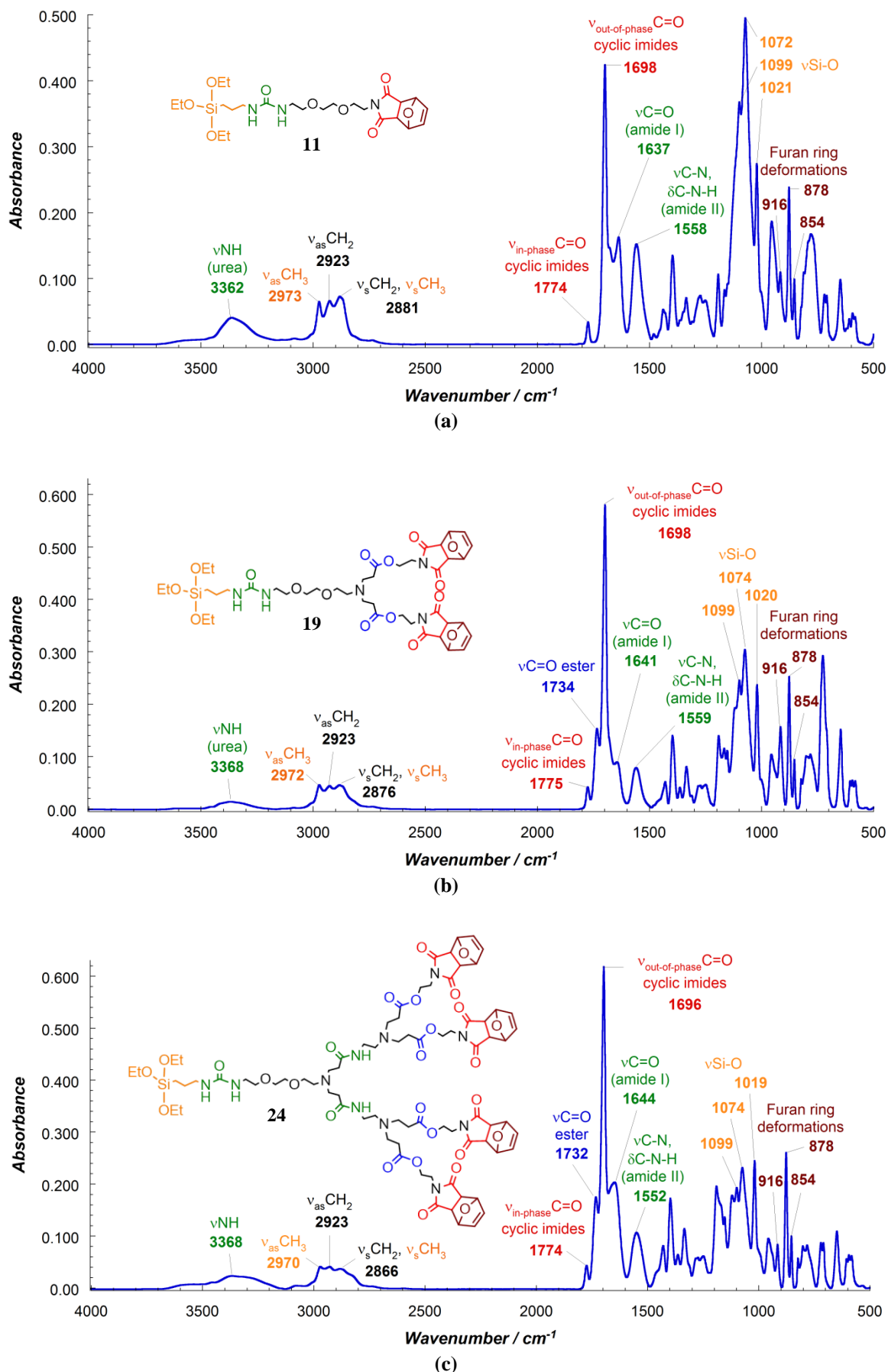


**Figure IV-2.** (a) ATR FT-IR spectrum of the linear silylated coupling agent **11**; (b) ATR FT-IR spectrum of the two-branched silylated coupling agent **19**; (c) ATR FT-IR spectrum of the four-branched silylated coupling agent **24**.

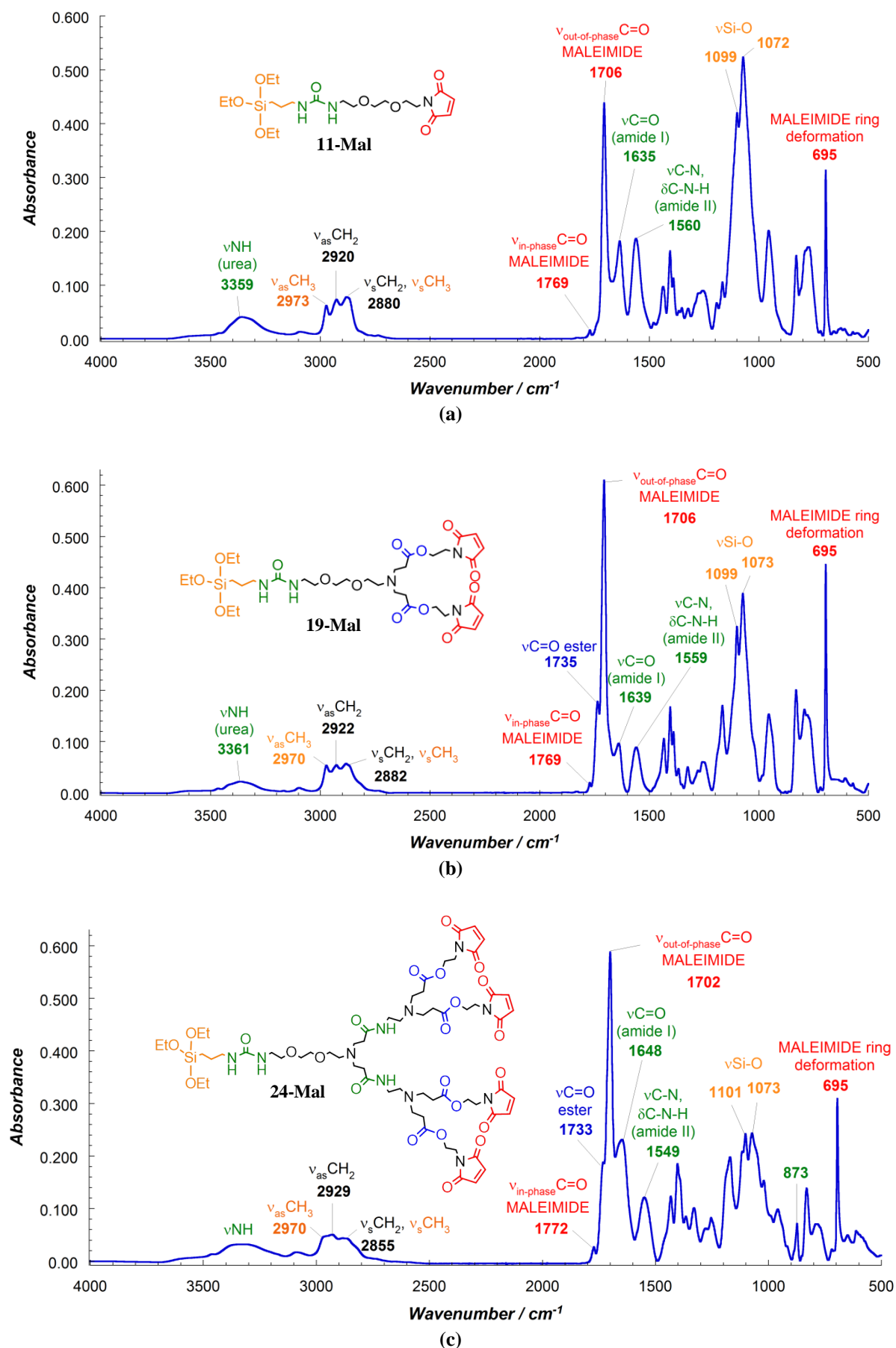


**Figure IV-3.** (a) ATR FT-IR spectrum of maleimide functional silane **11-Mal**; (b) ATR FT-IR spectrum of maleimide functional silane **19-Mal**; and (c) ATR FT-IR spectrum of maleimide functional silane **24-Mal**.

FT-IR spectra of  $\gamma\text{-Fe}_2\text{O}_3/\text{SiO}_2$  MNPs modified with coupling agents **11**, **19** and **24** ( $\gamma\text{-Fe}_2\text{O}_3/\text{SiO}_2@11$ ,  $\gamma\text{-Fe}_2\text{O}_3/\text{SiO}_2@19$ , and  $\gamma\text{-Fe}_2\text{O}_3/\text{SiO}_2@24$ ) and corresponding maleimide functionalized MNPs ( $\gamma\text{-Fe}_2\text{O}_3/\text{SiO}_2@11\text{-Mal}$ ,  $\gamma\text{-Fe}_2\text{O}_3/\text{SiO}_2@19\text{-Mal}$ , and  $\gamma\text{-Fe}_2\text{O}_3/\text{SiO}_2@24\text{-Mal}$ ) are presented in Figure IV-4, Figure IV-5 and Figure IV-6.

Figure IV-4 gather the spectra of native  $\gamma\text{-Fe}_2\text{O}_3/\text{SiO}_2$  MNPs ( $\gamma\text{-Fe}_2\text{O}_3/\text{SiO}_2\text{-OH}$ ) – in blue; the MNPs resulted after the grafting of the silylated linear coupling agent **11** ( $\gamma\text{-Fe}_2\text{O}_3/\text{SiO}_2@11$ ) – in green, and those obtained after the maleimide group deprotection ( $\gamma\text{-Fe}_2\text{O}_3/\text{SiO}_2@11\text{-Mal}$ ) – in red. Each spectrum represents an average of at least three experiments (corresponding to the three performed grafting or deprotection experiments).

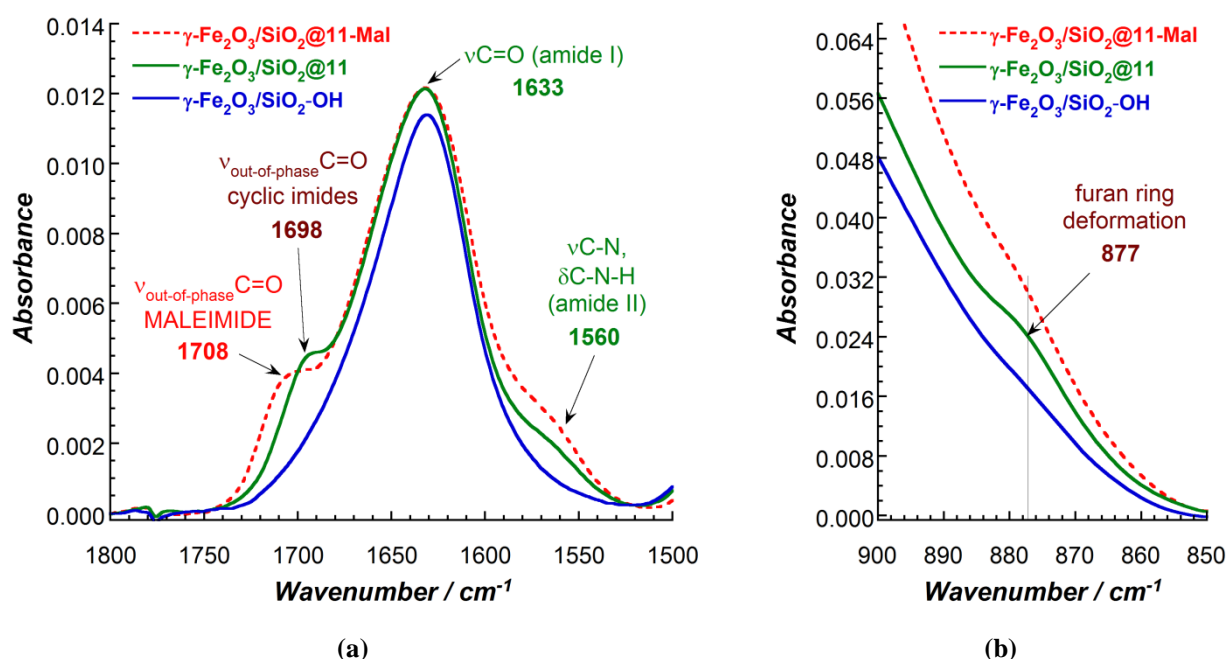


**Figure IV-4.** ATR FT-IR spectra of: native silica coated  $\gamma\text{-Fe}_2\text{O}_3$  MNPs ( $\gamma\text{-Fe}_2\text{O}_3/\text{SiO}_2\text{-OH}$ ) – solid line in blue, MNPs obtained after the grafting of linear silylated coupling agent **11** ( $\gamma\text{-Fe}_2\text{O}_3/\text{SiO}_2@11$ ) – solid line in green, and MNPs obtained after the cleavage of furan protection ( $\gamma\text{-Fe}_2\text{O}_3/\text{SiO}_2@11\text{-Mal}$ ) – dotted line in red (a) in the region 1800-1500 nm; and (b) in the region 900-850 nm.

The FT-IR spectrum of  $\gamma\text{-Fe}_2\text{O}_3/\text{SiO}_2@11$  (green solid line, Figure IV-4) showed the characteristic bands of silylated coupling agent **11**. The band at  $1698\text{ cm}^{-1}$  is assigned to the out-of-phase C=O stretching of cyclic imides. The shoulder around  $1560\text{ cm}^{-1}$  arises from the amide II mode ( $\nu\text{C-N}$  and  $\delta\text{C-N-H}$ ), while the increase of absorption band intensity around  $1633\text{ cm}^{-1}$  corresponds to the amide I mode ( $\nu\text{C=O}$ ), both revealing the presence of urea moiety. However, we must not forget that the increase of absorption band intensity around  $1633\text{ cm}^{-1}$  could be also due to the H-O-H bending vibration of water molecules adsorbed on MNPs' surface.<sup>20</sup> Another proof of the successful surface modification is the presence of the specific furan ring deformation band, seen at  $877\text{ cm}^{-1}$  (Figure IV-4 b). The FT-IR spectrum of maleimide functionalized  $\gamma\text{-Fe}_2\text{O}_3/\text{SiO}_2$  MNPs resulted after

the cleavage of furan protection –  $\gamma\text{-Fe}_2\text{O}_3/\text{SiO}_2@11\text{-Mal}$  (red dotted line, Figure IV-4) demonstrated the successful maleimide deprotection by the shift of characteristic cyclic imides out-of-phase C=O stretching band from  $1698\text{ cm}^{-1}$  to  $1708\text{ cm}^{-1}$  and disappearance of the furan ring deformation at  $877\text{ cm}^{-1}$ . Unfortunately, the appearance of a new peak at  $695\text{ cm}^{-1}$  could not be monitored, being completely covered by the peaks at  $696\text{ cm}^{-1}$  arising from  $\gamma\text{-Fe}_2\text{O}_3/\text{SiO}_2$  MNPs' core-shell structure.

Grafting of the silylated two-branched coupling agent **19** (FT-IR spectrum in green solid line, Figure IV-5) can be monitored by the presence of five characteristic bands: the out-of-phase C=O stretching at  $1699\text{ cm}^{-1}$ ; the well delimited absorption band arising from C=O stretching of ester groups at  $1740\text{ cm}^{-1}$ ; the increase of absorption band intensity around  $1633\text{ cm}^{-1}$  attributed to the amide I mode; the shoulder around  $1560\text{ cm}^{-1}$  indicating the presence of the amide II mode; and the furan specific ring deformation at  $877\text{ cm}^{-1}$  (Figure IV-5 b).

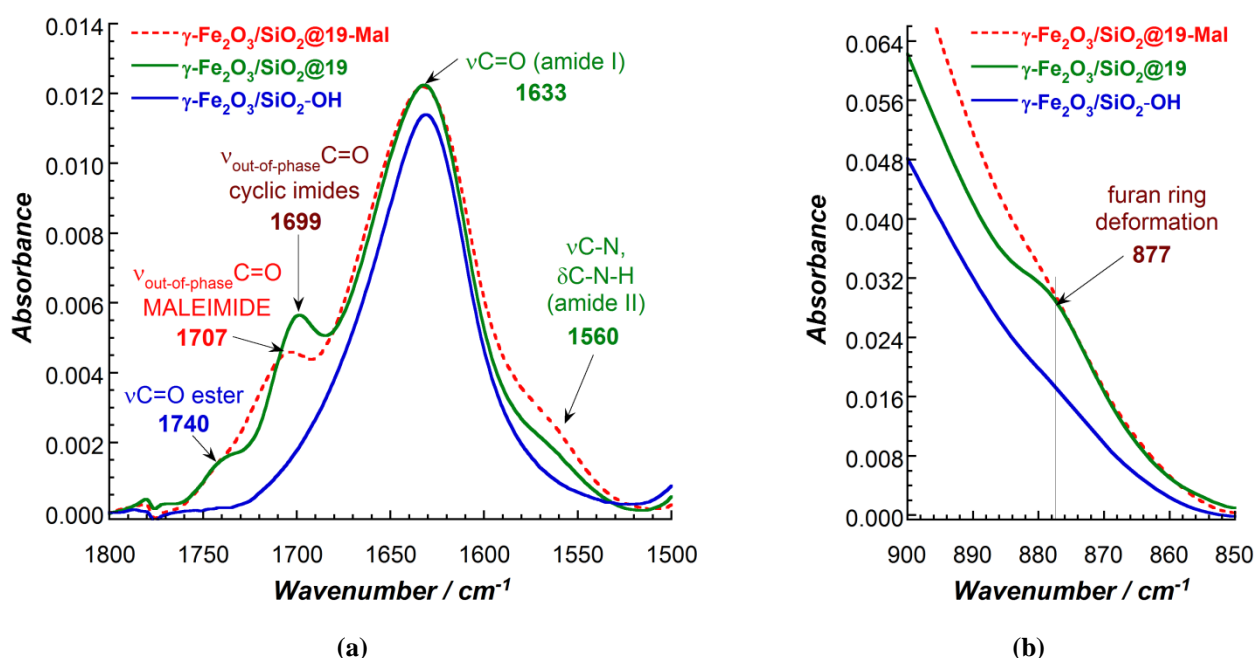


**Figure IV-5.** ATR FT-IR spectra of: native silica coated  $\gamma\text{-Fe}_2\text{O}_3$  MNPs ( $\gamma\text{-Fe}_2\text{O}_3/\text{SiO}_2\text{-OH}$ ) – solid line in blue, MNPs obtained after the grafting of two-branched silylated coupling agent **19** ( $\gamma\text{-Fe}_2\text{O}_3/\text{SiO}_2@19$ ) – solid line in green, and MNPs obtained after the cleavage of furan protection ( $\gamma\text{-Fe}_2\text{O}_3/\text{SiO}_2@19\text{-Mal}$ ) – dotted line in red (a) in the region 1800-1500 nm; and (b) in the region 900-850 nm.

In addition, the FT-IR spectrum of  $\gamma\text{-Fe}_2\text{O}_3/\text{SiO}_2@19$ , showed an increase in intensity of all compound's characteristic absorption bands, comparing to the recorded FT-IR spectrum of  $\gamma\text{-Fe}_2\text{O}_3/\text{SiO}_2@11$  (Figure IV-4) indicating the presence of a larger amount of functional groups on MNPs' surface. Thus, under the identical conditions of the grafting reaction, the grafting of the two-branched silylated coupling agent **19** allows achieving a larger number of functional groups comparing to the IR results obtained for the grafting of the linear silylated coupling agent **11**. FT-IR spectrum of  $\gamma\text{-Fe}_2\text{O}_3/\text{SiO}_2@19\text{-Mal}$  (red dotted line, Figure IV-5) demonstrated the successful maleimide

deprotection by the shift of out-of-phase C=O stretching band from  $1699\text{ cm}^{-1}$  to  $1707\text{ cm}^{-1}$  and complete disappearance of the furan ring deformation at  $877\text{ cm}^{-1}$ .

Grafting of the four-branched silylated coupling agent **24** (FT-IR spectrum in green solid line, Figure IV-6) revealed the presence of six characteristic bands. A very strong out-of-phase C=O stretching vibration (cyclic imides) is detected at  $1702\text{ cm}^{-1}$ , and even a weak in-phase C=O stretching vibration is visible at  $1774\text{ cm}^{-1}$ . The characteristic absorption band of the C=O stretching vibration of ester groups is well delimited at  $1734\text{ cm}^{-1}$ . Also, the apparition of a broad shoulder in the  $1560 - 1520\text{ cm}^{-1}$  region (arising from the amide II mode), as well as the increase in intensity of the absorption band around  $1640\text{ cm}^{-1}$  (amide I mode) confirm the presence of amide groups on MNPs' surface. Another indication for the high surface modification is the peak at  $877\text{ cm}^{-1}$  assigned to the furan specific ring deformation (Figure IV-6 b).

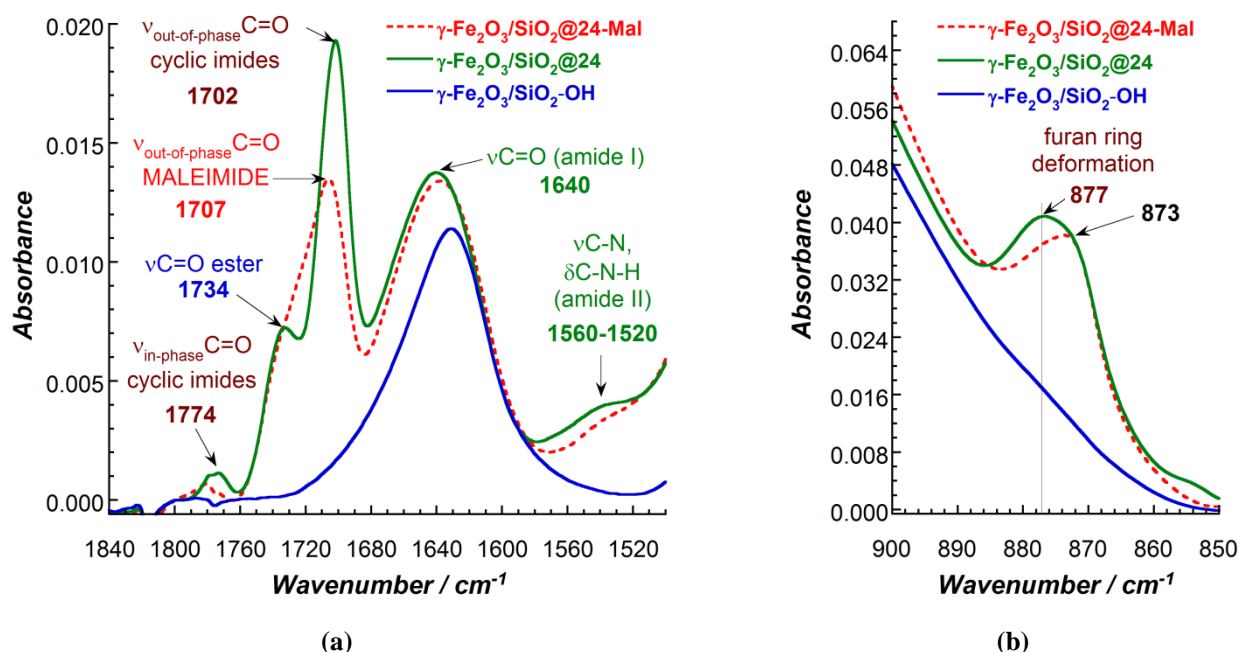


**Figure IV-6.** ATR FT-IR spectra of: native silica coated  $\gamma\text{-Fe}_2\text{O}_3$  MNPs ( $\gamma\text{-Fe}_2\text{O}_3/\text{SiO}_2\text{-OH}$ ) – solid line in blue, MNPs obtained after the grafting of four-branched silylated coupling agent **24** ( $\gamma\text{-Fe}_2\text{O}_3/\text{SiO}_2\text{@24}$ ) – solid line in green, and MNPs obtained after the cleavage of furan protection ( $\gamma\text{-Fe}_2\text{O}_3/\text{SiO}_2\text{@24-Mal}$ ) – dotted line in red (a) in the region 1840-1520  $\text{nm}$ ; and (b) in the region 900-850  $\text{nm}$ .

Surprisingly, the grafting of the four-branched silylated coupling agent **24** resulted in a considerable increase of all the characteristic absorption bands' intensities comparing to the IR spectra of MNPs functionalized with linear **11** or two-branched **19** silylated coupling agents (Figure IV-4 and Figure IV-5). This increasing intensity makes evident, that the number of functional groups present on MNPs' surface is dependent on the number of functional groups present in the coupling agent's structure (and thus, dependent on the dendron generation). However, the increase in intensity of the bands is not proportional to number of functional groups present in the coupling agents' structure used

for the surface modification, indicating that the dendron's generation does not represent the only factor in achieving of high surface functionalization. From the comparison of the spectra (Figure IV-4, Figure IV-5 and Figure IV-6) it is apparent that the grafting reaction is strongly dependent on the chemical nature of the coupling agents, being completely different in the case of the four-branched silylated coupling agent **24**. Silane **24** differs from the silanes **11** and **19** by the presence of amide groups in the backbone, and also has a higher molecular weight. These changes seem to have a significant influence on the chemical properties of silane, with a substantial influence on the reactivity.

FT-IR spectrum of  $\gamma$ -Fe<sub>2</sub>O<sub>3</sub>/SiO<sub>2</sub>@**24-Mal** (red dotted line, Figure IV-6) showed the characteristic shift of out-of-phase C=O stretching band from 1702 cm<sup>-1</sup> to 1707 cm<sup>-1</sup> and the disappearance of the furan ring deformation at 877 cm<sup>-1</sup> pointing out on the cleavage of furan protection. Similarly to the coupling agent **24** deprotection (Figure IV-3 c) the band at 783 cm<sup>-1</sup> was observed. However, the intensity of this band suggests that it could be partially generated by the residual Diels-Alder adduct (non-deprotected maleimide).

To conclude, the performed FT-IR study allowed confirming both, the successful grafting of silylated coupling agents **11**, **19** and **24** as well as the cleavage of the furan protection. Also, it showed that the amount of grafted molecule increases with increasing the dendron's generation. However, in the case of core-shell  $\gamma$ -Fe<sub>2</sub>O<sub>3</sub>/SiO<sub>2</sub> MNPs, it is possible that the surface modification efficiency is influenced by the dendron generation and also by the coupling agent's chemical nature.

#### IV.3.2.2. TGA coupled with MS study of $\gamma$ -Fe<sub>2</sub>O<sub>3</sub>/SiO<sub>2</sub> MNPs functionalized with silylated coupling agent **11**

The surface coverage of the modified core-shell  $\gamma$ -Fe<sub>2</sub>O<sub>3</sub>/SiO<sub>2</sub> MNPs as well as the occurring thermal decomposition processes were investigated by TGA coupled with MS. For this purpose three samples were submitted for analyses: native core-shell  $\gamma$ -Fe<sub>2</sub>O<sub>3</sub>/SiO<sub>2</sub> MNPs ( $\gamma$ -Fe<sub>2</sub>O<sub>3</sub>/SiO<sub>2</sub>-OH); MNPs obtained after the grafting of silylated coupling agent **11** ( $\gamma$ -Fe<sub>2</sub>O<sub>3</sub>/SiO<sub>2</sub>@**11**); and maleimide functionalized MNPs ( $\gamma$ -Fe<sub>2</sub>O<sub>3</sub>/SiO<sub>2</sub>@**11-Mal**). The recorded TGA curves are presented in Figure IV-7, Figure IV-9 and Figure IV-11 respectively. The mass loss seen in TGA was then associated with the corresponding key ions detected via MS at the given range of temperature (shown in Figure IV-8, Figure IV-10 and Figure IV-12 respectively).

TG measurement of native  $\gamma$ -Fe<sub>2</sub>O<sub>3</sub>/SiO<sub>2</sub> MNPs ( $\gamma$ -Fe<sub>2</sub>O<sub>3</sub>/SiO<sub>2</sub>-OH) is presented in Figure IV-7.

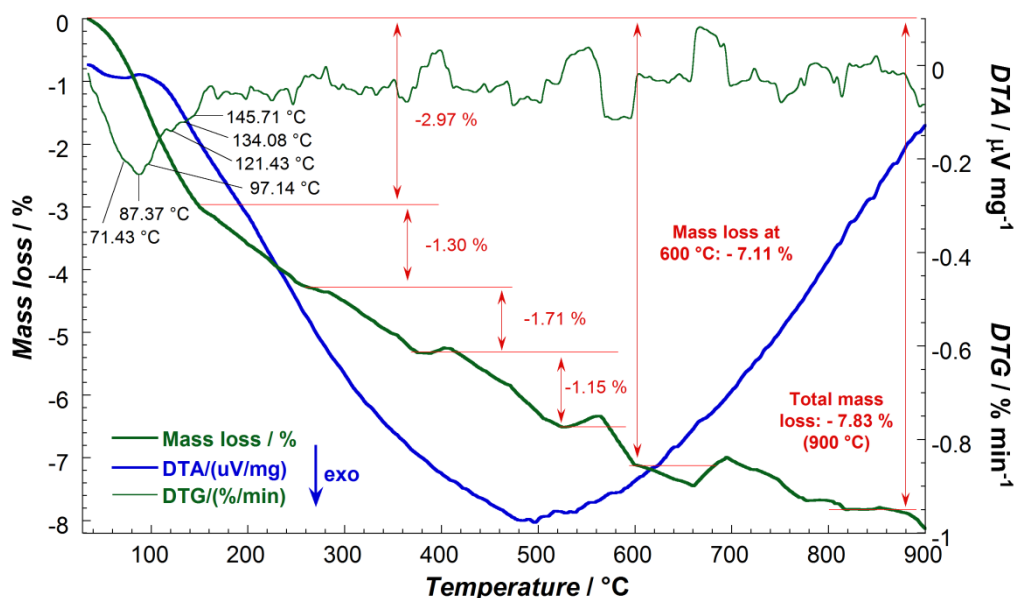
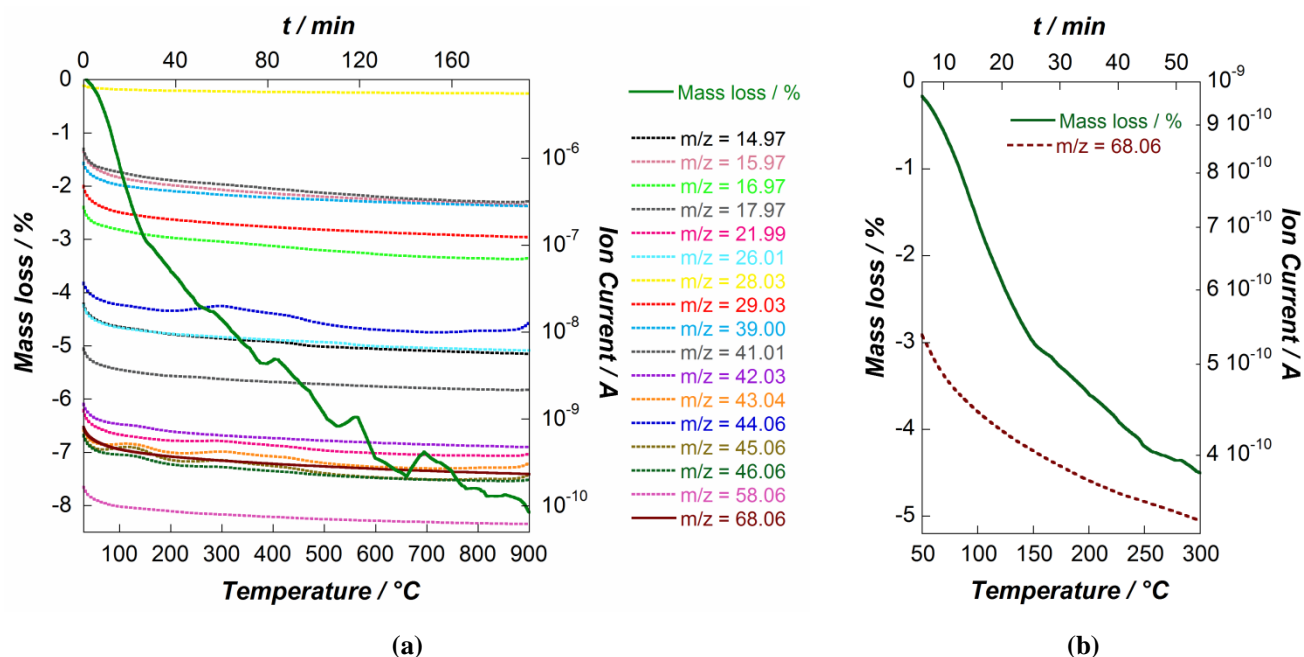


Figure IV-7. TG measurement of native  $\gamma\text{-Fe}_2\text{O}_3/\text{SiO}_2$  MNPs ( $\gamma\text{-Fe}_2\text{O}_3/\text{SiO}_2\text{-OH}$ ).

The TG curve of  $\gamma\text{-Fe}_2\text{O}_3/\text{SiO}_2\text{-OH}$  did not show well delimited steps of thermal decomposition, since there are several decomposition processes which take place simultaneously. Thus, according to R. P. W. Scott and S. Traiman: the layer of weakly adsorbed water on silica surface can be completely removed by heating to  $120^\circ\text{C}$ ; the layer of adsorbed water that is strongly held by hydrogen bonding does not commence to leave the surface until a temperature of  $200^\circ\text{C}$  is reached, and can be completely removed only about  $650^\circ\text{C}$ ; and the silanol groups can be converted to siloxyl groups when the silica is heated to  $450^\circ\text{C}$ , however, the significant loss of silanol groups does not appear to take place until  $750^\circ\text{C}$ .<sup>21</sup> Also, we must not forget that the TG curve comprises the mass of adsorbed solvents on MNPs' surface as well as the mass resulted after the decomposition processes related to the core-shell MNPs' content. The total mass loss for  $\gamma\text{-Fe}_2\text{O}_3/\text{SiO}_2\text{-OH}$  after heating the sample to  $900^\circ\text{C}$  constituted 7.83 % and showed to be an exothermic process.

The mass loss seen in TGA, associated with the corresponding key ions detected via MS at the given range of temperature, is presented in Figure IV-8 a. The MS spectra showed to be in a good coherence with the upper described decomposition processes. At the same time, the molecular ion current of furan ( $m/z = 68.06$ ) was not detected in the range of temperatures between  $50^\circ\text{C}$  and  $250^\circ\text{C}$  (corresponding to the range of temperatures when the retro Diels-Alder reaction occurs, Figure IV-8 b).





**Figure IV-8.** (a) Combination of the mass loss curve from TGA for native  $\gamma\text{-Fe}_2\text{O}_3/\text{SiO}_2$  MNPs ( $\gamma\text{-Fe}_2\text{O}_3/\text{SiO}_2\text{-OH}$ ) with the corresponding ion currents detected in MS in the range of temperatures between 30°C and 900°C; and (b) Combination of the mass loss curve from TGA for  $\gamma\text{-Fe}_2\text{O}_3/\text{SiO}_2\text{-OH}$  with the ion current corresponding to  $m/z = 68.06$  in the range of temperatures between 50°C and 300°C.

The TG and DTG curves of  $\gamma\text{-Fe}_2\text{O}_3/\text{SiO}_2@11$  (Figure IV-9) showed similar behaviour as that for  $\gamma\text{-Fe}_2\text{O}_3/\text{SiO}_2\text{-OH}$  (Figure IV-7), while the DTA curve showed to be different, pointing out on the change in thermal decomposition processes. For a better understanding of the thermal decomposition processes, the TG curve should be examined associated to the corresponding fragment ion currents detected in MS (Figure IV-10).

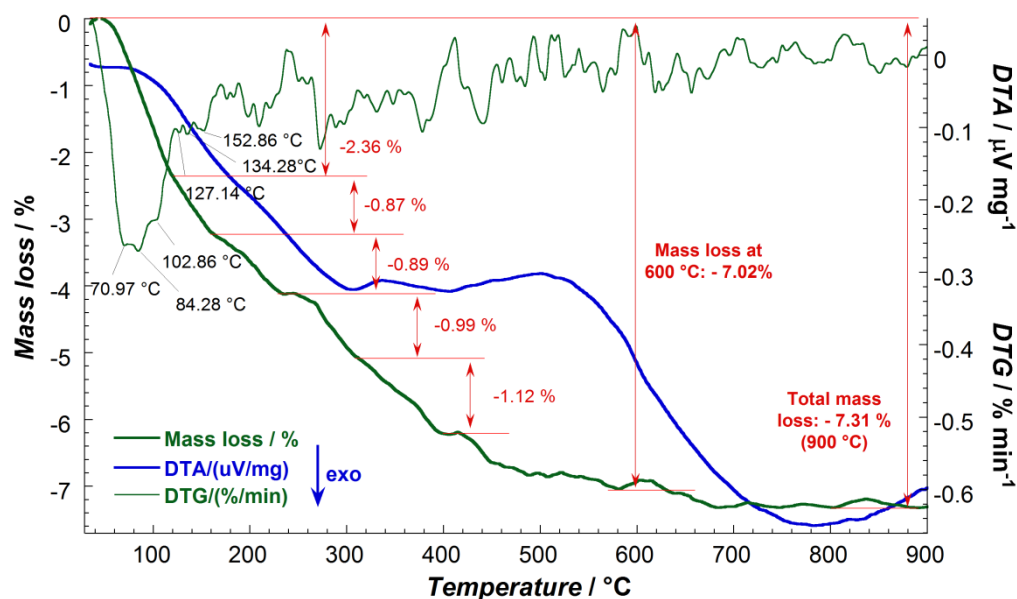


**Figure IV-9.** TG measurement of  $\gamma\text{-Fe}_2\text{O}_3/\text{SiO}_2$  MNPs resulted after the grafting of silylated linear coupling agent **11** ( $\gamma\text{-Fe}_2\text{O}_3/\text{SiO}_2@11$ ).

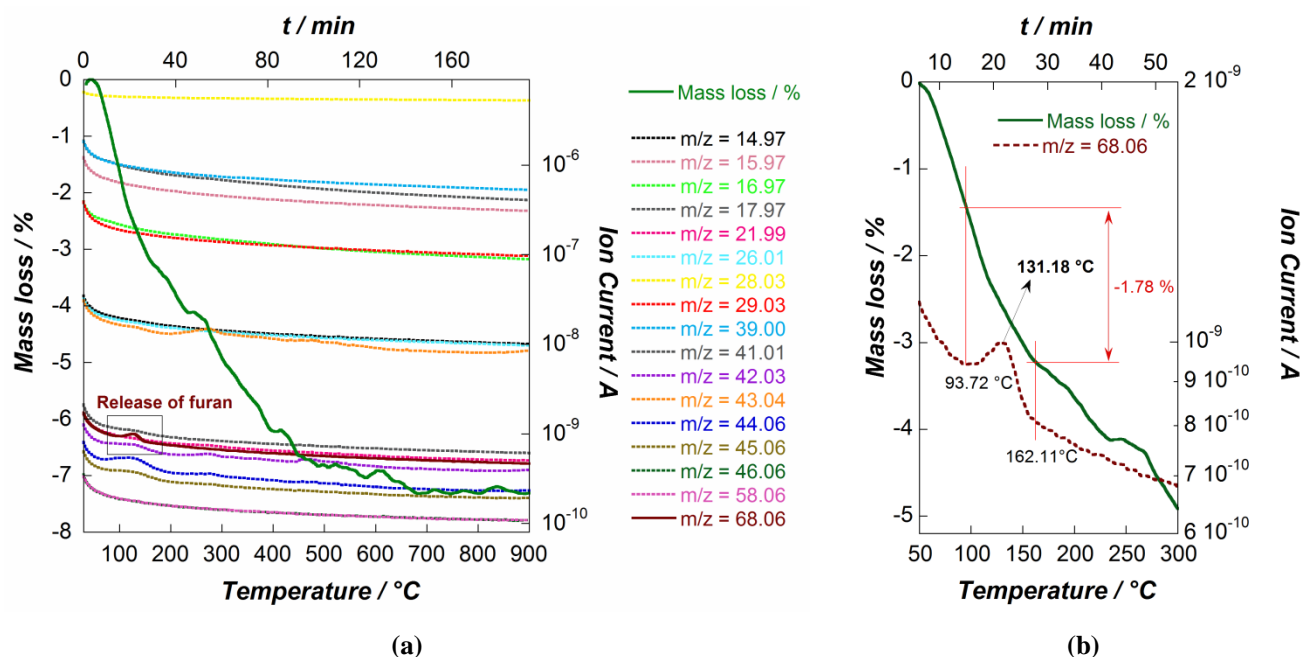


**Figure IV-10.** (a) Combination of the mass loss curve from TGA for  $\gamma\text{-Fe}_2\text{O}_3/\text{SiO}_2@11$  with the corresponding fragment ion currents detected in MS in the range of temperatures between 30°C and 900°C, and (b) Combination of the mass loss curve from TGA for  $\gamma\text{-Fe}_2\text{O}_3/\text{SiO}_2@11$  with the detected ion of furan ( $m/z = 68.06$ ) in the range of temperatures between 50°C and 300°C.

The mass loss until 240°C can be associated to the release of adsorbed onto the MNPs' surface water and ethanol, the ethanol resulted after the hydrolyses of ethoxy groups that did not hydrolyse during the grafting reaction, as well as the release of *uran*. The release of *uran* (Figure IV-10 b) begins at a temperature of around 94°C with the maximum at around 131°C and finishes around 162°C. The detected maximum of *uran* release (131°C) is coherent with the results obtained in Chapter III as well as the previously reported literature values.<sup>22</sup> However, the mass loss of 1.78 % found in this range of temperatures (Figure IV-10 b) cannot be attributed only to the *uran* mass loss (and to the mass loss due to the amount of grafted coupling agent, respectively), since the release of *uran* occurs simultaneously with the release of the water and ethanol (Figure IV-10 a). The detection of *uran* ion current additionally confirms the successful grafting of silylated linear coupling agent 11.

Further heating of the sample (at temperatures upper than 200°C) results in the thermal decomposition of the coupling agent (including maleimide functionality) that is associated with the decomposition processes related to the MNPs' core content. The total mass loss for  $\gamma\text{-Fe}_2\text{O}_3/\text{SiO}_2@11$  after heating the sample to 900°C constituted 7.31 % comparing to 7.83 % of total loss detected for  $\gamma\text{-Fe}_2\text{O}_3/\text{SiO}_2\text{-OH}$ . These results suggest that the total mass loss of the sample is strongly dependent on the quantity of adsorbed water and/or solvents, as well as on the core-shell structure of MNPs (silica coating and ferrofluid core).

In the case of  $\gamma$ -Fe<sub>2</sub>O<sub>3</sub>/SiO<sub>2</sub>@11-Mal (Figure IV-11) the TG, DTG and Differential Thermal Analysis (DTA) curves showed similar behaviour as in the case of  $\gamma$ -Fe<sub>2</sub>O<sub>3</sub>/SiO<sub>2</sub>@11 (Figure IV-9) indicating the similarity of the decomposition processes, except the release of furan (Figure IV-12).

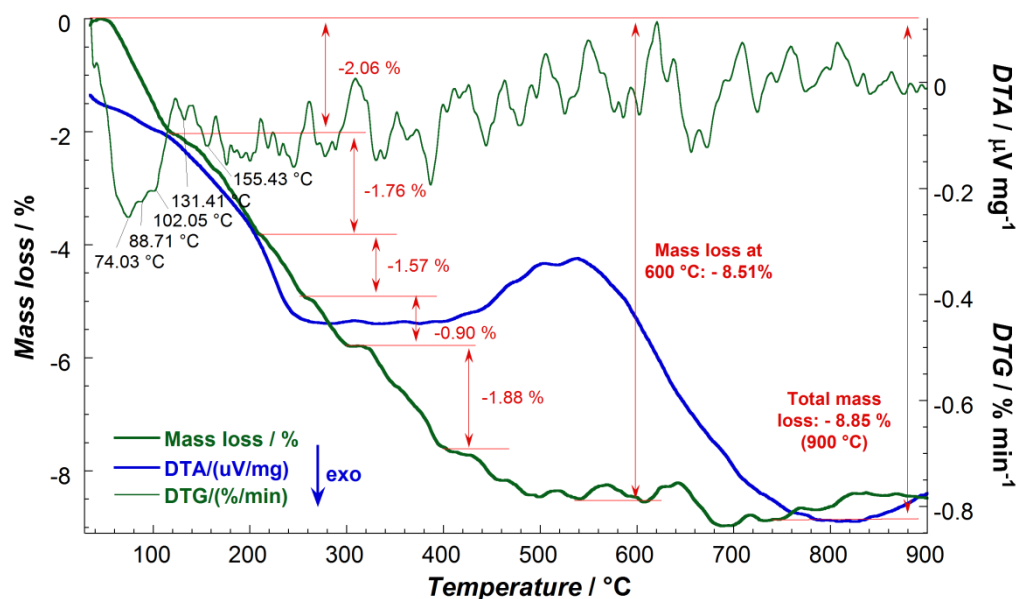


Figure IV-11. TG measurement of  $\gamma$ -Fe<sub>2</sub>O<sub>3</sub>/SiO<sub>2</sub>@11-Mal.

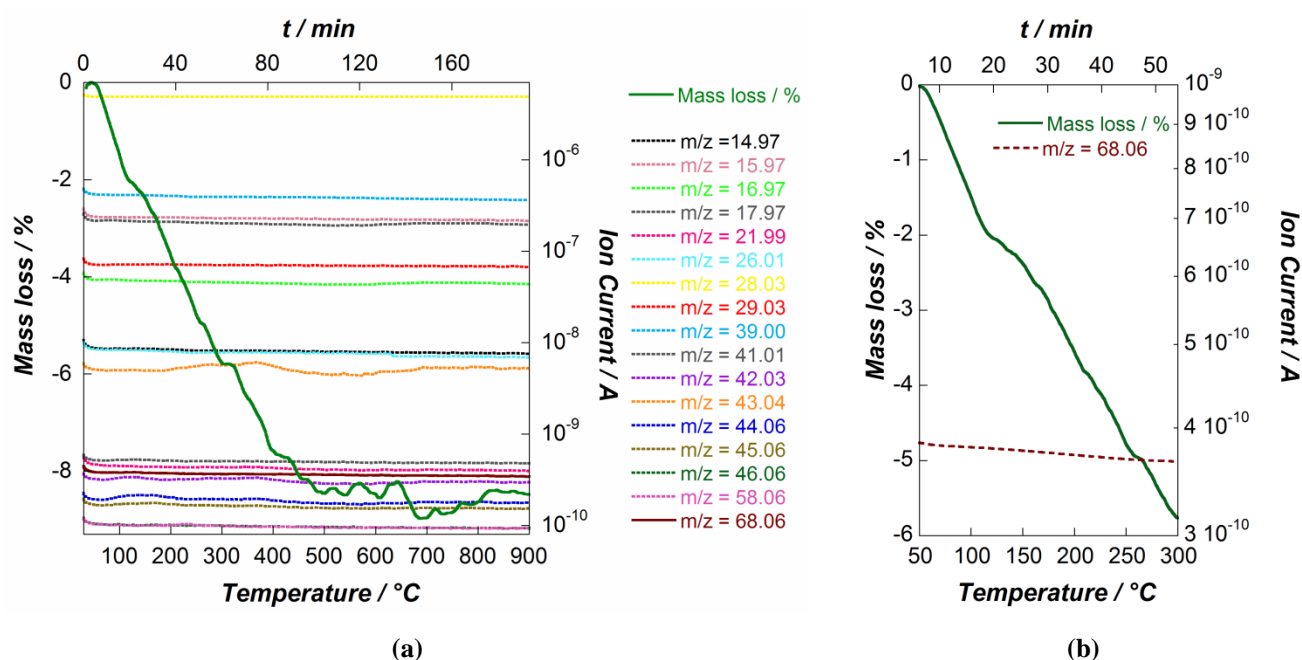


Figure IV-12. (a) Combination of the mass loss curve from TGA for  $\gamma$ -Fe<sub>2</sub>O<sub>3</sub>/SiO<sub>2</sub>@11-Mal with the corresponding fragment ion currents detected in MS in the range of temperatures between 30 °C and 900 °C, and (b) Combination of the mass loss curve from TGA for  $\gamma$ -Fe<sub>2</sub>O<sub>3</sub>/SiO<sub>2</sub>@11-Mal with the ion current corresponding to  $m/z = 68.06$  in the range of temperatures between 50 °C and 300 °C.

According to the MS spectra of  $\gamma$ -Fe<sub>2</sub>O<sub>3</sub>/SiO<sub>2</sub>@11-Mal (Figure IV-12) as it was expected, the furan ion current ( $m/z = 68.06$ ) was not detected in the range of temperatures between 50 °C and 250 °C, thus confirming the deprotection of maleimide functional group.

To conclude, TGA coupled with MS analysis gave an additional to IR technique confirmation of the successful grafting of silylated linear coupling agent **11**, as well as the proof of the complete cleavage of furan protection. However, these techniques cannot provide any information about the quantity of grafted molecules and, in addition, TGA represents a destructive high mass consuming technique (10 – 20 mg of MNPs). For these reasons, similar study was not investigated in the case of MNPs functionalized with dendritic silylated coupling agents **19** and **24**.

#### IV.3.2.3. TEM study of maleimide functionalized $\gamma\text{-Fe}_2\text{O}_3/\text{SiO}_2$ MNPs

To investigate the morphological changes (size, shape etc.) that can occur on the MNPs' surface upon surface modification chemistry, TEM images of the modified  $\gamma\text{-Fe}_2\text{O}_3/\text{SiO}_2$  MNPs:  $\gamma\text{-Fe}_2\text{O}_3/\text{SiO}_2@11$ ,  $\gamma\text{-Fe}_2\text{O}_3/\text{SiO}_2@19$ ,  $\gamma\text{-Fe}_2\text{O}_3/\text{SiO}_2@24$ ,  $\gamma\text{-Fe}_2\text{O}_3/\text{SiO}_2@11\text{-Mal}$ ,  $\gamma\text{-Fe}_2\text{O}_3/\text{SiO}_2@19\text{-Mal}$ , and  $\gamma\text{-Fe}_2\text{O}_3/\text{SiO}_2@24\text{-Mal}$  were recorded (Figure IV-13). These images confirmed that all the particles retain their integrity after the grafting procedure as well as after the maleimide group deprotection step. The general aspect of MNPs after the carried out surface modification did not show significant changes. In all the cases the shell of the particles remained homogeneous and no oligomerization on the MNPs' surface was observed as side reaction.

At the same time, a non-significant increase in shell thickness was observed. Thus, for  $\gamma\text{-Fe}_2\text{O}_3/\text{SiO}_2$  MNPs functionalized with linear coupling agent **11** the shell thickness increased with 1–2 nm (Figure IV-13 a and b), for those functionalized with two-branched coupling agent **19** (Figure IV-13 c and d) the shell thickness increased with 1–3 nm, while for those functionalized with four-branched coupling agent **24** (Figure IV-13 e and f) it increased with 3–5 nm (assuming that the shell thickness of the native core shell  $\gamma\text{-Fe}_2\text{O}_3/\text{SiO}_2$  MNPs was 20 nm). These results suggest that the grafting of coupling agents on the  $\gamma\text{-Fe}_2\text{O}_3$  MNPs' surface resulted in the formation of a thin homogeneous layer.

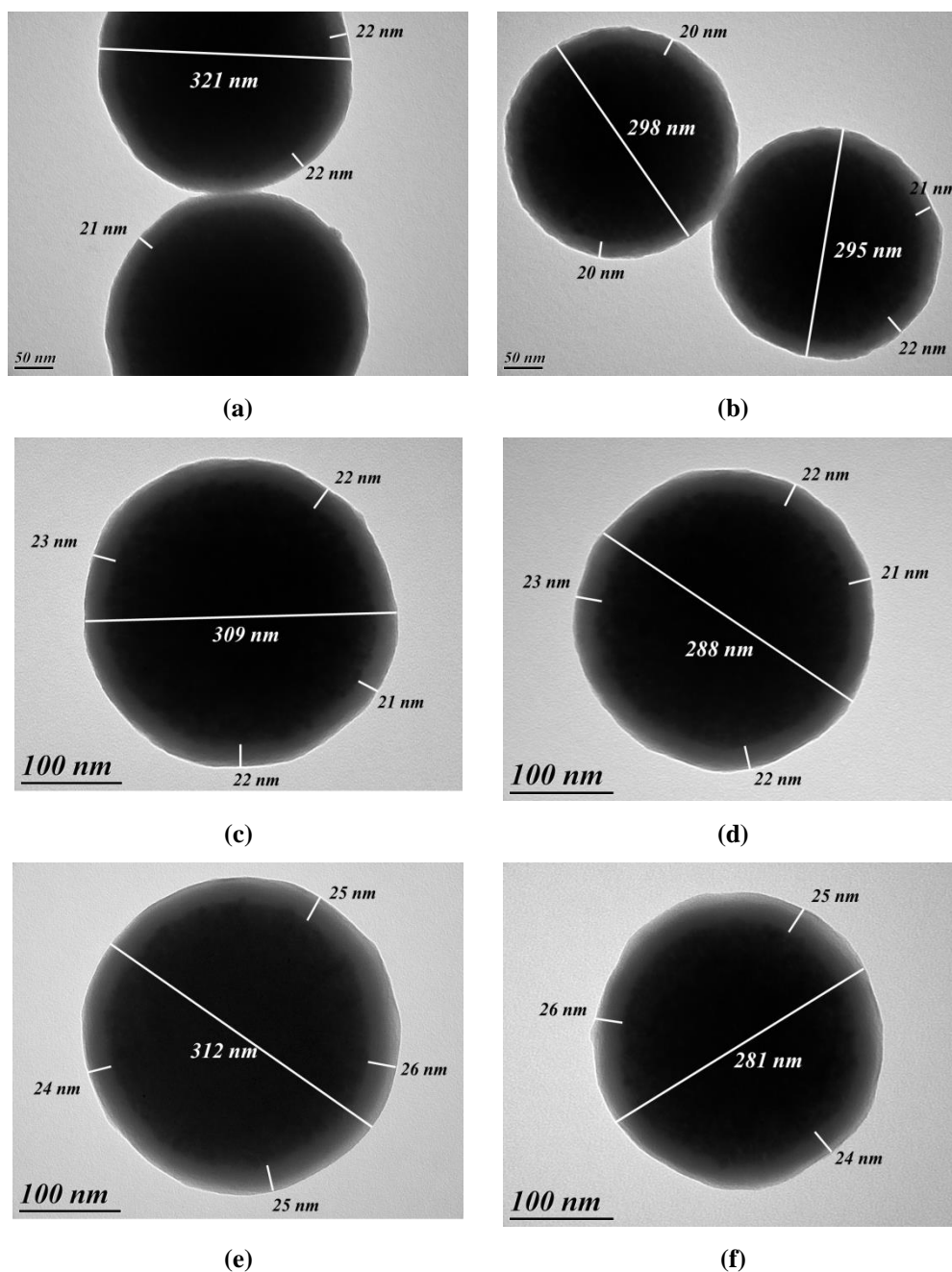


**Figure IV-13.** TEM images of (a)  $\gamma$ -Fe<sub>2</sub>O<sub>3</sub>/SiO<sub>2</sub>@11; (b)  $\gamma$ -Fe<sub>2</sub>O<sub>3</sub>/SiO<sub>2</sub>@11-Mal; (c)  $\gamma$ -Fe<sub>2</sub>O<sub>3</sub>/SiO<sub>2</sub>@19; (d)  $\gamma$ -Fe<sub>2</sub>O<sub>3</sub>/SiO<sub>2</sub>@19-Mal; (e)  $\gamma$ -Fe<sub>2</sub>O<sub>3</sub>/SiO<sub>2</sub>@24; (f)  $\gamma$ -Fe<sub>2</sub>O<sub>3</sub>/SiO<sub>2</sub>@24-Mal.

#### IV.3.2.4. Zeta potential measurements for maleimide functionalized $\gamma$ -Fe<sub>2</sub>O<sub>3</sub>/SiO<sub>2</sub> MNPs

Zeta potential measurements of diluted aqueous suspensions of native and functionalized  $\gamma$ -Fe<sub>2</sub>O<sub>3</sub>/SiO<sub>2</sub> MNPs were performed at 25°C by varying pH from 4.2 to 8.5. The pH of the  $\gamma$ -Fe<sub>2</sub>O<sub>3</sub>/SiO<sub>2</sub> MNPs samples was adjusted by adding 0.01 M solution of hydrochloric acid or 0.01 M sodium hydroxide solution. Figure IV-14 illustrates the results obtained after performing the measurement of zeta potential as function of pH.

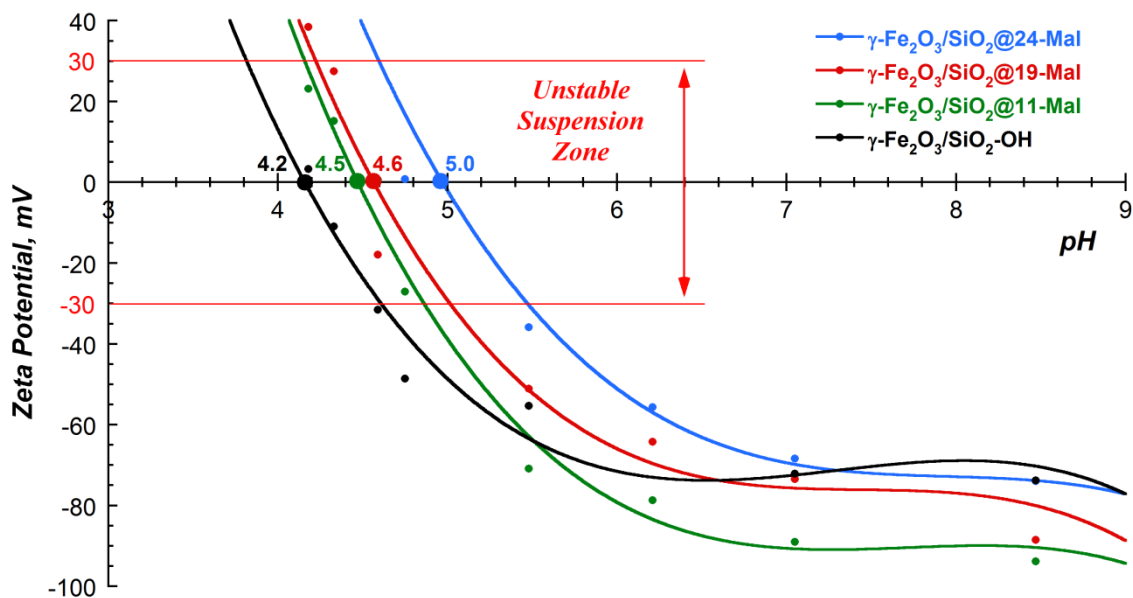


**Figure IV-14.** Effect of pH on the surface charge of native and functionalized  $\gamma\text{-Fe}_2\text{O}_3/\text{SiO}_2$  MNPs:  $\gamma\text{-Fe}_2\text{O}_3/\text{SiO}_2\text{@24-Mal}$ ;  $\gamma\text{-Fe}_2\text{O}_3/\text{SiO}_2\text{@19-Mal}$ ;  $\gamma\text{-Fe}_2\text{O}_3/\text{SiO}_2\text{@11-Mal}$ ; and  $\gamma\text{-Fe}_2\text{O}_3/\text{SiO}_2\text{-OH}$ .

As we can note, the curve profile of functionalized  $\gamma\text{-Fe}_2\text{O}_3/\text{SiO}_2$  MNPs is different from that of native  $\gamma\text{-Fe}_2\text{O}_3/\text{SiO}_2$  MNPs. Thus, the isoelectric point for all the samples of maleimide functionalized  $\gamma\text{-Fe}_2\text{O}_3$  MNPs has shifted towards higher values of pH, and constitutes: 4.5 for  $\gamma\text{-Fe}_2\text{O}_3/\text{SiO}_2\text{@11-Mal}$ ; 4.6 for  $\gamma\text{-Fe}_2\text{O}_3/\text{SiO}_2\text{@19-Mal}$ ; and 5.0 for  $\gamma\text{-Fe}_2\text{O}_3/\text{SiO}_2\text{@24-Mal}$ , comparing to 4.2 for native  $\gamma\text{-Fe}_2\text{O}_3/\text{SiO}_2\text{-OH}$ . This shift of isoelectric point values is due to the change of the surface charge of MNPs as the result of the surface modification. It is noteworthy that the isoelectric point for the  $\gamma\text{-Fe}_2\text{O}_3/\text{SiO}_2\text{@24-Mal}$  is a bit higher than for  $\gamma\text{-Fe}_2\text{O}_3/\text{SiO}_2\text{@11-Mal}$  and  $\gamma\text{-Fe}_2\text{O}_3/\text{SiO}_2\text{@19-Mal}$ , suggesting that the negative charge on the surface of MNPs is more shielded after the surface modification with coupling agent **24** than with coupling agents **11** or **19**, which is in a good coherence with a thicker shell thickness observed in TEM in the case of  $\gamma\text{-Fe}_2\text{O}_3/\text{SiO}_2\text{@24-Mal}$ .

#### IV.3.2.5. Colloidal state of maleimide functionalized $\gamma\text{-Fe}_2\text{O}_3/\text{SiO}_2$ MNPs in water

Colloidal state of native ( $\gamma\text{-Fe}_2\text{O}_3/\text{SiO}_2\text{-OH}$ ) and maleimide functionalized MNPs ( $\gamma\text{-Fe}_2\text{O}_3/\text{SiO}_2\text{@11-Mal}$ ,  $\gamma\text{-Fe}_2\text{O}_3/\text{SiO}_2\text{@19-Mal}$ , and  $\gamma\text{-Fe}_2\text{O}_3/\text{SiO}_2\text{@24-Mal}$ ) dispersed in ultrapure water was examined by Transmitted Light Microscopy (Figure IV-15).

The results of Transmitted Light Microscopy investigation are in good coherence with zeta potential measurements, according to which samples  $\gamma\text{-Fe}_2\text{O}_3/\text{SiO}_2\text{@11-Mal}$  (Figure IV-14 green line and Figure IV-15 b) and  $\gamma\text{-Fe}_2\text{O}_3/\text{SiO}_2\text{@19-Mal}$  (Figure IV-14 red line and Figure IV-15 c) are well dispersed in ultrapure water medium, while sample  $\gamma\text{-Fe}_2\text{O}_3/\text{SiO}_2\text{@24-Mal}$  (Figure IV-14 blue line and Figure IV-15 d) has the less stable colloidal state (in this medium). In this sample few aggregates

were observed. These aggregates negatively impact the colloidal stability of  $\gamma\text{-Fe}_2\text{O}_3/\text{SiO}_2@24\text{-Mal}$  in ultrapure water and result in a faster precipitation of MNPs comparing to other samples. Therefore, to improve the stability of the functionalized  $\gamma\text{-Fe}_2\text{O}_3/\text{SiO}_2$  MNPs in aqueous medium surfactants were employed.

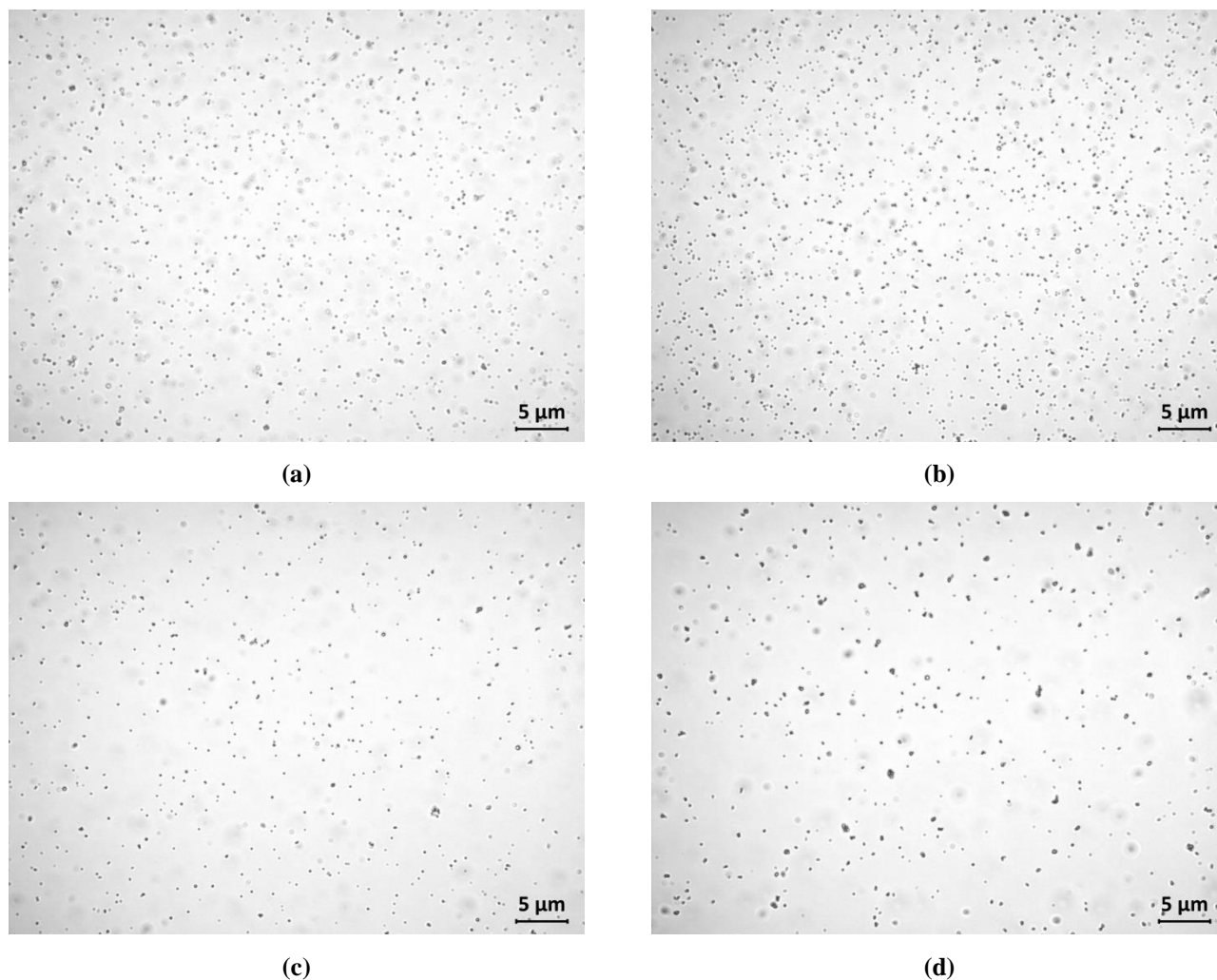


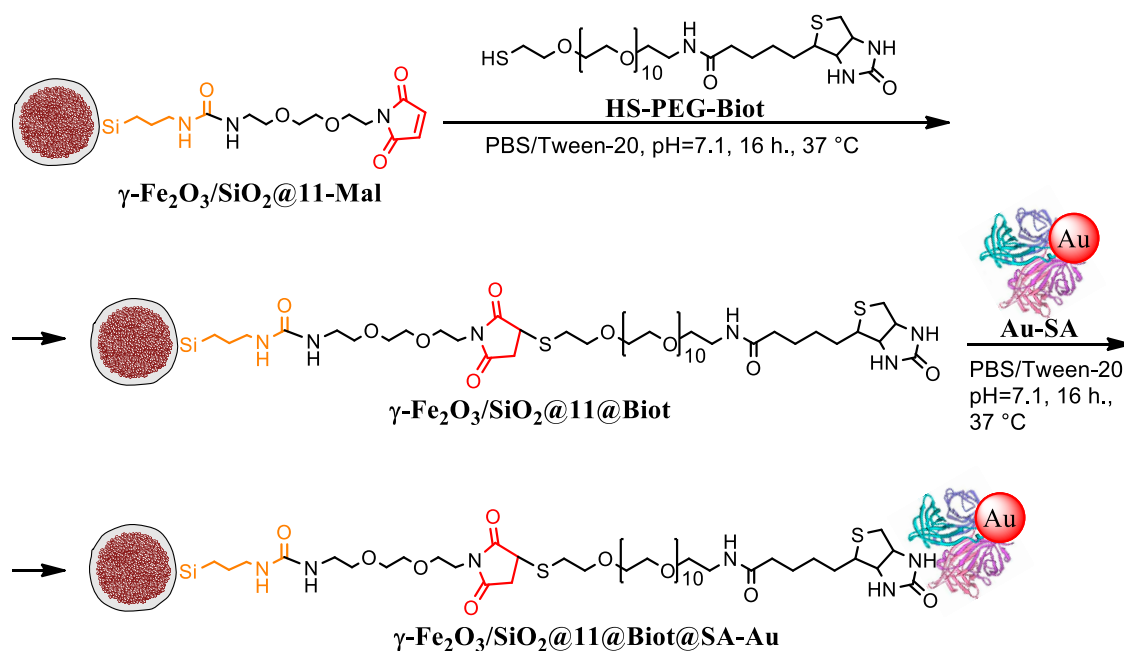
**Figure IV-15.** Transmitted Light Microscopy images of (a)  $\gamma\text{-Fe}_2\text{O}_3/\text{SiO}_2\text{-OH}$ ; (b)  $\gamma\text{-Fe}_2\text{O}_3/\text{SiO}_2@11\text{-Mal}$ ; (c)  $\gamma\text{-Fe}_2\text{O}_3/\text{SiO}_2@19\text{-Mal}$ ; (d)  $\gamma\text{-Fe}_2\text{O}_3/\text{SiO}_2@24\text{-Mal}$ .

#### IV.4. Immobilization tests

In order to study and compare the efficiency of maleimide functionalized  $\gamma\text{-Fe}_2\text{O}_3/\text{SiO}_2$  MNPs to immobilize thiol containing biomolecules two immobilization tests were performed and are presented below.

#### IV.4.1. Covalent coupling of thiol modified biotin with the maleimide functionalized $\gamma\text{-Fe}_2\text{O}_3/\text{SiO}_2$ MNPs and consequent recognition by SA-Au NPs

The labelling efficiency of maleimide functionalized  $\gamma\text{-Fe}_2\text{O}_3/\text{SiO}_2$  MNPs ( $\gamma\text{-Fe}_2\text{O}_3/\text{SiO}_2@11\text{-Mal}$ ,  $\gamma\text{-Fe}_2\text{O}_3/\text{SiO}_2@19\text{-Mal}$ , and  $\gamma\text{-Fe}_2\text{O}_3/\text{SiO}_2@24\text{-Mal}$ ) was tested according to the general strategy that was previously detailed in Chapter III (section III.3.3.3) and is illustrated in Scheme IV-14 (on the example of  $\gamma\text{-Fe}_2\text{O}_3/\text{SiO}_2@11\text{-Mal}$ ).



**Scheme IV-14.** Schematic representation of thiol modified biotin immobilization on  $\gamma\text{-Fe}_2\text{O}_3/\text{SiO}_2@11\text{-Mal}$  followed by immobilization of SA-Au NPs via Biotin-Streptavidin affinity.

The first step of this strategy involved the covalent coupling between HS-PEG-Biot and maleimide functionalized MNPs ( $\gamma\text{-Fe}_2\text{O}_3/\text{SiO}_2@11\text{-Mal}$ ,  $\gamma\text{-Fe}_2\text{O}_3/\text{SiO}_2@19\text{-Mal}$  or  $\gamma\text{-Fe}_2\text{O}_3/\text{SiO}_2@24\text{-Mal}$ ). The second step consists in the immobilization of SA-Au NPs via Biotin-Streptavidin affinity. Same reaction conditions as described in Chapter III, section III.3.3.3. were used for both steps. During the immobilization of SA-Au NPs, no sedimentation was observed in the case of  $\gamma\text{-Fe}_2\text{O}_3/\text{SiO}_2@11@Biot$ ; the microscopic colloidal aspect of  $\gamma\text{-Fe}_2\text{O}_3/\text{SiO}_2@19@Biot$  was less stable (at the end of reaction); while in the case of  $\gamma\text{-Fe}_2\text{O}_3/\text{SiO}_2@24@Biot$  a precipitation of the particles was observed (at the end of reaction).

UV-Vis spectroscopy measurements for the SA-Au NPs' solutions recovered after the immobilization reactions were performed (according to the procedure described in Chapter III, section III.3.3.3.) and the results are presented in Figure IV-16 a. TEM images of the  $\gamma\text{-Fe}_2\text{O}_3/\text{SiO}_2@11@Biot@SA\text{-Au}$ ,  $\gamma\text{-Fe}_2\text{O}_3/\text{SiO}_2@19@Biot@SA\text{-Au}$  and  $\gamma\text{-Fe}_2\text{O}_3/\text{SiO}_2@24@Biot@SA\text{-Au}$  are presented in Figure IV-16 b, c, d.



The calculations according to the calibration plot (Figure IV-16 a) showed that  $\gamma\text{-Fe}_2\text{O}_3/\text{SiO}_2@11@Biot$  immobilized  $1.62 \times 10^{12}$  of SA-Au NPs per 1mg (or  $0.73 \times 10^{11}$  of SA-Au NPs on 0.045mg\* of  $\gamma\text{-Fe}_2\text{O}_3/\text{SiO}_2@11@Biot$ );  $\gamma\text{-Fe}_2\text{O}_3/\text{SiO}_2@19@Biot$  immobilized  $1.76 \times 10^{12}$  of SA-Au NPs per 1mg (or  $0.65 \times 10^{11}$  of SA-Au NPs on 0.037mg\* of  $\gamma\text{-Fe}_2\text{O}_3/\text{SiO}_2@19@Biot$ ) and  $\gamma\text{-Fe}_2\text{O}_3/\text{SiO}_2@24@Biot$  immobilized  $2.24 \times 10^{12}$  of SA-Au NPs per 1mg (or  $0.55 \times 10^{11}$  of SA-Au NPs on 0.025mg\* of  $\gamma\text{-Fe}_2\text{O}_3/\text{SiO}_2@24@Biot$ ). TEM images (Figure IV-16 b, c and d) are in a good coherence with the UV/Vis study revealing a compact covering of the functionalized  $\gamma\text{-Fe}_2\text{O}_3/\text{SiO}_2$  MNPs with SA-Au NPs.

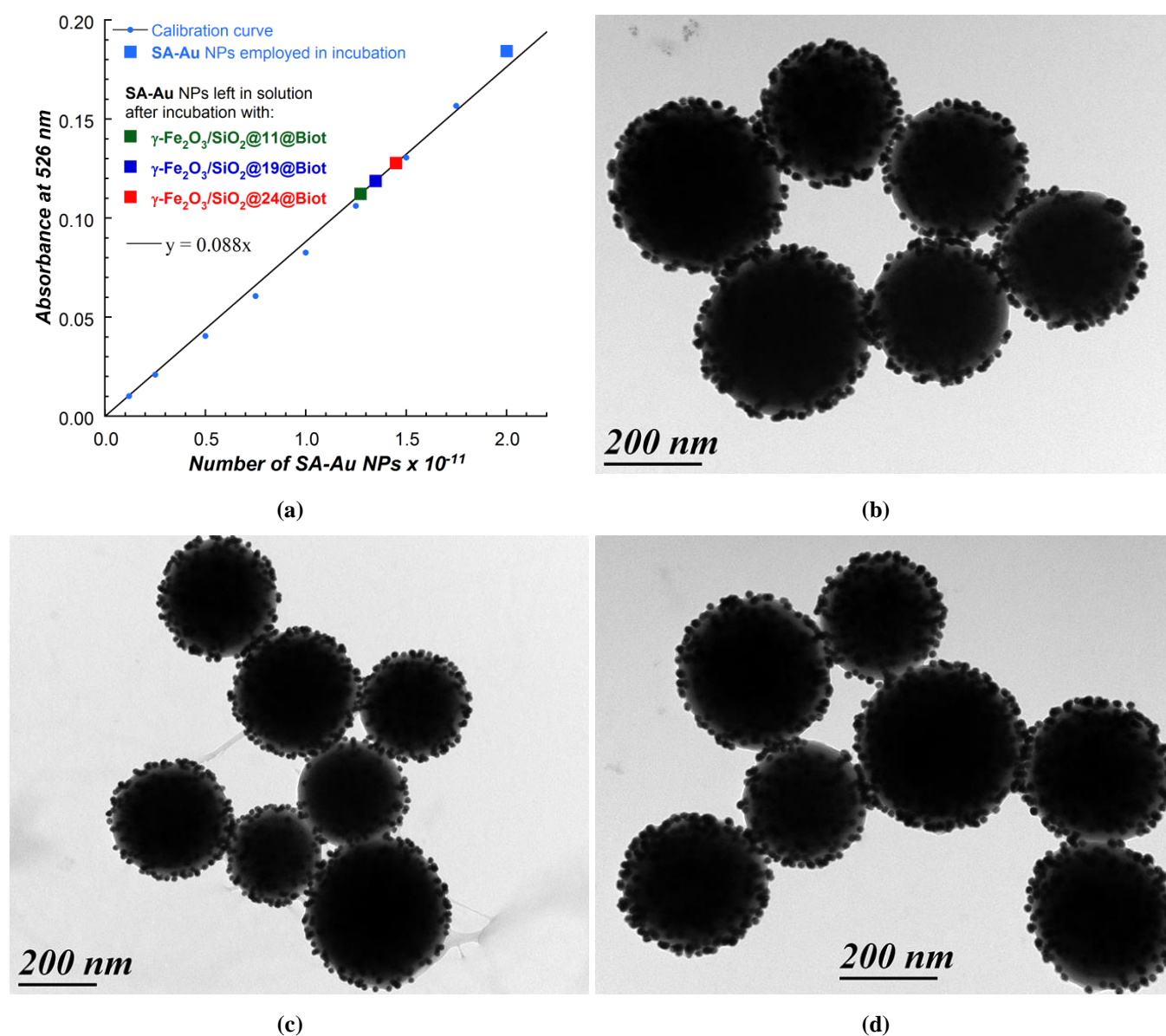


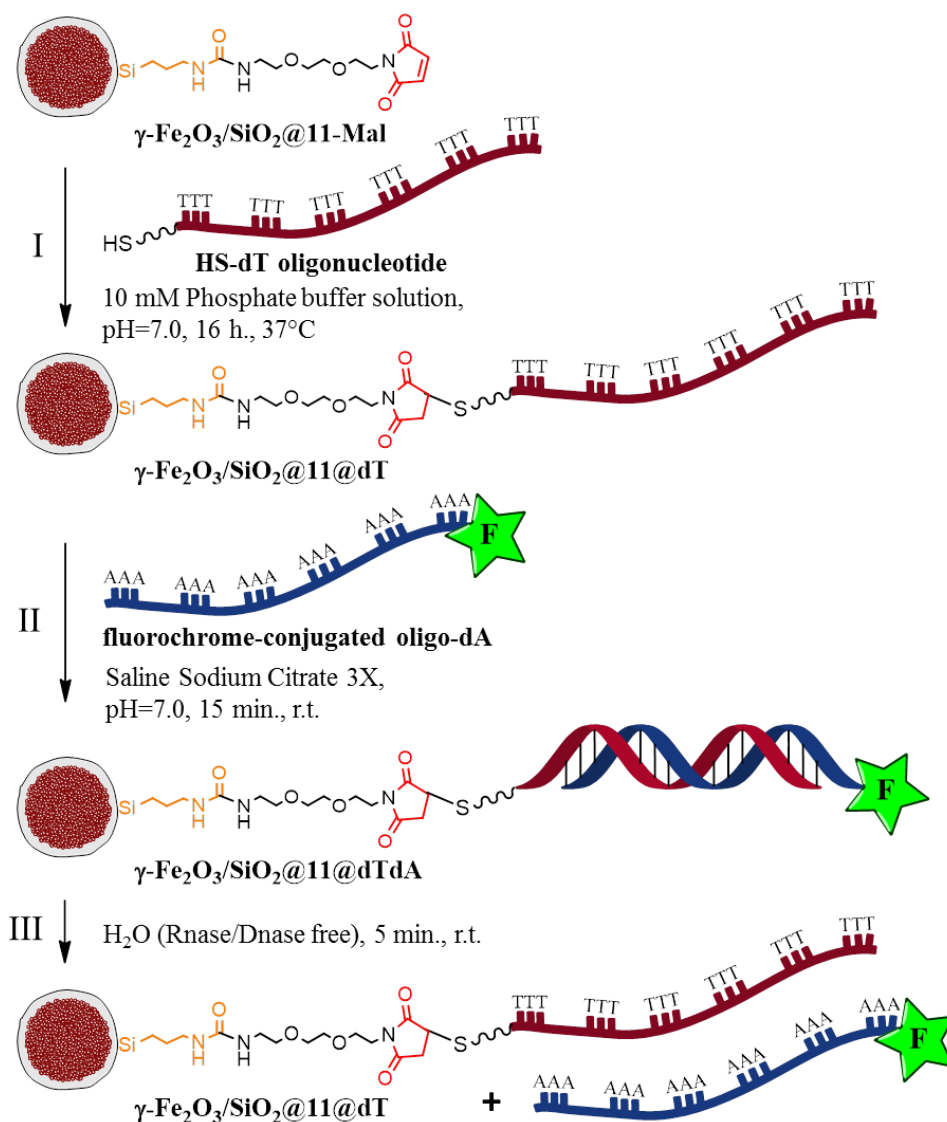
**Figure IV-16.** (a) Dependence of Absorbance at 526 nm as function of 15 nm SA-Au NPs number left in solution after the immobilization reaction; (b) TEM image of  $\gamma\text{-Fe}_2\text{O}_3/\text{SiO}_2@11@Biot@SA\text{-Au}$ ; (c) TEM image of  $\gamma\text{-Fe}_2\text{O}_3/\text{SiO}_2@19@Biot@SA\text{-Au}$ ; and (d) TEM image of  $\gamma\text{-Fe}_2\text{O}_3/\text{SiO}_2@24@Biot@SA\text{-Au}$ .

\*Concentration of maleimide functionalized MNPs ( $\gamma\text{-Fe}_2\text{O}_3/\text{SiO}_2@11@Biot$ ,  $\gamma\text{-Fe}_2\text{O}_3/\text{SiO}_2@19@Biot$  and  $\gamma\text{-Fe}_2\text{O}_3/\text{SiO}_2@24@Biot$ ) recalculated via optical density measurements.

To conclude, this strategy offered the possibility to verify (via Biotin-SA affinity) the capacity of maleimide functionalized MNPs to immobilize a thiol tagged biomolecule. All the samples of functionalized  $\gamma\text{-Fe}_2\text{O}_3/\text{SiO}_2$  MNPs showed to immobilise a high amount of SA-Au NPs, and therefore, these results indirectly confirm the successful homogeneous functionalization of MNPs.

#### IV.4.2. Covalent coupling of HS-dT oligonucleotide with maleimide functionalized $\gamma\text{-Fe}_2\text{O}_3/\text{SiO}_2$ MNPs and hybrid capture of its complementary sequence

Scheme IV-15 illustrates the steps of this strategy based on the example of  $\gamma\text{-Fe}_2\text{O}_3/\text{SiO}_2@11\text{-Mal}$ .



**Scheme IV-15.** I) Covalent coupling of HS-dT with  $\gamma\text{-Fe}_2\text{O}_3/\text{SiO}_2@11\text{-Mal}$ ; II) Hybrid capture of a complementary sequence oligo poly A (fluorochrome-conjugated oligo-dA Alexa Fluor) on  $\gamma\text{-Fe}_2\text{O}_3/\text{SiO}_2@11@dT$ ; and III) Dehybridization.

*In the first step* the HS-dT oligonucleotide was covalently immobilized on maleimide functionalized MNPs ( $\gamma\text{-Fe}_2\text{O}_3/\text{SiO}_2@11\text{-Mal}$ ,  $\gamma\text{-Fe}_2\text{O}_3/\text{SiO}_2@19\text{-Mal}$  or  $\gamma\text{-Fe}_2\text{O}_3/\text{SiO}_2@24\text{-Mal}$ ). *In*

the next step, the hybridization of the immobilized oligonucleotide dT with a complementary sequence oligo poly A of fluorochrome-conjugated oligo-dA (Alexa Fluor) was performed. The last step represents the dehybridization. The eluted in this step fluorochrome-conjugated oligo-dA was quantified on fluorescence microplate reader (Figure IV-17). A control experiment was also performed on  $\gamma\text{-Fe}_2\text{O}_3/\text{SiO}_2\text{-OH}$ . The hybridization, dehybridization and quantification of oligo-dA were performed by Ademtech SA.<sup>1</sup> The quantity of oligo-dA Alexa Fluor detected in Figure IV-17 is directly related to the quantity of HS-dT oligonucleotide immobilized on maleimide functionalized  $\gamma\text{-Fe}_2\text{O}_3/\text{SiO}_2$  MNPs.

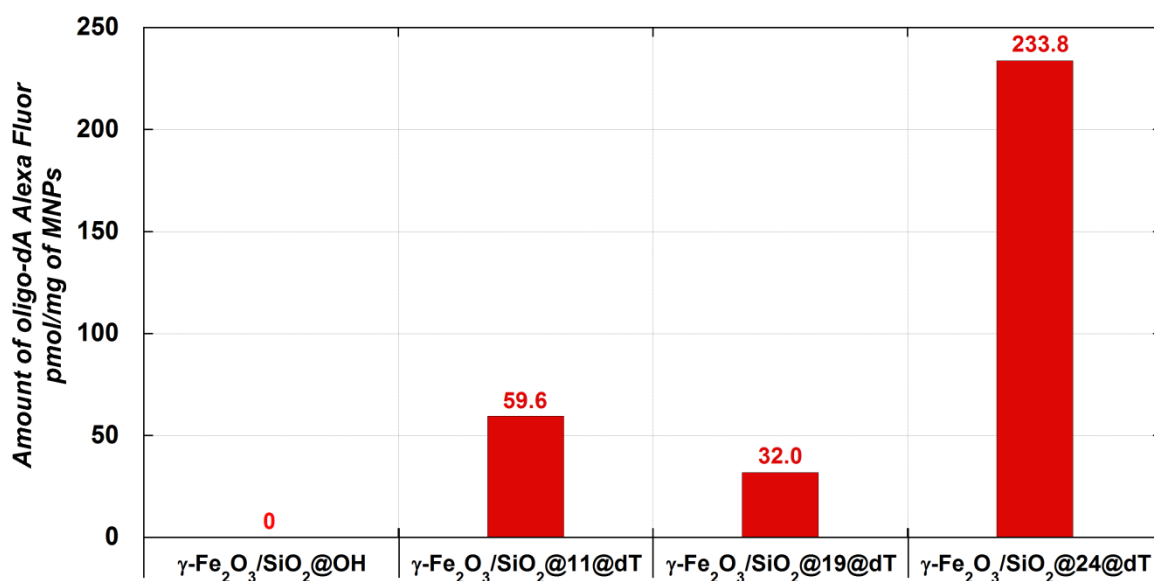


Figure IV-17. Results of the fluorescent quantification of the oligo-dA Alexa Fluor eluted after the dehybridization.

These results showed that maleimide functionalized  $\gamma\text{-Fe}_2\text{O}_3/\text{SiO}_2$  MNPs have an excellent capacity to immobilize HS-dT oligonucleotide. According to calculations,  $\gamma\text{-Fe}_2\text{O}_3/\text{SiO}_2\text{@11-Mal}$  immobilized 59.6 pmol/mg of HS-dT oligonucleotide;  $\gamma\text{-Fe}_2\text{O}_3/\text{SiO}_2\text{@19-Mal}$  – 32.0 pmol/mg of HS-dT oligonucleotide and  $\gamma\text{-Fe}_2\text{O}_3/\text{SiO}_2\text{@24-Mal}$  – 233.8 pmol/mg of HS-dT oligonucleotide, while native  $\gamma\text{-Fe}_2\text{O}_3/\text{SiO}_2\text{-OH}$  do not immobilize any HS-dT oligonucleotide (0 pmol/mg).

Even though, the performances in immobilization of HS-dT oligonucleotide of the sample  $\gamma\text{-Fe}_2\text{O}_3/\text{SiO}_2\text{@19-Mal}$  ( $\gamma\text{-Fe}_2\text{O}_3/\text{SiO}_2$  MNPs functionalized with two branched dendritic coupling agent) and  $\gamma\text{-Fe}_2\text{O}_3/\text{SiO}_2\text{@11-Mal}$  (functionalized with linear coupling agent) are comparable, these results prove the positive dendritic effect on the example of  $\gamma\text{-Fe}_2\text{O}_3/\text{SiO}_2\text{@24-Mal}$  (functionalized with four branched dendritic coupling agent). Moreover, these results showed that maleimide functionalized  $\gamma\text{-Fe}_2\text{O}_3/\text{SiO}_2$  MNPs are much more reactive in this HS-dT oligonucleotide immobilization ( $\gamma\text{-Fe}_2\text{O}_3/\text{SiO}_2\text{@24-Mal}$  immobilize 233.8 pmol/mg) comparing to their maleimide functionalized  $\gamma\text{-Fe}_2\text{O}_3/\text{Polymer}$  MNPs analogues ( $\gamma\text{-Fe}_2\text{O}_3/\text{SiO}_2\text{@23-Mal}$  immobilize 4.5 pmol/mg,

see Chapter III, section III.3.3.5.). These differences in the term of immobilization efficiency may be explained by several parameters, such as the nature of the shell (polymer versus silica), the quality of the MNPs' colloidal dispersion as well as the changes at the MNPs' surface.

## IV.5. Conclusion

In this chapter maleimide functionalization of core-shell  $\gamma\text{-Fe}_2\text{O}_3/\text{SiO}_2$  MNPs was investigated. The chemical modification of core-shell  $\gamma\text{-Fe}_2\text{O}_3/\text{SiO}_2$  MNPs was achieved via covalent attachment of previously synthesised silylated coupling agents (see Chapter II): linear coupling agent **11** (containing one functional group); two-branched coupling agent **19** (containing two functional groups) and four-branched dendritic coupling agent **24** (containing four functional groups).

The surface modification chemistry was mainly monitored by IR spectroscopy. The IR study proved the successful grafting of silylated coupling agents and showed that the amount of functional groups present on the functionalized  $\gamma\text{-Fe}_2\text{O}_3/\text{SiO}_2$  MNPs surface increases with the dendron's generation. However, it was not directly proportional to the number of functional groups present in the coupling agents' structure, as it was found in the case of  $\gamma\text{-Fe}_2\text{O}_3/\text{Polymer}$  MNPs functionalization (see Chapter III). In the case of  $\gamma\text{-Fe}_2\text{O}_3/\text{SiO}_2$  MNPs functionalization, the surface modification efficiency was probably influenced by both: the coupling agent's dendron generation and its chemical nature. Thus, according to IR spectroscopy study, the grafting reaction is strongly dependent on the chemical nature of the coupling agents, being completely different in the case of the four-branched silylated coupling agent **24** that ensures the highest amount of functional groups on MNPs' surface. TGA coupled with MS analyses gave an additional (to IR technique) confirmation of the successfully grafting, as well as the proof of the performed deprotection step (on the example of silylated linear coupling agent **11**). Another confirmation of the successful maleimide functionalization was obtained by performing zeta potential measurements.

The integrity of the maleimide functionalized  $\gamma\text{-Fe}_2\text{O}_3/\text{SiO}_2$  MNPs (in its protected and free form) has been monitored by TEM, according to which all the functionalized  $\gamma\text{-Fe}_2\text{O}_3/\text{SiO}_2$  MNPs preserved their morphology and integrity. At the same time, a slight increase in shell thickness was observed pointing out on the formation of a thin homogeneous layer of coupling agents on the  $\gamma\text{-Fe}_2\text{O}_3/\text{SiO}_2$  MNPs' surface.

The performances of maleimide functionalized  $\gamma\text{-Fe}_2\text{O}_3/\text{SiO}_2$  MNPs to immobilize biomolecules or a model of biomolecules were investigated by performing two immobilization tests. The first test

included the covalent immobilization of a thiol modified biotin (HS-PEG-Biot) on maleimide functionalized MNPs, and the efficiency of the immobilization was controlled via Biotin-SA affinity recognition. TEM revealed a homogeneous, compact covering with SA-Au NPs of all the biotin functionalized  $\gamma$ -Fe<sub>2</sub>O<sub>3</sub>/SiO<sub>2</sub> MNPs independent on the dendron generation. However, the UV-Vis study showed that the amount of the immobilized SA-Au NPs increases with the increase of the dendron generation.

In the second test, 3' thiol modified oligonucleotide poly T (HS-dT oligonucleotide) was immobilized on the maleimide functionalized  $\gamma$ -Fe<sub>2</sub>O<sub>3</sub>/SiO<sub>2</sub> MNPs. These results showed that maleimide functionalized  $\gamma$ -Fe<sub>2</sub>O<sub>3</sub>/SiO<sub>2</sub> MNPs have an excellent capacity to immobilize HS-dT oligonucleotide. The best results in immobilization of HS-dT oligonucleotide were observed for the  $\gamma$ -Fe<sub>2</sub>O<sub>3</sub>/SiO<sub>2</sub> MNPs modified with dendron **24** (233.8 pmol/mg), highlighting the efficiency of dendritic functionalization. Moreover, all the maleimide functionalized  $\gamma$ -Fe<sub>2</sub>O<sub>3</sub>/SiO<sub>2</sub> MNPs showed a higher capacity to immobilize a thiol modified oligonucleotide comparing to the maleimide functionalized  $\gamma$ -Fe<sub>2</sub>O<sub>3</sub>/Polymer MNPs (*Chapter III, section III.3.3.5.*).

## References:

- <sup>1</sup> <http://www.ademtech.com>
- <sup>2</sup> P. M. Price, J. H. Clark and D. J. Macquarrie, *J. Chem. Soc., Dalton Trans.* **2000**, 101–110
- <sup>3</sup> (a) D. Brunel, A. Cauvel, F. Di Renzo, F. Fajula, B. Fubini, B. Onida, and E. Garrone, *New J. Chem.* **2000**, 24, 807–813; (b) P. Sutra, F. Fajula, D. Brunel, P. Lentz, G. Daelen and J. B. Nagy, *Colloids Surf. A* **1999**, 158, 21–27.
- <sup>4</sup> (a) S. Cousinié, M. Gressier, P. Alphons and M.-J. Menu, *Chem. Mater.* **2007**, 19, 6492–6503; (b) C. P. Tripp and M. L. Hair, *Langmuir* **1992**, 8, 1961–1967; (c) P. Silberzan, J. L. Leger, D. Ausserre and J. J. Benattar, *Langmuir* **1991**, 7, 1647–1651; (d) K. Cheng and C. C. Landry, *J. Am. Chem. Soc.* **2007**, 129, 9674–9685.
- <sup>5</sup> (a) J. Zou, R. K. Baldwin, K. A. Pettigrew and S. M. Kauzlarich, *Nano Letters* **2004**, 4, 1181–1186; (b) F. Xu, J. H. Geiger, G. L. Baker and M. L. Bruening, *Langmuir*, **2011**, 27, 3106–3112; (c) X. Liu, Z. Ma, J. Xing and H. Liu, *J. Magn. Magn. Mater.* **2004**, 270, 1–6; (d) C. Pereira, A. M. Pereira, P. Quaresma, P. B. Tavares, E. Pereira, J. P. Araujo and C. Freire, *Dalton Trans.* **2010**, 39, 2842–2854; (e) J. W. Park, Y. J. Park and C.-H. Jun, *Chem. Commun.* **2011**, 47, 4860–4871; (f) R. A. Bini, R. F. C. Marques, F. J. Santos, J. A. Chaker, M. Jafelicci Jr, *J. Magn. Magn. Mater.* **2012**, 324, 534–539; (g) V. Maurice, T. Georgelin, J.-M. Siaugue, V. Cabuil, *J. Magn. Magn. Mater.* **2009**, 321, 1408–1413; (h) K. Yamaguchi, T. Kitabatake, M. Izawa, T. Fujiwara, H. Nishimura and T. Futami, *Chem. Lett.* **2000**, 3, 228–229; (i) C. Pathmamanoharan, P. Wijkens, D. M. Grove, and A. P. Philipse, *Langmuir* **1996**, 12, 4372–4377; (j) Z.-X. Guo and J. Yu, *J. Mater. Chem.* **2002**, 12, 468–472; (k) R. Wang, W. Jiao and B. Gao, *Appl. Surf. Sci.* **2010**, 256, 6029–6034; (l) Y. Ana, M. Chena, Q. Xue, W. Li, *J. Colloid Interface Sci.* **2007**, 311, 507–513; (m) E. Woo, K. M. Ponvel, I.-S. Ahn and C.-H. Le, *J. Mater. Chem.* **2010**, 20, 1511–1515; (n) Z. Ma, Y. Guan and H. Liu, *J. Magn. Magn. Mater.* **2006**, 301, 469–477; (o) N. T. K. Thanh and L. A. W. Green, *Nano Today* **2010**, 5, 213–230.
- <sup>6</sup> G. T. Hermanson, *Bioconjugate Techniques* – 2<sup>nd</sup> edition, Academic Press, San Diego, **2008**.
- <sup>7</sup> W. Stöber and A. Fink, *J. Coll. Interf. Sci.* **1968**, 26, 62–69.
- <sup>8</sup> N. Chekina, D. Horak, P. Jendelova, M. Trchova, M. J. Benes, M. Hruby, V. Herynek, K. Turnovcova and E. Sykova, *J. Mater. Chem.* **2011**, 21, 7630–7639.
- <sup>9</sup> I. J. Bruce and T. Sen, *Langmuir* **2005**, 21, 7029–7035.

- <sup>10</sup> M. W. Daniels, J. Sefcik, L. F. Francis and A. V. McCormick, *J. Colloid Interface Sci.* **1999**, 219, 351–356.
- <sup>11</sup> (a) J. Sagiv, *J. Am. Chem. Soc.* **1980**, 102, 92–98; (b) M. Ramin, *PhD Thesis*, Bordeaux 1 University **2010**; (c) A. del Campo, T. Sena, J.-P. Lellouchec and I. J. Bruce, *J. Magn. Magn. Mater.* **2005**, 293, 33–40; (d) A. C. Zettlemoyer and H. H. Hsing, *J. Colloid Interface Sci.* **1977**, 58, 263–274.
- <sup>12</sup> F. Luderer and U. Walschus, *Top. Curr. Chem.* **2005**, 260, 37–56.
- <sup>13</sup> M. P. J. Peeters, *J. Sol-Gel Sci. Technol.* **2000**, 19, 131–135.
- <sup>14</sup> R. Denoyel, J. C. Glez and P. Trens, *Colloids Surf., A* **2002**, 197, 213–223
- <sup>15</sup> F. D. Osterholtza and E. R. Pohl, *J. Adhes. Sci. Technol.* **1992**, 6, 127–149
- <sup>16</sup> (a) J. P. Blitz, R. S. Shreedhara Murthy, and D. E. Leyden, *J. Colloid Interface Sci.* **1988**, 126, 387–392; (b) J. P. Blitz, R. S. Shreedhara Murthy and D. E. Leyden, *J. Am. Chem. Soc.* **1987**, 109, 7141–7145.
- <sup>17</sup> (a) S. de Monredon, *PhD Thesis*, University of Paris VI, **2004**; (b) H. Rahma, *PhD Thesis*, University of Bordeaux 1, **2012**.
- <sup>18</sup> T. Woldbæk, P. Klaboe and C. J. Nielsen, *J. Mol. Struct.* **1975**, 27, 283–301.
- <sup>19</sup> T. Engel and G. Kickelbick, *Chem. Mater.* **2013**, 25, 149–157.
- <sup>20</sup> (a) R. Wagner, S. Benz, O. Moihler, H. Saathoff, M. Schnaiter, and U. Schurath, *J. Phys. Chem. A* **2005**, 109, 7099–7112; (b) E. Mendelovici, R. Villalba, A. Sagarzazu and O. Carias, *Clay Minerals*, **1995**, 30, 307–313.
- <sup>21</sup> R. P. W. Scott and S. Traiman, *Journal of Chromatography*, **1980**, 196, 193–205.
- <sup>22</sup> (a) T. Dispinar, R. Sanyal and A. Sanyal, *J. Polym. Sci., A: Polym. Chem.* **2007**, 45, 4545–4551; (b) L. Billiet, O. Gok, A. P. Dove, A. Sanyal, L.-T. T. Nguyen and F. E. D. Prez, *Macromolecules* **2011**, 44, 7874–7878; (c) T. Engel and G. Kickelbick, *Chem. Mater.* **2013**, 25, 149–157.

# **General conclusion**





In the field of biotechnology (such as proteomics, bio-catalysis and biomaterials), magnetic separation exploiting MNPs represents an attractive method for reliable capture, isolation, purification and controlled manipulation of biomolecules (proteins, enzymes, antibodies, peptides, lipids, nucleic acids, etc.), since it is a simple, fast and cheap method. With this goal in mind, the purpose of this work was to design stable, water-dispersible, functionalized MNPs that would ensure selective covalent immobilization of biomolecules. An indispensable step in elaboration of such MNPs is the surface modification. Moreover, a precise control over the surface functionalization of MNPs is crucial, because it governs their physicochemical properties, their colloidal stability, and their biological behaviour. In this work a comparative study regarding the dendritic effect on the functionalization of core-shell MNPs (with polymer or silica shell) was investigated.

The first part of the work was dedicated to the design and synthesis of linear and dendritic coupling agents. Since the surface modification chemistry was investigated on two types of core-shell MNPs (with polymer or silica), two “*families*” of coupling agents were synthesized. Each “*family*” of coupling agents possessed an *anchoring site* (amino or silane), capable to form covalent bonding with the available on MNPs’ surface groups (carboxyl or silanol) and a *functional group* (maleimide). In order to investigate the “*dendritic effect*” on the surface functionalization, three types of coupling agents were designed: linear coupling agents (containing one functional group: compounds **10** and **11**); two-branched coupling agents (containing two functional groups: compounds **18** and **19**) and four-branched dendritic coupling agents (containing four functional groups: compounds **23** and **24**). Since the majority of the tests in biotechnology are performed in aqueous medium it was indispensable to design hydrophilic coupling agents, therefore PEG chains or/and PAMAM chains were introduced in the coupling agents’ backbones. In addition, the PEG chain is considered to be one of the most inert chemical groups towards non-specific protein adsorption. Both “*families*” of coupling agents (amino and silane-based coupling agents) were successfully synthesized and characterized.

The second part of the work was dedicated to the grafting of maleimide functionalized coupling agents onto the core-shell  $\gamma$ -Fe<sub>2</sub>O<sub>3</sub>/Polymer MNPs and their characterization. The surface functionalization of MNPs with polymer shell was achieved by the grafting of amine containing coupling agents (linear coupling agent **10**, two-branched coupling agent **18** and four-branched dendritic coupling agent **23**) on carboxylic acid functionalized surface of MNPs (via EDC/NHS chemistry). This step has been controlled via FT-IR spectroscopy, which showed that the grafting efficiency strongly depends on the quantity of coupling agents employed into the grafting process. Thus, the maximum of surface functionalization with linear coupling agent **10** was achieved by adding *100 equivalents* of compound; with two-branched coupling agent **18** (dendron G1) *50 equivalents* of compound were necessary; while four-branched coupling agent **23** (dendron G2) allowed achieving the

maximum of surface functionalization by adding only 10 equivalents of compound. Moreover, the amount of functional groups on MNPs' surface increases with the growth of dendron's generation and was directly proportional to the number of functional groups present in the structure of the coupling agent, thus highlighting the positive "dendritic effect" on the surface functionalization. The surface functionalization was also confirmed by TGA coupled with MS analyses and zeta potential measurements. The maleimide modified  $\gamma$ -Fe<sub>2</sub>O<sub>3</sub>/Polymer MNPs preserved their integrity as well as their colloidal stability, since a good dispersion in aqueous solutions and polar solvents was maintained. The capacity of maleimide functionalized  $\gamma$ -Fe<sub>2</sub>O<sub>3</sub>/Polymer MNPs to immobilize biomolecules or models of biomolecules was investigated via a series of immobilization tests. All of them proved the efficiency of maleimide functionalization of  $\gamma$ -Fe<sub>2</sub>O<sub>3</sub>/Polymer MNPs to immobilize thiol containing biomolecules as well as the positive "dendritic effect" on the surface functionalization. Moreover, the reactivity of maleimide functionalized  $\gamma$ -Fe<sub>2</sub>O<sub>3</sub>/Polymer MNPs towards amino group, in the typical reaction conditions used for immobilization of thiols (pH in the range of 6.5-7.5), was explored. It was confirmed that the quantities of amine containing biomolecules that can be immobilized on maleimide functionalized  $\gamma$ -Fe<sub>2</sub>O<sub>3</sub>/Polymer MNPs remain negligible comparing to the quantities of thiol containing biomolecules.

The third part of the work was dedicated to the maleimide functionalization and characterization of the core-shell  $\gamma$ -Fe<sub>2</sub>O<sub>3</sub>/SiO<sub>2</sub> MNPs. The chemical modification of core-shell  $\gamma$ -Fe<sub>2</sub>O<sub>3</sub>/SiO<sub>2</sub> MNPs was achieved via hydrolysis-condensation reaction of silanol groups of silica shell with the silane groups of the coupling agents (linear coupling agent **11**, two-branched coupling agent **19** and four-branched dendritic coupling agent **24**). The surface modification chemistry of  $\gamma$ -Fe<sub>2</sub>O<sub>3</sub>/SiO<sub>2</sub> MNPs was monitored by IR spectroscopy. This study proved the successful grafting of silylated coupling agents (**11**, **19** and **24**) and showed that the amount of functional groups present on the surface of modified  $\gamma$ -Fe<sub>2</sub>O<sub>3</sub>/SiO<sub>2</sub> MNPs increases with the dendron's generation. The highest amount of functional groups on MNPs' surface was achieved by the grafting of four-branched dendritic coupling agent **24**, highlighting the efficiency of dendritic structures for the surface modification and proves once again the positive "dendritic effect" on the surface functionalization. The surface functionalization was also confirmed by TGA coupled with MS analyses and zeta potential measurements. TEM showed that maleimide functionalized  $\gamma$ -Fe<sub>2</sub>O<sub>3</sub>/SiO<sub>2</sub> MNPs preserved their morphology and integrity, while a slight increase of the shell thickness suggests the formation of a thin homogeneous layer of coupling agents on the  $\gamma$ -Fe<sub>2</sub>O<sub>3</sub>/SiO<sub>2</sub> MNPs' surface. Also, all the maleimide functionalized  $\gamma$ -Fe<sub>2</sub>O<sub>3</sub>/SiO<sub>2</sub> MNPs preserved a good colloidal stability in aqueous media. Finally, the capacity of maleimide functionalized  $\gamma$ -Fe<sub>2</sub>O<sub>3</sub>/SiO<sub>2</sub> MNPs to immobilize biomolecules was investigated by performing two immobilization tests: immobilization of thiol modified biotin and thiol modified oligonucleotide. Both tests proved the efficiency of the maleimide functionalized  $\gamma$ -Fe<sub>2</sub>O<sub>3</sub>/SiO<sub>2</sub> MNPs towards the

immobilization of thiol containing biomolecules. An excellent immobilization capacity of the maleimide functionalized  $\gamma$ -Fe<sub>2</sub>O<sub>3</sub>/SiO<sub>2</sub> MNPs for the thiol modified oligonucleotide was observed. The highest amount of immobilized HS-dT oligonucleotide (233.8 pmol/mg) was achieved in the case of  $\gamma$ -Fe<sub>2</sub>O<sub>3</sub>/SiO<sub>2</sub> MNPs modified with dendron **24**, highlighting again the efficiency of dendritic functionalization. Moreover, all the maleimide functionalized  $\gamma$ -Fe<sub>2</sub>O<sub>3</sub>/SiO<sub>2</sub> MNPs showed a higher capacity to immobilize a thiol modified oligonucleotide comparing to their analogues - maleimide functionalized  $\gamma$ -Fe<sub>2</sub>O<sub>3</sub>/Polymer MNPs. Also, it is noteworthy that the optimization of immobilization protocols can lead to even higher amount of immobilized HS-dT oligonucleotide. Therefore, it could be envisaged to perform a more detailed study regarding the specific immobilization of biomolecules in a complex medium.

As expected, this study proved the efficiency of the surface functionalization with dendritic structures. Moreover, it was determined that a variety of parameters strongly influences the efficiency of the MNPs' functionalization, among these the four most important factors are: (I) *the nature of the surface* (polymer or silica); (II) *the size of the particles*; (III) *the nature of the coupling agents*, (linear or dendritic structure, as well as the dendron's generation); and (IV) *the loading of the coupling agents* in the grafting reaction. Dendritic surface modification strategy can be extended to other surfaces as well (i.e. functionalization of other types of NPs). Moreover, it allows introducing on the surface a wide range of accessible functional groups.



# **Experimental part**



## 1. Solvents and reagents

Solvents and starting materials were purchased from Acros, Alfa Aesar or Aldrich. All reagents used as starting materials in this work were reagent-grade. All the solvents used for the synthesis were anhydrous, some of them were purchased: DMF, DMSO, Dioxane, THF,  $\text{CHCl}_3$ , EtOAc, AcOH, others were dried over dehydrating agents and distilled under an inert atmosphere:

- $\text{CH}_2\text{Cl}_2$ :  $\text{CaH}_2$ ;
- MeOH:  $\text{CaH}_2$ ;
- Toluene: Na/benzophenone.

Core-shell superparamagnetic nanoparticles [Silica-Adembeads ( $\gamma\text{-Fe}_2\text{O}_3/\text{SiO}_2\text{-OH}$ ) and Carboxyl-Adembeads ( $\gamma\text{-Fe}_2\text{O}_3/\text{Pol-COOH}$ )] were purchased from Ademtech SA; 15 nm Conjugate-Streptavidin Gold Nanoparticles, EM.STP15 (SA-Au NPs) from BBI Solutions; 20 nm Amino PEGylated Gold Nanoparticles, 24877 ( $\text{H}_2\text{N-Au}$  NPs) from Polysciences Inc; Biotin-PEG-Thiol, 41156-1095 (HS-PEG-Biot), from Polypure; and 3' thiol modified oligonucleotide poly T: TTT-TTT-TTT-TTT-TTT or Oligonucleotide-Thiol, (HS-dT) from Eurogentec.

## 2. Equipment:

### Nuclear Magnetic Resonance (NMR)

NMR spectra were performed at Institut des Sciences Moléculaires (ISM), CNRS-University of Bordeaux (Centre Nationale de la Recherche Scientifique), on the following spectrometers:

- Bruker DPX 200 FT NMR spectrometer ( $^1\text{H}$ : 200,  $^{13}\text{C}$ : 50 MHz);
- Bruker Avance 300 FT NMR spectrometer ( $^1\text{H}$ : 300,  $^{13}\text{C}$ : 75MHz);
- Bruker DPX 400 FT NMR spectrometer ( $^1\text{H}$ : 400,  $^{13}\text{C}$ : 101 MHz).
- Bruker DPX 600 FT NMR spectrometer ( $^1\text{H}$ : 600,  $^{13}\text{C}$ : 151 MHz).

Chemical shifts of  $^1\text{H}$  NMR signals were calibrated according to the signals of deuterated solvents quoted to internal standard TMS ( $\delta = 0.00$ ) and expressed as chemical shifts in parts per million (ppm,  $\delta$ ), multiplicity, coupling constant (Hz), and relative intensity.

### Mass Spectrometry (MS)

Mass spectra were performed by the Centre d'Etude Structurale et d'Analyse des Molécules Organiques (CESAMO), ISM, CNRS-University of Bordeaux, on a QStar Elite Mass Spectrometer equipped with an electrospray ionization (ESI) source (operated in a positive or negative ion mode).



### **Thermogravimetric (TG) measurements coupled with Mass spectrometry**

TG coupled with MS analyses was performed at ISM (C<sub>2</sub>M group), on Pyrolyzor coupled to a Balzers Instruments Thermostar quadrupolar mass spectrometer Type: Netzsch STA 409. The mass loss of the dried samples (10–20 mg) was monitored under argon at temperatures from 30°C to 1000°C with a heating rate of 5 K/min.

### **Elemental Analysis (EA)**

Chemical formula of compounds was achieved by elemental analysis, carried out by Service Centrale d'Analyse, CNRS at Lyon-Vernaison.

### **Fourier Transform Infrared (FT-IR) Analysis**

FT-IR spectra were recorded at ISM (Molecular Spectroscopy Group (GSM)) on the following spectrometers:

- FT-IR Spectrometer Perkin-Elmer 100
- FT-IR Spectrometer Nicolet iS50

The middle infrared region (approximately 4000–400 cm<sup>-1</sup>) was used to study the fundamental vibrations.

### **UV-Vis Analysis**

UV-Vis spectra were recorded between 200 and 800 nm using a PerkinElmer UV/Vis spectrophotometer Lambda 650 at ISM (GSM).

### **Transmitted Electron Microscopy (TEM)**

TEM images were obtained on Electronic Microscope HITACHI H7650, (120 Kv, high resolution, equipped with a GATAN 11MPx camera) at Bordeaux Imaging Centre (BIC). The samples were prepared by deposition of MNPs dispersed in ethanol or water (5-10µL, 0.25-0.5 mg/mL) on carbon coated copper grids and dried in the air.

### **Transmitted Light Microscopy**

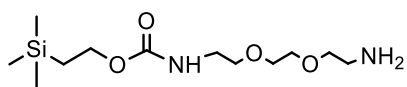
The colloidal state of the final maleimide functionalized MNPs dispersed in water was observed under Transmitted Light Microscope equipped with an AxioCam digital camera.

### **Zeta Potential**

Zeta Potential measurements were carried out on Horiba Scientific nanoparticle analyzer SZ-100 at ISM (PHotonics and Omics ENabled by Innovations in Chemical Synthesis (Phoenics) group). The measurements were performed at 25°C for diluted aqueous suspension of functionalized MNPs at pH varying from 3.5 to 9.0.

### 3. Synthesis of precursors and dendritic structures

#### Compound 1

Chemical Formula: C<sub>12</sub>H<sub>28</sub>N<sub>2</sub>O<sub>4</sub>Si

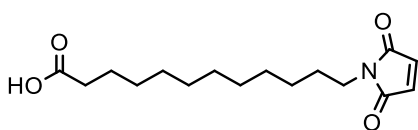
Molecular Weight: 292,45 g/mol

To a solution of 2,2-(ethylenedioxy)bis(ethylamine) (6.2 mL, 42.34 mmol, 6 eq. in 40 mL of dioxane), 2.0 mL of TEA (14.20 mmol; 2 eq.) were added. Then, a solution of TEOC-ONp (2.00 g, 7.06 mmol in 40 mL of dioxane) was added dropwise during 2.5 h. The reaction mixture was stirred overnight at room temperature. Afterwards, the solvent was evaporated and the residue was solubilized in 40 mL of H<sub>2</sub>O, next compound **1** was extracted with CH<sub>2</sub>Cl<sub>2</sub> (5×20 mL). The organic phase was washed with brine (5×50 mL), dried over magnesium sulphate (MgSO<sub>4</sub>), filtrated and evaporated to dryness to yield compound **1** (83 %) as a pale yellow oil.

<sup>1</sup>H NMR (300 MHz, CDCl<sub>3</sub>) δ 5.37 (s, 1H, -NH-), 4.21 – 4.03 (m, 2H, -CH<sub>2</sub>-OCO), 3.59 (s, 4H, -O-CH<sub>2</sub>-CH<sub>2</sub>-O-), 3.52 (d, *J* = 5.2 Hz, 4H, -CH<sub>2</sub>-O-), 3.34 (d, *J* = 5.0 Hz, 2H, -CH<sub>2</sub>-NH-), 2.87 (t, *J* = 5.2 Hz, 2H, -CH<sub>2</sub>-NH<sub>2</sub>), 2.23 (s, 2H, -NH<sub>2</sub>), 1.01 – 0.88 (m, 2H, -CH<sub>2</sub>-Si), 0.00 (s, 9H, -Si-CH<sub>3</sub>).

<sup>13</sup>C NMR (75 MHz, CDCl<sub>3</sub>) δ 156.91 (s, 1C, -O(C=O)NH-), 73.27 (s, 2C, -O-CH<sub>2</sub>-), 70.20 (s, 2C, -O-CH<sub>2</sub>-CH<sub>2</sub>-O-), 62.90 (s, 1C, -CH<sub>2</sub>-OCO), 41.60 (s, 1C, -CH<sub>2</sub>-NH<sub>2</sub>), 40.74 (s, 1C, -CH<sub>2</sub>-NH-), 17.80 (s, 1C, -CH<sub>2</sub>-Si), -1.47 (s, 3C, -Si-CH<sub>3</sub>).

#### Compound 4

Chemical Formula: C<sub>16</sub>H<sub>25</sub>NO<sub>4</sub>

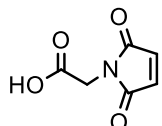
Molecular Weight: 295.37 g/mol

To a solution of maleic anhydride (0.23 g, 2.30 mmol, 1 eq. in 5 mL of glacial AcOH) a solution of 12-aminolauric acid (0.50 g, 2.30 mmol in 5 mL of glacial AcOH) was added. The obtained slurry was stirred for 8 h under argon, at room temperature. The resulting white precipitate (intermediate maleamic acid) was filtrated and washed with H<sub>2</sub>O (3×30 mL), then re-dispersed in 50 mL of H<sub>2</sub>O and refluxed for 2 h. Afterwards, the H<sub>2</sub>O was removed under vacuum to yield N-maleimidolauric acid (72 %) as a white powder.

<sup>1</sup>H NMR (300 MHz, DMSO) δ 7.68 (s, 1H, OH), 6.04 (s, 2H, CH=CH<sub>maleimide</sub>), 2.77 (s, 2H, -CH<sub>2</sub>-N), 2.18 (s, 2H, -CH<sub>2</sub>-COOH), 1.49 (s, 4H, -CH<sub>2</sub>-CH<sub>2</sub>-COOH, -CH<sub>2</sub>-CH<sub>2</sub>-N), 1.24 (s, 14H, -CH<sub>2</sub>-).

$^{13}\text{C}$  NMR (75 MHz, DMSO)  $\delta$  174.91 (s, 1C, C=O<sub>acid</sub>), 167.76 (s, 2C, -N(C=O)-), 136.53 (s, 2C, CH=CH<sub>maleimide</sub>), 39.33 (s, 1C, -CH<sub>2</sub>-N), 34.14 (s, 1C, -CH<sub>2</sub>-COOH), 29.30 (s, 4C, -CH<sub>2</sub>-), 29.00 (s, 2C, -CH<sub>2</sub>-), 27.43 (s, 1C, -CH<sub>2</sub>-), 26.20 (s, 1C, -CH<sub>2</sub>-), 24.96 (s, 1C, -CH<sub>2</sub>-).

### Compound 5



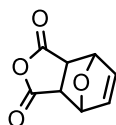
Chemical Formula: C<sub>6</sub>H<sub>5</sub>NO<sub>4</sub>  
Molecular Weight: 155.11 g/mol

To a solution of maleic anhydride (9.80 g, 0.10 mol, 1 eq. in 100 mL of glacial AcOH) 7.50 g of glycine (0.10 mol) were added. The resulting slurry was stirred for 8 h under argon at room temperature. The white precipitate (intermediate compound) was collected by filtration and washed with cold H<sub>2</sub>O (2×20 mL), then re-dispersed in 200 mL of H<sub>2</sub>O and refluxed for 30 min. Afterwards, the mixture was concentrated and the resulting white precipitate was collected by filtration, washed with cold H<sub>2</sub>O (20 mL), and dried under high vacuum to yield 2-maleimidoacetic acid (55 %) as a white powder.

$^1\text{H}$  NMR (300 MHz, DMSO)  $\delta$  6.06 (s, 2H, CH=CH<sub>maleimide</sub>), 3.65 (s, 2H, -CH<sub>2</sub>-).

$^{13}\text{C}$  NMR (75 MHz, DMSO)  $\delta$  169.09 (s, 1C, C=O<sub>acid</sub>), 167.32 (s, 2C, -N(C=O)-), 134.75 (s, 2C, CH=CH<sub>maleimide</sub>), 39.91 (s, 1C, -CH<sub>2</sub>-).

### Compound 8



Chemical Formula: C<sub>8</sub>H<sub>6</sub>O<sub>4</sub>  
Molecular Weight: 166,13 g/mol

#### Method A:

To a dried 500 mL round-bottom flask with a magnetic stirring bar, 40.0 g of maleic anhydride (0.41 mol, 1 eq.), 200 mL of benzene and 30 mL of furan (0.41 mol, 1 eq.) were added. The reaction mixture was stirred at room temperature for 24 h under argon atmosphere. The precipitated out product was collected via vacuum filtration, washed with diethyl ether and dried under vacuum to yield compound **8** (58 %) as small white needles, which were used without further purification.

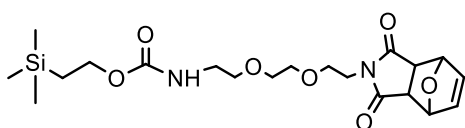
Method B:

Maleic anhydride (30.0 g, 0.31 mol) was suspended in 150 mL of toluene, the suspension was warmed up to 80°C and 33 mL of furan (0.46 mol, 1.3 eq.) were added. The turbid solution was stirred for 6 h and then cooled to room temperature without stirring. White crystals, which precipitated out of solution after 1 h, were collected by vacuum filtration, washed with petroleum ether (2×30 mL) and dried under vacuum to yield compound **8** (58 %) as small white needles.

<sup>1</sup>H NMR (400 MHz, DMSO) δ 6.58 (s, 2H, CH=CH), 5.35 (s, 2H, CHO), 3.31 (s, 2H, CH).

<sup>13</sup>C NMR (101 MHz, DMSO) δ 171.53 (s, 2C, C=O), 136.85 (s, 2C, CH=CH), 81.64 (s, 2C, CHO), 49.08 (s, 2C, CH).

FT IR (cm<sup>-1</sup>) = 1858, 1780 (ν<sub>C=O</sub> five membered ring anhydrides); 921, 878, 849, 822, 813, 691 (maleic anhydride ring deformation).

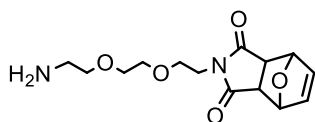
Compound 9

Chemical Formula: C<sub>20</sub>H<sub>32</sub>N<sub>2</sub>O<sub>7</sub>Si  
Molecular Weight: 440.56 g/mol

A solution of compound **8** (0.84 g, 5.03 mmol, 1.5 eq. in 20 mL of anhydrous MeOH) was added dropwise to a solution of compound **1** (0.98 g, 3.35 mmol, 1 eq. in 10 mL of anhydrous MeOH) at room temperature and then refluxed for 4 h. Afterwards, the solvent was removed under vacuum and the residue was solubilized in 20 mL of CH<sub>2</sub>Cl<sub>2</sub>, washed first with H<sub>2</sub>O (2×10 mL) and then with brine (2×10 mL) (in order to remove the excess of compound **8**). The organic layer was dried over MgSO<sub>4</sub>, filtrated and concentrated under vacuum. The residue was purified by silica gel chromatography (AcOEt) to yield compound **9** (10 %) as a pale yellow oil.

<sup>1</sup>H NMR (200 MHz, CDCl<sub>3</sub>) δ 6.49 (s, 2H, CH=CH), 5.24 (s, 2H, CHO), 4.12 (s, 2H, CH<sub>2</sub>), 3.80 – 3.41 (m, 10H, -CH<sub>2</sub>-O-CH<sub>2</sub>-CH<sub>2</sub>-O-CH<sub>2</sub>-CH<sub>2</sub>-), 3.33 (s, 2H, CH<sub>2</sub>-NH), 2.84 (s, 2H, CH), 0.96 (t, 2H, CH<sub>2</sub>-Si), 0.01 (s, 9H, CH<sub>3</sub>).

<sup>13</sup>C NMR (75 MHz, CDCl<sub>3</sub>) δ 176.26 (s, 2C, C=O), 156.98 (s, 1C, (C=O)NH), 136.65 (s, 2C, CH=CH), 81.01 (s, 2C, CH), 72.33 (s, 1C, OCH<sub>2</sub>), 70.69 – 69.95 (d, 2C, OCH<sub>2</sub>), 67.30 (s, 1C, OCH<sub>2</sub>), 63.01 (s, 1C, CH<sub>2</sub>OCO), 47.58 (s, 2C, CH), 40.90 (s, 1C, CH<sub>2</sub>-NH), 38.29 (s, 1C, CH<sub>2</sub>-N), 17.93 (s, 1C, CH<sub>2</sub>-Si), -1.37 (s, 3C, CH<sub>3</sub>).

**Compound 10**

Chemical Formula: C<sub>14</sub>H<sub>20</sub>N<sub>2</sub>O<sub>5</sub>  
 Molecular Weight: 296,32 g/mol

**Method A:**

A solution of compound **8** (1.00 g, 6 mmol in 40 mL of anhydrous dioxane) was added dropwise to a solution of 2,2-(ethylenedioxy)bis(ethylamine) (7.50 g, 51 mmol, 8.5 eq. in 30 mL of anhydrous dioxane) at room temperature. The resulting mixture was then heated to 80°C and stirred overnight. At the end of reaction the solvent was evaporated and the obtained residue was solubilized in 200 mL of CH<sub>2</sub>Cl<sub>2</sub>, washed firstly with H<sub>2</sub>O (2×100 mL), then with brine (2×100 mL) (to remove the excess of 2,2-(ethylenedioxy)bis(ethylamine)) and dried over MgSO<sub>4</sub>. Afterwards, the solution was filtrated and concentrated under vacuum. The residue was purified by column chromatography on basic alumina (CH<sub>2</sub>Cl<sub>2</sub>/MeOH, v/v 98:2) to yield compound **10** (20 %) as a viscous pale yellow oil.

**Method B:**

Compound **8** (1.00 g, 6 mmol) and 2,2-(ethylenedioxy)bis(ethylamine) (7.50 g, 51 mmol, 8.5 eq.) were mixed at room temperature, and then the mixture was heated to 80°C upon which the solid anhydride gradually dissolved. The resulting mixture was then left under stirring (at 80°C) for 3 h. After cooling to room temperature, the mixture was solubilized in 200 mL of CH<sub>2</sub>Cl<sub>2</sub> and washed firstly with H<sub>2</sub>O (2×100 mL) and then with brine (2×100 mL) (to remove the excess of 2,2-(ethylenedioxy)bis(ethylamine)). The organic phase was dried over MgSO<sub>4</sub>, filtrated and concentrated in vacuum. The compound was purified by column chromatography on basic alumina, first with a mixture of CH<sub>2</sub>Cl<sub>2</sub>/MeOH (v/v 98:2) in order to remove the side product and then with a mixture of CH<sub>2</sub>Cl<sub>2</sub>/MeOH (v/v 5:1) to yield compound **10** (27 %) as viscous pale yellow oil.

**<sup>1</sup>H NMR** (200 MHz, CDCl<sub>3</sub>) δ 6.48 (s, 2H, CH=CH), 5.23 (s, 2H, CH), 3.64 (m, 4H, -CH<sub>2</sub>-O), 3.56 (m, 4H, -O-CH<sub>2</sub>-CH<sub>2</sub>-O-), 3.45 (t, 2H, -CH<sub>2</sub>-N), 2.81 (s, 2H, CH), 2.83 (t, 2H, -CH<sub>2</sub>-NH<sub>2</sub>), 1.41 (s, 2H, -NH<sub>2</sub>).

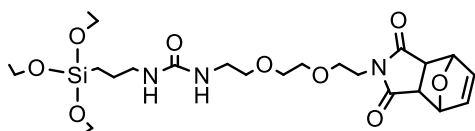
**<sup>13</sup>C NMR** (151 MHz, CDCl<sub>3</sub>) δ 176.12 (s, 2C, C=O), 136.51 (s, 2C, CH=CH), 80.86 (s, 2C, CHO), 72.97 (s, 1C, -CH<sub>2</sub>-O), 70.20 (d, *J* = 34.6 Hz, 2C, -O-CH<sub>2</sub>-CH<sub>2</sub>-O-), 67,11 (s, 1C, CH<sub>2</sub>-O), 47.43 (s, 1C, CH), 41.62 (s, 1C, -CH<sub>2</sub>-NH<sub>2</sub>), 38.13 (s, 1C, -CH<sub>2</sub>-N).

**MS (ESI, m/z)** [M+H]<sup>+</sup> calc. – 297.1398, found – 297.1411; [M+Na]<sup>+</sup> calc. – 319.1264, found – 319.1277

**EA** calc.: C, 56.75; H, 6.80; N, 9.45; O, 27.00; found: C, 56.49; H, 6.86; N, 9.20; O, 28.60

**FT IR (cm<sup>-1</sup>)** = 3373 ( $\nu_{\text{as}}$  NH<sub>2</sub>), 2918 ( $\nu_{\text{as}}$  CH<sub>2</sub>); 2865 ( $\nu_{\text{s}}$  CH<sub>2</sub>); 1772, 1693 ( $\nu_{\text{C=O}}$  cyclic imides in five membered ring); 915, 876, 852, 824, 813 (maleimide ring deformation).

### **Compound 11**



Chemical Formula: C<sub>24</sub>H<sub>41</sub>N<sub>3</sub>O<sub>9</sub>Si  
Molecular Weight: 543.68 g/mol

A solution of compound **10** (0.20 g, 6.75 mmol in 20 mL of freshly distilled CH<sub>2</sub>Cl<sub>2</sub>) was cooled to 0 °C and 0.17 mL of isocyanato propyl tri-(etoxy)silane (6.75 mmol, 1 eq.) were added dropwise. The mixture was stirred at room temperature overnight under argon atmosphere. Afterwards, the solvent was evaporated under vacuum to yield quantitatively compound **11** as pale yellow oil.

**<sup>1</sup>H NMR** (200 MHz, CDCl<sub>3</sub>)  $\delta$  6.51 (s, 2H, CH=CH), 5.25 (t+s, 3H, CH, NH), 5.05 (t,  $J$  = 5.2 Hz, 1H, NH), 3.79 (q,  $J$  = 7.0 Hz, 6H, -O-CH<sub>2</sub>-CH<sub>3</sub>), 3.66 (dd,  $J$  = 9.4, 4.2 Hz, 4H, -CH<sub>2</sub>-O), 3.55 – 3.45 (m, 6H, -O-CH<sub>2</sub>-CH<sub>2</sub>-O-, -CH<sub>2</sub>-N), 3.42 – 3.32 (m, 2H, -CH<sub>2</sub>-NH-), 3.18 (dd,  $J$  = 13.0, 7.0 Hz, 2H, -CH<sub>2</sub>-NH-), 2.86 (s, 2H, CH), 1.68 – 1.49 (m, 2H, -CH<sub>2</sub>-CH<sub>2</sub>-Si), 1.19 (t,  $J$  = 7.0 Hz, 9H, -CH<sub>3</sub>), 0.68 – 0.57 (m, 2H, -CH<sub>2</sub>-CH<sub>2</sub>-Si).

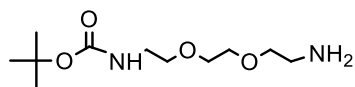
**<sup>13</sup>C NMR** (101 MHz, CDCl<sub>3</sub>)  $\delta$  176.82 (s, 2C, -(C=O)-N), 158.61 (s, 1C, NH-(C=O)-NH), 136.71 (s, 2C, CH=CH), 81.01 (s, 2C, CH), 70.59 (s, 1C, -O-CH<sub>2</sub>-), 70.18 (d,  $J$  = 26.9 Hz, 2C, -O-CH<sub>2</sub>-CH<sub>2</sub>-O-), 67.47 (s, 1C, -CH<sub>2</sub>-O-), 58.50 (s, 6C, -O-CH<sub>2</sub>-CH<sub>3</sub>), 47.64 (s, 2C, CH), 43.03 (s, 1C, -CH<sub>2</sub>-NH-), 39.95 (s, 1C, -CH<sub>2</sub>-NH-), 38.89 (s, 1C, -CH<sub>2</sub>-N), 23.97 (s, 1C, -CH<sub>2</sub>-CH<sub>2</sub>-Si), 18.42 (s, 3C, -CH<sub>3</sub>), 7.86 (s, 1C, -CH<sub>2</sub>-Si).

**MS (ESI, m/z)** [M+Na]<sup>+</sup> calc. – 566.2504, found – 566.2494

**EA calc.:** C, 53.02; H, 7.60; N, 7.73; Si, 5.17; found: C, 50.75; H, 7.00; N, 7.87; Si, 5.03

**FT IR (cm<sup>-1</sup>)** = 3362 ( $\nu_{\text{NH}}$  NH(C=O)NH); 2973 ( $\nu_{\text{as}}$  CH<sub>3</sub>); 2923 ( $\nu_{\text{as}}$  CH<sub>2</sub>); 2881 ( $\nu_{\text{s}}$  CH<sub>2</sub>); 1774, 1698 ( $\nu_{\text{C=O}}$  cyclic imides in five membered ring); 1637 ( $\nu_{\text{C=O}}$  urea) amide I; 1558 ( $\nu_{\text{CN}}$ ,  $\delta_{\text{NH}}$  C-N-H) amide II; 1099, 1072, 1021 ( $\nu_{\text{Si-O}}$  Si-OEt); 916, 877, 854, 824 (maleimide ring deformation).

### **Compound 12**



Chemical Formula: C<sub>11</sub>H<sub>24</sub>N<sub>2</sub>O<sub>4</sub>  
Molecular Weight: 248,32 g/mol

A solution of di-*tert*-butyl dicarbonate (11.25g, 0.05 mol, 1 eq. in 125 mL of anhydrous dioxane) was added dropwise to a solution of 2,2-(ethylenedioxy)bis(ethylamine) (44 mL, 45.75 g, 0.31 mol, 6 eq. in 125 mL of anhydrous dioxane). The mixture was stirred at room temperature overnight under

argon atmosphere. Afterwards, the solvent was evaporated, the residue was solubilized in 400 mL of  $\text{CH}_2\text{Cl}_2$  and washed with  $\text{H}_2\text{O}$  ( $3 \times 200$  mL) (to remove the excess of 2,2-(ethylenedioxy)bis(ethylamine)). The organic phase was dried over  $\text{MgSO}_4$ , filtrated and concentrated under vacuum. A column chromatography on basic alumina was then performed (AcOEt 100%) to yield compound **12** (88 %) as pale yellow oil.

$^1\text{H NMR}$  (300 MHz,  $\text{CDCl}_3$ )  $\delta$  5.15 (s, 1H, NH), 3.59 (s, 4H, -O- $\text{CH}_2$ - $\text{CH}_2$ -O-), 3.55 - 3.47 (m, 4H, -O- $\text{CH}_2$ -), 3.29 (dd,  $J = 10.4, 5.2$  Hz, 2H,  $\text{CH}_2$ -NH-), 2.86 (t,  $J = 5.2$  Hz, 2H, - $\text{CH}_2$ - $\text{NH}_2$ ), 1.57 (s, 2H, - $\text{NH}_2$ ), 1.42 (s, 9H, - $\text{CH}_3$ ).

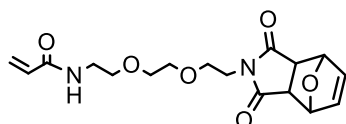
$^{13}\text{C NMR}$  (101 MHz,  $\text{CDCl}_3$ )  $\delta$  156.08 (s, 1C, O-(C=O)-NH-), 79.18 (s, 1C,  $\text{C}_q$ ), 73.28 (s, 2C, -O- $\text{CH}_2$ -), 70.26 (s, 2C, -O- $\text{CH}_2$ - $\text{CH}_2$ -O-), 41.70 (s, 1C, - $\text{CH}_2$ - $\text{NH}_2$ ), 40.38 (s, 1C, - $\text{CH}_2$ -NH-), 28.46 (s, 3C,  $\text{CH}_3$ ).

**MS (ESI, m/z)**  $[\text{M}+\text{H}]^+$  calc. – 249.1818, found – 249.1808

**EA** calc.: C, 53.20; H, 9.74; N, 11.28; O, 25.77; found: C, 52.73; H, 9.61; N, 10.84; O, 26.35

**FT IR** ( $\text{cm}^{-1}$ ) = 3361 ( $\nu_{\text{as}}$   $\text{NH}_2$ ); 2974 ( $\nu_{\text{as}}$   $\text{CH}_3$ ); 2926 ( $\nu_{\text{as}}$   $\text{CH}_2$ ); 2866 ( $\nu_{\text{s}}$   $\text{CH}_2$ ); 1704 ( $\nu_{\text{C=O}}$  O(C=O)NH); 1518 ( $\nu_{\text{CN}}$ ,  $\delta_{\text{NH}}$  C-N-H) amide II.

### **Compound 13**



Chemical Formula:  $\text{C}_{17}\text{H}_{22}\text{N}_2\text{O}_6$   
Molecular Weight: 350.37 g/mol

A mixture formed of compound **10** (2.40 g, 8.11 mmol, 1 eq. in 40 mL of freshly distilled  $\text{CH}_2\text{Cl}_2$ ) and TEA (1.81 mL, 1.31 g, 12.98 mmol, 1.6 eq.) was cooled to  $0^\circ\text{C}$  and 1.81 mL of acryloyl chloride (0.9546 g, 0.01 mmol, 1.3 eq.) were added dropwise. The mixture was stirred at room temperature overnight under argon atmosphere. The formed precipitate (salt of triethylammoniumchloride) was then eliminated by filtration. Then, 1 mL of 0.01% 4-Methoxyphenol (MEHQ) (100ppm) were added to the obtained clear yellow solution, as an inhibitor (to avoid polymerization). The solvent, excess of acryloyl chloride and TEA were evaporated under vacuum. The resulting residue was solubilized in 150 mL of  $\text{CH}_2\text{Cl}_2$ , washed with brine ( $3 \times 100$  mL), dried over  $\text{MgSO}_4$  and filtrated. Again, 1 mL of 0.01% MEHQ (100ppm) were added to the organic solution. The solvent was evaporated under vacuum to yield compound **13** (77 %) as viscous brown oil.

$^1\text{H NMR}$  (400 MHz,  $\text{CDCl}_3$ )  $\delta$  6.50 (s, 3H,  $\text{CH}=\text{CH}$ , NH), 6.26 (qd,  $J = 17.0, 6.0$  Hz, 2H,  $\text{CH}_2$ =), 5.62 (dd,  $J = 9.7, 2.2$  Hz, 1H, - $\text{CH}$ =), 5.24 (s, 2H, CH), 3.73 – 3.49 (m, 12H, N- $\text{CH}_2$ - $\text{CH}_2$ -O- $\text{CH}_2$ - $\text{CH}_2$ -O- $\text{CH}_2$ - $\text{CH}_2$ -NH-), 2.84 (s, 2H, CH).

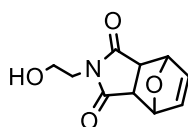
<sup>13</sup>C NMR (101 MHz, CDCl<sub>3</sub>) δ 176.42 (s, 2C, -(C=O)-N), 165.76 (s, C, -(C=O)-NH-), 136.67 (s, 2C, CH=CH), 131.15 (s, 1C, -CH=), 126.35 (s, 1C, CH<sub>2</sub>=), 81.02 (s, 1C, CHO), 70.37 (s, 1C, -O-CH<sub>2</sub>-), 69.95 (d, *J* = 20.7 Hz, 2C, -O-CH<sub>2</sub>-CH<sub>2</sub>-O-), 67.38 (s, 1C, -O-CH<sub>2</sub>-), 47.61 (s, 1C, CH), 39.35 (s, 1C, -CH<sub>2</sub>-NH-), 38.45 (s, 1C, -CH<sub>2</sub>-N).

MS (ESI, *m/z*) MS [M+Na]<sup>+</sup> calc. – 373.1370, found – 373.1378

EA calc.: C, 58.28; H, 6.33; N, 8.00; O, 27.40 found: C, 57.35; H, 6.04; N, 7.33; O, 28.65

FT IR (cm<sup>-1</sup>) = 3321 (ν<sub>NH</sub> (C=O)NH); 2947 (ν<sub>as</sub> CH<sub>2</sub>); 2872 (ν<sub>s</sub> CH<sub>2</sub>); 1773, 1696 (ν<sub>C=O</sub> cyclic imides in five membered ring); 1627 (ν<sub>C=O</sub> (C=O)NH) amide I; 1536 (ν<sub>CN</sub>, δ<sub>NH</sub> C-N-H) amide II; 916, 877, 854 (maleimide ring deformation).

### Compound 15



Chemical Formula: C<sub>10</sub>H<sub>11</sub>NO<sub>4</sub>  
Molecular Weight: 209,20 g/mol

Compound **8** (10.00 g, 60.19 mmol) was dispersed in 20 mL of MeOH and the suspension cooled to 0 °C. Then, a solution of ethanolamine (3.6 mL, 60.19 mmol, 1 eq.) in 20 mL of MeOH) was added dropwise during 10 min. The resulting clear yellow solution was stirred first, for 5 min. at 0 °C, then 30 min. at room temperature, and finally refluxed for 4 h. At the end of reaction the flask was cooled to room temperature, and after 2 h the product began to crystallize. The mixture was stored in the freezer overnight, and the precipitated out crystals were collected by vacuum filtration (yield: 44 %).

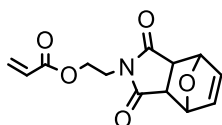
<sup>1</sup>H NMR (300 MHz, CDCl<sub>3</sub>) δ 6.51 (s, 2H, CH=CH), 5.26 (s, 2H, CH), 3.70 (dt, *J* = 10.0, 3.5 Hz, 4H, -CH<sub>2</sub>-N-, HO-CH<sub>2</sub>-), 2.88 (s, 2H, CH), 2.40 (s, 1H, -OH).

<sup>13</sup>C NMR (75 MHz, CDCl<sub>3</sub>) δ 176.89 (s, 2C, N-(C=O)-), 136.62 (s, 2C, CH=CH), 81.08 (s, 2C, OCH), 60.30 (s, 1C, -CH<sub>2</sub>-OH), 47.60 (s, 2C, CH), 41.84 (s, 1C, -CH<sub>2</sub>-N).

MS (ESI, *m/z*) [M+Na]<sup>+</sup> calc. – 232.0580, found – 232.0587

FT IR (cm<sup>-1</sup>) = 3473 (ν OH); 2932 (ν<sub>as</sub> O-CH<sub>2</sub>); 2866 (ν<sub>s</sub> CH<sub>2</sub>); 1768, 1683 (ν<sub>C=O</sub> cyclic imides in five membered ring); 918,875, 851 (maleic anhydride ring deformation).

### Compound 16



Chemical Formula: C<sub>13</sub>H<sub>13</sub>NO<sub>5</sub>  
Molecular Weight: 263,25 g/mol



A mixture formed of compound **15** (2.00 g, 9.56 mmol, 1 eq. in 40 mL of freshly distilled  $\text{CH}_2\text{Cl}_2$ ) and anhydrous TEA (2.2 mL, 1.55 g, 15.3 mmol, 1.6 eq.) was cooled to 0 °C and 1 mL of acryloyl chloride (1.13 g, 12.43 mmol, 1.3 eq.) were added dropwise. The mixture was stirred at room temperature overnight under argon atmosphere. The solvent, excess of acryloyl chloride and TEA were evaporated under vacuum. The resulting residue was re-solubilized in 150 mL of  $\text{CH}_2\text{Cl}_2$ , washed with brine (3×100 mL), dried over  $\text{MgSO}_4$ , filtrated and concentrated in vacuum. Next, the obtained residue was purified by column chromatography on silica gel (AcOEt 100%) to yield compound **16** (60%) as white crystals.

$^1\text{H NMR}$  (300 MHz,  $\text{CDCl}_3$ )  $\delta$  6.51 (s, 2H,  $\text{CH}=\text{CH}$ ), 6.37 (d,  $J = 17.3$  Hz, 1H,  $\text{CH}_2=$ ), 6.06 (dd,  $J = 17.3, 10.5$  Hz, 1H,  $=\text{CH}-$ ), 5.83 (d,  $J = 11.9$  Hz, 1H,  $\text{CH}_2=$ ), 5.25 (s, 2H,  $\text{CH}$ ), 4.30 (t,  $J = 5.4$  Hz, 2H,  $-\text{O}-\text{CH}_2-$ ), 3.80 (t,  $J = 5.4$  Hz, 2H,  $-\text{CH}_2-\text{N}-$ ), 2.86 (s, 2H,  $\text{CH}$ ).

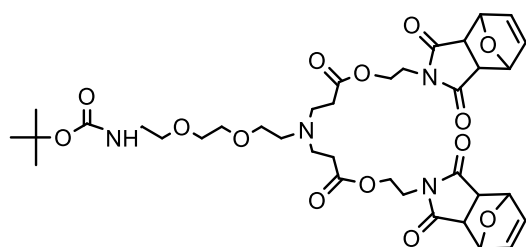
$^{13}\text{C NMR}$  (75 MHz,  $\text{CDCl}_3$ )  $\delta$  176.07 (s, 2C,  $-\text{N}-(\text{C}=\text{O})-$ ), 165.84 (s, 1 C,  $-(\text{C}=\text{O})-\text{O}-$ ), 136.66 (s, 2C,  $\text{CH}=\text{CH}$ ), 131.41 (s, 1C,  $\text{CH}_2=$ ), 128.07 (s, 1C,  $=\text{CH}-$ ), 81.02 (s, 2C,  $-\text{CH}-\text{O}$ ), 60.81 (s, 2C,  $-\text{O}-\text{CH}_2-$ ), 47.56 (s, 2C,  $-\text{CH}-$ ), 37.89 (s, 2C,  $-\text{CH}_2-\text{N}-$ ).

**MS (ESI, m/z)**  $[\text{M}+\text{Na}]^+$  calc. – 286.0685, found – 286.0692

**EA** calc.: C, 59.31; H, 4.98; N, 5.32; O, 30.39; found: C, 59.64; H, 5.03; N, 5.27; O, 29.66

**FT IR** ( $\text{cm}^{-1}$ ) = 2907 ( $\nu_{\text{as}} \text{O}-\text{CH}_2$ ); 1773, 1690 ( $\nu_{\text{C}=\text{O}}$  cyclic imides in five membered ring); 1723 ( $\nu_{\text{C}=\text{O}}$  ester); 914,873, 850, 824 (maleimide ring deformation).

### Compound 17



Chemical Formula:  $\text{C}_{37}\text{H}_{50}\text{N}_4\text{O}_{14}$   
Molecular Weight: 774,81 g/mol

To the solution of compound **12** (2.00 g; 8.05 mmol in 15 mL of anhydrous DMF) a solution of compound **16** (8.48 g; 32.22 mmol; 4 eq. in 35 mL of DMF) was added. The reaction mixture was stirred at 40 °C during 5 days. Afterwards the solvent was evaporated and the residue was purified by column chromatography on silica gel, first the excess of compound **16** was eluted with a mixture of  $\text{CH}_2\text{Cl}_2/\text{AcOEt}$  (v/v 90:10), then an elution with AcOEt (100%) was performed to yield compound **17** (56 %).

$^1\text{H NMR}$  (400 MHz,  $\text{CDCl}_3$ )  $\delta$  6.50 (s, 4H,  $\text{CH}=\text{CH}$ ), 5.24 (s, 4H,  $\text{CH}$ ), 5.08 (s, 1H,  $\text{NH}$ ), 4.19 (t,  $J = 5.4$  Hz, 4H,  $-(\text{C}=\text{O})-\text{O}-\text{CH}_2-$ ), 3.73 (t,  $J = 5.4$  Hz, 4H,  $-\text{CH}_2-\text{N}(\text{cycle})$ ), 3.51 (dd,  $J = 21.9, 13.1$  Hz,

8H, -O-CH<sub>2</sub>-), 3.29 (d, *J* = 4.8 Hz, 2H, -NH-CH<sub>2</sub>-), 2.86 (s, 4H, -CH-), 2.76 (t, *J* = 7.2 Hz, 4H, -N-CH<sub>2</sub>-), 2.63 (t, *J* = 6.1 Hz, 2H, -CH<sub>2</sub>-N-), 2.39 (t, *J* = 7.2 Hz, 4H, -CH<sub>2</sub>-(C=O)-O-), 1.42 (s, 9H, -CH<sub>3</sub>).

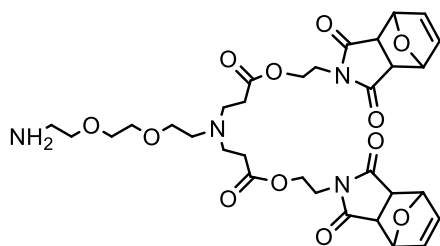
<sup>13</sup>C NMR (101 MHz, CDCl<sub>3</sub>) δ 176.12 (s, 4C, -N-(C=O)-), 172.30 (s, 2C, -(C=O)-O-), 156.11 (s, 1C, -(C=O)-O-), 136.65 (s, 4C, CH=CH), 81.02 (s, 4C, -CH-O), 79.23 (s, 1C, =C=), 70.34 (d, *J* = 6.7 Hz, 2C, -CH<sub>2</sub>-O-), 69.63 (d, *J* = 71.2 Hz, 2C, -CH<sub>2</sub>-O-), 60.63 (s, 2C, -(C=O)-O-CH<sub>2</sub>-), 53.21 (s, 1C, -CH<sub>2</sub>-N-), 49.61 (s, 2C, -N -CH<sub>2</sub>-), 47.56 (s, 2C, -CH-), 40.46 (s, 1C, -NH-CH<sub>2</sub>-), 37.91 (s, 2C, -CH<sub>2</sub>-N-(cycle)), 32.42 (s, 2C, -CH<sub>2</sub>-(C=O)-O -), 28.53 (s, 3C, -CH<sub>3</sub>).

MS (ESI, *m/z*) [M+H]<sup>+</sup> calc. – 775.3402, found – 775.3404; MS [M+Na]<sup>+</sup> calc. – 797.3221, found – 797.3249

EA calc.: C, 57.36; H, 6.50; N, 7.23; O, 28.91; found: C, 57.21; H, 6.75; N, 7.22, O, 29.77

FT IR (cm<sup>-1</sup>) = 3382 (ν<sub>NH</sub> (C=O)NH); 2970 (ν<sub>as</sub> CH<sub>3</sub>); 2929 (ν<sub>as</sub> CH<sub>2</sub>); 2868 (ν<sub>s</sub> CH<sub>2</sub>); 1773, 1695 (ν<sub>C=O</sub> cyclic imides in five membered ring); 1732 (ν<sub>C=O</sub> ester); 1515 (ν<sub>CN</sub>, δ<sub>NH</sub> C-N-H) amide II; 915,876, 853, 824 (maleimide ring deformation).

### Compound 18



Chemical Formula: C<sub>32</sub>H<sub>42</sub>N<sub>4</sub>O<sub>12</sub>  
Molecular Weight: 674,70 g/mol

Compound **17** (3.50g) was solubilized in 100 mL of freshly distilled CH<sub>2</sub>Cl<sub>2</sub> and gaseous HCl was bubbled through the solution during 30 min. At the end of the reaction the solvent was evaporated under vacuum and the obtained residue was solubilized in 100 mL of H<sub>2</sub>O, washed with CH<sub>2</sub>Cl<sub>2</sub> (3×100 mL) and dried in vacuum to yield compound **18** (65 %) as a slightly yellow very hygroscopic foam (foamy oil).

<sup>1</sup>H NMR (400 MHz, D<sub>2</sub>O) δ 6.65 (s, 4H, CH=CH), 5.32 (s, 4H, CH), 4.38 (t, *J* = 5.0 Hz, 4H, -(C=O)O-CH<sub>2</sub>-), 3.92 (t, 2H, -O-CH<sub>2</sub>-), 3.85 (t, *J* = 5.0 Hz, 4H, -CH<sub>2</sub>-N-), 3.80 (t, 2H, -CH<sub>2</sub>-O-), 3.76 (s, 4H, -O-CH<sub>2</sub>-CH<sub>2</sub>-O-), 3.55 (t, *J* = 6.4 Hz, 4H, -N-CH<sub>2</sub>-), 3.50 (t, 2H, -CH<sub>2</sub>-N-), 3.25 (t, 2H, -CH<sub>2</sub>-NH<sub>2</sub>) 3.17 (s, 4H, CH), 2.90 (t, *J* = 6.8 Hz, 4H, -CH<sub>2</sub>-(C=O)O-).

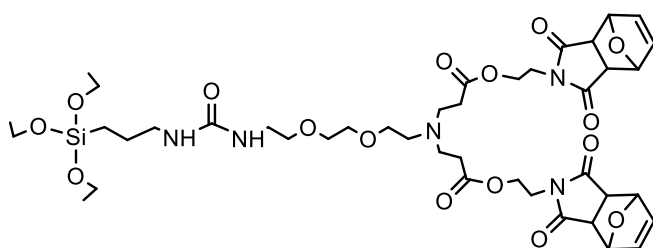
<sup>13</sup>C NMR (101 MHz, D<sub>2</sub>O) δ 179.83 (s, 4C, N(C=O)<sub>2</sub>), 172.20 (s, 2C, -(C=O)O-), 137.00 (s, 4C, CH=CH), 81.61 (s, 4C, CH), 70.36 (s, 1C, -CH<sub>2</sub>-O-), 70.12 (s, 1C, -O-CH<sub>2</sub>-), 66.97 (s, 1C, -CH<sub>2</sub>-O-), 64.43 (s, 1C, -O-CH<sub>2</sub>-), 62.22 (s, 2C, -(C=O)O-CH<sub>2</sub>-), 54.04 (s, 1C, -CH<sub>2</sub>-N-), 49.76 (s, 2C, -N-CH<sub>2</sub>-), 47.62 (s, 4C, CH), 39.61 (s, 1C, -CH<sub>2</sub>-NH<sub>2</sub>), 38.10 (s, 2C, -CH<sub>2</sub>-N), 28.66 (s, 2C, -CH<sub>2</sub>-(C=O)O-).

MS (ESI, *m/z*) [M+H]<sup>+</sup> calc. – 675.2877, found – 675.2878; MS [M+Na]<sup>+</sup> calc. – 697.2697, found – 697.2648

**EA** ( $M \times 4H_2O \times 2HCl$ ) calc.: C, 46.95; H, 6.28; Cl, 8.66; N, 6.84; O, 31.27; found: C, 47.54; H, 6.44; Cl, 9.91; N, 7.01; O, 29.36

**FT IR** ( $cm^{-1}$ ) = 3449 ( $\nu_{as} NH_2$ ); 2956 ( $\nu_{as} CH_2$ ); 2868 ( $\nu_s CH_2$ ); 1770, 1693 ( $\nu_{C=O}$  cyclic imides in five membered ring); 1735 ( $\nu_{C=O}$  ester); 914, 876, 852, 824 (maleimide ring deformation).

### **Compound 19**



Chemical Formula:  $C_{42}H_{63}N_5O_{16}Si$   
Molecular Weight: 922,06 g/mol

A solution formed of compound **18** (0.675 g, 1.0 mmol in 30 mL of freshly distilled  $CH_2Cl_2$ ) and TEA (0.56 mL, 0.41 g, 4.0 mmol, 4 eq.) was cooled to  $0^\circ C$  and 0.2350 g of isocyanato propyl tri-(etoxy)silane (0.95 mmol, 0.95 eq.) were added dropwise. The mixture was stirred at room temperature overnight under argon atmosphere. Afterwards, the solvent was evaporated under vacuum and 10 mL of THF was added to the obtained residue. The precipitated out powder ( $TEA \times HCl$ ) was filtrated and the solution was concentrated under vacuum to yield compound **19** as viscous yellowish transparent oil (99 %).

**$^1H$  NMR** (300 MHz,  $CDCl_3$ )  $\delta$  6.50 (s, 4H,  $CH=CH$ ), 5.24 (s, 4H,  $CH$ ), 5.03 (s, 1H,  $NH$ ), 4.88 (s, 1H,  $NH$ ), 4.19 (t,  $J = 5.4$  Hz, 4H,  $-(C=O)O-CH_2-$ ), 3.79 (q,  $J = 7.0$  Hz, 6H,  $-O-CH_2-CH_3$ ), 3.72 (t,  $J = 5.4$  Hz, 4H,  $-CH_2-N$ ), 3.55 (s, 4H,  $-O-CH_2-CH_2-O-$ ), 3.50 (dd,  $J = 11.8, 5.6$  Hz, 4H,  $-O-CH_2-$ ,  $-CH_2-O-$ ), 3.35 (dd,  $J = 10.2, 5.2$  Hz, 2H,  $-NH-CH_2-$ ), 3.14 (dd,  $J = 13.1, 6.9$  Hz, 2H,  $-CH_2-NH-$ ), 2.86 (s, 4H,  $CH$ ), 2.76 (t,  $J = 7.2$  Hz, 4H,  $-N-CH_2-$ ), 2.61 (t,  $J = 5.8$  Hz, 2H,  $-CH_2-N-$ ), 2.39 (t,  $J = 7.2$  Hz, 4H,  $-CH_2-(C=O)O-$ ), 1.57 (dt,  $J = 15.5, 7.7$  Hz, 2H,  $-CH_2-$ ), 1.20 (t,  $J = 7.0$  Hz, 9H,  $-O-CH_2-CH_3$ ), 0.65 – 0.56 (m, 2H,  $-Si-CH_2-$ ).

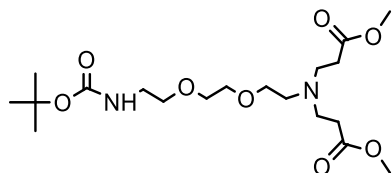
**$^{13}C$  NMR** (101 MHz,  $CDCl_3$ )  $\delta$  176.21 (s, 4C,  $N(C=O)_2$ ), 172.36 (s, 2C,  $-(C=O)O-$ ), 158.58 (s, 1C,  $C=O_{urea}$ ), 136.67 (s, 4C,  $CH=CH$ ), 81.05 (s, 4C,  $CH$ ), 71.13 (s, 1C,  $-CH_2-O-$ ), 70.75 (d,  $J = 56.7$  Hz, 2C,  $-O-CH_2-CH_2-O-$ ), 69.45 (s, 1C,  $-O-CH_2-$ ), 60.75 (s, 2C,  $-(C=O)O-CH_2-$ ), 58.51 (s, 3C,  $-O-CH_2-CH_3$ ), 53.31 (s, 1C,  $-CH_2-N$ ), 49.58 (s, 2C,  $-N-CH_2-$ ), 47.60 (s, 4C,  $CH$ ), 43.07 (s, 1C,  $-CH_2-NH-$ ), 40.34 (s, 1C,  $-NH-CH_2-$ ), 37.91 (s, 2C,  $-CH_2-N$ ), 32.27 (s, 2C,  $-CH_2-(C=O)O-$ ), 23.83 (s, 1C,  $-CH_2-$ ), 18.42 (s, 3C,  $-CH_3$ ), 7.78 (s, 1C,  $-Si-CH_2-$ ).

**MS (ESI, m/z)**  $[M+H]^+$  calc. – 922.4111, found – 922.4108;  $MS [M+Na]^+$  calc. – 944.3914, found – 944.3710

**EA** calc.: C, 54.71; H, 6.89; N, 7.60; O, 27.76; Si, 3.05; found: C, 52.48; H, 6.74; N, 7.73; Si, 3.15

**FT IR (cm<sup>-1</sup>)** = 3368 ( $\nu_{\text{NH}}$  NH(C=O)NH); 2972 ( $\nu_{\text{as}}$  CH<sub>3</sub>); 2923 ( $\nu_{\text{as}}$  CH<sub>2</sub>); 2876 ( $\nu_{\text{s}}$  CH<sub>2</sub>); 1775, 1698 ( $\nu_{\text{C=O}}$  cyclic imides in five membered ring); 1734 ( $\nu_{\text{C=O}}$  ester); 1641 ( $\nu_{\text{C=O}}$  urea) amide I; 1559 ( $\nu_{\text{CN}}$ ,  $\delta_{\text{NH}}$  C-N-H) amide II; 1099, 1074, 1020 ( $\nu_{\text{Si-O}}$  Si-OEt); 916, 877, 854, (maleimide ring deformation).

### **Compound 20**



Chemical Formula: C<sub>19</sub>H<sub>36</sub>N<sub>2</sub>O<sub>8</sub>

Molecular Weight: 420,50 g/mol

To a solution of compound (**12**) (6.00 g, 24.16 mmol in 100 mL freshly distilled MeOH), 22 mL of methyl acrylate (20.8 g, 241.6 mmol, 10 eq.) were added. The mixture was stirred for 3 days at 50 °C. At the end of reaction the excess of methyl acrylate and MeOH was evaporated under vacuum to yield compound (**20**) (quantitatively) as yellow oil.

**<sup>1</sup>H NMR** (300 MHz, CDCl<sub>3</sub>)  $\delta$  5.07 (s, 1H, NH), 3.64 (s, 6H, -O-CH<sub>3</sub>), 3.56 (s, 4H, -O-CH<sub>2</sub>-CH<sub>2</sub>-O-), 3.51 (t,  $J$  = 5.4 Hz, 4H, -O-CH<sub>2</sub>-), 3.28 (dd,  $J$  = 10.4, 5.2 Hz, 2H, -CH<sub>2</sub>-NH-), 2.81 (t,  $J$  = 7.1 Hz, 4H, -N-CH<sub>2</sub>-), 2.66 (t,  $J$  = 6.1 Hz, 2H, -CH<sub>2</sub>-N-), 2.44 (t,  $J$  = 7.1 Hz, 4H, -CH<sub>2</sub>-COO), 1.41 (s, 9H, -CH<sub>3</sub>).

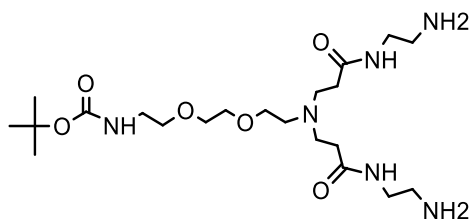
**<sup>13</sup>C NMR** (75 MHz, CDCl<sub>3</sub>)  $\delta$  173.03 (s, 2C, -(C=O)-O-), 156.09 (s, 1C, -(C=O)-NH-), 79.22 (s, 1C, C<sub>q</sub>), 70.43 (d,  $J$  = 10.1 Hz, 2C, -O-CH<sub>2</sub>-CH<sub>2</sub>-O-), 69.79 (s, 2C, -CH<sub>2</sub>-O-), 53.36 (s, 1C, -CH<sub>2</sub>-N-), 51.63 (s, 2C, -O-CH<sub>3</sub>), 50.04 (s, 2C, -N-CH<sub>2</sub>), 40.48 (s, 1C, -CH<sub>2</sub>-NH-), 32.68 (s, 2C, -CH<sub>2</sub>-COO-), 28.52 (s, 2C, -CH<sub>3</sub>).

**MS (ESI, m/z)** [M+H]<sup>+</sup> calc. – 421.2544, found – 421.2554; MS [M+Na]<sup>+</sup> calc. – 443.2431, found – 443.2441

**EA** calc.: C, 54.27; H, 8.63; N, 6.66; O, 30.44; found: C, 54.66; H, 8.54; N, 6.60; O, 30.64

**FT IR (cm<sup>-1</sup>)** = 3374 ( $\nu_{\text{NH}}$  O(C=O)NH); 2976 ( $\nu_{\text{as}}$  CH<sub>3</sub>); 2951 ( $\nu_{\text{as}}$  CH<sub>2</sub>); 2867 ( $\nu_{\text{s}}$  CH<sub>2</sub>); 1735 ( $\nu_{\text{C=O}}$  ester); 1711 ( $\nu_{\text{C=O}}$  O(C=O)NH); 1513 ( $\nu_{\text{CN}}$ ,  $\delta_{\text{NH}}$  C-N-H) amide II.

### **Compound 21**



Chemical Formula: C<sub>21</sub>H<sub>44</sub>N<sub>6</sub>O<sub>6</sub>

Molecular Weight: 476,61 g/mol

To a solution of compound **20** (11.00 g, 26.16 mmol in 100 mL freshly distilled MeOH), 140 mL of ethylene diamine (126g, 2.09 mol, 80 eq.) were added. The mixture was stirred for 5 days at 25 °C. At the end of reaction the excess of ethylene diamine and MeOH was evaporated under vacuum to yield compound **21** (quantitatively) as a very viscous brown oil.

**<sup>1</sup>H NMR** (400 MHz, CDCl<sub>3</sub>) δ 7.46 (s, 2H, -NH-), 5.65 (s, 1H, -NH-), 3.56 – 3.47 (m, 8H, -CH<sub>2</sub>-O-CH<sub>2</sub>-CH<sub>2</sub>-O-CH<sub>2</sub>-), 3.24 (dd, *J* = 11.7, 5.8 Hz, 6H, -CONH-CH<sub>2</sub>-), 2.81 – 2.69 (m, 8H, N-CH<sub>2</sub>-, -CH<sub>2</sub>-NH<sub>2</sub>), 2.62 (t, *J* = 5.3 Hz, 2H, -CH<sub>2</sub>-N), 2.33 (t, *J* = 6.2 Hz, 4H, -CH<sub>2</sub>-CONH-), 2.03 (s, 4H, -NH<sub>2</sub>), 1.40 (s, 9H, -CH<sub>3</sub>).

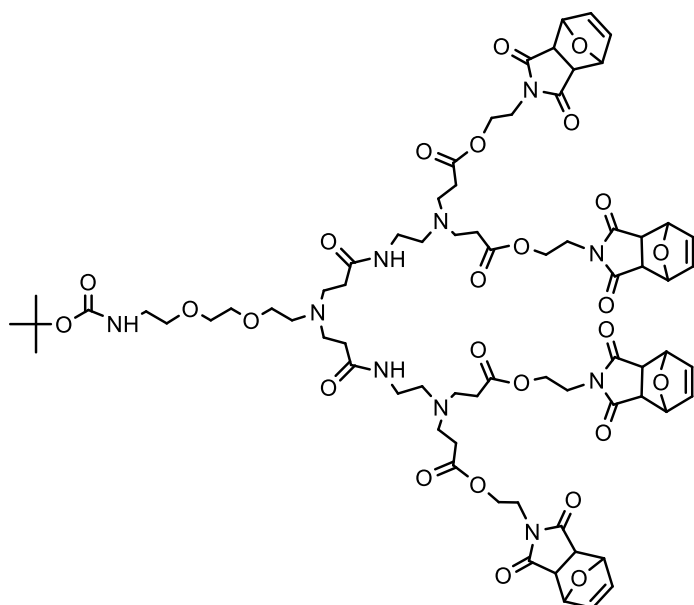
**<sup>13</sup>C NMR** (151 MHz, CDCl<sub>3</sub>) δ 171.93 (s, 2C, -(C=O)NH), 155.26 (s, 1C, -O(C=O)NH), 78.22 (s, 1C, C<sub>q</sub>), 69.32 (s, 2C, -O-CH<sub>2</sub>-CH<sub>2</sub>-O-), 68.34 (s, 2C, -O-CH<sub>2</sub>-), 52.77 (s, 1C, -CH<sub>2</sub>-N), 50.01 (s, 2C, -N-CH<sub>2</sub>-), 41.14 (s, 1C, -OCONH-CH<sub>2</sub>-), 40.46 (s, 2C, -CH<sub>2</sub>-NH<sub>2</sub>), 39.38 (s, 2C, -CONH-CH<sub>2</sub>-), 33.36 (s, 2C, -CH<sub>2</sub>-CONH-), 27.52 (s, 3C, -CH<sub>3</sub>).

**MS (ESI, m/z)** [MH<sup>+</sup>] calc. – 477.3395, found – 477.3398; MS [MNa<sup>+</sup>] calc. – 499.3240, found – 499.3243

**EA** calc.: C, 52.92; H, 9.31; N, 17.63; O, 20.14; found: C, 52.12; H, 9.20; N, 16.88 O, 21.15

**FT IR** (cm<sup>-1</sup>) = 3295 (ν<sub>NH</sub> (C=O)NH); 2970 (ν<sub>as</sub> CH<sub>3</sub>); 2929 (ν<sub>as</sub> CH<sub>2</sub>); 2866 (ν<sub>s</sub> CH<sub>2</sub>); 1702 (ν<sub>C=O</sub> O(C=O)NH); 1644 (ν<sub>C=O</sub>) amide I; 1537 (ν<sub>CN</sub>, δ<sub>NH</sub> C-N-H) amide II.

## Compound 22



Chemical Formula: C<sub>73</sub>H<sub>96</sub>N<sub>10</sub>O<sub>26</sub>  
Molecular Weight: 1529,59 g/mol

To a solution of compound **21** (1.81 g, 3.80 mmol in 20 mL of anhydrous DMF) a solution of compound **16** (8.00 g, 30.39 mmol, 8 eq. in 40 mL of anhydrous DMF) was added. The reaction mixture was stirred at 40°C during 5 days. At the end of reaction, the solvent was evaporated and the

residue was purified relying on the difference of solubility of the mixture in Toluene. The compound **22** is not soluble in Toluene while the starting material (compound **16**) added in a large excess is. Thus, the residue was solubilized in a minimal volume of  $\text{CH}_2\text{Cl}_2$  and added dropwise to a large volume of toluene, and then the solution volume was reduced twice. After two days the precipitated out gluey mass was separated from the solution by decantation and the procedure was repeated again (at least three times). By this procedure compound **22** was obtained in 46 % yield.

**$^1\text{H}$  NMR** (300 MHz,  $\text{CDCl}_3$ )  $\delta$  6.51 (s, 8H,  $\text{CH}=\text{CH}$ ), 5.24 (s, 8H, CH), 4.20 (s, 8H,  $-(\text{C}=\text{O})\text{O}-\text{CH}_2-$ ), 3.73 (t,  $J = 5.3$  Hz, 8H,  $-\text{CH}_2-\text{N}$ ), 3.58 (s, 4H,  $-\text{O}-\text{CH}_2-\text{CH}_2-\text{O}-$ ), 3.51 (t, 4H,  $-\text{CH}_2-\text{O}-, -\text{O}-\text{CH}_2-$ ), 3.27 (dd,  $J = 10.0, 5.0$  Hz, 6H,  $-\text{NH}-\text{CH}_2-$ ), 2.85 (d,  $J = 19.2$  Hz, 12H, CH,  $-\text{N}-\text{CH}_2-$ ), 2.71 (t,  $J = 6.7$  Hz, 8H,  $-\text{N}-\text{CH}_2-$ ), 2.50 (t,  $J = 5.8$  Hz, 6H,  $-\text{CH}_2-\text{N}-$ ), 2.42 – 2.29 (m, 12H,  $-\text{CH}_2-(\text{C}=\text{O})\text{O}$ ,  $-\text{CH}_2-(\text{C}=\text{O})\text{NH}$ ), 1.43 (s, 9H,  $-\text{CH}_3$ ).

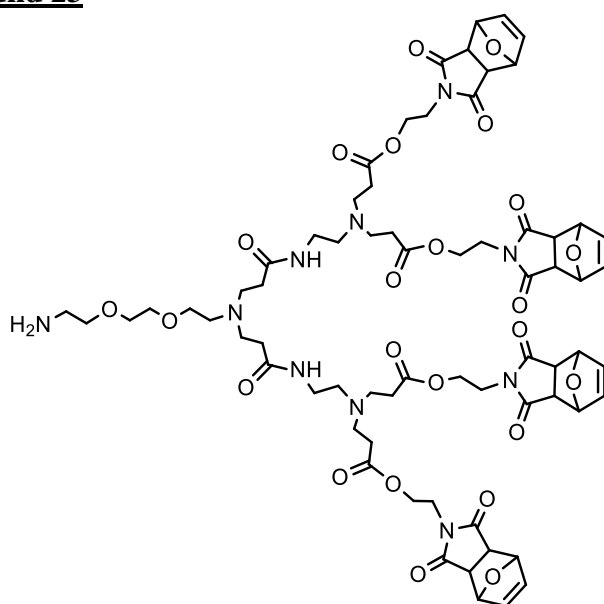
**$^{13}\text{C}$  NMR** (101 MHz,  $\text{CDCl}_3$ )  $\delta$  176.25 (s, 8C,  $-\text{N}(\text{C}=\text{O})_2$ ), 172.42 (s, 6C,  $-(\text{C}=\text{O})\text{O}-$ ,  $-(\text{C}=\text{O})\text{NH}-$ ), 156.21 (s, 1C,  $-\text{O}(\text{C}=\text{O})\text{NH}-$ ), 136.72 (s, 8C,  $\text{CH}=\text{CH}$ ), 81.09 (s, 8C, CH), 79.24 (s, 1C,  $\text{C}_q$ ), 70.39 (s, 4C,  $-\text{CH}_2-\text{O}-\text{CH}_2-\text{CH}_2-\text{O}-\text{CH}_2-$ ), 60.86 (s, 4C,  $-(\text{C}=\text{O})\text{O}-\text{CH}_2-$ ), 52.87 (d,  $J = 18.6$  Hz, 3C,  $-\text{CH}_2-\text{N}$ ), 50.29 (s, 2C,  $\text{N}-\text{CH}_2-$ ), 48.91 (s, 4C,  $\text{N}-\text{CH}_2-$ ), 47.65 (s, 8C, CH), 40.51 (s, 1C,  $-\text{O}(\text{C}=\text{O})\text{NH}-\text{CH}_2-$ ), 37.94 (s, 4C,  $-\text{CH}_2-\text{N}$ ), 37.24 (s, 2C,  $(\text{C}=\text{O})\text{NH}-\text{CH}_2-$ ), 32.43 (s, 6C,  $-\text{CH}_2-(\text{C}=\text{O})\text{NH}-$ ,  $-\text{CH}_2-(\text{C}=\text{O})\text{O}-$ ), 28.60 (s, 3C,  $-\text{CH}_3$ ).

**MS (ESI, m/z)**  $[\text{M}]^{2+}$  calc. – 765.3321, found – 765.3329; MS  $[\text{M}]$  calc. – 1529.6570, found – 1529.6210; MS  $[\text{M}+\text{Na}]^+$  calc. – 1551.6345, found – 1551.5985

**EA** calc.: C, 57.32; H, 6.33; N, 9.16; O, 27.20; found: C, 57.76; H, 6.39; N, 9.03; O, 26.96

**FT IR** ( $\text{cm}^{-1}$ ) = 3372 ( $\nu_{\text{as}}$   $\text{NH}_2$ ); 2958 ( $\nu_{\text{as}}$   $\text{CH}_3$ ); 2923 ( $\nu_{\text{as}}$   $\text{CH}_2$ ); 2869 ( $\nu_{\text{s}}$   $\text{CH}_2$ ); 1774, 1695 ( $\nu_{\text{C}=\text{O}}$  cyclic imides in five membered ring); 1730 ( $\nu_{\text{C}=\text{O}}$  ester); 1640 ( $\nu_{\text{C}=\text{O}}$  amide I; 1527 ( $\nu_{\text{CN}}$ ,  $\delta_{\text{NH}}$  C-N-H) amide II; 915, 876, 853, 824 (maleimide ring deformation)

### Compound 23



Chemical Formula:  $\text{C}_{68}\text{H}_{88}\text{N}_{10}\text{O}_{24}$   
Molecular Weight: 1429,48 g/mol

Compound **22** (3.00g) was solubilized in freshly distilled CH<sub>2</sub>Cl<sub>2</sub> (40 mL) and gaseous HCl was bubbled through the solution during 25 min. At the end of the reaction, the solvent, *t*-butanol and excess of HCl were evaporated under vacuum. Next, the residue was solubilized in 100 mL of H<sub>2</sub>O, washed with CH<sub>2</sub>Cl<sub>2</sub> (3×100 mL) and dried in vacuum to yield compound **23** (77 %) as a yellow-orange very viscous oil.

<sup>1</sup>H NMR (300 MHz, D<sub>2</sub>O) δ 6.65 (s, 8H, CH=CH), 5.32 (s, 8H, CH), 4.36 (t, *J* = 5.1 Hz, 8H, -(C=O)O-CH<sub>2</sub>-), 3.94 (d, *J* = 4.4 Hz, 2H, O-CH<sub>2</sub>-), 3.83 (dd, *J* = 9.4, 4.7 Hz, 10H, -CH<sub>2</sub>-O-, -CH<sub>2</sub>-N-), 3.78 (s, 4H, -O-CH<sub>2</sub>-CH<sub>2</sub>-O-), 3.72 – 3.65 (m, 4H, -(C=O)NH-CH<sub>2</sub>-), 3.55 (dd, *J* = 13.8, 6.9 Hz, 14H, -N-CH<sub>2</sub>-, -CH<sub>2</sub>-N), 3.43 (t, *J* = 5.7 Hz, 4H, -CH<sub>2</sub>-N), 3.28 – 3.22 (t, 2H, -CH<sub>2</sub>-NH<sub>2</sub>), 3.16 (s, 8H, CH), 2.91 (d, *J* = 6.4 Hz, 12H, -CH<sub>2</sub>-(C=O)NH-, -CH<sub>2</sub>-(C=O)O-).

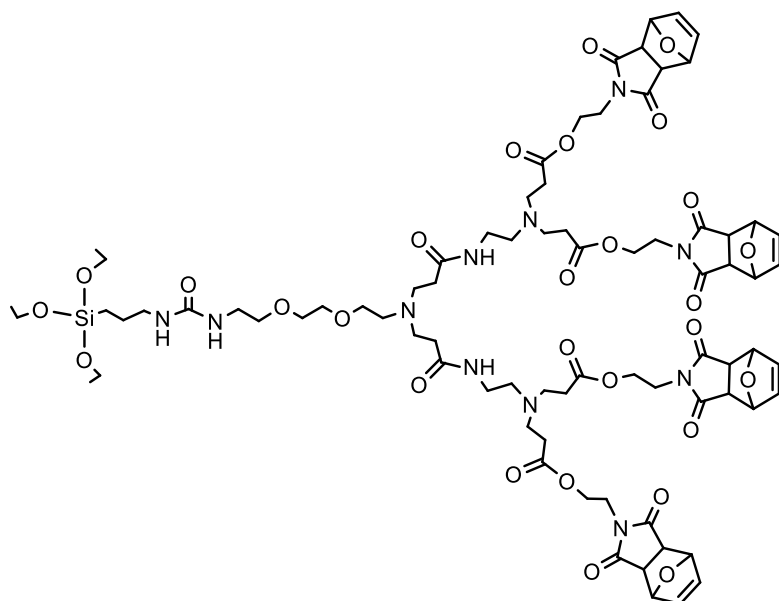
<sup>13</sup>C NMR (75 MHz, D<sub>2</sub>O) δ 179.31 (s, 8C, -N(C=O)<sub>2</sub>), 172.81 (s, 2C, (C=O)NH), 172.61 (s, 4C, (C=O)O), 136.56 (s, 8C, CH=CH), 81.16 (s, 8C, CH), 69.79 (d, *J* = 19.5 Hz, 2C, -O-CH<sub>2</sub>-CH<sub>2</sub>-O-), 66.54 (s, 1C, -CH<sub>2</sub>-O-), 64.09 (s, 1C, -O-CH<sub>2</sub>-), 61.88 (s, 4C, (C=O)O-CH<sub>2</sub>-), 53.09 (s, 2C, -CH<sub>2</sub>-N), 52.91 (s, 1C, -CH<sub>2</sub>-N), 49.85 (s, 8C, N-CH<sub>2</sub>-), 49.14 (s, 2C, N-CH<sub>2</sub>-), 47.54 (s, 8C, CH), 39.17 (s, 1C, -CH<sub>2</sub>-NH<sub>2</sub>), 37.11 (s, 4C, -CH<sub>2</sub>-N), 34.53 (s, 2C, -CH<sub>2</sub>-(C=O)NH-), 28.77 (s, 4C, -CH<sub>2</sub>-(C=O)O-), 28.23 (s, 2C, -CH<sub>2</sub>-(C=O)NH-).

MS (FD, *m/z*) [M+H]<sup>+</sup> calc. – 1429.6051, found – 1429.6008

EA (M×5H<sub>2</sub>O×4HCl) calc: C, 49.04; H, 6.17; Cl, 8.52; N, 8.41; O, 27.86; found: C, 48.76; H, 6.16; Cl, 9.58; N, 8.72; O, 26.92.

FT IR (cm<sup>-1</sup>) = 3389 (ν<sub>as</sub> NH<sub>2</sub>); 2956 (ν<sub>as</sub> CH<sub>2</sub>); 2866 (ν<sub>s</sub> CH<sub>2</sub>); 1772, 1693 (ν<sub>C=O</sub> cyclic imides in five membered ring); 1735 (ν<sub>C=O</sub> ester); 1551 (ν<sub>CN</sub>, δ<sub>NH</sub> C-N-H) amide II; 1184 cm<sup>-1</sup> (C-N-C stretch); 914, 877, 852, 824 (maleimide ring deformation)

## Compound 24



Chemical Formula: C<sub>78</sub>H<sub>109</sub>N<sub>11</sub>O<sub>28</sub>Si  
Molecular Weight: 1676,84 g/mol

To 1.00 g of compound **23** (0.70 mmol) dispersed in 30 mL of freshly distilled CH<sub>2</sub>Cl<sub>2</sub>, 1.46 mL of TEA (1.06 g, 10.50 mmol, 15 eq) were added. After compound **23** was solubilized, the solution was cooled to 0 °C and 0.1732 g of isocyanato propyl tri-(etoxy)silane (0.70 mmol, 1 eq.) were added dropwise. The reaction proceeded at room temperature, under argon atmosphere, overnight. Afterwards the solvent and excess of TEA were evaporated, and the obtained residue was purified by gel permeation chromatography. Three successive size exclusion columns with Biorad S-X3 beads swelled with CH<sub>2</sub>Cl<sub>2</sub> allowed yielding compound **24** in 73 %.

**<sup>1</sup>H NMR** (300 MHz, CDCl<sub>3</sub>) δ 6.50 (s, 8H, CH=CH), 5.50 (s, 1H, NH), 5.22 (s, 8H, CH), 4.17 (s, 8H, -(C=O)O-CH<sub>2</sub>-), 3.77 (d, *J* = 7.0 Hz, 6H, -O-CH<sub>2</sub>-CH<sub>3</sub>), 3.71 (s, 4H, -CH<sub>2</sub>-N), 3.54 (s, 4H, -O-CH<sub>2</sub>-CH<sub>2</sub>-O-), 3.48 (t, 4H, -CH<sub>2</sub>-O-, -O-CH<sub>2</sub>-), 3.32 (s, 2H, NH(C=O)NH-CH<sub>2</sub>-), 3.24 (s, 4H, (C=O)NH-CH<sub>2</sub>-), 3.11 (d, *J* = 6.2 Hz, 2H, -CH<sub>2</sub>-NH(C=O)NH), 2.86 (s, 8H, CH), 2.84 – 2.76 (m, 4H, N-CH<sub>2</sub>-), 2.69 (s, 8H, N-CH<sub>2</sub>-), 2.48 (s, 6H, -CH<sub>2</sub>-N), 2.35 (s, 12H, -CH<sub>2</sub>-(C=O)NH-, -CH<sub>2</sub>-(C=O)O-), 1.55 (s, 2H, -CH<sub>2</sub>-), 1.18 (t, *J* = 7.0 Hz, 9H, -CH<sub>3</sub>), 0.59 (s, 2H, -Si-CH<sub>2</sub>-).

**<sup>13</sup>C NMR** (101 MHz, CDCl<sub>3</sub>) δ 176.25 (s, 8C, -N(C=O)<sub>2</sub>), 172.44 (s, 6C, (C=O)NH, (C=O)O), 158.90 (s, 1C, C=O<sub>urea</sub>), 136.66 (s, 8C, CH=CH), 81.03 (s, 8C, CH), 70.74 (d, *J* = 84.0 Hz, 4C, -CH<sub>2</sub>-O-CH<sub>2</sub>-CH<sub>2</sub>-O-CH<sub>2</sub>-), 60.80 (s, 4C, (C=O)O-CH<sub>2</sub>-), 58.45 (s, 3C, -O-CH<sub>2</sub>-CH<sub>3</sub>), 52.84 (s, 3C, -CH<sub>2</sub>-N-), 50.39 (s, 2C, -N-CH<sub>2</sub>-), 48.84 (s, 4C, -N-CH<sub>2</sub>-), 47.59 (s, 8C, CH), 42.96 (s, 1C, -CH<sub>2</sub>-NH-), 40.15 (s, 1C, -NH-CH<sub>2</sub>-), 37.85 (s, 4C, -CH<sub>2</sub>-N), 37.23 (s, 2C, (C=O)NH-CH<sub>2</sub>-), 33.48 (s, 2C, -CH<sub>2</sub>-(C=O)NH-), 32.39 (s, 4C, -CH<sub>2</sub>-(C=O)O-), 23.92 (s, 1C, -CH<sub>2</sub>-), 18.40 (s, 3C, -CH<sub>3</sub>), 7.78 (s, 1C, -Si-CH<sub>2</sub>-).

**MS (FD, m/z)** [M+H]<sup>+</sup> calc. – 1676.7291, found – 1676.7123

**EA** calc: C, 55.87; H, 6.55; N, 9.19; O, 26.72; Si, 1.67; found: C, 51.57; H, 6.68; N, 9.44; Si, 1.69

**FT IR (cm<sup>-1</sup>)** = 3368 (ν<sub>NH</sub> NH(C=O)NH); 2970 (ν<sub>as</sub> CH<sub>3</sub>); 2923 (ν<sub>as</sub> CH<sub>2</sub>); 2866 (ν<sub>s</sub> CH<sub>2</sub>); 1774, 1696 (ν<sub>C=O</sub> cyclic imides in five membered ring); 1732 (ν<sub>C=O</sub> ester); 1644 (ν<sub>C=O</sub> urea) amide I; 1549 (ν<sub>CN</sub>, δ<sub>NH</sub> C-N-H) amide II; 1099, 1074, 1019 (ν<sub>Si-O</sub> Si-OEt); 915, 877, 853, (maleimide ring deformation).

## 4 General grafting and maleimide functional group deprotection procedures

### Grafting of coupling agents **10**, **18** or **23** on core-shell γ-Fe<sub>2</sub>O<sub>3</sub>/Polymer MNPs

First, 5 mg of γ-Fe<sub>2</sub>O<sub>3</sub>/Polymer MNPs were dispersed in 1 mL of 50 mM MES/0.3 % PF solution. Next, 2.85 mg of EDC (corresponding to 8.5 eq. per equivalent of available COOH groups on γ-Fe<sub>2</sub>O<sub>3</sub>/Polymer MNPs, which is ~350 μmol COOH/g) solubilized in 1 mL of 50 mM MES/0.3 % PF solution and 5.99 mg of NHS (3.5 eq. per equivalent of EDC quantity) solubilized in 1 mL of 50 mM MES/0.3 % PF solution were added. Then, 10, 25, 35, 50 or 100 equivalents of coupling agents **10** or **18** or **23** (per equivalent of available COOH groups on γ-Fe<sub>2</sub>O<sub>3</sub>/Polymer MNPs) solubilized in 1 mL of



50 mM MES/0.3 % PF solution were loaded in the grafting reaction, corresponding to 15 grafting experiments (see Table 1):

**Table 1.** Different loading of coupling agents **10**, **18** or **23** in the grafting reaction.

Compound 10	Compound 18	Compound 23
$\gamma\text{-Fe}_2\text{O}_3/\text{Pol}@10/10\text{eq}$	$\gamma\text{-Fe}_2\text{O}_3/\text{Pol}@18/10\text{eq}$	$\gamma\text{-Fe}_2\text{O}_3/\text{Pol}@23/10\text{eq}$
$\gamma\text{-Fe}_2\text{O}_3/\text{Pol}@10/25\text{eq}$	$\gamma\text{-Fe}_2\text{O}_3/\text{Pol}@18/25\text{eq}$	$\gamma\text{-Fe}_2\text{O}_3/\text{Pol}@23/25\text{eq}$
$\gamma\text{-Fe}_2\text{O}_3/\text{Pol}@10/35\text{eq}$	$\gamma\text{-Fe}_2\text{O}_3/\text{Pol}@18/35\text{eq}$	$\gamma\text{-Fe}_2\text{O}_3/\text{Pol}@23/35\text{eq}$
$\gamma\text{-Fe}_2\text{O}_3/\text{Pol}@10/50\text{eq}$	$\gamma\text{-Fe}_2\text{O}_3/\text{Pol}@18/50\text{eq}$	$\gamma\text{-Fe}_2\text{O}_3/\text{Pol}@23/50\text{eq}$
$\gamma\text{-Fe}_2\text{O}_3/\text{Pol}@10/100\text{eq}$	$\gamma\text{-Fe}_2\text{O}_3/\text{Pol}@18/100\text{eq}$	$\gamma\text{-Fe}_2\text{O}_3/\text{Pol}@23/100\text{eq}$

The total reaction volume for each grafting experiment was brought up to 5 mL (corresponding to the final concentration of 1 mg of MNPs/mL of solution) and then all the samples were sonicated (~10 sec, 60W). The grafting proceeded in a thermomixer (300 rpm) at 25°C for 16 h. During all the grafting period the particles remained well dispersed and no sedimentation or aggregation was observed. At the end of the grafting, MNPs were separated from the reaction mixture by magnetic decantation, washed with: MES (1x5mL), H<sub>2</sub>O (1x5mL), EtOH (3x5mL), re-dispersed in EtOH (5 mg/mL) and stored in the fridge.

### Grafting of silylated coupling agents **11**, **19** or **24** on core-shell $\gamma\text{-Fe}_2\text{O}_3/\text{SiO}_2$ MNPs

Grafting of coupling agents **11** and **19** on  $\gamma\text{-Fe}_2\text{O}_3/\text{SiO}_2$  MNPs can be performed by two procedures, in the absence of DMF (*protocol a*) or in the presence of DMF (*protocol b*), as described below. Regardless the grafting protocol (*a* or *b*) the grafting efficiency is the same (according to the IR study), therefore procedure *a* was used for the grafting of coupling agents **11** and **19**. Grafting of coupling agent **24** can be performed exclusively by *protocol b*, since adding of a small amount of DMF is necessary for the complete solubilisation of coupling agent **24** in EtOH.

*a)* First, 10 mg of  $\gamma\text{-Fe}_2\text{O}_3/\text{SiO}_2$  MNPs were dispersed in a mixture formed of 0.5 mL of 0.21 % Tx-405 solution, 0.5 mL of EtOH and a catalytic amount of 30 % NH<sub>4</sub>OH commercial solution (87.5  $\mu\text{L}$ ). Then, 0.125 mmol of functional silylated coupling agent **11** (0.068 g) or **19** (0.115 g) was solubilized in 1 mL of dry EtOH. The grafting was performed in a thermomixer (300 rpm) at 25°C for 2.5 h, during which, the coupling agent solution (**11** or **19**) was added dropwise (13  $\mu\text{L}$  every 2 min) to the dispersed  $\gamma\text{-Fe}_2\text{O}_3/\text{SiO}_2$  MNPs. Afterwards, the suspension was stirred additionally for 1 h at 40°C. At the end of the grafting reaction the modified  $\gamma\text{-Fe}_2\text{O}_3/\text{SiO}_2$  MNPs ( $\gamma\text{-Fe}_2\text{O}_3/\text{SiO}_2@11$  or

$\gamma\text{-Fe}_2\text{O}_3/\text{SiO}_2@19$ ) were separated by magnetic decantation from the reaction mixture, washed with EtOH ( $5 \times 1$  mL), re-dispersed in EtOH (5mg/mL) and stored in the fridge.

b) First, 10 mg of  $\gamma\text{-Fe}_2\text{O}_3/\text{SiO}_2$  MNPs were dispersed in 0.5 mL of 0.21 % Tx-405 solution and a catalytic amount of 30 %  $\text{NH}_4\text{OH}$  (87.5  $\mu\text{L}$ ). Then, 0.125 mmol of functional silylated coupling agent **11** (0.068 g), **19** (0.115 g) or **24** (0.21 g) was solubilized in the mixture formed of 1.5 mL of dry EtOH and 0.18 mL of anhydrous DMF. The grafting was performed in a thermomixer (300 rpm) at 25°C for 2.5 h, during which, the coupling agent solution (**11**, **19** or **24**) was added dropwise (22.4  $\mu\text{L}$  every 2 min) to the dispersed  $\gamma\text{-Fe}_2\text{O}_3/\text{SiO}_2$  MNPs. Afterwards, the suspensions were stirred for 1 h at 40°C. At the end of the grafting reaction the modified  $\gamma\text{-Fe}_2\text{O}_3/\text{SiO}_2$  MNPs ( $\gamma\text{-Fe}_2\text{O}_3/\text{SiO}_2@11$ ,  $\gamma\text{-Fe}_2\text{O}_3/\text{SiO}_2@19$  or  $\gamma\text{-Fe}_2\text{O}_3/\text{SiO}_2@24$ ) were separated by magnetic decantation from the reaction medium, washed with EtOH ( $5 \times 1$  mL), dispersed in EtOH (5 mL) and stored in the fridge.

#### Maleimide group deprotection

10 mg of the modified MNPs ( $\gamma\text{-Fe}_2\text{O}_3/\text{Pol}@10$ ,  $\gamma\text{-Fe}_2\text{O}_3/\text{Pol}@18$ ,  $\gamma\text{-Fe}_2\text{O}_3/\text{Pol}@23$ ,  $\gamma\text{-Fe}_2\text{O}_3/\text{SiO}_2@11$ ,  $\gamma\text{-Fe}_2\text{O}_3/\text{SiO}_2@19$ , or  $\gamma\text{-Fe}_2\text{O}_3/\text{SiO}_2@24$ ) were dispersed in 1 mL of anhydrous DMSO and the cleavage of furan protection proceeded in a thermomixer (300 rpm) at 99°C during 5 h. At the end of deprotection reaction the resulting maleimide functionalized MNPs:  $\gamma\text{-Fe}_2\text{O}_3/\text{Pol}@10\text{-Mal}$ ,  $\gamma\text{-Fe}_2\text{O}_3/\text{Pol}@18\text{-Mal}$ ,  $\gamma\text{-Fe}_2\text{O}_3/\text{Pol}@23\text{-Mal}$ ,  $\gamma\text{-Fe}_2\text{O}_3/\text{SiO}_2@11\text{-Mal}$ ,  $\gamma\text{-Fe}_2\text{O}_3/\text{SiO}_2@19\text{-Mal}$ , or  $\gamma\text{-Fe}_2\text{O}_3/\text{SiO}_2@24\text{-Mal}$  were separated from the reaction mixture by magnetic decantation, washed with EtOH ( $5 \times 1$  mL), dispersed in EtOH (5 mL) and stored in the fridge.

The cleavage of furan protection on silylated coupling agents was performed by refluxing 50 mg of silylated coupling agents **11**, **19** and **24** over 2 hours in the appropriate dry solvent (10 mL) (silanes **11** and **19** were refluxed in toluene, while silane **24** was refluxed in dioxan, since it is not soluble in toluene). At the end of the deprotection reaction the solvent was evaporated.

## 5. Immobilization tests

#### Covalent coupling of thiol modified biotin (HS-PEG-Biot) with the maleimide functionalized $\gamma\text{-Fe}_2\text{O}_3/\text{Polymer}$ or $\gamma\text{-Fe}_2\text{O}_3/\text{SiO}_2$ MNPs

1 mg of maleimide functionalized MNPs ( $\gamma\text{-Fe}_2\text{O}_3/\text{Pol}@10\text{-Mal}$ ,  $\gamma\text{-Fe}_2\text{O}_3/\text{Pol}@18\text{-Mal}$ ,  $\gamma\text{-Fe}_2\text{O}_3/\text{Pol}@23\text{-Mal}$ ,  $\gamma\text{-Fe}_2\text{O}_3/\text{SiO}_2@11\text{-Mal}$ ,  $\gamma\text{-Fe}_2\text{O}_3/\text{SiO}_2@19\text{-Mal}$  or  $\gamma\text{-Fe}_2\text{O}_3/\text{SiO}_2@24\text{-Mal}$ ) was dispersed in 0.375 mL of 0.01 M PBS/0.05% Tween-20 buffer solution (adjusted to pH=7.1 with 1 M HCl solution), and 2.76 mg of HS-PEG-Biot solubilized in 0.125 mL of 0.01 M PBS/0.05%

Tween-20 buffer solution were added to the MNPs' suspension. The reaction mixture was incubated in a thermomixer (300 rpm) at 37°C for 16 h. During the incubation period the particles remained well dispersed and no sedimentation or aggregation was observed. At the end of incubation reaction, MNPs ( $\gamma\text{-Fe}_2\text{O}_3/\text{Pol}@10@\text{Biot}$ ,  $\gamma\text{-Fe}_2\text{O}_3/\text{Pol}@18@\text{Biot}$ ,  $\gamma\text{-Fe}_2\text{O}_3/\text{Pol}@23@\text{Biot}$ ,  $\gamma\text{-Fe}_2\text{O}_3/\text{SiO}_2@11@\text{Biot}$ ,  $\gamma\text{-Fe}_2\text{O}_3/\text{SiO}_2@19@\text{Biot}$  or  $\gamma\text{-Fe}_2\text{O}_3/\text{SiO}_2@24@\text{Biot}$ ) were separated from the reaction mixture by magnetic decantation, washed with 0.01 M PBS/0.05% Tween-20 buffer solution, then re-dispersed in 1 mL of the same buffer solution and stored in the fridge.

### **Immobilization of 15 nm SA-Au NPs on biotin functionalized $\gamma\text{-Fe}_2\text{O}_3/\text{Polymer}$ or $\gamma\text{-Fe}_2\text{O}_3/\text{SiO}_2$ MNPs**

First, the storage buffer solution (Tris buffer saline pH=8.2, containing 1 % BSA, 15 mM  $\text{NaN}_3$  and 30 % glycerol) of 15 nm SA-Au NPs' was replaced with 0.01 M PBS/0.05% Tween-20 buffer solution (adjusted to pH=7.1 with 1 M HCl solution) according to the following procedure: 1 mL of SA-Au NPs (13.65  $\mu\text{g}/\text{mL}$  of protein,  $1.4 \times 10^{12}$  particles/mL) was transferred into a conical tube and 1 mL of 0.01 M PBS/0.05% Tween-20 buffer solution was added. The particles were vortexed and then centrifuged during 1 h at the speed of 9000 rpm. The solution was separated from the particles with a pipet. Next, the particles were re-dispersed in 2 mL of same buffer solution, vortexed and centrifuged during 1 h at the same speed. The procedure was repeated 2 times and then particles were dispersed in 1.4 mL (corresponding to  $1.00 \times 10^{12}$  part/mL) of the same buffer solution and stored in the fridge.

Next, to 0.05 mg of biotin modified MNPs ( $\gamma\text{-Fe}_2\text{O}_3/\text{Pol}@10@\text{Biot}$ ,  $\gamma\text{-Fe}_2\text{O}_3/\text{Pol}@18@\text{Biot}$ ,  $\gamma\text{-Fe}_2\text{O}_3/\text{Pol}@23@\text{Biot}$ ,  $\gamma\text{-Fe}_2\text{O}_3/\text{SiO}_2@11@\text{Biot}$ ,  $\gamma\text{-Fe}_2\text{O}_3/\text{SiO}_2@19@\text{Biot}$ , or  $\gamma\text{-Fe}_2\text{O}_3/\text{SiO}_2@24@\text{Biot}$ )  $2.00 \times 10^{11}$  SA-Au NPs (15 nm) dispersed in 0.2 mL of 0.01 M PBS/0.05% Tween-20 buffer solution (pH=7.1) were added (corresponding to  $4.0 \times 10^{12}$  SA-Au NPs/mg of functionalized MNPs). The reaction mixture was incubated in a thermomixer (300 rpm) at 37°C for 16 h. and no sedimentation or aggregation was observed during all this period, except sample  $\gamma\text{-Fe}_2\text{O}_3/\text{SiO}_2@24@\text{Biot}$  where the precipitation of the particles was observed (at the end of incubation time). Afterwards, MNPs were separated from the reaction mixture by magnetic decantation and the solutions of SA-Au NPs were analysed by UV-Vis Spectroscopy. The resulting MNPs ( $\gamma\text{-Fe}_2\text{O}_3/\text{Pol}@10@\text{Biot}@SA\text{-Au}$ ,  $\gamma\text{-Fe}_2\text{O}_3/\text{Pol}@18@\text{Biot}@SA\text{-Au}$ ,  $\gamma\text{-Fe}_2\text{O}_3/\text{Pol}@23@\text{Biot}@SA\text{-Au}$ ,  $\gamma\text{-Fe}_2\text{O}_3/\text{SiO}_2@11@\text{Biot}@SA\text{-Au}$ ,  $\gamma\text{-Fe}_2\text{O}_3/\text{SiO}_2@19@\text{Biot}@SA\text{-Au}$  or  $\gamma\text{-Fe}_2\text{O}_3/\text{SiO}_2@24@\text{Biot}@SA\text{-Au}$ ) were washed with water ( $5 \times 1$  mL), then re-dispersed 0.2 mL of water, and stored in the fridge.

### **Incubation of biotin functionalized $\gamma$ -Fe<sub>2</sub>O<sub>3</sub>/Polymer MNPs with 20 nm H<sub>2</sub>N-PEG-Au NPs**

First, 20 nm H<sub>2</sub>N-Au NPs were dispersed in 0.01 M PBS/0.05% Tween-20 buffer solution (adjusted to pH=7.1 with 1 M HCl solution) according to the following procedure: 0.2 mL of H<sub>2</sub>N-Au NPs' aqueous solution (corresponding to  $6.8 \times 10^{12}$  H<sub>2</sub>N-Au NPs) were transferred into a conical tube and 2 mL of 0.01 M PBS/0.05% Tween-20 buffer solution was added. The dispersion was vortexed and then centrifuged during 40 min. at the speed of 8500 rpm. Then, the solution was separated from the particles with a pipet. Next the particles were dispersed in 2 mL of same buffer solution, vortexed and centrifuged during 40 min at the same speed. The procedure was repeated one more times and then particles were dispersed in in 6.8 mL of buffer solution and stored in the fridge ( $1 \times 10^{12}$  particles/mL).

Next, 0.05 mg of biotin functionalized  $\gamma$ -Fe<sub>2</sub>O<sub>3</sub>/Polymer MNPs ( $\gamma$ -Fe<sub>2</sub>O<sub>3</sub>/Pol@10@Biot,  $\gamma$ -Fe<sub>2</sub>O<sub>3</sub>/Pol@18@Biot or  $\gamma$ -Fe<sub>2</sub>O<sub>3</sub>/Pol@23@Biot) were incubated with  $2.00 \times 10^{11}$  H<sub>2</sub>N-PEG-Au NPs of 20 nm dispersed in 0.2 mL of 0.01 M PBS/0.05% Tween-20 buffer solution (pH=7.1). The incubation proceeded in a thermomixer (300 rpm) at 37°C during 16 h. At the end of the incubation time, MNPs were separated from the reaction mixture, and the solutions of H<sub>2</sub>N-PEG-Au NPs were analysed by UV-Vis Spectroscopy, while MNPs were washed with water (5×1 mL), then re-dispersed 0.2 mL of water, and stored in the fridge.

### **Immobilization of 20 nm H<sub>2</sub>N-PEG-Au NPs on maleimide functionalized $\gamma$ -Fe<sub>2</sub>O<sub>3</sub>/Polymer MNPs**

To 0.05 mg of native or maleimide functionalized MNPs ( $\gamma$ -Fe<sub>2</sub>O<sub>3</sub>/Pol-COOH,  $\gamma$ -Fe<sub>2</sub>O<sub>3</sub>/Pol@10-Mal,  $\gamma$ -Fe<sub>2</sub>O<sub>3</sub>/Pol@18-Mal and  $\gamma$ -Fe<sub>2</sub>O<sub>3</sub>/Pol@23-Mal)  $2.00 \times 10^{11}$  H<sub>2</sub>N-PEG-Au NPs (20 nm) dispersed in 0.2 mL of 0.01 M PBS/0.05% Tween-20 buffer solution (adjusted to pH=7.1 with 1 M HCl solution) were added. The reaction mixtures were incubated in a thermomixer (300 rpm) at 37°C for 16 h. and no sedimentation or aggregation was observed during all this period. Afterwards, MNPs ( $\gamma$ -Fe<sub>2</sub>O<sub>3</sub>/Pol-COOH,  $\gamma$ -Fe<sub>2</sub>O<sub>3</sub>/Pol@10@Au,  $\gamma$ -Fe<sub>2</sub>O<sub>3</sub>/Pol@18@Au and  $\gamma$ -Fe<sub>2</sub>O<sub>3</sub>/Pol@23@Au) were separated from the reaction mixture, and the solutions of H<sub>2</sub>N-PEG-Au NPs were analysed by UV-Vis Spectroscopy, while MNPs were washed with water (5×1 mL), then re-dispersed 0.2 mL of water, and stored in the fridge.

### **Immobilization of HS-dT oligonucleotide on maleimide functionalized $\gamma$ -Fe<sub>2</sub>O<sub>3</sub>/Polymer or $\gamma$ -Fe<sub>2</sub>O<sub>3</sub>/SiO<sub>2</sub> MNPs and hybrid capture of its complementary sequence**

First, 1 mg of maleimide functionalized MNPs ( $\gamma$ -Fe<sub>2</sub>O<sub>3</sub>/Pol-COOH,  $\gamma$ -Fe<sub>2</sub>O<sub>3</sub>/Pol@10-Mal,  $\gamma$ -Fe<sub>2</sub>O<sub>3</sub>/Pol@18-Mal,  $\gamma$ -Fe<sub>2</sub>O<sub>3</sub>/Pol@23-Mal,  $\gamma$ -Fe<sub>2</sub>O<sub>3</sub>/SiO<sub>2</sub>-OH,  $\gamma$ -Fe<sub>2</sub>O<sub>3</sub>/SiO<sub>2</sub>@11-Mal,  $\gamma$ -Fe<sub>2</sub>O<sub>3</sub>/SiO<sub>2</sub>@19-Mal, or  $\gamma$ -Fe<sub>2</sub>O<sub>3</sub>/SiO<sub>2</sub>@24-Mal) was dispersed in 100  $\mu$ L of 10 mM phosphate buffer solution (adjusted to pH=7.0 with a 0.1 M HCl solution), then 10  $\mu$ L of 1 mM aqueous HS-dT

solution (10 nmol, 0.0774 mg) were added to the MNPs' suspension. The incubation reaction proceeded in the thermomixer (300 rpm) at 37°C during 16 h. All samples showed a good dispersion from the beginning until the end of the incubation period. At the end of the incubation time, oligonucleotide modified MNPs ( $\gamma\text{-Fe}_2\text{O}_3/\text{Pol}@10@dT$ ,  $\gamma\text{-Fe}_2\text{O}_3/\text{Pol}@18@dT$ ,  $\gamma\text{-Fe}_2\text{O}_3/\text{Pol}@23@dT$ ,  $\gamma\text{-Fe}_2\text{O}_3/\text{SiO}_2@11@dT$ ,  $\gamma\text{-Fe}_2\text{O}_3/\text{SiO}_2@19@dT$ , or  $\gamma\text{-Fe}_2\text{O}_3/\text{SiO}_2@24@dT$ ) were separated from the reaction mixture by magnetic decantation, washed with water (5×1 mL), re-dispersed in 0.1 mL of water and stored in the fridge.

*Hybridization* of the immobilized oligonucleotide dT with a complementary sequence oligo poly A of fluorochrome-conjugated oligo-dA Alexa Fluor (performed by Ademtech): 100 µg of oligonucleotide modified MNPs ( $\gamma\text{-Fe}_2\text{O}_3/\text{Pol}@10@dT$ ,  $\gamma\text{-Fe}_2\text{O}_3/\text{Pol}@18@dT$ ,  $\gamma\text{-Fe}_2\text{O}_3/\text{Pol}@23@dT$ ,  $\gamma\text{-Fe}_2\text{O}_3/\text{SiO}_2@11@dT$ ,  $\gamma\text{-Fe}_2\text{O}_3/\text{SiO}_2@19@dT$ , or  $\gamma\text{-Fe}_2\text{O}_3/\text{SiO}_2@24@dT$ ) were dispersed in 50 µL of SSC 3X (Saline Sodium Citrate) hybridization buffer and 1 µL of 100 µM oligo-dA-Alexa Fluor (100 pmol) was added. The incubation reaction proceeded in the thermomixer (1000 rpm) during 15min. At the end of the incubation time, the resulting MNPs ( $\gamma\text{-Fe}_2\text{O}_3/\text{Pol}@10@dTdA$ ,  $\gamma\text{-Fe}_2\text{O}_3/\text{Pol}@18@dTdA$ ,  $\gamma\text{-Fe}_2\text{O}_3/\text{Pol}@23@dTdA$ ,  $\gamma\text{-Fe}_2\text{O}_3/\text{SiO}_2@11@dTdA$ ,  $\gamma\text{-Fe}_2\text{O}_3/\text{SiO}_2@19@dTdA$ , or  $\gamma\text{-Fe}_2\text{O}_3/\text{SiO}_2@24@dTdA$ ) were separated from the reaction mixture by magnetic decantation and washed with SSC 0.3X (2×50 µL).

*The elution* of oligo-dA Alexa Fluor (performed by Ademtech) was achieved by incubation of the hybridized MNPs ( $\gamma\text{-Fe}_2\text{O}_3/\text{Pol}@10@dTdA$ ,  $\gamma\text{-Fe}_2\text{O}_3/\text{Pol}@18@dTdA$ ,  $\gamma\text{-Fe}_2\text{O}_3/\text{Pol}@23@dTdA$ ,  $\gamma\text{-Fe}_2\text{O}_3/\text{SiO}_2@11@dTdA$ ,  $\gamma\text{-Fe}_2\text{O}_3/\text{SiO}_2@19@dTdA$ , or  $\gamma\text{-Fe}_2\text{O}_3/\text{SiO}_2@24@dTdA$ ) with 50 µL of Rnase/Dnase free water, for 5 min at 50°C (1000rpm). Then, the supernatant was diluted in 950 µL of PBS and analysed on fluorescence microplate reader FLUOROSKAN.

# **List of abbreviations**



AcOEt	Ethyl acetate
AcOH	Acetic acid
Aloc or Alloc	Allyloxycarbonyl
APTES	3-aminopropyltrimethoxysilane
ATR	Attenuated Total Reflectance
ATRP	Atom Transfer Radical Polymerization
BIC	Bordeaux Imaging Centre
Boc	<i>tert</i> -Butyloxycarbonyl
Boc anhydride	Di- <i>tert</i> -butyl dicarbonate
C2M	Molecular Chemistry and Materials
Cbz	Carbobenzyloxy
CESAMO	Centre d'Etude Structurale et d'Analyse des Molécules Organiques
CLIO	Cross-linked Iron Oxide
CNRS	Centre Nationale de la Recherche Scientifique
COSY	Correlation Spectroscopy
CRP	Control Radical Polymerization
CuAAC	Cu <sup>I</sup> -mediated [3 + 2] azide–alkyne cycloaddition
Cu-free AAC	Strain-promoted AAC - “copper-free click chemistry”
Cys	Cysteine
DA	Diels-Alder
DCM	Dichloromethane
DEPT	Distortionless Enhancement by Polarization Transfer
DIAD	Diisopropyl azodicarboxylate
DMAP	4-Dimethylaminopyridine
DMF	Dimethylformamide
DMSO	Dimethylsulfoxide
DNA	Deoxyribonucleic acid
DTA	Differential Thermal Analysis
DTG	Derivative of the Thermogravimetric curve
EDA	Ethylenediamine
EDC or EDAC	N-Ethyl-N'-(3-dimethylaminopropyl)carbodiimide
EDTA	Ethylenediaminetetraacetic acid
ESI	Electrospray Ionization



Et <sub>2</sub> O	Diethyl ether
EtOH	Ethanol
FD	Field Desorption
FISH	Fluorescent In Situ Hybridization
Fmoc	9-Fluorenylmethyloxycarbonyl
FT-IR	Fourier Transformed Infrared Spectrometry
G	Generation
GA	Glutaraldehyde
GLYMO	3-glycidoxypropyltrimethoxysilane
GSM	Molecular Spectroscopy Group
H <sub>2</sub> N-PEG-Au NPs	Amino PEGylated gold nanoparticles
HMBC	Heteronuclear Multiple Bond Coherence
HOBt	Hydroxybenzotriazole
HS-dT oligonucleotide	3' thiol modified oligonucleotide poly T: TTT-TTT-TTT-TTT-TTT-TTT
HS-PEG-Biot	Thiol modified biotin
HSQC	Heteronuclear Single Quantum Coherence
IMAC	Immobilized Metal Affinity Chromatography
IO	Iron Oxide
IONPs	Iron Oxide Nanoparticles
IR	Infrared Spectroscopy
ISM	Institut des Sciences Moléculaires
MEHQ	Hydroquinone monomethyl ether
MeOH	Methanol
MES	4-Morpholineethanesulfonic acid
MNPs	Magnetic nanoparticles
MS	Mass Spectrometry
NHS	N-hydroxysuccinimide
NMP	Nitroxide-mediated Polymerization
NMR	Nuclear Magnetic Resonance
NP	Nanoparticle
NTA	Nitrilotriacetic acid
OA	Oleic acid
OEG	Oligo(ethylene glycol)

P(OEGMA-co-MAA)	Poly(oligo(ethylene glycol) methacrylate-co-methacrylic acid)
PAMAM	Poly(amidoamine)
PBS	Phosphate buffered saline
PEA	Poly(ester amine)
PEG	Poly(ethylene glycol)
PEI	Poly(ethylene imine)
PEO	Poly(ethylene oxide)
PF	Pluronic F-127
Ph <sub>3</sub> P	Triphenylphosphine
Phoenics	PHotonics and Omics ENabled by Innovations in Chemical Synthesis
Phth	Phtalimide
Poly(St-AA)	Poly(styrene-co-acrylic acid)
Poly(TMSMA-r-PEGMA-r-NAS)	Poly(3-(trimethoxysilyl)propyl methacrylate-r-PEG methyl ether methacrylate-r-N-acryloxysuccinimide)
PVA	Poly(vinyl alcohol)
RAFT	Reversible Addition-fragmentation Transfer Polymerization
RNA	Ribonucleic acid
SA	Streptavidin
SA-Au NPs	Streptavidin coated gold nanoparticles
SMCC	Succinimidyl-4-(N-maleimidomethyl)cyclohexane-1-carboxilate
SP	Superparamagnetism
SP IONPs	Superparamagnetic Iron Oxide Nanoparticles
SP NPs	Superparamagnetic Nanoparticles
SSC	Saline Sodium Citrate
ssDNA	Single-stranded Deoxyribonucleic acids
ssRNA	Single-stranded Ribonucleic acid
Sulpho-SMCC	Sulphosuccinimidyl-4-(N-maleimidomethyl)cyclohexane-1-carboxilate
TBAF	Tetrabutylammonium Fluoride hydrate
TCL-SPION	Thermally Cross-linked Superparamagnetic Iron Oxide Nanoparticle
TEA	Triethylamine
TEM	Transmission Electron Microscopy

TEM	Transmission Electron Microscopy
Troc	2,2,2-trichloroethyloxycarbonyl
Teoc	2-(trimethylsilyl)ethyloxycarbonyl
Teoc-ONp	4-Nitrophenyl-2-(trimethylsilyl)ethyl carbonate
TEOS	Tetraethyl Orthosilicate or Tetraethoxysilane
TGA	Thermogravimetric Analyses
THF	Tetrahydrofuran
Triton X-405 or Tx	Polyethylene glycol tert-octylphenyl ether
UV-Vis	Ultraviolet–visible



## Fonctionnalisation dendritique de nanoparticules magnétiques cœur-écorce pour la biotechnologie

**Résumé :** Le but de ce travail a été d'élaborer des nanoparticules magnétiques (MNPs) fonctionnalisées avec un groupement maléimide, stables, dispersibles dans l'eau et qui assureront une immobilisation covalente, sélective et efficace de biomolécules. Bien qu'un large choix de MNPs soit disponible dans le commerce, la modification chimique de surface des MNPs reste une étape indispensable pour l'élaboration de matériaux spécifiques. Un contrôle précis de la fonctionnalisation de surface des MNPs est crucial, car en découlent leurs propriétés physico-chimiques, leur stabilité colloïdale, et la préservation de l'activité biologique de la biomolécule immobilisée. Dans ce travail, nous proposons d'augmenter le nombre de groupes fonctionnels (maléimide) accessibles à la surface de MNPs, en la modifiant par des agents de couplage dendritiques. Deux types de MNPs cœur-écorce de 300 nm (avec un noyau de  $\gamma$ -Fe<sub>2</sub>O<sub>3</sub> et une écorce de polymère ou de silice) ont été utilisés. Afin d'étudier l'effet «dendritique» sur la fonctionnalisation de surface, trois types d'agents de couplage ont été conçus: des agents de couplage linéaires (contenant un groupe maléimide), des agents de couplage dendritiques à deux branches (contenant deux groupes maléimide) et des agents de couplage dendritiques à quatre branches (contenant quatre groupes maléimide). L'efficacité de ces MNPs fonctionnalisées pour immobiliser des biomolécules ou des modèles de biomolécules a été étudiée. Cette étude a démontré l'intérêt de la fonctionnalisation de la surface des MNPs cœur-écorce par des structures dendritiques pour une immobilisation efficace et spécifique de biomolécules.

**Mots clés :** fonctionnalisation de surface, agents de couplage dendritiques, nanoparticules magnétiques cœur-écorce, immobilisation covalente de biomolécules.

---

### Dendritic functionalization of core-shell magnetic nanoparticles for biotechnology

**Abstract:** The purpose of this work is to design stable, water-dispersible, maleimide functionalized magnetic nanoparticles (MNPs) that will ensure selective covalent immobilization of biomolecules. While, a large choice of MNPs is now commercially available, the surface modification of MNPs remains an indispensable step in the elaboration of such MNPs. A precise control over the surface functionalization of MNPs is crucial, because it governs their physicochemical properties, their colloidal stability, and their biological behaviour. In this work with the aim to increase the number of functional groups on MNPs' surfaces, it was proposed to functionalize MNPs with dendritic coupling agents and to compare their efficiency with those functionalized with a linear analogue. Moreover, it was decided to investigate the "dendritic effect" of the surface functionalization on two types of core-shell MNPs (300 nm) that consist of a maghemite ( $\gamma$ -Fe<sub>2</sub>O<sub>3</sub>) ferrofluid core coated with: (I) polymer shell or (II) silica shell. Therefore, three types of coupling agents (that possess an amino or silane anchoring site) were synthesized: linear coupling agents (containing one maleimide functional group); two-branched coupling agents (containing two maleimide functional groups) and four-branched dendritic coupling agents (containing four maleimide functional groups). Then, the capacity of MNPs functionalized with dendritic or linear coupling agents to immobilize biomolecules or models of biomolecules was investigated. This study proved the efficiency of the surface functionalization with dendritic structures for the immobilization of biomolecules.

**Keywords:** surface functionalization, dendritic coupling agents, core-shell magnetic nanoparticles, covalent immobilization of biomolecules.

---